ASPECTS OF INTERACTING ELECTRONS ON GRAPHENE HONEYCOMB LATTICE

by

Bitan Roy

B.Sc, University of Calcutta, 2004

M.Sc, Indian Institute of Technology-Bombay, 2006

M.Sc, Simon Fraser University- Burnaby, 2008

A THESIS SUBMITTED IN PARTIAL FULFILLMENT
OF THE REQUIREMENTS FOR THE DEGREE OF
DOCTOR OF PHILOSOPHY
in the Department
of
Physics

SIMON FRASER UNIVERSITY
Summer 2011

APPROVAL

Name:	Bitan Roy
Degree:	Doctor of Philosophy
Title of thesis:	Aspects of interacting electrons on Graphene Honeycomb Lattice
Examining Committee:	Dr. George Kirczenow Chair
	Dr. Igor Herbut, Senior Supervisor Professor, Department of Physics
	Dr. Malcolm Kennett, Supervisor Assistant Professor, Department of Physics
	Dr. Howard Trottier, Supervisor Professor, Department of Physics
	Dr. J. Steven Dodge, SFU Examiner Associate Professor, Department of Physics
	Dr. Vladimir A. Miransky, External Examiner Professor, Department of Applied Mathematics, University of Western Ontario
Date Approved:	August 17, 2011.

Partial Copyright Licence

Abstract

In this thesis, we study the electron-electron interaction on the graphene honeycomb lattice theoretically. Even though pristine graphene behaves like a semimetal, sufficiently strong interactions can place the system in ordered phases.

First, we derive a general Lagrangian for repulsive, short-ranged quartic interactions. The number of parameters in the Lagrangian is restricted by the symmetries present in the lattice, and the emergent ones. Then, we study the interacting theory in the framework of the renormalization group. All the critical points describing the transitions from the semimetallic phase to insulating phases reside in a Lorentz symmetric subspace. All the transitions are continuous and weak Lorentz symmetry breaking is irrelevant near the critical points. We also study the behaviour of various physical observables near the criticality.

In the presence of an attractive interaction, we study the superconducting ground state, when fermions living on the nearest-neighbour sites of the honeycomb lattice attract each other strongly. A spatially inhomogeneous, spin-triplet, odd under sublattice exchange, Kekule superconductor turns out to be the variational ground state. Within the mean field approximation, the Kekule superconductor is energetically the best solution at and close to filling one-half.

Even though all the transitions in neutral graphene can only take place at strong couplings, penetration of either real or pseudo magnetic field lowers the critical strength for insulation to zero. We study the problem of interacting fermions in the presence of the two magnetic fields, as well as when both of them are present. Moreover, our analysis includes the formation of insulators in the presence of inhomogeneous fields. We take analytical and

numerical approaches to convey the central message: irrespective of the form of the fields, as long as there exists a finite density of states near zero energy, graphene finds itself in an ordered phase even at infinitesimal interactions. However, in the presence of real (pseudo) magnetic field the order parameter breaks the chiral (time reversal) symmetry. We present a thorough study of the scaling of the interaction induced gap, universal amplitudes and finite size effects.

Keywords: Graphene; Interactions; Insulators; Superconductors; Renormalization group; Magnetic catalysis.

To my parents Anuradha and Bikash Behari Roy

Acknowledgments

During three and half years I was in Simon Fraser University and many people supported me to achieve Ph.D. degree. It is my pleasure to acknowledge them.

First of all, I am greatly indebted to Prof. Igor Herbut for his scientific and moral support during the time I spent at Simon Fraser University. He introduced me to the physics of graphene which was a completely new area for me at the time I started my Master's studies in 2006. He continued great amount of support in my scientific career during my doctoral studies too. He was a brilliant supervisor and his ideas profoundly influenced my work during this period. Apart from our regular scientific discussion, I thoroughly enjoyed discussions and debates on movies, sports, politics, philosophy etc. Despite of occasional hiccups among us, I feel great honor to declare him my friend, guide and philosopher. He influenced my life in many different ways and stood by me in difficult periods of my life. Thanks Igor!

It is a pleasure to express my gratitude to Dr. Vladimir Juričić, who was a post-doc in the group. I worked extensively with Vladimir and we are currently involved in few projects. He always provided great amount of help scientifically, which played a crucial role to shape my scientific career. However, he is more than a collaborator to me and it is my privilege to have a friend like Vladimir. Author of this thesis also admires many valuable discussion with Dr. Chi-Ken Lu, current post-doc in the group.

Here I would like to take the opportunity to thank the other members of my supervising committee, Malcolm Kennett and Howard Trottier. Their critical comments about my work shaped my work towards completeness. I am thankful to Prof. Steven Dodge for assigning a healthy amount of travel grant, which made some of my scientific travel possible. My attendance in the 28^{th} Winter School in Theoretical Physics held in Jerusalem and

Korrelationstage 2011 in Dresden provided me ample opportunity to get to know some other related topics in Condensed Matter Physics. I owe at least a thank to Michael Plischke, for providing ample opportunity to learn statistical physics from him and also working with me on some interesting ideas. Andrew DeBenedictis is a good friend of mine over last few years. I also appreciate his patience to discuss some physics with me.

The great course work structure of Department of Physics provided an excellent background for my research work. David Broun, Levon Pogosian, Andrei Frolov, Malcolm Kennett, Igor Herbut showed their great skill of teaching and provided fantastic learning environment. I appreciate their effort. It was a great experience to take two courses in Quantum Field theory in UBC with Gordon Semenoff and Ariel Zhitnitsky. I am thankful to the graduate secretaries of Department of Physics, Margaret, Misty, Amy and Rose for taking care of credit transfer and for providing reminders of committee meetings every year ! In particular, special thanks to Rose for answering my repeated questions patiently about the formalities regarding the thesis submission.

I was a great pleasure to share office with Peter Smith, Maysam Emadi, Sara Sadeghi, Greg Miller, Yiwei Zhang, Hildur Knutsdottir, Sarah Reeve, Kelly Cheung, Nuri Yazdani. I am thankful to Peter for patiently sharing his expertise on computational physics. I am also greatfull to Nuri for involving me in many social activities. Having friends like Michel Trottier-McDonald, Kamran Kaveh, Suvayu Ali, Somshubra Sharangi, Natasha Ghosh, Rasoul Narimani, Kallol Mitra, Richard Bolton, Daniel Haft, Mehrdad Rastan, Himadri Ganguli, Subinoy Das, Bananin Chakraborty, Pallab Basu, Payam Masouvi, Amir Farhani was a great pleasure to me. Special thanks to Pallab for introducing Ads-CFT correspondence to me. I am indebted to Ananth Narayan Sankaranarayanan, who provided critical comments about the thesis.

I also thank Dilip Bhattacharya, my uncle for proving some support in need. At last but not the least I would like to thank my parents Anuradha and Bikash Behari Roy for providing moral support during my entire academic period and the sacrifices they made to facilitate my study.

Thanks all of you !

Contents

List of Tables

List of Figures

Chapter 1

Introduction and basic philosophy

At the dawn of time, our planet was a gaseous fireball covered by a thick layer of carbon di- and mono-oxide. With time, they started to dissolve leaving the globe with copious amount of oxygen, suitable for habitation of living elements. Nevertheless, carbon remained as one of the crucial ingredients of almost all the living creatures. Development of modern civilization is based on consumption of fossil fuels, which are primarily carbon based. Moreover, bio-fuels, one of the replacement of fossil fuels, are carbon based compounds. In the recent era, carbon based compounds became the prime element in the study of organic chemistry. Due to flexibility in its bonding, carbon based materials offers a wide variety of electronic properties depending on structure and dimensionality, for example, fullerene (C_{60}), carbon based nanotubes (see Fig. 1.1). Yet another carbon based material, 'graphene' was successfully synthesized in 2004 [1]. Vast studies on graphite explored that, it is comprised of stacks of two dimensional arrangement of carbon atoms in a honeycomb pattern, with the adjacent layers glued by a weak Van-der Waals force. Still, it took more than a decade after successful fabrication of fullerene to isolate a single layer of graphite, nowadays commonly known as 'graphene'. This was the first realization of an isolated 2 dimensional system, with thickness of the order of angstrom. Apart from technical complications involved in the isolation of a single layer graphite, thermodynamic aspects kept the stability of such two dimensional system under question. Synthesis of GaAs heterostructure provided ample opportunity to test various aspects of physics, purely arising due to the reduced dimensionality of the system, e.g., integer and fractional quantum Hall effects. Following graphene's successful fabrication, the discoverers, Andrei Geim and Konstantin Novoselov, were awarded the Nobel prize in 2010.

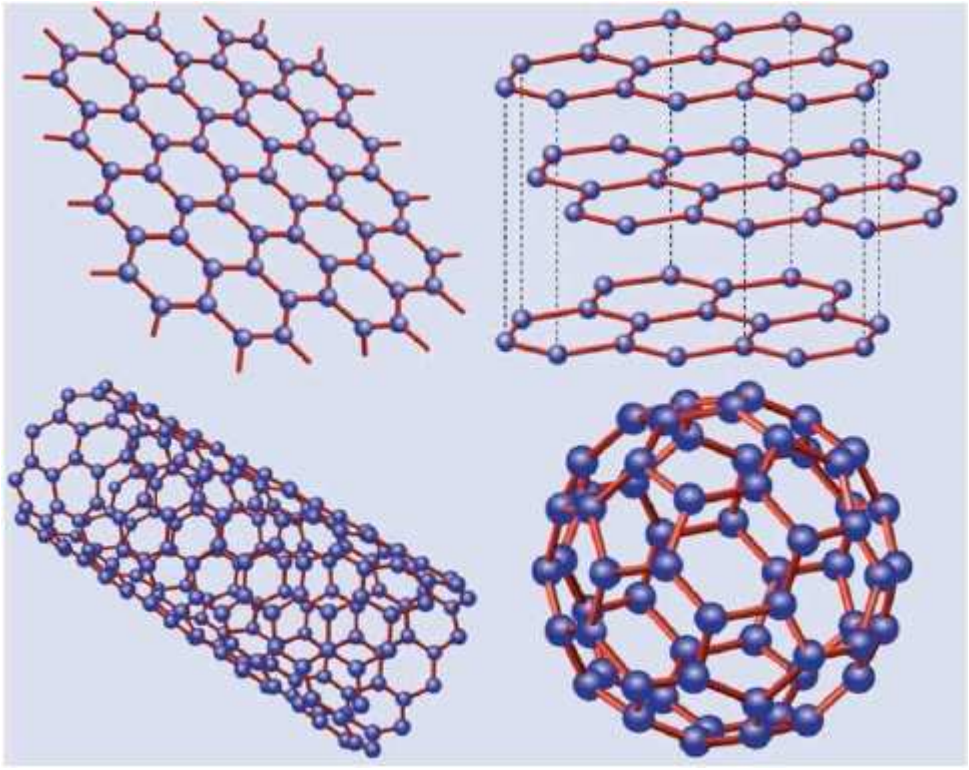

Figure 1.1: Graphene (top left) consists of hexagonal honeycomb lattice of carbon atoms. Top right one showing Graphite consists of graphene layers. In bottom it is carbon nanotube in the left and 3-D allotrope of carbon on a spherical surface in right. Figure reprinted with permission from A. H. Castro Neto et al., [1]. Copyright 2009 by the American Physical Society.

The hexagonal honeycomb lattice comprised of carbon atoms, opened a new frontier in condensed matter physics in the last few years. Peculiarities in its electronic behavior arise from the underlying lattice structure which lacks inversion symmetry around a site. Unlike a square lattice, the valence and the conduction band touch each other at the edges of the Brillouin zone. At half-filling, when the number of electrons residing in the lattice is equal to the number of carbon atoms, the valence band is filled, while the conduction band remains empty. The quasi particle excitations then can be described as massless Dirac fermions with a linearized conical dispersion around the corners of the Brillouin zone. It is admitted

that such linearized band structure remains valid up to an energy scale smaller than the bandwidth. The momentum range, over which the linear approximation of density of states holds is therefore always accompanied by a cutoff ($\Lambda = 1/a$), a is the lattice spacing. In the presence of a $\pi-$flux square lattice one can also end up with Dirac fermions at single zero-energy points in the Brillouin zone, but the unit cell consists of four lattice sites [2]. However, experimental limitations to implement such proposal made the community wait for almost two decades before the Dirac quantization in graphene was first observed in a laboratory. As a consequence, graphene is expected to mimic the physics of quantum electrodynamics but at a much smaller velocity than the usual photon. Measurement of Fermi velocity (v_F), playing the role of velocity of light (c), found $v_F = c/300$ [1].

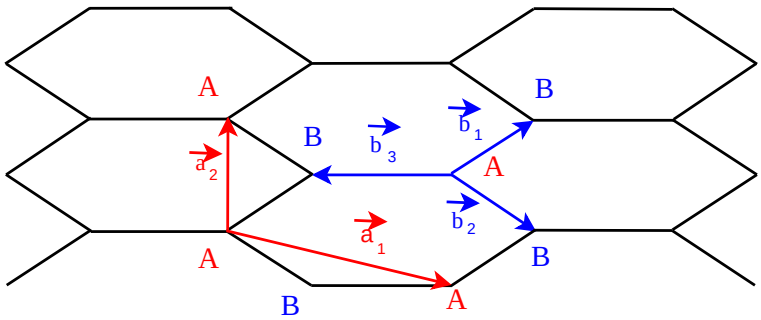

Figure 1.2: Lattice structure of the graphene honeycomb lattice showing sublattices A (red) and B (blue) with different lattice vectors that generate two interlocked triangular sublattices.

In a recent work, a construction by Affleck and Marston has been generalized to the cubic lattice in three dimension. The 3D $\pi-$flux lattice can give rise to Dirac fermions near with a single Dirac point. However the unit cell then consists of 8 sites [3]. The connection between the minimal representation of the Dirac fermions with the dimensionality of the system has been established recently [4]. It shows that in a *two* dimensional lattice the minimal dimensionality of spinless Dirac fermions is always 4, while that in a *three* dimensional lattice is 8.

1.1 Graphene

The lattice structure of honeycomb lattice is described in terms of two inter-penetrating triangular sublattices, shown in Fig. 1.2. One of the sublattices (A) is generated by the linear combination of the basis vectors $\vec{a}_1 = (\sqrt{3}, -1)a$, $\vec{a}_2 = (0, 1)a$. The other sublattice (B) is then at $\vec{B} = \vec{A} + \vec{b}$, with $\vec{b}$ being $\vec{b}_1 = (1/\sqrt{3}, 1)a/2$, $\vec{b}_2 = (1/\sqrt{3}, -1)a/2$, or $\vec{b}_3 = (-1/\sqrt{3}, 0)a$, where a is the lattice spacing $= 2.5\mathring{A}$, for graphene. The reciprocal lattice is also a hexagon, defined in terms of the vectors the vectors $\vec{R}_1 = \frac{4\pi}{\sqrt{3}a}(1, 0)$ and $\vec{R}_2 = \frac{4\pi}{\sqrt{3}a}(\frac{1}{2}, \frac{\sqrt{3}}{2})$, see Fig. 1.3 [5, 6].

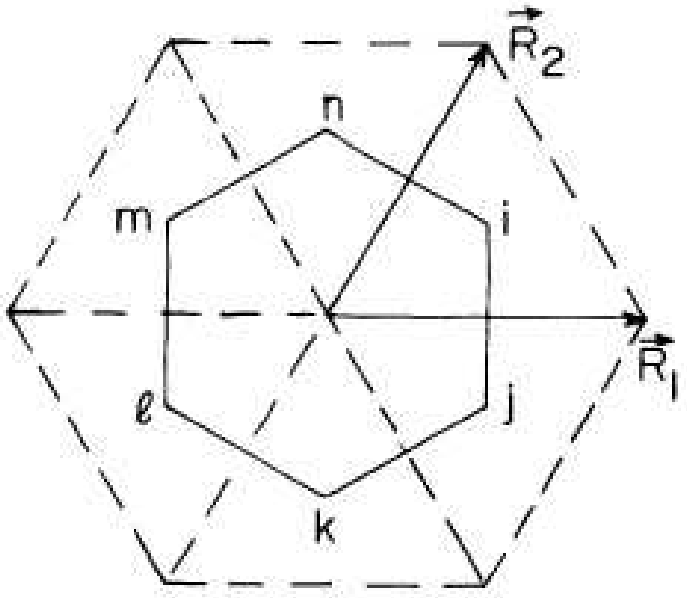

Figure 1.3: The Brillouin zone. The reciprocal-lattice vectors are $\vec{R_1} = (4\pi/\sqrt{3}a)(1, 0)$, $\vec{R_2} = (4\pi/\sqrt{3}a)(1/2, \sqrt{3}/2)$. The degeneracy points occur at the corners i j k l m n, of the Brillouin zone. Figure reprinted with permission from G. W. Semenoff, [6]. Copyright 1984 by the American Physical Society.

Next we try to understand the behavior of the free fermions hopping on carbon honeycomb lattice. The electronic structure of Carbon is $1s^2 2s^2 2p^2$. Therefore it has 4 electrons

in the outer shell. Out of these, 3 electrons form bonds with nearest neighbor sites by sp^2 hybridization and the fourth electron in the p_z orbital can hop through the system. Large overlap of the wave functions among the nearest-neighbor sites yields a strong hopping amplitude in graphene $t \sim 2.5$ eV [7]. Keeping only the nearest-neighbor hopping, one can write down the free Hamiltonian associated with the tight binding model as

$$\begin{aligned} H_t = & - t \sum_{\vec{A},i,\sigma=\pm 1} \left[{u_\sigma}^\dagger(\vec{A}) v_\sigma(\vec{A}+\vec{b_i}) + H.c. \right] \\ & + \beta \sum_{\vec{A},\sigma=\pm 1} \left[{u_\sigma}^\dagger(\vec{A}) u_\sigma(\vec{A}) - {v_\sigma}^\dagger(\vec{A}+\vec{b_1}) v_\sigma(\vec{A}+\vec{b_1}) \right], \end{aligned} \tag{1.1}$$

where $u^\dagger$ and u ($v^\dagger$ and v) are the electron creation and annihilation operators on the sublattice A (B) of the honeycomb lattice. The second term counts the difference in onsite energy among the two sublattices. The relevance of such a term will be discussed soon. Defining the Fourier modes

$$u(\vec{A}) = \int \frac{d^2k}{(2\pi)^2}\, e^{i\vec{k}\cdot\vec{A}}\, u(\vec{k}) \ , \quad v(\vec{B}) = \int \frac{d^2k}{(2\pi)^2}\, e^{i\vec{k}\cdot\vec{B}}\, v(\vec{k}), \tag{1.2}$$

and dropping the spin indices, one can also write down the Hamiltonian H_t as

$$\begin{aligned} H_t = & \int \frac{d^2k}{(2\pi)^2} \left[u^\dagger(\vec{k}), v^\dagger(\vec{k}) \right] \\ & \times \begin{pmatrix} \beta & -t(e^{i\vec{k}\cdot\vec{b_1}} + e^{i\vec{k}\cdot\vec{b_2}} + e^{i\vec{k}\cdot\vec{b_3}}) \\ -t(e^{i\vec{k}\cdot\vec{b_1}} + e^{i\vec{k}\cdot\vec{b_2}} + e^{i\vec{k}\cdot\vec{b_3}}) & -\beta \end{pmatrix} \times \begin{bmatrix} u(\vec{k}) \\ v(\vec{k}) \end{bmatrix}. \end{aligned} \tag{1.3}$$

Diagonalizing the tight binding Hamiltonian one gets the doubly degenerate energy eigenvalues to be

$$E(k) = \pm \left(\beta^2 + t^2 |e^{i\vec{k}\cdot\vec{b_1}} + e^{i\vec{k}\cdot\vec{b_2}} + e^{i\vec{k}\cdot\vec{b_3}}|^2 \right)^{1/2}. \tag{1.4}$$

With one electron per site, all the negative energy states (valence band) are filled, leaving those at positive energy (conduction band) empty. The separation between these two bands is minimum at the zeros of the function $f(k) = \left(e^{i\vec{k}\cdot\vec{b_1}} + e^{i\vec{k}\cdot\vec{b_2}} + e^{i\vec{k}\cdot\vec{b_3}} \right)$. The minima of this function occurs at the six edges of the Brillouin zone. Out of those six such points, only two are inequivalent and suitably chosen to be at $\vec{K_1} = (4\pi/\sqrt{3}a)(1/2, 1/2\sqrt{3})$ and $\vec{K_2} = -\vec{K_1}$. At those points the band gap is 2 $|\beta|$. Taking $\beta = 0$ one finds that the valence and the conduction bands touch each other at the corners of the Brillouin zone. These special points in the Brillouin zone are named as Dirac points. A trivial value of β

signifies that the two subattices are identical. This is indeed the case in graphene, as both the triangular sublattices are occupied by carbon atoms. Thus graphene in its pristine state behaves like a semimetal. On the other hand for boron nitride $\beta \neq 0$ and hence it is a trivial insulator [8]. The symmetry under the exchange of two sublattices is one of the reflection symmetries, to be discussed in detail in the next chapter. The other one is the invariance of the theory under the exchange of two inequivalent Dirac points. Such reflection symmetry is associated with the time reversal symmetry of the problem. Incorporation of further remote hopping does not remove the Dirac points from the spectrum, only shifts them in energy.

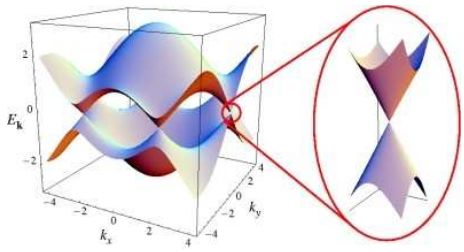

Figure 1.4: Conical dispersion in graphene around the Dirac point. Figure reprinted with permission from A. H. Castro Neto et al., [1]. Copyright 2009 by the American Physical Society.

Setting $\beta = 0$, let us compute the dispersion relation in the vicinity of the Dirac points. Expanding the function $f(k)$ around $\vec{K}_1$ to linear order in momentum yields

$$f(\vec{K}_1 + \vec{q}) = -i\frac{t\sqrt{3}}{2}e^{-i\frac{2\pi}{3}}\, q_x + i\,\frac{t}{2}\,\left(e^{i\frac{2\pi}{3}} - 1\right)\, q_y. \tag{1.5}$$

A similar expansion can be performed near the other point at $\vec{K}_2$ and gives

$$f(\vec{K}_2 + \vec{q}) = -f^*(\vec{K}_1 + \vec{q}). \tag{1.6}$$

Thus the dispersion near the two Dirac points becomes conical and isotropic, and reads as

$$\omega^2 = \frac{3t^2}{4}({q_x}^2 + {q_y}^2) + O(q^3). \tag{1.7}$$

Finally incorporating the spin degrees of freedom one can write down the low energy Hamiltonian as

$$\begin{aligned} H_t &= -\frac{t\sqrt{3}}{2}\sum_{\sigma=\pm}\int_{\vec{K}_1+\vec{q}}^{\Lambda}\frac{d^2\vec{q}}{(2\pi a)^2}(u_\sigma^\dagger(\vec{K}_1+\vec{q}),v_\sigma^\dagger(\vec{K}_2+\vec{q}))\,\mathcal{P}_+\begin{pmatrix} u_\sigma(\vec{K}_1+\vec{q}) \\ v_\sigma(\vec{K}_1+\vec{q})\end{pmatrix} \\ &- \frac{t\sqrt{3}}{2}\sum_{\sigma=\pm}\int_{\vec{K}_2+\vec{q}}^{\Lambda}\frac{d^2\vec{q}}{(2\pi a)^2}(u_\sigma^\dagger(\vec{K}_2+\vec{q}),v_\sigma^\dagger(\vec{K}_2+\vec{q}))\,\mathcal{P}_-\begin{pmatrix} u_\sigma(\vec{K}_2+\vec{q}) \\ v_\sigma(\vec{K}_2+\vec{q})\end{pmatrix} \end{aligned} \tag{1.8}$$

where $\mathcal{P}_\pm = \pm\, q_x\,\sigma_x - q_y\,\sigma_y$, and σ_x, σ_y are the Pauli matrices. Here the frame of reference is conveniently rotated to $q_x = \vec{q}\cdot\vec{K}/q$ and $q_y = (\vec{K}\times\vec{q})\times\vec{K}/K^2$. One can cast the above low energy Hamiltonian in Dirac notation

$$H_t = \sum_{\sigma=\pm}\Psi_\sigma^\dagger(\vec{x})\,(i\,\gamma_0\,\gamma_i\,p_i)\,\Psi_\sigma(\vec{x}), \tag{1.9}$$

with

$$\Psi_\sigma^\dagger(\vec{x}) = \int^{\Lambda}\frac{d\vec{q}}{(2\pi a)^2}e^{i\vec{q}\cdot\vec{x}}\,\left(u_\sigma^\dagger(\vec{K}+\vec{q}),v_\sigma^\dagger(\vec{K}+\vec{q}),u_\sigma^\dagger(-\vec{K}+\vec{q}),v_\sigma^\dagger(-\vec{K}+\vec{q})\right). \tag{1.10}$$

The four component Hermitian gamma matrices belong to the 'graphene representation', namely $\gamma_0 = I_2\otimes\sigma_3, \gamma_1 = \sigma_3\otimes\sigma_2$ and $\gamma_2 = I_2\otimes\sigma_1$. To complete the Clifford algebra, one can define the remaining two anticommuting gamma matrices as $\gamma_3 = \sigma_1\otimes\sigma_2$ and $\gamma_5 = \sigma_2\otimes\sigma_2$. Here the gamma matrices satisfy the following algebra $\{\gamma_\mu,\gamma_\nu\} = 2\delta_{\mu\,\nu}$, where $\mu,\nu = 0,1,2,3,5$ [9].

1.2 Fingerprint of graphene

Isolation of a monolayer of graphite, graphene, nevertheless requires to be confirmed experimentally. The electronic properties of graphene reflect the Dirac nature of the low energy quasiparticles. The linear dependence of the Hamiltonian on momentum places the Hall states at fillings $\nu = \pm 4(n+\frac{1}{2})$, where $n = 0,1,2,\cdots$ citermp. Measurement of Hall conductivity at relatively low magnetic field confirmed such quantization of the off-diagonal conductivity (See Fig. 1.5). If, on the other hand, there are two layers of graphene (bilayer graphene) the energy dispersion becomes quadratic in momentum in the vicinity of the Dirac points, leading to a completely different quantization of the Hall conductivity. For bilayer graphene, however the Hall states reside at filling $\nu = \pm 4(n+1)$ (See Inset

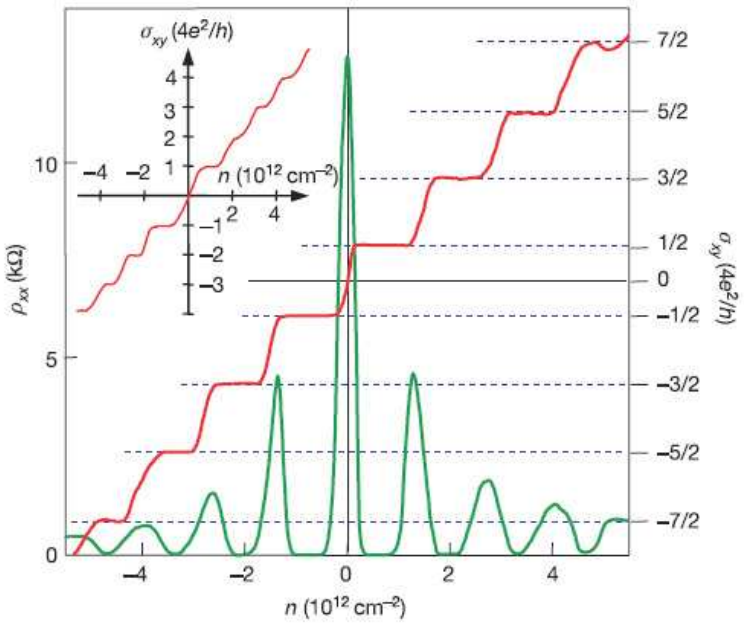

Figure 1.5: Figure shows the anomalous quantum hall plateaus for single layer graphene. Inset diagram is for bilayer graphene. Reprinted by permission from Macmillan Publishers Ltd. (Nature): K. S. Novoselov, et al.,[10], copyright 2005.

of Fig. 1.5) [10, 11]. The additional degeneracy of the zeroth Landau level arises from the quadratic nature of the dispersion. The quantization of the Hall conductivity can therefore be implemented as a litmus test of the monolayer graphene. Recent experiments found quantization of the Hall conductivity at fillings $\nu = \pm 4(n + \frac{3}{2})$ in a tri-layer graphene [12].

1.3 Many body physics in graphene

One of the most fundamental problems in condensed matter physics is the understanding of quantum properties of systems with very large number of degrees of freedom. Condensed matter systems are comprised of electrons, which interact among themselves via Coulomb interactions. Electron-electron interactions lead to plethora of effects, e.g., magnetic transitions of metal towards ferromagnetic ground states. The failure of dipole-dipole type interactions to explain high Curie temperature ($\sim$ 770 K in Iron, 1130 K in Cobalt etc.) was one of the primitive examples which can only be resolved in the framework of Coulomb

interaction. There are many other effects, where interactions play a dominant role, such as high temperature superconductivity, the Kondo problem etc. In other branches of physics, interactions among the fundamental particles play crucial role, for example quark-gluon plasma in heavy ion collision and asymptotic freedom in QCD.

One of the greatest achievement of early twentieth century was Landau's Fermi liquid theory. In a weakly interacting system, such a framework essentially treats the quasi particle excitations like a gas of non-interacting electrons, in terms of various *renormalized* parameters of the free electron system [13]. The most fundamental assumption in that picture is the existence of a Fermi surface even in an interacting system. Later this assumption was justified by Luttinger, which is known as the 'Luttinger theorem' [14]. Nevertheless, in many instances the Fermi liquid ground state becomes unstable, leading to a completely new ground state. One of the celebrated examples is the BCS instability of the Fermi system towards the superconducting ground state. Apart from the static ions in a solid, electrons interact with their vibrational modes, phonons. In the presence of strong screening, electron-phonon interactions can lead to an effective attraction among electrons, which may lead the Fermi system to a superconducting ground state. This class of new problems initiated the journey of many body physics in the second half of the last century [15].

In the system of our concern, graphene, Coulomb interactions are important too. The absence of electronic states at the Fermi energy keeps the long range Coulomb interaction unscreened. Therefore it is expected to play a crucial role in the behaviour of the system in the strong coupling limit. Nevertheless, smallness of Fermi velocity yields a large fine structure constant ($\alpha \sim 1$) in graphene system, in comparison to that in QED ($\alpha \approx 1/137$). Effect of the Coulomb interaction is expected to be enhanced in a suspended graphene [16]. Besides its long ranged tail, the short ranged components of the Coulomb interaction can take the system through the quantum semimetal-insulator transition if it is sufficiently strong. On the other hand, if the net interaction has an attractive component then system may also find itself in a superconducting ground state.

1.4 Central theme of the work

Our discussion takes the semimetallic ground state of graphene as a starting point and then systematically takes the effect of electron-electron interactions into account. The short-ranged interactions among the fermions living on honeycomb lattice can take the system into various insulating as well as superconducting ground states. From simple power counting, one finds that the long ranged Coulomb interaction is irrelevant, however only marginally. The least irrelevant short ranged interactions are the quartic interactions. Irrelevance of the quartic interactions is much faster than that for long ranged Coulomb interaction. However, recent numerical and analytical studies found that the critical exponents near the quantum transitions, driven by either long or short ranged interaction, are close to each other. It might, therefore, be the case that these two seemingly different type of transitions belong to the same universality class [16, 17]. Thus as a convenient point of departure, we now on consider only the quartic short ranged interactions among the fermions. Another way to justify the omission of the long ranged Coulomb interaction is the following. It was reported that when graphene is deposited on SiO_2 substrate, there exists a layer of water between the graphene flake and the substrate. Since the dielectric constant of water (~ 80) is much larger than that for SiO_2 (~ 4), accumulation of a water layer significantly reduces the strength of long ranged interactions. However, in suspended graphene such screening is immediately removed.

We here study the formation of the gapped phases out of the semimetal graphene, with special emphasis given to the universality classes of the quantum transitions, critical exponents, and variation of physical observables near the criticality. The effect of repulsive and attractive interactions are taken into account to study the structure of various insulating and superconducting ground states. We also consider the effect of electromagnetic gauge potentials in the system, which may considerably reduce the strength of the critical interaction for insulation. The effect of yet another gauge potential which may arise from the wrinkling of graphene is also considered. In the following discussions we pursue both analytical and numerical approaches. This analysis allowed us to establish remarkably good agreement among the results found with these two procedures. The numerical approach allowed us to study some problems which are analytically not tractable, for example, the behaviour of interacting fermions in the presence of inhomogeneous magnetic fields (real or

pseudo). Next we provide a brief outline of our work.

1.5 Outline of the thesis

We devote the next chapter to arrive at most general form of the Lagrangian for interacting fermions containing quartic terms. Starting from a general interaction terms we systematically impose the symmetries offered by the lattice along with translational invariance, time reversal symmetry, and two other low energy emergent symmetries; pseudo Lorentz symmetry and chiral symmetry. Performing a one-loop renormalization group calculation we capture all the possible metal-insulator transitions in graphene. The relevance of the low energy symmetry breaking has been studied in detail. Following the instability of semimetallic graphene towards gapped insulating phases, we then revert our focus onto superconducting instabilities. Chapter 3 is devoted to exploring the superconducting transitions in graphene. Our study mainly concerns the variational superconducting ground state when fermions living on the nearest-neighbour site of the honeycomb lattice experience strong attraction among themselves. Irrespective of the nature of the ordered phase, we found that any order-disorder transition in neutral graphene can take place only at finite interaction. The underlying reason behind the strong coupling instability is the vanishing density of states at the Fermi energy.

However, in the presence of a magnetic field, kinetic energy is completely quenched, leading to a band structure consisting of a set of non-dispersing Landau levels. The existence of a zero energy Landau level can bring the critical strength of insulation down to zero and that way catalyze the formation of an ordered phase. We discuss this issue in detail in Chapter 4. We also consider the electronic ground state in neutral graphene in the presence of a magnetic field, and study the scaling and broken symmetry of the interaction induced gap at filling ± 1. There we study the problem in a continuum description, which remains valid even at strong magnetic field ~ 40 T, at which the magnetic length is still much larger than the lattice spacing. We also confirm the catalysis mechanism in Chapter 5 for spinless fermions by numerically diagonalizing the interacting Hamiltonian at Hartree level. Our numerical analysis is in accord with the results found in the continuum description. However, our main focus is on the spatial distribution of the interaction induced gap in the presence of an *inhomogeneous* magnetic field. When the condition of uniformity of the magnetic field

is relaxed, the density of states are impossible to calculate analytically, unless a specific modulation of the field is assumed. Numerically diagonalizing the interacting Hamiltonian in the presence of a nonuniform field, we see that the gap varies with the local strength of the magnetic field.

Yet another gauge field may penetrate in graphene, which on the other hand does not break the time reversal symmetry. A random realization of such fictitious gauge potential can be found in normal graphene in the form of ripples. Nevetheless via specific deformation of the flake one can induce a finite flux of the pseudo magnetic field in the system. Motivated by this possibility, we construct a mechanism to realize a pseudo magnetic field through a particular change in the nearest neighbor hopping amplitude. The existence of a finite number of states, proportional to the flux penetrating the system, can catalyze a time reversal symmetry breaking order even at an infinitesimal strength of the next nearest-neighbour repulsion. A detailed analysis of this problem can be found in Chapter 6.

The absence of quantum Hall states at fillings $\nu = \pm 3, \pm 5, \cdots$ even at the highest laboratory magnetic field is due to the presence of 'valley' degeneracy in higher Landau levels. One way to remove such degeneracy is placing the system in the presence of both the magnetic fields mentioned above. In that setup, two inequivalent valleys are exposed to different effective magnetic fields. This way one may observe plateaus in the Hall conductivity quantized at all the integer factors of e^2/h. Restricting our analysis to, when the real magnetic field is much stronger than the pseudo magnetic field, we performed a detailed analysis of Hall conductivity, scaling of the interaction induced gap, and the nature of the gap for quasiparticle excitations etc. The reader can find a pedagogical formulation of the problem in Chapter 7.

Some further details of our studies which do not belong to the central theme of the thesis are presented in the appendices.

Chapter 2

Electron-electron interactions in graphene

The general low-energy theory of electrons interacting via repulsive short-range interactions on graphene's honeycomb lattice at half filling is developed in this chapter. For simplicity we take the fermions to be spinless. The exact symmetry of the Lagrangian with local quartic terms for the Dirac four-component field dictated by the lattice is identified as $D_2 \times U_c(1) \times$time reversal, where D_2 is the dihedral group, and $U_c(1)$ is a subgroup of the $SU_c(2)$ "chiral" group of the non-interacting Lagrangian, that represents translations in Dirac language. The Lagrangian describing spinless particles respecting this symmetry is parameterized by six independent coupling constants. We show how first imposing the rotational, then Lorentz, and finally chiral symmetry to the quartic terms - in conjunction with the Fierz transformations - eventually reduces the set of couplings to just two, in the "maximally symmetric" local interacting theory. For quartic interactions among the Dirac fermions, however, the rotational symmetry is exact and the interacting Lagrangian without the pseudo relativistic and chiral symmetry is described in terms of only *four* linearly independent quartic terms. We identify the two critical points in such a Lorentz and chirally symmetric theory as describing metal-insulator transitions into the states with either time-reversal or chiral symmetry being broken. The latter is proposed to govern the continuous transition in both the Thirring and Nambu-Jona-Lasinio models in 2+1 dimensions and with a single Dirac field. In the site-localized, "atomic", limit of the interacting Hamiltonian, under the assumption of emergent Lorentz invariance, the low-energy theory

describes continuous transitions into the insulator with either a finite Haldane's (circulating currents) or Semenoff's (staggered density) masses, both in the universality class of the Gross-Neveu model. The simple picture of the metal-insulator transition on a honeycomb lattice emerges at which the residue of the quasiparticle pole at the metallic, and the mass-gap in the insulating phase both vanish continuously as the critical point is approached. In contrast to these two critical quantities, we argue that the Fermi velocity is non-critical as a consequence of the dynamical exponent being fixed to unity by the emergent Lorentz invariance near criticality. Possible effects of the long-range Coulomb interaction, and the critical behavior of the specific heat, the interaction induced gap in the presence of magnetic fields and conductivity are discussed.

2.1 Introduction and results

The two-dimensional honeycomb lattice of carbon atoms may be viewed as the mother of all other forms of carbon. Its crucial electronic property, which arises as a consequence of the absence of the inversion symmetry around the lattice site, is that the usual Fermi surface is reduced to just two points. The electronic dispersion may be linearized around these two points, after which it becomes isotropic and dependent on the single dimensionful parameter, the Fermi velocity (v_F). In graphene, the Fermi velocity is large $v_F \approx c/300$, due to large hopping parameter among the nearest-neighbour sites. The pseudo-relativistic nature of the electronic motion in graphene has, since its synthesis, placed this material at the center stage of condensed matter physics [1].

In this chapter we discuss the low-energy theory and the metal-insulator quantum phase transitions of *interacting* Dirac electrons on the honeycomb lattice. In the first approximation, *all* weak interactions of Dirac electrons in graphene may be neglected at half filling, when the Fermi surface consists of the Dirac points [9]. This is because short-range interactions are represented by local terms which are quartic in the electron fields, which makes them irrelevant near the non-interacting fixed point by power counting. The same conclusion turns out to apply to the long-range tail of the Coulomb interaction, which remains unscreened in graphene, although only marginally so [1] [18, 9, 19]. Nevertheless, if strong

[1] In the simple Thomas-Fermi picture of 'jellium model' the screening length is inversely proportional to

enough, the same interactions would turn graphene into a gapped Mott insulator. As an example, at a strong on-site repulsion the system is likely to be the usual Néel antiferromagnet [9, 20]. It is not *a priori* clear on which side of this metal-insulator transition graphene should be. With the standard estimate for the nearest-neighbor hopping in graphene of $t = 2.5eV$ and the Hubbard interaction of $U \approx 7 - 12eV$, it seems that the system is below yet not too far from the critical point estimated to be at $U/t \approx 4 - 5$ [9, 21, 22, 23, 24]. If sufficiently weak, the electron-electron interactions only provide corrections to scaling of various quantities, which ultimately vanish at low temperatures or frequencies. At, what is probably a more realistic, an intermediate strength, the flow of interactions and the concomitant low-energy behaviour may be influenced by the existence of metal-insulator critical points. It is possible that some of the consequences of such interaction-dominated physics have already been observed in the quantization of the Hall conductance at filling factors zero and one [25, 26, 27, 28, 29, 30]. We will discuss this issue later in Chapter 4. The long ranged Coulomb interaction may also be responsible for anomalously large value of the minimal conductivity [31, 32], a logarithmic correction to the Fermi velocity near the charge neutral point [33].

The above discussion raises some basic questions. What is the minimal description of interacting electrons in graphene at "low" energies ? What is the symmetry of the continuum interacting theory, and how does it constrain the number of coupling constants ? What kinds of order may be expected at strong coupling, and what is the nature of the metal-insulator quantum phase transition ? In this chapter we address these and some related issues. During rest of the introduction we would like to present an outline of our main result.

The simplest prototypical system that exhibits the physics of interacting Dirac fermions which we seek to understand is a collection of spinless electrons interacting via short-range interactions at half-filling. For present purposes an interaction may be considered as "short-ranged" if its Fourier transform at vanishing wavevector is finite [2]. The least irrelevant quartic terms one can add to the non-interacting Dirac Lagrangian will then be local in

---

the density of states at Fermi energy. So for a half filled honeycomb lattice the screening length diverges due to the absence of any states at the apex of the conical band. See 'A Quantum Approach to Condensed Matter Physics' by P. L. Taylor and O. Heinonen, Cambridge University Press, 2002.

[2] By this definition the interaction that at large particle separation decays as a power law $V(r) \sim 1/r^a$ is short ranged provided that $a > 2$.

space-time, and of course quartic in terms of the four-component Dirac fields that describe the electronic modes near the two inequivalent Dirac points at wavevectors $\pm\vec{K}$ at the edges of the Brillouin zone. The most general local quartic term in the Lagrangian would be of the form

$$L_{int} = (\Psi^\dagger(\vec{x},\tau)M_1\Psi(\vec{x},\tau))(\Psi^\dagger(\vec{x},\tau)M_2\Psi(\vec{x},\tau)), \tag{2.1}$$

where M_1 and M_2 are four-dimensional Hermitian matrices. The symmetry alone, however, immediately drastically reduces the number of independent couplings from the apparent 136 to just *nine*. Although the point group of the honeycomb lattice is C_{6v}, the exact spatial discrete symmetry of the Lagrangian is only the *dihedral group* D_2, or the *vierergruppe*, which consists of the reflections through the two coordinate axis shown in Fig. 2.1, and the inversion through the origin. Such a small symmetry results from the very choice of two inequivalent Dirac points out of six corners of the Brillouin zone, which reduces the symmetry to the simple exchange of the two sublattices (reflection around A axis), the exchange of Dirac points (reflection around B axis), and their product (the inversion through the origin). D_2, the time-reversal, and the translational invariance are shown to leave fifteen possible different local quartic terms in the Lagrangian. The interacting Lagrangian in Eq. [2.1] transforms as a scalar under rotation around the Dirac point. After imposing the rotational symmetry around the Dirac points L_{int} is described by nine coupling constants.

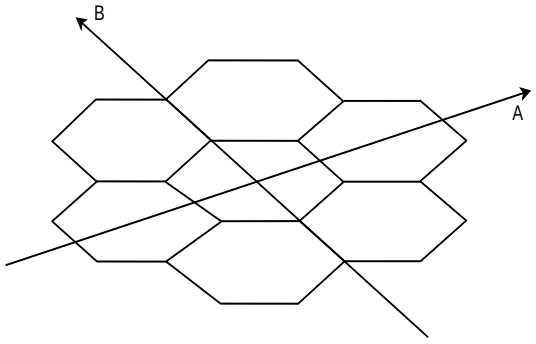

Figure 2.1: Two axis of symmetry of the low-energy theory of graphene, in real space. The Dirac points in this coordinate frame are at $\pm\vec{K} = (1,0)(4\pi/3a)$, i. e. along the A-axis. Figure reprinted with permission from I. F. Herbut et al., [80]. Copyright 2009 by the American Physical Society.

Fortunately, not all of these still numerous quartic terms are independent, and there are linear constraints between them implied by the algebraic Fierz identities [34]. The Fierz transformations are rewritings of a given quartic term in terms of others, and we provide the general formalism for determining the number and the type of independent quartic couplings of a given symmetry. For the case at hand we find that spinless electrons interacting with short-range interactions on honeycomb lattice are in fact described by only *four* independent local quartic terms. The inclusion of electron spin should double this number to *eight*. However, a recent study found this number to be *nine* [35].

The linearized noninteracting Lagrangian for Dirac electrons,

$$L_0 = \bar{\Psi}(\vec{x},\tau)\gamma_\mu \partial_\mu \Psi(\vec{x},\tau) \tag{2.2}$$

as well-known, exhibits Lorentz and global $SU_c(2)$ ("chiral") symmetry. The latter, generated by $\{\gamma_3, \gamma_5, \gamma_{35}\}$, with $\gamma_{35} = -i\gamma_3\gamma_5$, is nothing but the "rotation" of the "pseudospin", or "valley", corresponding to two inequivalent Dirac points [3][36]. A general quartic term allowed by the lattice symmetry, on the other hand, has a much smaller symmetry, as already mentioned. Nevertheless, we will argue that near the metal-insulator quantum critical points, all, or nearly all of the larger symmetry possessed by the non-interacting part of the Lagrangian gets restored. This conclusion is supported by the, admittedly uncontrolled, but nevertheless quite informative one-loop calculation. First, we find three distinct critical points in the theory, all of which have not only the rotational, but the full Lorentz-symmetric form. This immediately implies that the dynamical critical exponent is always $z = 1$. This is quite remarkable in light of the fact that the microscopic theory is not even rotationally invariant, and that the critical points in question are purely short-ranged [4][37]. The fact that $z = 1$ has important implications for several key physical observables near the critical point, as we discuss shortly. Furthermore, we find that two out of three critical points in the theory exhibit a full chiral symmetry as well. We identify the three fixed points in the theory as corresponding to three possible order parameters, or "masses" that develop in the insulating phase at strong coupling.

[3] Similar emergent low energy chiral symmetry is also present in d-wave superconductors.

[4] At the critical point at a finite Coulomb interaction in two-dimensions z is always unity.

1. $\langle\bar{\Psi}\gamma_{35}\Psi\rangle$, which preserves chiral, but breaks time-reversal symmetry. Microscopically, this order parameter may be understood as a specific pattern of circulating currents, as discussed in the past [38].

2. $\langle\bar{\Psi}\Psi\rangle$, which preserves the time-reversal symmetry, and the single chiral generator γ_{35}, which will be shown to correspond to translational invariance. This order parameter describes a finite staggered density, i.e. the difference between the average densities on the two sublattices of the honeycomb lattice [6].

3. $\langle\bar{\Psi}(\gamma_3\cos\alpha+\gamma_5\sin\alpha)\Psi\rangle$, which preserves the time-reversal, but breaks translational invariance (γ_{35}). This order parameter can be understood as the specific "Kekule" modulation of the nearest-neighbor hopping integrals [39].

In a one-loop calculation all three critical points have the same correlation length exponent $\nu=1$, which we believe is an artifact of the quadratic approximation. The result that the dynamical critical exponent $z=1$ is, on the other hand, possibly exact. If we denote the relevant interaction parameter with V, the Fermi velocity near the transition scales as

$$v_F\sim(V_c-V)^{\nu(z-1)} \tag{2.3}$$

so the above value of z would simply imply that it stays regular at the transition. This appears to be in agreement with the picture of the transition as the opening of the relativistic "mass" in the spectrum. The mass-gap in the insulating phase scales as usual [40] as

$$m\sim(V-V_c)^{z\nu}. \tag{2.4}$$

The transition on the metallic side is manifested as vanishing of the residue of the quasiparticle pole [41]

$$Z\sim(V_c-V)^{\nu\eta_\Psi}. \tag{2.5}$$

where we assumed $z=1$. (A more general power-law is discussed in the chapter.) At one-loop the fermion anomalous dimension η_Ψ vanishes, but in general it is a positive, small, and critical-point-dependent number. The overall picture of the metal-insulator transition that emerges is presented in Fig. 2.2.

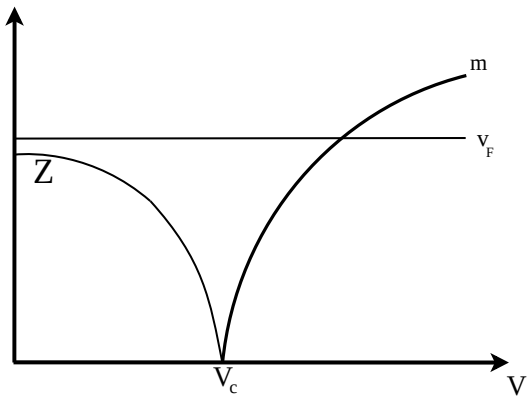

Figure 2.2: The behavior of the the Fermi velocity(v_F), strength of the quasiparticle pole (Z), and the gap (m) near the metal-insulator transition. Figure reprinted with permission from I. F. Herbut et al., [80]. Copyright 2009 by the American Physical Society.

For graphene's p_z-orbitals well localized on carbon sites, a further significant simplification takes place. All the terms without equal numbers of creation and annihilation operators for each of the two sublattices must vanish. Assuming again the emergent Lorentz symmetry at low energies this allows one to finally write the simplest internally consistent interacting theory as

$$L = L_0 + g_{D2}(\bar{\Psi}\gamma_{35}\Psi)^2 + g_{C1}(\bar{\Psi}\Psi)^2. \tag{2.6}$$

This Lagrangian provides the minimal low-energy description of interacting spinless electrons on honeycomb lattice. It has two critical points, corresponding to transitions into insulators 1) and 2) in the above, both corresponding to Gross-Neveu criticality in 2+1 dimensions. We discuss the internal consistency and the sufficiency of this Lagrangian and some of the peculiarities of the ensuing phase diagram.

2.2 Symmetries and short-range interactions

Let us begin the discussion by considering a collection of free fermions on a honeycomb lattice. We set up our notational convention here followed by a detailed analysis of electron-electron interactions on symmetry grounds.

2.2.1 Hamiltonian and the Lagrangian

As the simplest microscopic model that contains the relevant physics we may consider the tight-binding Hamiltonian on graphene's honeycomb lattice, defined as

$$H_0 = \tilde{t}\sum_{\vec{A},i} u^\dagger(\vec{A})v(\vec{A}+\vec{b_i}) + H.c., \tag{2.7}$$

where u and v are the electron annihilation operators on the two triangular sublattices of the honeycomb lattice. Here, $\vec{A}$ denotes sites of the sublattice generated by linear combinations of basis vectors $\vec{a_1} = (\sqrt{3}, -1)a$, $\vec{a_2} = (0, 1)a$, whereas $\vec{B} = \vec{A} + \vec{b}$ are the sites on the second sublattice, with $\vec{b}$ being $\vec{b_1} = (1/\sqrt{3}, 1)a/2, \vec{b_2} = (1/\sqrt{3}, -1)a/2$, or $\vec{b_3} = (-1/\sqrt{3}, 0)a$, and a is the lattice spacing.

Within the framework of the tight-binding model the energy spectrum is doubly degenerate $E(\vec{k}) = \pm\tilde{t}|\sum_i \exp[\vec{k}\cdot\vec{b_i}]|$, and becomes linear and isotropic in the vicinity of six Dirac points, at the edge of the Brillouin zone, among which only two, hereafter chosen to be at $\pm\vec{K}$ with $\vec{K} = (1, 1/\sqrt{3})(2\pi/a\sqrt{3})$, are inequivalent. Retaining only the Fourier components in the vicinity of these two inequivalent points, the quantum mechanical action corresponding to H_0 at low energies can be written in the form $S = \int_0^{1/T} d\tau d\vec{x} L_0$, with the free Lagrangian density L_0 defined as in Eq. [2.2], with τ the imaginary time and T the temperature. The matrices γ_μ satisfy the Clifford algebra $\{\gamma_\mu, \gamma_\nu\} = 2\delta_{\mu\nu}$, $\mu, \nu = 0, 1, 2$, $\bar{\Psi} = \Psi^\dagger\gamma_0$. The summation over repeated space-time indices is assumed hereafter. The fermionic field $\Psi(\vec{x}, \tau)$ is defined as

$$\Psi^\dagger(\vec{x}, \tau) = T\sum_{\omega_n}\int^\Lambda \frac{d\vec{q}}{(2\pi a)^2}\, e^{i\omega_n\tau + i\vec{q}\cdot\vec{x}} \qquad (u^\dagger(\vec{K}+\vec{q}, \omega_n), v^\dagger(\vec{K}+\vec{q}, \omega_n), u^\dagger(-\vec{K}+\vec{q}, \omega_n), v^\dagger(-\vec{K}+\vec{q}, \omega_n)). \tag{2.8}$$

Here, the reference frame is conveniently rotated so that $q_x = \vec{q}\cdot\vec{K}/K$, $q_y = (\vec{K}\times\vec{q})\times\vec{K}/K^2$, $\omega_n = (2n+1)\pi T$ are the fermionic Matsubara frequencies, $\Lambda \sim 1/a$ is a high-energy cutoff, and we set $\hbar = k_B = v_F = 1$, where $v_F = \tilde{t}a\sqrt{3}/2$ is the Fermi velocity. Choosing

$$\gamma_0 = \begin{pmatrix} \sigma_z & 0 \\ 0 & \sigma_z \end{pmatrix},$$

implies

$$\gamma_1 = \begin{pmatrix} \sigma_y & 0 \\ 0 & -\sigma_y \end{pmatrix}, \quad \gamma_2 = \begin{pmatrix} \sigma_x & 0 \\ 0 & \sigma_x \end{pmatrix}. \tag{2.9}$$

The two remaining anticommuting matrices may then be taken as

$$\gamma_3 = \begin{pmatrix} 0 & \sigma_y \\ \sigma_y & 0 \end{pmatrix}, \quad \gamma_5 = \begin{pmatrix} 0 & -i\sigma_y \\ i\sigma_y & 0 \end{pmatrix}. \tag{2.10}$$

This defines the "graphene representation" of γ-matrices [9]. $\vec{\sigma}$ are the standard Pauli matrices.

Considering a more general model with further hoppings or weak anisotropies [42] can be seen not to destroy the Dirac points, but only to shift them in energy. As this can always be compensated by a shift of the chemical potential, the Lagrangian (Eq. [2.2]) provides the low-energy description of the general free electronic Hamiltonian on a honeycomb lattice, with the chemical potential tuned to the Dirac point.

Note that the free Lagrangian besides the Lorentz symmetry also possesses another chiral, pseudospin or "valley", global $SU_c(2)$ symmetry, generated by $\{\gamma_3, \gamma_5, \gamma_{35}\}$. Both the Lorentz and the chiral symmetry of the free Lagrangian emerge only at low energies, however, and the term quadratic in derivatives in L_0, for example, would spoil it. [5] As will be shown shortly, both symmetries are also violated by the leading irrelevant quartic couplings introduced by the interactions.

Let us now consider the electron-electron interactions. The Hamiltonian of a general four-fermion interaction has the form

$$H_{int} = \sum_{\alpha,\beta,\gamma,\delta} \langle \alpha\beta \mid V \mid \gamma\delta \rangle {r_\alpha}^\dagger {r_\beta}^\dagger r_\delta r_\gamma, \tag{2.11}$$

where $r = u$ or v are fermionic annihilation operators, and the matrix element corresponding to the interaction potential $V(\vec{r})$ is given by

$$\langle \alpha\beta \mid V \mid \gamma\delta \rangle = \int d\vec{x} d\vec{y} \varphi^*_\alpha(\vec{x}) \varphi^*_\beta(\vec{y}) V(\vec{x} - \vec{y}) \varphi_\gamma(\vec{x}) \varphi_\delta(\vec{y}). \tag{2.12}$$

Here we can take $\varphi_\alpha(\vec{x})$ to be a localized p_z-orbital on the site α, so that it belongs to either one of the two sublattices of the honeycomb lattice. In general, there is no restriction on the overlap of the wave-functions, and all the matrix elements $\langle \alpha\beta \mid V \mid \gamma\delta \rangle$ are in principle

[5] Consult Appendix A for exact form of the quadratic Hamiltonian

finite. Their relative sizes, however, may be rather different, and we discuss important simplifications that follow in the limit of well localized orbitals later. In the following we will consider general "short-ranged" interactions, which are defined by the interaction $V(\vec{x})$ with a regular Fourier component $V(\vec{k}=0)$. Without a loss in generality one may then take the interacting Lagrangian for spinless fermions corresponding to H_{int} as in Eq. [2.1] where M_1 and M_2 are some constant 4×4 Hermitian matrices. The interacting Lagrangian contains therefore at most $16+(16\times 15/2)=136$ independent real coupling constants. However, the number of couplings in L_{int} is severely reduced by the lattice symmetries, as we discuss next.

2.2.2 Reflection symmetries

Two obvious discrete symmetries of the honeycomb lattice that have not been broken by our choice of the Dirac points are the reflection symmetries through the lines A and B in Fig. 2.1. Let us consider the former symmetry first. It exchanges the two sublattices, but not the two Dirac points. The low-energy Lagrangian thus has to be invariant under the exchange of the spinor components belonging to different sublattices, $u(\vec{k})\leftrightarrow v(\vec{k})$. Consequently, the symmetry operator acting on the four-component Dirac spinor defined in Eq. [2.8] has the form

$$S = I\otimes\sigma_x = \gamma_2. \tag{2.13}$$

Since under this reflection $q_x\to q_x$ and $q_y\to -q_y$, L_0 is evidently invariant under S. The invariance of L_{int} under this reflection symmetry requires both matrices M_1 and M_2 to either commute or anticommute with the operator S:

$$[S,M_1]=[S,M_2]=0, \tag{2.14}$$

or

$$\{S,M_1\}=\{S,M_2\}=0. \tag{2.15}$$

Similarly, the reflection symmetry through the line B exchanges the two Dirac points, while not exchanging the sublattice labels. It corresponds therefore to

$$T = i\gamma_1\gamma_5 = \begin{pmatrix} 0 & I_2 \\ I_2 & 0 \end{pmatrix}. \tag{2.16}$$

Recalling that under this transformation $q_x \to -q_x$ and $q_y \to q_y$, it is evident that the free Lagrangian in graphene representation is indeed invariant under T as well. Demanding the interacting Lagrangian L_{int} to be invariant under the action of the operator T on the Dirac spinor, implies that both matrices M_1 and M_2 either commute or anticommute with T as well. In other words, both matrices M_1 and M_2 have to be either even or odd with respect to T:

$$[T, M_1] = [T, M_2] = 0, \tag{2.17}$$

or

$$\{T, M_1\} = \{T, M_2\} = 0. \tag{2.18}$$

Together with the combination of the two reflections S and T, and the identity operation, the two symmetry operations form the *dihedral group* (or Klein's *vierergrouppe*, in older literature) D_2: $D_2 = \{1, S, T, ST\} = Z_2 \times Z_2$, the symmetry group of a rectangle. Note that the transformation ST is just space inversion, and that the rotation by $\pi/2$ *does not* belong to D_2.

One may now classify all the four-dimensional matrices into four categories, according to their transformation under the two reflection symmetries S and T, respectively:

1. even-even: $A \equiv \{I, \gamma_2, i\gamma_0\gamma_3, i\gamma_1\gamma_5\}$,
2. even-odd: $B \equiv \{i\gamma_0\gamma_1, \gamma_{35}, i\gamma_0\gamma_5, i\gamma_1\gamma_3\}$,
3. odd-even: $C \equiv \{\gamma_0, i\gamma_0\gamma_2, \gamma_3, i\gamma_2\gamma_3\}$,
4. odd-odd: $D \equiv \{\gamma_1, i\gamma_1\gamma_2, \gamma_5, i\gamma_2\gamma_5\}$.

The interacting Lagrangian symmetric under the D_2 is thus restricted to be of the following form

$$\begin{aligned} L_{int} = a_{ij}(\Psi^\dagger A_i \Psi)(\Psi^\dagger A_j \Psi) + b_{ij}(\Psi^\dagger B_i \Psi)(\Psi^\dagger B_j \Psi) &+ c_{ij}(\Psi^\dagger C_i \Psi)(\Psi^\dagger C_j \Psi) \\ &+ d_{ij}(\Psi^\dagger D_i \Psi)(\Psi^\dagger D_j \Psi), \end{aligned} \tag{2.19}$$

where o_{ij}, $o = a, b, c, d$, and $i, j = 1, ..., 4$, are real and symmetric. The maximal number of independent real parameters specifying the allowed couplings is thus already reduced to forty, since each o_{ij} has ten independent components.

2.2.3 Translational invariance

The generator $\gamma_{35} = \sigma_z \otimes I_2$ of the chiral symmetry plays a special role. It is in fact the generator of translations. To see this recall that under a translation by $\vec{R}$ the electron fields transform as

$$r(\vec{k}, \omega) \to e^{i\vec{k}\cdot\vec{R}} r(\vec{k}, \omega) \tag{2.20}$$

where $r = u, v$. The Dirac field under the same transformation thus changes as

$$\Psi(\vec{q}, \omega) \to e^{i(\vec{K}\cdot\vec{R})\gamma_{35}} e^{i\vec{q}\cdot\vec{R}} \Psi(\vec{q}, \omega), \tag{2.21}$$

or, in real space,

$$\Psi(\vec{x}, \tau) \to e^{i(\vec{K}\cdot\vec{R})\gamma_{35}} \Psi(\vec{x} + \vec{R}, \tau). \tag{2.22}$$

Translational invariance requires therefore that L_{int} is a scalar under the transformations generated by γ_{35}, which we will denote as $U_c(1)$. It is easy to see that this is precisely the same as demanding the conservation of momentum in the interaction terms. The reader is also invited to convince herself that the terms with higher-order derivatives in L_0 would also be invariant under the $U_c(1)$. [6]

First, we observe that there are eight linearly independent bilinears that are *scalars* under $U_c(1)$:

$$X_{Fi} = \Psi^\dagger F_i \Psi, \tag{2.23}$$

where $F = A, B, C, D$ and $i = 1, 2$. The remaining eight bilinears can be grouped into four *vectors* under the same $U_c(1)$:

$$\vec{\alpha} = (\Psi^\dagger A_3 \Psi, \Psi^\dagger B_3 \Psi), \tag{2.24}$$

$$\vec{\beta} = (\Psi^\dagger B_4 \Psi, \Psi^\dagger A_4 \Psi), \tag{2.25}$$

$$\vec{\gamma} = (\Psi^\dagger C_3 \Psi, \Psi^\dagger D_3 \Psi), \tag{2.26}$$

$$\vec{\delta} = (\Psi^\dagger C_4 \Psi, \Psi^\dagger D_4 \Psi), \tag{2.27}$$

[6] See Appendix A

The invariance under $U_c(1)$ implies therefore that the interacting Lagrangian has the following form

$$L_{int} = \sum_{Fi} g_{Fi} X_{Fi}^2 + \sum_{F} g_F X_{F1} X_{F2} + g_{\alpha\beta} \vec{\alpha} \times \vec{\beta} + g_{\gamma\delta} \vec{\gamma} \cdot \vec{\delta} + \sum_{\rho=\alpha,\beta,\gamma,\delta} g_\rho \vec{\rho} \cdot \vec{\rho}. \tag{2.28}$$

The number of possible independent couplings is down to eighteen.

2.2.4 Time-reversal

The set of allowed couplings is further reduced by time-reversal symmetry. The microscopic interacting Hamiltonian (Eq. [2.11]) is invariant under time-reversal, and therefore the corresponding low-energy Lagrangian has to possess the same invariance. The time-reversal symmetry requires that $I_t H {I_t}^{-1} = H$, where I_t is the antiunitary operator representing the time-reversal symmetry, and thus has the form $I_t = UK$, with U representing the unitary part of I_t and K is the complex conjugation. To find the form of I_t let us consider first the *massive* Dirac Hamiltonian

$$H = i\gamma_0\gamma_i p_i + m_1\gamma_0, \tag{2.29}$$

with the mass m_1 describing the imbalance in the chemical potential on the two sublattices [6]. Recalling that momentum changes sign under the time-reversal, $I_t p_i {I_t}^{-1} = -p_i$, in the graphene representation the invariance of the above Hamiltonian under the same transformation implies

$$\{U, i\gamma_0\gamma_1\} = [U, i\gamma_0\gamma_2] = [U, \gamma_0] = 0, \tag{2.30}$$

and hence

$$U = ie^{i\phi}\gamma_1(\cos\theta\gamma_3 + \sin\theta\gamma_5). \tag{2.31}$$

One may arrive at the same form of the time reversal symmetry operator by replacing $m_1\gamma_0$ by a different mass term m_4 $i\gamma_1\gamma_2$ in Eq. [2.29]. On the honeycomb lattice such a mass term corresponds to a circulating current among the sites of same sublattice. Otherwise, the current propagates in opposite directions on two sublattices and breaks the time reversal symmetry. In the 'graphene representation' $i\gamma_1\gamma_2 = \sigma_3 \otimes \sigma_3$, therefore

$$\{U,\ i\gamma_1\gamma_2\} = 0. \tag{2.32}$$

Along with the first two constraints in Eq. [2.30] this yields the announced form of the time reversal symmetry operator in Eq. [2.31]. Within the simplest framework of the tight-binding model with uniform hopping the time-reversal operator is not uniquely determined. We thus consider a generalized tight-binding model with anisotropic hopping defined as

$$H_{aniso} = \sum_{\vec{A},i} (\tilde{t} + \delta\tilde{t}_{\vec{A},i}) u^{\dagger}(\vec{A}) v(\vec{A} + \vec{b_i}) + H.c., \tag{2.33}$$

where

$$\delta\tilde{t}_{\vec{A},i} = \frac{1}{3}\Delta(\vec{A}) e^{i\vec{K}\cdot\vec{b_i}} e^{i\vec{G}\cdot\vec{A}} + c.c. \tag{2.34}$$

represents a non-uniform hopping, and $\vec{G} = 2\vec{K}$ [39]. On a lattice, this particular set of hoppings generates the so-called Kekule texture. Near the two Dirac points the Hamiltonian H_{aniso} reads

$$H_{aniso} = i\gamma_0\gamma_i p_i + m_2 i\gamma_0\gamma_5 + m_3 i\gamma_0\gamma_3, \tag{2.35}$$

where $m_2 = Im(\Delta(\vec{r}))$ and $m_3 = Re(\Delta(\vec{r}))$. The two masses m_2 and m_3 therefore provide the low-energy representation of a completely real microscopic Hamiltonian, so that we postulate that H_{aniso} is also time-reversal symmetric. In the graphene representation this requires the unitary part of the time-reversal operator to obey the following algebra:

$$[U, i\gamma_0\gamma_3] = \{U, i\gamma_0\gamma_5\} = 0. \tag{2.36}$$

The matrix $T = i\gamma_1\gamma_5$ satisfies the conditions (2.36) and thus the unitary part of the operator I_t acting on the spinless Dirac field (Eq. [2.8]) is [43]

$$U = T = i\gamma_1\gamma_5 = \begin{pmatrix} 0 & I_2 \\ I_2 & 0 \end{pmatrix}, \tag{2.37}$$

with I_2 as the 2×2 unity matrix. The unitary part of the time-reversal operator thus simply exchanges the components of the Dirac spinor $\Psi(\vec{x}, \tau)$ with different valley indices, as expected. It also happens to be the same as one of the two matrices representing the reflection operators from D_2.

Another way of arriving at the same form for the time-reversal operator is to postulate that an arbitrary chiral transformation of the Dirac Hamiltonian in Eq. [2.29] yields a time-reversal invariant Hamiltonian. Alternatively, our derivation may be understood as a

demonstration of commutativity of the chiral and time-reversal transformations.

Since we have already used the invariance under T to restrict the interacting Lagrangian, time-reversal invariance will be observed if the remaining terms are even under complex conjugation. All the terms X_{Fi}^2 and $\vec{\rho}\cdot\vec{\rho}$ are thus automatically invariant under time-reversal, but among the remaining six mixed terms, the terms $X_{C1}X_{C2}$, $X_{D1}X_{D2}$, and $\vec{\gamma}\cdot\vec{\delta}$ are odd. Time-reversal invariance implies therefore that

$$g_C = g_D = g_{\gamma\delta} = 0, \tag{2.38}$$

which leaves then at most fifteen independent couplings.

2.2.5 Rotational symmetry

Since the rotation by $\pi/2$ is not a member of the D_2, the matrices γ_1 and γ_2 appear asymmetrically in L_{int}. If we demand that they appear symmetrically, L_{int} becomes fully rotationally invariant. This is achieved if

$$g_A = g_B = g_{\alpha\beta} = g_{A2} - g_{D1} = g_{B1} - g_{C2} = g_\beta - g_\delta = 0. \tag{2.39}$$

Let us call the interacting Lagrangian with the rotational invariance imposed this way $L_{int,rot}$. It would be described by at most nine couplings. The interacting Lagrangian enjoying rotational invariance therefore reads as

$$\begin{aligned} L_{int,rot} &= g_{A1}(\bar{\Psi}\gamma_0\Psi)^2 + g_{B1}(\bar{\Psi}\gamma_i\Psi)^2 + g_{B2}(\bar{\Psi}\gamma_0\gamma_{35}\Psi)^2 + g_{A2}(\bar{\Psi}\gamma_i\gamma_{35}\Psi)^2 + g_{C1}(\bar{\Psi}\Psi)^2 \\ &+ g_{D2}(\bar{\Psi}\gamma_{35}\Psi)^2 + g_\alpha[(i\bar{\Psi}\gamma_3\Psi)^2 + (i\bar{\Psi}\gamma_5\Psi)^2] + g_\gamma[(\bar{\Psi}\gamma_0\gamma_3\Psi)^2 + (\bar{\Psi}\gamma_0\gamma_5\Psi)^2] \\ &+ g_\beta[(\bar{\Psi}\gamma_i\gamma_3\Psi)^2 + (\bar{\Psi}\gamma_i\gamma_5\Psi)^2] \qquad (2.40) \\ &\equiv g_{A1}S_1 + g_{B1}V_2 + g_{B2}S_2 + g_{A2}V_1 + g_{C1}S_3 + g_{D2}S_4 + g_\alpha S_5 + g_\gamma S_6 + g_\beta V_3. \qquad (2.41) \end{aligned}$$

However, the rotational invariance is an exact symmetry if one considers only the quartic interaction. The generator of the rotation around the Dirac points is

$$Q = (\vec{x}\times\vec{p})_z + i\gamma_1\gamma_2. \tag{2.42}$$

Therefore, $L_{int,rot}$ must invariant under the $U_R(1)$ symmetry generated by $i\gamma_1\gamma_2$. Which restricts the form of the interaction Lagrangian to Eq. [2.40]. Note that the free Hamiltonian to the leading order in momentum transforms as a scalar under Q. The reader should consult Appendix A for a more detailed discussion on this issue.

2.3 Enlargement of symmetry

The interacting Lagrangian respecting all the symmetries offered by the lattice restricts the number of coupling constants to nine. However the collection of free fermions on honeycomb lattice enjoys some additional symmetries, which are emergent and present in the low energy description, e.g., pseudo Lorentz, chiral $SU_c(2)$ symmetry. One might enforce those symmetries in the interacting theory as well. Enlargement of the symmetries, nevertheless reduces the number of coupling constants in the interacting Lagrangian. The relevance of breaking such symmetries can be tested via renormalization group study, which we present later in this chapter.

2.3.1 Lorentz invariance

Imposing further the Lorentz invariance would require that on top of the above restrictions one also has that

$$g_{A1} + g_{B1} = g_{A2} + g_{B2} = g_\gamma + g_\beta = 0. \tag{2.43}$$

With the restrictions in the previous two equations the Lagrangian has only six coupling constants, and may be cast in a manifestly Lorentz invariant form, worth displaying:

$$\begin{aligned} L_{int,lor} &= g_{A1}(\bar{\Psi}\gamma_\mu\Psi)^2 + g_{B2}(\bar{\Psi}\gamma_\mu\gamma_{35}\Psi)^2 + g_{C1}(\bar{\Psi}\Psi)^2 + g_{D2}(\bar{\Psi}\gamma_{35}\Psi)^2 \\ &+ g_\alpha[(i\bar{\Psi}\gamma_3\Psi)^2 + (i\bar{\Psi}\gamma_5\Psi)^2] + g_\gamma[(\bar{\Psi}\gamma_\mu\gamma_3\Psi)^2 + (\bar{\Psi}\gamma_\mu\gamma_5\Psi)^2]. \end{aligned} \tag{2.44}$$

2.3.2 Chiral invariance

Finally, the maximally invariant interacting Lagrangian would be with the full, i.e. both the Lorentz and the chiral, symmetry of the non-interacting part. This is achieved by setting

in the last equation

$$g_{C1} - g_\alpha = g_{B2} - g_\gamma = 0. \tag{2.45}$$

The interacting Lagrangian can in this case be written as

$$L_{int,max} = g_{A1} S_\mu^2 + g_{D2} S^2 + g_{C1} \vec{V}^2 + g_{B2} \vec{V}_\mu^2, \tag{2.46}$$

where the participating bilinears in Dirac fields,

$$S_\mu = \bar{\Psi} \gamma_\mu \Psi, \tag{2.47}$$

$$S = \bar{\Psi} \gamma_{35} \Psi, \tag{2.48}$$

$$\vec{V} = (\bar{\Psi}\Psi, i\bar{\Psi}\gamma_3\Psi, i\bar{\Psi}\gamma_5\Psi), \tag{2.49}$$

$$\vec{V}_\mu = (\bar{\Psi}\gamma_\mu\gamma_{35}\Psi, \bar{\Psi}\gamma_\mu\gamma_3\Psi, \bar{\Psi}\gamma_\mu\gamma_5\Psi), \tag{2.50}$$

are the scalar (vector), scalar (scalar), vector (scalar), and vector (vector) under the chiral (Lorentz) transformation. The last form makes the Lorentz and the chiral symmetry of the Lagrangian $L_0 + L_{int,max}$ manifest. Such a *maximally symmetric* Lagrangian contains therefore at most only four coupling constants.

2.4 Fierz transformations

The number of independent couplings is further reduced by the existence of algebraic identities between seemingly different quartic terms. Let us provide the derivation of the so-called Fierz transformation, which allows one to write a given local quartic term in terms of other quartic terms. Assume a basis $\{\Gamma^a, a = 1, ..16\}$ in the space of four-dimensional matrices, and choose $(\Gamma^a)^\dagger = \Gamma^a = (\Gamma^a)^{-1}$. Then any Hermitean matrix M can be written as

$$M = \frac{1}{4}(TrM\Gamma^a)\Gamma^a, \tag{2.51}$$

with the summation over repeated indices assumed. This can be rewritten as

$$4\delta_{li}\delta_{mj}M_{lm} = \Gamma^a_{ml}\Gamma^a_{ij}M_{lm}, \tag{2.52}$$

and therefore it follows that

$$\delta_{li}\delta_{mj} = \frac{1}{4}\Gamma^a_{ml}\Gamma^a_{ij}. \tag{2.53}$$

Applying this identity to the product of two matrix elements then yields

$$M_{ij}N_{mn} = \frac{1}{16}(TrM\Gamma^a N\Gamma^b)\Gamma^b_{in}\Gamma^a_{mj}. \tag{2.54}$$

Finally, this leads to the expansion of a quartic term as

$$\begin{aligned}(\bar{\Psi}(x)M\Psi(x))(\bar{\Psi}(y)N\Psi(y)) = \\ -\frac{1}{16}(TrM\Gamma^a N\Gamma^b)(\bar{\Psi}(x)\Gamma^b\Psi(y))(\bar{\Psi}(y)\Gamma^a\Psi(x))\end{aligned} \tag{2.55}$$

which is used in the text for $x = y$. The minus sign in the last line derives from the Grassmann nature of the fermionic fields. A systematic application of this transformation allows one to reduce the number of independent couplings for a given symmetry of the interacting Lagrangian.

2.4.1 General problem

The application of the Fierz identity to the set of quartic terms allowed by the assumed symmetry in principle leads to a set of linear constraints of the form

$$FX = 0, \tag{2.56}$$

where F is a real, typically asymmetric matrix, and X is a column vector; the elements of which are the quartic terms allowed by the symmetry. Of course, only the quartic terms which share the same symmetry may be related by Fierz transformations. For example, in the maximally symmetric case $X^\top = (S^2, S_\mu^2, \vec{V}^2, \vec{V}_\mu^2)$.

Let us next establish a general representation of any asymmetric matrix. Any real N-dimensional matrix M can obviously be written as

$$M = \sum_{i=1}^{N} M_i \otimes e_i^\top \tag{2.57}$$

where $M_i^\top = (M_{1i}, M_{2i}, ...M_{Ni})$, and $(e_i)_j = \delta_{ij}$. In Dirac notation,

$$M = \sum_{i=1}^{N} |M_i\rangle\langle e_i|, \tag{2.58}$$

and

$$M^\top = \sum_{i=1}^{N} |e_i\rangle\langle M_i| \tag{2.59}$$

is the transposed matrix. There exists such a representation of the matrix M in any basis of vectors $|\tilde{e}_i\rangle$, as can be seen by multiplying M from the right with $1 = \sum_i |\tilde{e}_i\rangle\langle\tilde{e}_i|$.

Let us now form a related symmetric matrix $S_M = M^\top M$. Being symmetric, it can be written in the usual spectral form

$$S_M = \sum_{i=1}^{N} \mu_i |\mu_i\rangle\langle\mu_i| \tag{2.60}$$

where $\langle\mu_i|\mu_j\rangle = \delta_{ij}$. We can now write, however, the matrix M in the particular eigenbasis of the associated symmetric matrix [44] S_M

$$M = \sum_{i=1}^{N} |K_i\rangle\langle\mu_i|. \tag{2.61}$$

From the definition of S and its spectral form we see that $\langle K_i|K_j\rangle = \mu_i\delta_{ij}$, and therefore

$$M = \sum_{i=1}^{N} \sqrt{\mu_i}|\nu_i\rangle\langle\mu_i| \tag{2.62}$$

where $|K_i\rangle = \sqrt{\mu_i}|\nu_i\rangle$, and $\langle\nu_i|\nu_j\rangle = \delta_{ij}$. For a general asymmetric matrix, the basis μ and ν are different, and the last equation generalizes the more familiar form for a symmetric matrix, where they are the same.

Hence an asymmetric matrix such as the Fierz matrix F can be written in the diadic form as

$$F = \sum_i \mu_i^{1/2} |\nu_i\rangle\langle\mu_i| \tag{2.63}$$

where $\{\mu_i\}$ is the real spectrum of the related symmetric matrix $S_F = F^\top F$. In the eigenbasis of S_F we can write, in Dirac notation,

$$|X\rangle = \sum_i |\mu_i\rangle\langle\mu_i|X\rangle, \tag{2.64}$$

so that the above linear equations can be written as

$$FX = \sum_i \mu_i^{1/2} \langle\mu_i|X\rangle|\nu_i\rangle = 0. \tag{2.65}$$

Since the vectors $\{|\nu_i\rangle\}$ also form a basis, it must be that either:
a) for $\mu_i \neq 0$, $\langle\mu_i|X\rangle = 0$, or

b) $\mu_i = 0$, so that $\langle \mu_i | X \rangle \neq 0$.

The first set provides us then with the linearly independent constraints, and the second with the set of remaining linearly independent quartic terms. Since the matrices F and S_F obviously have the same kernels, the number of independent coupling constants allowed by the symmetry is simply the dimension of the kernel of the appropriate Fierz matrix.

2.4.2 Maximally symmetric case

Let us consider the simplest example of the quartic term with the full Lorentz and chiral symmetry, $L_{int,max}$ first. Defining the vector X as in the above leads to the Fierz matrix

$$F = \begin{pmatrix} 3 & 3 & 3 & -1 \\ 5 & 1 & 1 & 1 \\ 3 & 3 & 3 & -1 \\ 9 & -3 & -3 & 5 \end{pmatrix}, \tag{2.66}$$

with the two-dimensional kernel with the zero-eigenstates

$$\langle \mu_1 | = \frac{1}{\sqrt{2}}(0, -1, 1, 0), \tag{2.67}$$

$$\langle \mu_2 | = \frac{1}{2\sqrt{3}}(-1, 1, 1, 3), \tag{2.68}$$

and $\mu_1 = \mu_2 = 0$. The remaining two eigenvalues are $\mu_3 = 64$, and $\mu_4 = 144$. The general method explained above implies that the general maximally symmetric interacting Lagrangian can be written as

$$L_{int,max} = \lambda_1(\vec{V}^2 - S_\mu^2) + \lambda_2(-S^2 + S_\mu^2 + \vec{V}^2 + 3\vec{V}_\mu^2), \tag{2.69}$$

with the "physical" couplings

$$\lambda_1 = \frac{g_{C1} - g_{A1}}{2}, \tag{2.70}$$

$$\lambda_2 = \frac{-g_{D2} + g_{A1} + g_{C1} + 3g_{B2}}{12}. \tag{2.71}$$

The two remaining linearly independent combinations vanish due to Fierz identity. So the maximally symmetric interacting theory is specified by only two quartic coupling constants, which may be chosen to be any linearly independent combinations of the above λ_1 and λ_2.

2.4.3 Lorentz-symmetric case

We may then proceed to find the independent couplings for the next case in order in complexity, $L_{int,lor}$, with the chiral symmetry broken down to $U_c(1)$. If we define the six-dimensional vector

$$X^\top = (S^2, S_\mu^2, V_1^2, V_2^2 + V_3^2, S_{1\mu}^2, S_{2\mu}^2 + S_{3\mu}^2) \tag{2.72}$$

the Fierz matrix is found to be

$$F = \begin{pmatrix} 1 & 1 & 5 & -1 & 1 & -1 \\ 3 & 3 & -1 & 5 & -7/3 & -1/3 \\ 3 & 3 & 3 & 3 & -1 & -1 \\ 5 & 1 & 1 & 1 & 1 & 1 \\ 3 & -1 & 3 & -3 & 3 & 1 \\ 3 & -1 & -3 & 0 & 1 & 2 \end{pmatrix}, \tag{2.73}$$

with the three-dimensional kernel spanned by

$$\langle \mu_1| = \frac{1}{5\sqrt{2}}(-2, 3, 1, 0, 0, 6), \tag{2.74}$$

$$\langle \mu_2| = \frac{1}{5\sqrt{2}}(-1, 4, -2, 0, 5, 2), \tag{2.75}$$

$$\langle \mu_3| = \frac{1}{2\sqrt{55}}(-3, -7, 3, 10, 7, 2). \tag{2.76}$$

$L_{int,lor}$ can now be written in terms of only three linearly independent quartic terms, in complete analogy with the maximally symmetric case.

2.4.4 Rotationally symmetric case

Next we find the number of independent quartic interaction once the previous two low energy emergent symmetries are removed from the interacting Lagrangian. Define a *nine* dimensional vector as

$$X^\top = (S_1^2, S_2^2, S_3^2, S_4^2, S_5^2, S_6^2, V_1^2, V_2^2, V_3^2), \tag{2.77}$$

the Fierz matrix reads as

$$F = \begin{pmatrix} 5 & 1 & 1 & 1 & 1 & 1 & -1 & -1 & -1 \\ -1 & -1 & 1 & 1 & -1 & 1 & 2 & 0 & 0 \\ -1 & -1 & 1 & 1 & 1 & -1 & 0 & 2 & 0 \\ 1 & 5 & 1 & 1 & -1 & -1 & -1 & -1 & 1 \\ 1 & 1 & 5 & 1 & -1 & -1 & 1 & 1 & -1 \\ 1 & 1 & 1 & 5 & 1 & 1 & 1 & 1 & 1 \\ 3 & -7/3 & -1 & 3 & 5 & -1/3 & -7/3 & 3 & -1/3 \\ -1 & 1 & 1 & -1 & 0 & -2 & -1 & 1 & 0 \\ 1 & -1 & 1 & -1 & 0 & 0 & 0 & 0 & -1 \end{pmatrix}, \tag{2.78}$$

with the four dimensional kernel spanned by

$$\langle \mu_1 | = \frac{1}{2\sqrt{5}} (1, -1, 1, -1, , 0, 0, 0, 0, 4) \tag{2.79}$$

$$\langle \mu_2 | = \frac{1}{\sqrt{10}} (1, 0, -1, 0, -2, 0, 0, 2, 0) \tag{2.80}$$

$$\langle \mu_3 | = \frac{1}{\sqrt{10}} (0, 1, 0, -1, 2, 0, 2, 0, 0) \tag{2.81}$$

$$\langle \mu_4 | = \frac{1}{2\sqrt{3}} (-1, 1, 1, -1, 2, 2, 0, 0, 0) \tag{2.82}$$

Therefore the interacting Lagrangian possessing only the rotational symmetry can be described in terms of only *four* independent couplings.

2.5 Renormalization group

Having determined the independent coupling constants for each symmetry, we now proceed to study their changes with the decrease of the upper cutoff Λ. We will be particularly interested in fixed points of such renormalization group transformations, as they will provide the information on the quantum metal-insulator transitions that can be induced by increase in interactions.

2.5.1 Maximally symmetric theory

Let us again begin with the maximally symmetric Lagrangian, $L = L_0 + L_{int,max}$. There are only two coupling constants to consider in this case, and we choose them to be g_{D2} and g_{A1}, which correspond to S^2 and S_μ^2 quartic terms, respectively. If any of the other two terms would become generated by the renormalization transformation we would use the Fierz identity to rewrite it in terms of S^2 and S_μ^2. Alternatively, one may wish to renormalize the theory as written in terms of physical couplings in Eq. [2.69]. This procedure is completely equivalent to what is pursued here. As we integrate the fermionic modes lying in the 2+1 dimensional momentum shell [45] from Λ/b to Λ, with $b > 1$ [7], to quadratic order in coupling constants we find

$$\frac{dg_{D2}}{d\ln b} = -g_{D2} - g_{D2}^2 + 2g_{A1}^2 + 3g_{D2}g_{A1}, \tag{2.83}$$

$$\frac{dg_{A1}}{d\ln b} = -g_{A1} + g_{A1}^2 + g_{D2}g_{A1}. \tag{2.84}$$

We rescaled the couplings here as $2g\Lambda/\pi^2 \to g$. To this order no other types of quartic terms actually get generated, and the Fierz transformation turns out not to be necessary. The limit of the above equations that survives the extension to a large number of Dirac fields also agrees with the previous calculation [46].

The above flows, besides the Gaussian, exhibit three fixed points at finite couplings (Fig. 2.3). The first critical point (A) is at $g_{D2} = -1$, $g_{A1} = 0$, and the second critical point (C) is at $g_{D2} = (\sqrt{5}-1)/2$, $g_{A1} = (3-\sqrt{5})/2$. There is also a bicritical fixed point (B) that separates the domains of attraction of the two critical points, at $g_{D2} = -(\sqrt{5}+1)/2$, $g_{A1} = (\sqrt{5}+3)/2$.

The physical interpretation of the critical point A is obvious. Since we can tune through it by keeping $g_{A1} = 0$ and increasing g_{D2} over a certain negative value, it should describe the transition into the insulator with the gap that breaks the time-reversal symmetry, described by

$$\langle \bar{\Psi}\gamma_{35}\Psi \rangle \neq 0. \tag{2.85}$$

This state is obviously favored at a large and negative g_{D2}. Note that since γ_{35} commutes with γ_μ, the line $g_{A1} = 0$ is invariant under RG. In fact, the perturbative β-function along

[7] Here we integrate out the fast Fourier modes within the momentum shell $\Lambda < (\omega^2 + k^2)^{1/2} < \Lambda/b$

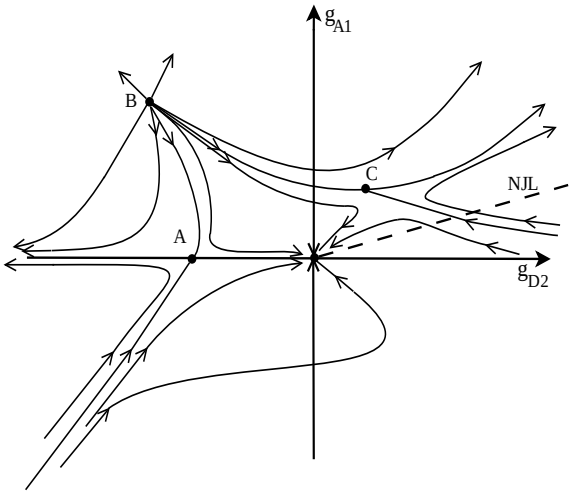

Figure 2.3: Schematic flow diagram of the two coupling constants in the maximally symmetric theory. The fixed point A describes the continuous transition into a time-reversal symmetry broken insulator, and C the dynamical generation of the chiral symmetry breaking mass. The line $g_{D2} = 0$ describes the Thirring model, and the dashed line the Nambu-Jona-Lasinio model in 2+1 dimensions. Figure reprinted with permission from I. F. Herbut et al., [80]. Copyright 2009 by the American Physical Society.

this line has to be identical as the one in the Gross-Neveu model. We can therefore simply use the already existing higher-order estimates [47, 48] and the numerical results [49, 50] to find the critical exponents describing this particular metal-insulator transition. We return to this fixed point shortly.

The physical interpretation of the critical point C is less obvious, but we can think of it as follows. First, note that the line $g_{D2} = 0$, $g_{A1} > 0$, which describes the Thirring model, [51] belongs to the domain of attraction of C. Also, the Fierz transformations in Eq. [2.66] imply

$$g_{D2}S^2 + g_{A1}S_\mu^2 = (g_{D2} - 2g_{A1})S^2 - g_{A1}\vec{V}^2. \tag{2.86}$$

The line $g_{D2} - 2g_{A1} = 0$ for $g_{A1} > 0$, which we name the Nambu-Jona-Lasinio (NJL) line, [52] also falls into the domain of attraction of the critical point C. Along this line, however, there should be a transition into an insulating state with

$$\langle \vec{n} \cdot \vec{V} \rangle \neq 0, \tag{2.87}$$

where $\vec{n}$ is a unit vector. Such a state is clearly favored at a large and positive g_{A1} along the NJL line, and breaks the chiral $SU_c(2)$ symmetry down to $U_c(1)$. We therefore identify C as the metal-insulator critical point governing the chiral-symmetry breaking transition in *both* Thirring and NJL models with a single Dirac field. A recent $1/N$ expansion also confirmed our claim [53]. However the enlarged chiral $SU_c(2)$ symmetry is only an emergent one. As one incorporates the next to the leading order terms in momentum such symmetry is reduced to only a $U(1)$ invariance under γ_{35}. The $U_c(1)$ symmetry under γ_{35} dictates the translational invariance of the system [8]. Therefore, even if system finds itself in an ordered phase by breaking a *continuous* chiral symmetry, there exists no massless Goldstone modes in the broken symmetric phase.

The picture suggested by the above one-loop calculation in the maximally symmetric theory appears quite natural. There are two possible insulating phases, each breaking either chiral or time-reversal symmetry, which correspond to possible "masses" for the Dirac fermions. Both metal-insulator transitions are continuous, and are described by different critical points.

Of course, the true low-energy theory on the honeycomb lattice is much less symmetric than the one studied in this section. Nevertheless, we will argue that the two identified critical points may in fact be stable at least with respect to weak manifest breaking of the Lorentz and chiral symmetries.

Before we proceed to study the infrared behaviour of a broken chiral symmetric interacting theory, it is worth pausing to provide an alternative formulation of the renormalization group transformation in the presence of constraints imposed by the Fierz identity. Instead of choosing two independent couplings and using Fierz transformation at intermediate stages of the calculation to transform any other generated quartic terms back into the chosen ones, one may use the kernel of the Fierz matrix to write the Lagrangian in terms only of the physical couplings from the outset, as in Eq. [2.69]. The advantage of doing this is that no other quartic term besides the ones corresponding to the physical couplings can ever get generated then by the renormalization transformation. The set of couplings λ_1 and λ_2 is

[8] The free Hamiltonian, quadratic in momentum reads as $H_0^{quad} = \gamma_2(\frac{p_x^2 - p_y^2}{2m}) + \gamma_1(\frac{-2p_x p_y}{2m})$, therefore commutes with only one of generators of the chiral symmetry, γ_{35}. Consult Appendix A for more details.

therefore closed under renormalization. The computation to the quadratic order then yields

$$\frac{d\lambda_1}{d\ln b} = -\lambda_1 - 24\lambda_1^2 - 72\lambda_1\lambda_2, \tag{2.88}$$

$$\frac{d\lambda_2}{d\ln b} = -\lambda_2 - 72\lambda_2^2 - 4\lambda_1^2. \tag{2.89}$$

The connection to Eqs. [2.83]-[2.84] in the text can be established as follows. Since the Fierz transformations in this case imply

$$\vec{V}_\mu^2 = -3S^2, \tag{2.90}$$

$$\vec{V}^2 = S_\mu^2 - 2S^2, \tag{2.91}$$

the Lagrangian $L_{int,max}$ in Eq. [2.46] can obviously also be written as

$$L_{int,max} = (g_{D2} - 3g_{B2} - 2g_{C1})S^2 + (g_{A1} - g_{C1})S_\mu^2 \tag{2.92}$$

In the text we therefore have simply named the entire first bracket g_{D2}, and the second g_{A1}. But these can be recognized as particular linear combinations of the physical couplings λ_1 and λ_2:

$$g_{D2} - 3g_{B2} - 2g_{C1} = -2\lambda_1 - 12\lambda_2, \tag{2.93}$$

$$(g_{A1} - g_{C1}) = -2\lambda_1. \tag{2.94}$$

Such a connection is of course completely general, and in particular may be established between the three chosen couplings next in the Eq. [2.95] and the "physical couplings" determined by the vectors in Eqs. [2.74]-[2.76].

2.5.2 Broken chiral symmetry

The simplest quartic term with the full Lorentz symmetry, and only $U_c(1)$ subgroup of the full chiral symmetry may be written as

$$L_{int,lor} = g_{D2}S^2 + g_{C1}V_1^2 + g_\alpha(V_2^2 + V_3^2). \tag{2.95}$$

The Fierz transformation matrix given above implies that these three quartic terms are indeed linearly independent. When $g_{C1} = g_\alpha$, the Lagrangian $L_{int,lor}$ acquires the full chiral $SU_c(2)$ symmetry, and may be rewritten as $L_{int,max}$.

Using the Fierz transformation, and after a convenient rescaling of the couplings as $g\Lambda/3\pi^2 \to g$, to the quadratic order one finds

$$\frac{dg_{D2}}{d\ln b} = -g_{D2} - 6g_{D2}^2 - 4g_\alpha^2 + 6g_{D2}g_{C1} + 12g_{D2}g_\alpha - 8g_{C1}g_\alpha, \quad (2.96)$$

$$\frac{dg_{C1}}{d\ln b} = -g_{C1} - 6g_{C1}^2 - 8g_\alpha^2 + 6g_{D2}g_{C1} - 4g_{C1}g_\alpha, \quad (2.97)$$

$$\frac{dg_\alpha}{d\ln b} = -g_\alpha - 8g_\alpha^2 + 6g_{D2}g_\alpha - 10g_\alpha g_{C1}. \quad (2.98)$$

The two chirally symmetric critical points from the previous section now appear at $g_{D2} = -1/6$, $g_{C1} = g_\alpha = 0$ (A), and $g_{D2} = (3\sqrt{5} - 7)/12$, $g_{C1} = g_\alpha = (\sqrt{5} - 3)/12$ (C), and both remain critical, even in absence of chiral symmetry in the Lagrangian. There is, however, an additional critical point (E) at $g_{D2} = (\sqrt{5} - 2)/6$, $g_{C1} = -2g_\alpha = (\sqrt{5} - 3)/6$. Note also that the plane $g_\alpha = 0$ is invariant under the renormalization group, but whereas the fixed point A in that plane is critical, the fixed point (D) at $g_{D2} = 0$, $g_{C1} = -1/6$ is bicritical. One also finds that the line $g_{D2} = 0$, $g_{C1} < 0$, g_α-infinitesimal and positive intersects the critical surface which contains the point E, whereas for g_α-infinitesimal and negative the critical behavior is governed by C. For weak g_α therefore there is a crossover from the fixed point at D toward either C or E, depending on the sign. Interestingly, for negative g_α chiral symmetry becomes fully restored at the transition, at least within our one-loop calculation [54] [9].

2.5.3 Broken Lorentz symmetry

The explicit breaking of Lorentz symmetry down to the rotational symmetry can be easily implemented by adding to $L_{int,max}$ a symmetry breaking term

$$g_{A1}(\bar{\Psi}\gamma_0\Psi)^2. \quad (2.99)$$

The interacting theory can then be represented in terms of the following four coupling constants

$$L_{int,rot} = g_{C1}\,(\bar{\Psi}\Psi)^2 \;+\; g_{D2}(\bar{\Psi}\gamma_{35}\Psi)^2 \;+\; g_\alpha\,\left[(\bar{\Psi}i\,\gamma_3\Psi)^2 + (\bar{\Psi}i\,\gamma_5\Psi)^2\right] \;+\; g_{A1}(\bar{\Psi}\gamma_0\Psi)^2. \quad (2.100)$$

[9] In the purely bosonic Φ^4-theories, the $O(3)$ symmetry is currently believed not to emerge at the critical point out of $Z_2 \times O(2)$, in three dimensions. The critical behavior is governed by the "biconal" fixed point, which however, appears to be extremely close the $O(3)$-symmetric point in the coupling space.

g_{A1} by virtue of being only rotational symmetric is guaranteed to be linearly independent of remaining of the interactions in $L_{int,rot}$. The remaining *five* quartic terms can be expressed as linear combinations of these four as

$$\begin{aligned} V_1^2 &= S_1^2 - S_3^2 + S_5^2, && (2.101)\\ V_2^2 &= -S_1^2 - S_3^2 - 2S_4^2 - S_5^2, && (2.102)\\ V_3^2 &= 2S_1^2 + 2S_3^2, && (2.103)\\ S_2^2 &= -S_1^2 - S_3^2 - S_4^2, && (2.104)\\ S_6^2 &= -2S_1^2 - 2S_4^2 - S_5^2. && (2.105) \end{aligned}$$

Next we study the low energy behaviour of the interacting theory after integrating out the fast Fourier modes in the momentum shell $\Lambda/b < (\omega^2 + k^2)^{1/2} < \Lambda$, with $b > 1$ [10]. The infrared behaviour of the coupling constants can be captured in terms of their differential flow equations

$$\begin{aligned} \frac{dg_{C1}}{d\ln b} &= -g_{C1} - 6g_{C1}^2 + 6g_{C1}g_{D2} - 4g_{C1}g_\alpha + 2g_{C1}g_{A1} - 4g_{D2}g_{A1}\\ &+ 8g_\alpha g_{A1} - 8g_\alpha^2, && (2.106)\\ \frac{dg_{D2}}{d\ln b} &= -g_{D2} - 6g_{D2}^2 + 6g_{C1}g_{D2} + 12g_{D2}g_\alpha - 2g_{D2}g_{A1} - 8g_{C1}g_\alpha - 4g_\alpha^2, && (2.107)\\ \frac{dg_\alpha}{d\ln b} &= -g_\alpha - 8g_\alpha^2 - 10g_\alpha g_{C1} + 6g_\alpha g_{D2} + 6g_\alpha g_{A1} + 4g_{C1}g_{A1} - 4g_{D2}g_{A1}, && (2.108)\\ \frac{dg_{A1}}{d\ln b} &= -g_{A1} + 2g_{A1}^2 + 2g_{A1}g_{C1} - 6g_{D2}g_{A1} + 4g_\alpha g_{A1}. && (2.109) \end{aligned}$$

We rescaled the couplings as $g\Lambda/3\pi^2 \to g$.

The topology of the flow is as follows. Two chirally symmetric critical points now appear at $g_{C1} = 0, g_{D2} = -0.167, g_\alpha = 0, g_{A1} = 0$ (A) and $g_{C1} = g_\alpha = -0.0637, g_{D2} = -0.024, g_{A1} = 0$ (C). The third critical point is located at $g_{C1} = -0.127, g_{D2} = 0.039, g_\alpha = 0.0637, g_{A1} = 0$ (E). The critical point (E) lacks chiral symmetry. However, the pseudo Lorentz symmetry is restored near all the three critical points. Hence the dynamical critical

[10] The pseudo-relativistic invariance is respected during the momentum-shell integration. However, one might introduce a different shell integration scheme with $-\infty < \omega < \infty$ and $\Lambda/b < |\vec{k}| < \Lambda$, which on the other hand does not preserve this symmetry. The reader may consult Appendix B for details.

exponent is exactly equal to *unity* in the vicinity of all the critical points. It is interesting to note that even though the interacting Lagrangian is symmetric only under spatial rotation, the relativistic invariance emerges near all the critical points describing the semimetal-insulator quantum phase transitions. It is worth mentioning that there are no other critical points in the four dimensional space spanned by the coupling constants.

2.6 Atomic limit

Motivated by the one-loop results, we will assume hereafter that the Lorentz symmetry becomes restored at long distances in the domain of interest, and that we need only consider $L_{int,lor}$ with the three couplings from the last section. The situation however, can then be simplified even further, as we discuss in this section.

Consider the interaction Hamiltonian in Eq. [2.11]. If the p_z-orbitals are well localized on their corresponding lattice sites, we may neglect the matrix elements with $\alpha \neq \gamma$ or $\beta \neq \delta$. Keeping only the remaining, dominant matrix elements then one obtains the "atomic limit" of the general interaction Hamiltonian

$$H_{int} \to H_{lat} = \sum_{\alpha,\beta} V_{\alpha,\beta} n_\alpha n_\beta \tag{2.110}$$

where n_α is the electron number operator at site α. The class of Hamiltonians H_{lat} is evidently still rather broad, and would for example include all lattice interacting Hamiltonians.

Writing the lattice Hamiltonian H_{lat} in terms of the Dirac fields, however, imposes yet another restriction on the coupling constants. Since H_{lat} is written in terms of lattice-site particle number operators, any Dirac quartic term evidently must contain an equal number of $u^\dagger$ ($v^\dagger$) and u (v) fields. On the other hand, the g_α-term from above in momentum space can be written schematically as

$$(V_2^2 + V_3^2) \sim (u_1^\dagger v_2 + v_1^\dagger u_2)(u_2^\dagger v_1 + v_2^\dagger u_1) \tag{2.111}$$

and thus contains terms forbidden in the atomic limit,[11] such as $u_1^\dagger v_2 u_2^\dagger v_1$. The index 1 and 2 refers here to the two Dirac points. This implies that for any lattice Hamiltonian H_{lat} we

[11] The terms allowed in the atomic limit are already contained in the terms S^2 and V_1^2.

must have

$$g_\alpha = 0. \tag{2.112}$$

Note that the plane $g_\alpha = 0$ is invariant under the change of cutoff in the above one-loop calculation. It is easy to see that this feature of the β-functions for g_{D2}, g_{C1} and g_α is in fact true to all orders in perturbation theory. The matrices γ_{35} and I in the remaining two terms in $L_{int,lor}$ commute with the Dirac propagator, and therefore an arbitrary diagram containing g_{D2} and g_{C1} terms can contribute only to the renormalized g_{D2} and g_{C1} couplings. So imposing $g_\alpha = 0$ at an arbitrary cutoff guarantees its vanishing at all others.

It is therefore not only physically justified but also internally consistent to consider only the two couplings g_{D2} and g_{C1} in the Lorentz symmetric, but chirally asymmetric low-energy theory. The one-loop result in this plane is depicted in Fig. 2.4. The transition is either into the time-reversal-symmetry-broken, or into chiral-symmetry-broken insulator. Several features of this flow diagram that should be generally valid are worth mentioning.

1. There should be two critical points, both unstable in a single direction. Bicriticality of A, for example, would imply that the transition for negative g_{D2} at a weak positive g_{C1} is first order. This, however, seems unlikely on physical grounds, and, also, it is not found in the explicit large-N generalization of the theory, when the two β-functions are known to decouple [46].

2. The two critical points have identical critical behavior. This is because the term $\bar{\Psi}\gamma_{35}\Psi$, in graphene representation, under the transformation

$$\Psi \to \frac{1}{2}[i(I_2 + \sigma_z) \otimes \sigma_z + (I_2 - \sigma_z) \otimes I_2]\Psi, \tag{2.113}$$

$$\Psi^\dagger \to \frac{1}{2}\Psi^\dagger[i(I_2 + \sigma_z) \otimes \sigma_z + (I_2 - \sigma_z) \otimes I_2], \tag{2.114}$$

goes into $\bar{\Psi}\Psi$, and vice versa, while L_0 remains invariant. This also means that the two β-functions are symmetric under the exchange $g_{D2} \leftrightarrow g_{C1}$. Both critical points are thus in the universality class of the Gross-Neveu model.

3. At the line $g_{D2} = g_{C1}$ the single β-function becomes

$$\frac{dg_{D2}}{d\ln b} = -g_{D2}, \tag{2.115}$$

i. e. g_{D2} flows according solely to its canonical dimension. This is because

$$(\bar{\Psi}\gamma_{35}\Psi)^2 + (\bar{\Psi}\Psi)^2 = 2(\Psi_+^\dagger \sigma_z \Psi_+)^2 + 2(\Psi_-^\dagger \sigma_z \Psi_-)^2, \tag{2.116}$$

where $\Psi^\dagger = (\Psi_+^\dagger, \Psi_-^\dagger)$. Since all γ_μ are block-diagonal, $+\vec{K}$ and $-\vec{K}$ components at this line decouple. The partition function factorizes into a product of two Gross-Neveu partition functions, each containing a single *two-component* Dirac fermion. Along this line the system is believed to have the metal-insulator transition, possibly continuous, [50] but the β-function vanishes at least to the order g_{D2}^3 [48].

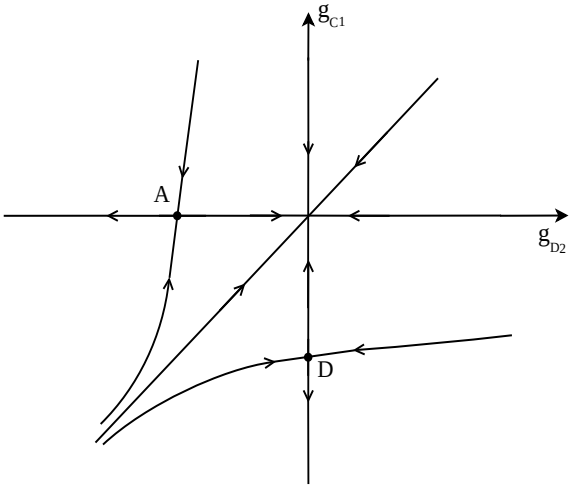

Figure 2.4: The flow diagram in the $g_{D2} - g_{C1}$ plane. The possible non-perturbative fixed point at the $g_{D2} = g_{C1}$ line, which governs the transition in the two-component Gross-Neveu theory is not shown. Figure reprinted with permission from I. F. Herbut et al., [80]. Copyright 2009 by the American Physical Society.

2.7 Critical exponents

Each identified metal-insulator transition is characterized by a set of critical exponents. We will here focus on the three already mentioned in the introduction: the correlation length

exponent ν, the dynamical exponent z, and the Dirac fermion anomalous dimension η_Ψ. The other exponents can then be obtained from the usual scaling relations [40].

First, since all the identified critical points exhibit Lorentz symmetry,

$$z = 1. \tag{2.117}$$

We also find that the exponent ν is unity at all critical points as well, but this is clearly an artifact of the one-loop calculation. In general, ν is expected to be different at different critical points. The same goes for η_Ψ, which vanishes in one-loop calculation, but will be finite in general.

In the atomic limit, when under the assumed Lorentz invariance we need only two coupling constants, the values of the critical exponents are better known. First, in a perturbative calculation in powers of coupling constants, the exponents at critical points A and D will be identical. We may thus expect that in a lattice theory with short-range repulsion the transition is either into the time-reversal symmetry or chiral symmetry broken insulator, in either case with [50]

$$\nu = 0.74 - 0.93 \tag{2.118}$$

$$\eta_\Psi = 0.071 - 0.105. \tag{2.119}$$

Note that since there is only a single Dirac field involved the numerical values of the exponents ν and η_Ψ differ significantly from the large-N values of unity and zero, respectively. This raises hope that this non-trivial critical behaviour may be observable in numerical simulations of lattice models.

Although not of immediate relevance to graphene, it would still be of interest to determine the critical exponents at the chirally symmetric critical point C, which we proposed to control the critical behavior of the Thirring and the NJL model. We, however, are not aware of any analytical nor numerical study of the NJL model that goes beyond the leading order in large-N calculation.

2.8 Fermi velocity and residue of quasiparticle pole

The critical exponents, as usual, govern for example the critical behaviour of the gap on the insulating side of the transition, as mentioned in the introduction. In the present case,

however, there are massless fermionic excitations on the metallic side, and one may wonder if and how the approach to the critical point is reflected onto these. Let us therefore generalize slightly and provide support for the results already announced in the introduction.

First, the usual scaling [40] implies that at the cutoff Λ/b the electron's two-point correlation function near the critical point and at zero temperature satisfies

$$G = b^x \tilde{F}(bk, b^z\omega, tb^{1/\nu}), \tag{2.120}$$

where ω is the Matsubara frequency and $t \sim (V_c - V) > 0$ is the transition's tuning parameter. Setting $tb^{1/\nu} = 1$ we thus find the usual scaling law

$$G = t^{-x\nu} F(t^{-\nu}k, t^{-z\nu}\omega) \tag{2.121}$$

where $F(x_1, x_2) = \tilde{F}(x_1, x_2, 1)$ is a universal scaling function. From here we can extract the scaling of the Fermi velocity and quasiparticle residue as follows. First, if upon the analytical continuation to real frequencies G has a pole at

$$\omega = v_F(t)k \tag{2.122}$$

the scaling relation immediately dictates that

$$v_F(t) = t^{\nu(z-1)} v_F. \tag{2.123}$$

Let us next set $\omega = 0$, take $k > 0$, and let $t \to 0$. In this limit

$$G \sim \frac{1}{k^{1-\eta_k}} \tag{2.124}$$

and therefore $F(x_1 \to \infty, 0) \sim 1/x_1^{1-\eta_k}$. In order to cancel the t-dependence of the prefactor in Eq. [2.121] in this limit it must be that

$$x = 1 - \eta_k, \tag{2.125}$$

where η_k is the (momentum) anomalous dimension. Analogously, assuming that for $k = 0$, $G \sim 1/\omega^{1-\eta_\omega}$, one finds that also

$$x = z(1 - \eta_\omega). \tag{2.126}$$

On the other hand, in the opposite limit $t > 0$ and $\omega \to 0$, in the metallic phase at low energies we have fermionic quasiparticles. This implies that, for example, $F(0, x_2 \to 0) \sim 1/x_2$, i. e.

$$G = \frac{Z}{\omega}, \tag{2.127}$$

with $Z \sim t^{(z-x)\nu}$. Combining with the previous relation, the quasiparticle pole's residue behaves as

$$Z \sim t^{z\eta_\omega \nu}. \tag{2.128}$$

For $z = 1$, the two anomalous dimensions are the same, $\eta_k = \eta_\omega = \eta_\Psi$, where η_Ψ is the Dirac fermion's anomalous dimension, and the scaling announced in the introduction follows. The special form of this relation for a large number of Dirac components when besides $z = 1$, also $\nu = 1$, was previously proposed [9]. The quasiparticle residue vanishes upon the approach to the metal-insulator transition, as proposed long-ago by Brinkman and Rice [41], but here in a decidedly non-mean-field fashion.

2.9 Discussion and related issue

There are at least two obvious generalizations important for real graphene: the addition of spin, and the inclusion of the long-range tail of Coulomb repulsion. Adding spin would simply double the number of couplings for each symmetry, since each independent quartic term would then require a separate coupling in the singlet and in the triplet channels. The minimal internally consistent low-energy theory would then be the generalization of the Lorentz invariant Lagrangian in Eq. [2.95], with $g_\alpha = 0$:

$$L^{spin}_{int,lor} = \sum g_{M,i} (\bar{\Psi}_\alpha M \sigma^i_{\alpha\beta} \Psi_\beta)(\bar{\Psi}_\gamma M \sigma^i_{\gamma\delta} \Psi_\delta), \tag{2.129}$$

where the sum goes over $M = I, \gamma_{35}$, and $i = 0, x, y, z$, with $\sigma_0 = I_2$, and $g_{M,x} = g_{M,y} = g_{M,z}$. The Lagrangian with $g_{\gamma_{35},i} = 0$ would represent the extended Hubbard model with on-site and nearest neighbor repulsion, considered before in the limit of large number of Dirac fermions in ref. [9]. The interplay between the various instabilities in the theory equivalent to the above Lagrangian was recently studied in [55], where it was pointed out that the second-nearest-neighbor repulsion implies a negative coupling $g_{\gamma_{35},0}$ for example. The form of the above minimal spinful Lagrangian allows one to perform a systematic study of the metal-insulator transition in the Hubbard model. In a recent work [56], a controlled epsilon expansion is performed near three dimensions by defining $d = 3 - \epsilon$, while ϵ being the expansion parameter.

A few comments on the importance of long-range tail of Coulomb interaction are also in order. Weak Coulomb ($\sim e^2/r$) interaction is an (marginally) irrelevant perturbation at the Gaussian fixed point, and this remains true at the metal-insulator critical point at large-N as well [18, 9, 19]. Furthermore, the entire β-function for the charge coupling e^2 can be computed at large-N, and it does not exhibit any non-trivial zeroes [57, 58]. On the other hand, several calculations show that by increasing the coupling e^2 beyond a certain point and for small enough N the system can be tuned through a metal-insulator transition at which the chiral symmetry becomes spontaneously broken [59, 27, 60, 16, 61]. The nature of such a putative metal-insulator transition is currently an open question. Nevertheless, a controlled ϵ expansion of Gross-Neveu (GN) theory for spinless fermions near $d = 1$, with a long ranged Coulomb interaction showed that upon increasing the strength of the long ranged interaction the critical strength for insulation decreases, however the transition always belongs to the GN universality class [17]. Whereas it is possible that it is described by a new "charged" critical point [19] corresponding to the non-trivial zero of the $\beta(e^2)$, it also seems conceivable that the charge is always irrelevant and that the transition is still in the universality class of the critical point C, in our nomenclature. Yet another possibility is a discontinuous transition. More work is obviously needed in order to be able to address this issue more conclusively. It may also be interesting to note that in the related bosonic problem, when a systematic expansion near four dimension is readily available, there are no charged critical points in the theory to the leading order [62]. This may also be contrasted with the well-known example of (albeit Lorentz invariant) scalar Higgs electrodynamics, for which the critical points, when they exist, are always charged [40, 63].

Probably the central message of this work is that provided Lorentz invariance becomes emergent near criticality, for the p_z-orbitals well localized on carbon atoms the Lagrangian may be taken to contain only two (or with the physical spin, four) coupling constants. If there are no intervening first-order transitions, one can infer then that there are two possible continuous metal-insulator transitions, both governed by the same Gross-Neveu model in 2+1 dimensions, into states that break either time-reversal or chiral symmetry. The residue of the quasiparticle pole on the metallic side plays the role of the metal's order parameter, and it vanishes continuously with a small critical exponent proportional to the fermion's

anomalous dimension. In contrast, the specific heat coefficient

$$\lim_{T\to 0} \frac{C_v}{T^2}, \tag{2.130}$$

being dependent on the Fermi velocity only, at the transition vanishes discontinuously from a finite value on the metallic side. Near the critical point and for temperatures much below the bandwidth we may assume that the specific heat obeys the scaling relation

$$C_v = T^{2/z} v_F^{-2} R\left(\frac{T}{t^{z\nu}}\right). \tag{2.131}$$

For small arguments the universal scaling function $R(x)$ behaves as $R(x) \sim x^{2(z-1)/z}$, so that in the metallic phase one finds the usual quadratic temperature dependence

$$C_v \sim T^2 v_F^{-2} t^{2\nu(1-z)}. \tag{2.132}$$

Recognizing the proportionality of the specific heat coefficient as $(v_F(t))^{-2}$ gives us yet another way to deduce Eq. [2.123]. At criticality, on the other hand,

$$\lim_{T\to 0} \frac{C_v v_F^2}{T^{2/z}} = R(\infty), \tag{2.133}$$

with $R(\infty)$ expected to be finite. When $z = 1$, the specific heat coefficient near criticality jumps therefore from $R(0)$ in the metallic phase to $R(\infty)$ at the critical point, and finally to zero in the insulating phase. [12]

Similarly, the optical conductivity near the metal-insulator transition will obey the scaling relation for $t > 0$

$$\sigma(\omega) = H\left(\frac{\omega}{t^{z\nu}}\right)\frac{e^2}{h}, \tag{2.134}$$

with $H(x)$ as a universal function, and with

$$H(0) = \frac{\pi}{4}, \tag{2.135}$$

as the familiar universal dc conductivity per Dirac field in the metallic phase [31]. In contrast to the specific heat, there is no (non-universal) dimensionful quantity such as v_F

[12] For spinless fermions considered here, both insulators break the discrete Ising symmetry, so there are no Nambu-Goldstone bosons.

in the scaling expression for conductivity, and consequently $\sigma(0)$ is constant and universal in the entire metallic phase. Right at the transition then

$$\sigma(\omega) = H(\infty)\frac{e^2}{h}, \tag{2.136}$$

so the dc conductivity, while still universal, at criticality should be different than in the metallic phase. Finally, in the insulator the dc conductivity vanishes, so that the dc conductivity, similar to the specific heat coefficient, in principle should show two universal discontinuities at the metal-insulator transition.

One obstacle to experimental observation of these predictions is that it has not been possible yet to tune the parameter ∼(interaction/bandwidth) in graphene, and sample different phases of the system. The application of magnetic field, however, changes this, since the kinetic energy becomes completely quenched, and infinitesimal interaction immediately induces a finite gap. If the parameters of the system place it not too far from the metal-insulator transition, the gap m would obey [29]

$$\frac{m}{v_F\Lambda} = \left(\frac{a}{l}\right)^z G(lt^\nu), \tag{2.137}$$

where l is the magnetic length, $a = 1/\Lambda$ is the lattice constant, and t is the tuning parameter. $G(x)$ is a (universal) scaling function. The computation of the scaling function in the large-N limit, and the consequences of this scaling relation for experiment will be discussed later in Chapter 4 [29]. Here we only wish to underline that the emergent Lorentz invariance of the metal-insulator critical point, via its consequence that $z = 1$, implies precise proportionality between the interaction gap and the Landau level separation at criticality,

$$m = v_F\sqrt{B}G(0), \tag{2.138}$$

where $G(0)$ is a universal number. Such a square-root magnetic field dependence of the gap is well known to arise from the long-range tail of the Coulomb interactions, but the above derivation serves to show that its origin may in principle lie in purely short-range interactions as well. In the presence of a real magnetic field the order parameter breaks the chiral symmetry. However, once a pseudo magnetic field, which may arise from specific distortion of a graphene flake, penetrates the system, a time reversal symmetric ordered phase may develop at infinitesimal interaction. Nevertheless, the scaling behaviour remains identical. A detailed discussion of pseudo magnetic catalysis can be found in Chapter 6.

2.10 Summary

We have presented the theory of electrons interacting via short-range interactions on the honeycomb lattice, and in particular, determined the number and types of independent quartic terms in the low-energy Lagrangian. Metal-insulator quantum critical points and the concomitant quantum critical behaviour were discussed, with particular attention paid to the consequences of the emergent Lorentz invariance. The minimal internally consistent local Lagrangian for spinless fermions is shown to contain only two Gross-Neveu-like quartic terms. Generalizations that would include long-range Coulomb interaction and spin degrees of freedom of electrons were briefly considered. We also discussed the critical behaviour of several key physical quantities on the metallic side of the transition, such as the Fermi velocity, the residue of the quasiparticle pole, specific heat, and the frequency dependent conductivity.

If on the other hand fermions on a honeycomb lattice experience attractive interactions, they may condense into various superconducting states. In the next chapter we study various possible superconducting states available for electrons in graphene to pair.

Chapter 3

Superconducting instabilities in graphene

A spatially non-uniform superconducting phase is proposed as the electronic variational ground state for the attractive interactions between nearest-neighbours on graphene's honeycomb lattice, close to and right at the filling one-half. The state spontaneously breaks the translational invariance of the lattice into the Kekule pattern of bond order parameters, and it is gapped, spin-triplet, and odd under sublattice exchange. With the increase of attractive interactions we first find a transition from the semimetallic phase into the p-Kekule superconductor, odd under the exchange of Dirac points, with the additional discontinuous superconductor-superconductor transition into the even s-Kekule state, deep within the superconducting phase. Topological excitations of the Kekule superconductor and its competition with other superconducting states on the honeycomb lattice are discussed [64].

3.1 Introduction

In the previous chapter we studied various possible transition in graphene out of the symmetric semimetallic phase to insulating phases. We found that fermions on graphene's honeycomb lattice can in principle find themselves in a plethora of insulating phases, depending on the relative magnitudes of different components of a finite-range repulsive interaction. If the net interaction has an attractive component, on the other hand, there would be a

variety of superconducting states available to Dirac quasiparticles for pairing and condensation. Some of them are quite conventional: on-site attraction would clearly favour the usual s-wave singlet pairing [65]. Others are already less so; the second-nearest-neighbour attraction, for example, leads to an f-wave superconductor [66], whose order parameter changes sign six times around the Brillouin zone. Another exotic superconducting state on honeycomb lattice was argued to arise from the nearest-neighbour attraction [67]: instead of gapping the Dirac points it lowers the energy of the Dirac-Fermi sea by effectively increasing the Fermi velocity. Only away from the half-filling does this state acquire a finite superconducting gap, which is then proportional to the chemical potential. A closely related superconducting ground state was also discussed in the context of the t-J-U model and graphite [68]. This *hidden* superconducting order is otherwise a spin-singlet, and even under the exchange of the two sublattices and/or the Dirac points. Since the electrons in graphene have three sets of discrete indices, the sublattice, valley, and real spin, possible superconducting states may exhibit various symmetries with respect to spatial and time inversions [69, 70]. Together with the observation of superconductivity in graphite [71], the intricate structure of the superconducting vortex [72, 70, 73], novel proximity phenomena [74] and the quantum criticality [56, 75], this makes the problem of superconductivity in graphene or in an optical honeycomb lattice attractive from theoretical as well as experimental points of view.

In the following discussion we will be concerned with the forms of the superconducting condensate on the honeycomb lattice at, and therefore also near, half-filling. As a convenient point of departure we consider the problem of graphene with the chemical potential right at the Dirac point and with the attraction only between the electrons residing on the nearest-neighbours of the honeycomb lattice. The motivation for studying such a pairing interaction of a finite range comes in part from the theories of boson-fermion mixtures in optical lattices, where the nearest-neighbor attraction between fermions arises upon integration over the bosonic degrees of freedom [76]. Also, since the fermions in reality certainly experience a strong repulsion when on the same site, the attraction between the nearest neighbours appears to be the simplest reasonable assumption that would still lead to pairing. Our conclusion about the superconducting ground state that arises as the BCS mean-field solution in this model is unusual and qualitatively different from the previous study [67]. Within the standard mean-field approach we find the superconducting state with the lowest energy

to be the spin-triplet, *non-uniform* condensate, which is odd under the exchange of the two sublattices. The spatial Kekule pattern [39, 77] of bonds between the paired electrons on nearest-neighbors has the periodicity of $2\vec{Q}$, where $\pm\vec{Q}$ are the Dirac points, which allows it to connect the two Dirac valleys and that way open the mass-gap in the Bogoliubov quasiparticle spectrum. It is an example of Fulde-Ferrell-Larkin-Ovchinikov [78, 79] type of superconducting phase appropriate to the honeycomb lattice.

Here we will argue that the development of such a non-uniform superconductor at T=0 may preempt the formation of the previously proposed hidden order, which in our approximation we indeed find to be suppressed at all couplings. The Kekule superconductor breaks the exact particle-number and the spin-rotational symmetries, and exhibits three massless and three massive modes in the ordered phase. It also rather weakly breaks the internal and approximate $U(1)$ symmetry between various Kekule patterns. Near the semimetal-superconductor transition we find the p-Kekule state, odd under the valley exchange, to have the lowest energy, with an additional discontinuous transition *within* the superconducting phase into the s-Kekule state, even under the valley exchange, at a stronger attractive interaction.

The target space of the Kekule order parameter is S_3, the surface of sphere in four dimensions. The topology of this space implies that there are no stable topological defects in our two-dimensional system, and therefore presumably no sharp finite temperature phase transition. Explicit breaking of the rotational symmetry, by an external magnetic field or the spin-orbit interaction, for instance, changes the target space for the order parameter and restores the possibility of topologically distinct defects. The cases of easy plane and easy axis, introduced by the two terms mentioned above, are both discussed. We also list all other gapped and hidden (gapless) superconducting states, as well as all the insulating orders on the honeycomb lattice.

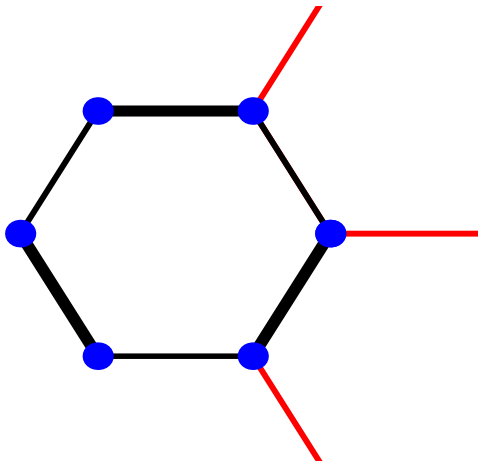

Figure 3.1: The unit cell of the Kekule lattice of superconducting bond order parameters. The red line corresponds to $\Delta\cos\alpha$, the bold line to $\Delta\cos(\alpha+2\pi/3)$, and the thin line to $\Delta\cos(\alpha-2\pi/3)$. The unit cell contains six sites (blue points) and nine bonds. When periodically arranged in a triangular lattice of period 3 it yields the Kekule pattern. The blue dots correspond to the local strength of the inhomogeneous magnetic field. Figure reprinted with permission from B. Roy et. al., [64]. Copyright 2010 by the American Physical Society.

3.2 BdG-Dirac Hamiltonian and the Kekule ansatz

Consider the usual tight-binding Hamiltonian for spin-1/2 fermions on honeycomb lattice at half-filling, with an attractive interaction between nearest neighbors,

$$H = H_t - V\sum_{\langle\vec{x},\vec{y}\rangle}\sum_{\sigma,\sigma'=\uparrow,\downarrow} n_\sigma(\vec{x})n_{\sigma'}(\vec{y}), \tag{3.1}$$

$$H_t = t\sum_{\langle\vec{x},\vec{y}\rangle}\sum_{\sigma,\sigma'=\uparrow,\downarrow} u^\dagger_\sigma(\vec{x})v_\sigma(\vec{y}) + h.c., \tag{3.2}$$

where $V>0$. $u_\sigma(\vec{x})$ and $v_\sigma(\vec{y})$ are the fermionic operators at two triangular sublattices of the honeycomb lattice. Decoupling the interaction term in the particle-particle channel yields the Bogoliubov-de Gennes (BdG) Hamiltonian

$$H_{BdG} = H_t - \sum_{\langle\vec{x},\vec{y}\rangle}\sum_{\sigma,\sigma'=\uparrow,\downarrow} \Delta_{\sigma\sigma'}(\vec{y},\vec{x})u^\dagger_{\sigma'}(\vec{x})v^\dagger_\sigma(\vec{y}) + h.c., \tag{3.3}$$

with the superconducting order parameters to be determined self-consistently as

$$\Delta_{\sigma\sigma'}(\vec{y},\vec{x}) = V\langle v_\sigma(\vec{y})u_{\sigma'}(\vec{x})\rangle. \tag{3.4}$$

Assuming the order parameters to be much smaller than the bandwidth the condensation energy comes mainly from the pairing of the quasiparticle states near the two Dirac points. Let us form a 16-component Dirac-Nambu fermion $\Psi = (\Psi_p, \Psi_h)^\top$, with $\Psi_p = (\Psi_{p\uparrow}, \Psi_{p\downarrow})^\top$ and $\Psi_h = (\Psi_{h\downarrow}, -\Psi_{h\uparrow})^\top$, and

$$\Psi^\top_{p\sigma}(\vec{q}) = (u_\sigma(\vec{Q}+\vec{q}), v_\sigma(\vec{Q}+\vec{q}), u_\sigma(-\vec{Q}+\vec{q}), v_\sigma(-\vec{Q}+\vec{q})), \tag{3.5}$$

$$\Psi^\top_{h\sigma}(\vec{q}) = (v^\dagger_\sigma(\vec{Q}-\vec{q}), u^\dagger_\sigma(\vec{Q}-\vec{q}), v^\dagger_\sigma(-\vec{Q}-\vec{q}), v^\dagger_\sigma(-\vec{Q}-\vec{q})). \tag{3.6}$$

The tight-binding Hamiltonian at low energies then becomes

$$H_t = \sum_{\vec{q}} \Psi^\dagger(\vec{q}) H_D \Psi(\vec{q}) + O(q^2), \tag{3.7}$$

with H_D as the Dirac Hamiltonian in two dimensions, which in our construction and in the first quantization assumes a particularly simple form,

$$H_D = \tau_0 \otimes \sigma_0 \otimes i\gamma_0\gamma_i q_i. \tag{3.8}$$

Here, $\gamma_0 = \sigma_0 \otimes \sigma_3$, $\gamma_1 = \sigma_3 \otimes \sigma_2$, $\gamma_2 = \sigma_0 \otimes \sigma_1$, are the usual four-component anticommuting Hermitian gamma-matrices [80]. The two-component Pauli matrices $\{\tau_0, \vec{\tau}\}$ operate on Nambu's, and $\{\sigma_0, \vec{\sigma}\}$ on the spin indices. We will also define the remaining two gamma-matrices as $\gamma_3 = \sigma_1 \otimes \sigma_2$, and $\gamma_5 = \sigma_2 \otimes \sigma_2$. For convenience, hereafter we also set the Fermi velocity $v_F = \sqrt{3}t/2 = 1$ and the lattice spacing a to unity.

Next, we define the *Kekule ansatz* for the superconducting order parameter:

$$\Delta_{\sigma\sigma}(\vec{x}, \vec{y}) = \Delta_\sigma \cos(\vec{Q} \cdot (\vec{x} + \vec{y}) + \alpha), \tag{3.9}$$

$$\frac{1}{2}(\Delta_{\downarrow\uparrow}(\vec{x}, \vec{y}) + \Delta_{\uparrow\downarrow}(\vec{x}, \vec{y})) = \Delta \cos(\vec{Q} \cdot (\vec{x} + \vec{y}) + \alpha), \tag{3.10}$$

$$\frac{1}{2}(\Delta_{\downarrow\uparrow}(\vec{x}, \vec{y}) - \Delta_{\uparrow\downarrow}(\vec{x}, \vec{y})) = \Delta'. \tag{3.11}$$

The components of the triplet are assumed to be spatially periodic, with periodicity of $2\vec{Q}$, whereas the singlet component is simply uniform. The "angle" α parameterizes different spatial patterns of the order parameter. The unit cell of the Kekule lattice is depicted in Fig. 3.1.

3.3 s-Kekule ground state

We determine first the optimal Kekule ground state for $\alpha = 0$, and then consider a more general solution. With the above ansatz the BdG Hamiltonian can be rewritten as

$$H_{BdG} = H_t + \sum_{\vec{q}} \Psi^\dagger(\vec{q})(M + M')\Psi(\vec{q}) \tag{3.12}$$

where the two matrices appearing in the last term are

$$M' = i(Re[\Delta']\tau_1 + Im[\Delta']\tau_2) \otimes \sigma_0 \otimes i\gamma_0\gamma_3)H_D, \tag{3.13}$$

and

$$M = [(R_+\tau_2 + I_+\tau_1) \otimes \sigma_2 + (I_-\tau_2 - R_-\tau_1) \otimes \sigma_1 + (X\tau_1 - Y\tau_2) \otimes \sigma_3] \otimes \gamma_0, \tag{3.14}$$

where

$$R_\pm = \frac{1}{2}(Re(\Delta_\uparrow) \pm Re(\Delta_\downarrow)), \tag{3.15}$$

$$I_\pm = \frac{1}{2}(Im(\Delta_\uparrow) \pm Im(\Delta_\downarrow)), \tag{3.16}$$

and

$$\Delta = X + iY. \tag{3.17}$$

Before proceeding with the diagonalization of the BdG Hamiltonian it is worth pausing to register its symmetries. The Dirac Hamiltonian, H_D, commutes with $N = \tau_3 \otimes \sigma_0 \otimes I$ and $P = \tau_3 \otimes \sigma_0 \otimes i\gamma_3\gamma_5$, which in our representation stand for the particle-number operator and the generator of translations. It also commutes with $I_K = \tau_0 \otimes \sigma_0 \otimes i\gamma_1\gamma_5$, and $I_{uv} = \tau_0 \otimes \sigma_0 \otimes \gamma_2$, when accompanied with the axis inversions $q_1 \to -q_1$, and $q_2 \to -q_2$, respectively. The latter two operations represent the exchanges of the two Dirac-points and the two sublattices, respectively. H_D also commutes with all three generators of rotations of electron spin, $\vec{S} = \tau_0 \otimes \vec{\sigma} \otimes I$. The matrix M does not commute with N, P, and I_{uv}, but, for $\alpha = 0$ under consideration at the moment, it does commute with I_K. It therefore represents a spatially *non-uniform* superconducting condensate, which is odd under the sublattice exchange and even under the exchange of Dirac points. We will call it the *s-Kekule superconductor*. Since it violates the spin-rotational symmetry, the matrix

M represents a triplet superconducting state, which breaks two generators of spin rotations.

The matrix M', on the other hand, is a product of the Dirac Hamiltonian and another matrix which, in our representation, by itself would represent the singlet s-wave order parameter. Since the two factors anticommute the presence of the imaginary unit in Eq. [3.13] makes the matrix M' Hermitian, and at the same time causes it to break the time-reversal symmetry. The matrix M' represents the hidden superconducting order [67]. This superconducting state, however, suffers from an energetic disadvantage: since M' vanishes precisely at the Dirac points, opening of the order parameter Δ' seems like an ineffective way to lower the energy of the filled Dirac-Fermi sea. We will argue shortly that in competition with the Kekule triplet the hidden order is likely to be energetically inferior. Therefore we set $\Delta' = 0$ for the time being, to return to the issue of the hidden superconducting order only after we determine the optimal triplet s-Kekule order parameters.

Setting then $\Delta' = 0$ one finds

$$(H_D + M)^2 = (q^2 + m^2)(\tau_0 \otimes \sigma_0 \otimes I) + 2\tau_3 \otimes (\vec{n} \cdot \vec{\sigma}) \otimes I, \tag{3.18}$$

where the vector $\vec{n}$ has the components:

$$\vec{n} = (XR_+ + YI_+, YR_- - XI_-, R_+R_- + I_+I_-), \tag{3.19}$$

and the mass-gap is

$$m^2 = X^2 + Y^2 + R_+^2 + I_+^2 + R_-^2 + I_-^2. \tag{3.20}$$

The mean-field ground state energy per site of honeycomb lattice is therefore

$$\frac{E}{2N} = \frac{3m^2}{2V} - \sum_{s=\pm} \int \frac{d\vec{q}}{(2\pi)^2} (q^2 + m^2 + 2s|\vec{n}|)^{1/2}, \tag{3.21}$$

where N is the number of points in the first Brillouin zone. We also assume an ultraviolet cutoff Λ in the integral over momenta, which is here performed only near the two Dirac points. Differentiating with respect to $|\vec{n}|$ immediately shows that for any value of the mass m the minimum of energy lies at $|\vec{n}| = 0$. We set therefore $n_1 = 0$ and $n_2 = 0$. Viewed as a set of two linear equations for the variables X and Y they will have a non-trivial solution only if

$$R_+R_- + I_+I_- = 0, \tag{3.22}$$

which also happens to be the remaining equation $n_3 = 0$. The condition $|\vec{n}| = 0$ yields therefore only two, and not three independent equations. The last equation then yields

$$|\Delta_\uparrow| = |\Delta_\downarrow| \tag{3.23}$$

and the remaining condition constrains the order parameter's phases as

$$\phi_\uparrow + \phi_\downarrow = 2\phi + \pi, \tag{3.24}$$

where $\Delta_\sigma = |\Delta_\sigma| \exp(i\phi_\sigma)$, and $\Delta = |\Delta| \exp(i\phi)$. Finally, the minimum of energy is at the value of the mass-gap $m = m_0$ determined by the gap equation:

$$1 = \frac{2V}{3} \int \frac{d\vec{q}}{(2\pi)^2} \frac{1}{(q^2 + m_0^2)^{1/2}}. \tag{3.25}$$

which has a solution for $V > V_c$. At the minimum, after some straightforward algebra the matrix M can be written as:

$$M = m_0(\tau_1 \cos\phi - \tau_2 \sin\phi) \otimes [\sin\theta(\sigma_1 \cos(\phi_\downarrow - \phi) + \sigma_2 \sin(\phi_\downarrow - \phi)) + \sigma_3 \cos\theta] \otimes \gamma_0, \tag{3.26}$$

where $|\Delta| = m_0 \cos\theta$, and $|\Delta_\uparrow| = |\Delta_\downarrow| = m_0 \sin\theta$. At the minimum of the energy the Kekule state has three hard and three soft modes: the angles $(\theta, \phi_\downarrow - \phi)$ determine the preferred spin axis for the triplet state, and ϕ is the superconducting phase. Note that the condition for the energy minimum $|\vec{n}| = 0$ eliminated three out of six linearly independent matrices that appear in the matrix M in Eq. [3.14]. The remaining three matrices anticommute among themselves as well as with the Dirac Hamiltonian and therefore enter as a sum of squares into the expression of the ground state energy. This quite generally appears to be the optimal way for the filled Dirac-Fermi sea to lower its energy. Another example of this rule is the emergence of the easy plane for the Néel order parameter for the antiferromagnetic state on the honeycomb lattice in the magnetic field [81]. Further consequences of this rule for the form of the order parameter in the presence of the terms that break rotational symmetry will be discussed in Sec. 3.9.

3.4 Hidden order parameter

Let us now restore the possibility of the hidden superconducting order, while retaining the energy-minimum condition $\vec{n} = 0$. The mean-field energy per site is now modified to:

$$\frac{E}{2N} = \frac{3(m^2 + 2|\Delta'|^2)}{2V} - 2 \int \frac{d\vec{q}}{(2\pi)^2} [q^2(1 + |\Delta'|^2) + m^2]^{1/2}. \tag{3.27}$$

In writing this expression we assumed the relative phase between the hidden and the Kekule order parameters to be $\pi/2$, so that the matrices M' in Eq. [3.13] and M in Eq. [3.26] anti-commute and enter the energy expression as a sum of squares. The relative factor of two in the first term derives from the sum of order parameters over a Kekule unit cell (Fig. 3.1). The critical interaction for the appearance of the s-Kekule order is therefore $V_c = 3\pi/\Lambda$, whereas for the hidden order, in absence of the Kekule state, *it would be* $V_c' = 18\pi/\Lambda^3$. Choosing the cutoff Λ even as big as unity, which, for instance, would represent the interval of the energies over which the tight-binding density of states is approximately linear, we see that by increasing the interaction at $V = V_c$ the system first becomes the Kekule superconductor, with $m_0 \neq 0$. Upon further increase of the interaction the amplitude of the order parameter m_0 grows, and then suppresses any appearance of the hidden order. We believe the reason for this outcome of the competition to be quite physical: given the choice whether to open the gap in spectrum or increase the velocity of excitations, all the rest being equal, the system chooses the former option as energetically preferable. The reader should be warned, however, that this conclusion could in principle be overturned upon inclusion of the states farther from the Fermi level into the energy calculation. The pure hidden order, or even the coexistence of the two orders, seem conceivable as well. Since the presence of the residual repulsive interactions in a real system will always broaden the single-particle states away from the Fermi level, it is difficult to say anything more definite on this issue beyond the low-energy approximation we employed.

We have checked, nevertheless, that our conclusion remains unaltered within the present mean-field calculation that keeps *all* quasiparticle states perfectly sharp, upon inclusion of the states from the entire first Brillouin zone. This way we find the two critical interactions defined above to be $V_c' = 3/0.786 = 3.816$ and $V_c = ((3/2)/0.727) = 2.063$, in qualitative agreement with the conclusion based on the linear approximation to quasiparticle dispersion. For further details of this computation the reader should consult Appendix C.

3.5 Other non-uniform superconductors

In a recent study [82], other superconducting phases have been proposed for attractive interactions among the spinless fermions living on the nearest-neighbour sites of the honeycomb

lattice. The BdG Hamiltonian is invariant under a C_{3v} group. Therefore, any permutation of the components $\vec{\delta}$ leads to another mean field solution, where $\delta_\alpha = \langle b_j a_i \rangle$. The permutation group $\mathcal{S}_3$ splits the order parameter space into direct sum of two orthogonal invariant subspaces. One is spanned by $u_1 = \frac{1}{\sqrt{3}}(1,1,1)$, while the other one is spanned by the linear combination of two vectors $u_2 = \frac{1}{\sqrt{6}}(2,-1,-1)$ and $u_3 = \frac{1}{\sqrt{2}}(0,1,-1)$. The last two superconducting orders are identical to the Kekule order parameters around a site of the honeycomb, whereas u_1 corresponds to the hidden order parameter originally proposed in [67]. However, u_2 and u_3 do not break the translational symmetry, as opposed to the Kekule orders. Nor are they proportional to the Dirac Hamiltonian. Therefore, u_2 or u_3 or any linear combination neither commutes nor anticommutes with the Dirac Hamiltonian and thus do not lower the energy of the filled Dirac Fermi sea optimally. Nevertheless, one can proceed with these orders and compute the critical strength of the interaction to open a superconducting gap. In Ref. [82] a detailed calculation has been performed. Here we briefly review their results and argue how the Kekule order is energetically a better variational ground state, at least at and close to filling one-half.

Defining a Fermi-Hubbard Hamiltonian for interacting spinless fermions as

$$H = -t \sum_{\langle i,j \rangle} \left(u_i^\dagger v_j + v_j^\dagger u_i \right) - V \sum_{\langle i,j \rangle} u_i^\dagger v_j^\dagger u_i v_j, \tag{3.28}$$

the superconducting order parameter

$$\Delta_k = -V \vec{\delta} \cdot \vec{f}(\vec{k}) \tag{3.29}$$

has been computed self consistently, with $\delta = \sum_\alpha \eta_\alpha u_\alpha$. Here

$$\vec{f}(\vec{k}) \;=\; \left(e^{-i\vec{k}\cdot\vec{b}_1}, e^{-i\vec{k}\cdot\vec{b}_2}, e^{-i\vec{k}\cdot\vec{b}_3} \right), \tag{3.30}$$

with $\vec{b}_i$s are the nearest-neighbour connecting vectors. The self consistent solution yields a series of first-order discontinuous transitions. The first one taking place at $V/t \approx 3.36 \equiv V_1$, while the second for $V/t \approx 7.12 \equiv V_2$, followed by the third and the final one occurring when $V/t \approx 9.15 \equiv V_3$. For $V_1 < V < V_2$, one of the components δ_α is always zero while remaining two are opposite to each other. Thus the order parameter is proportional to δ_3. When $V > V_2$ the order parameter reads as $\delta = \eta_1 u_1 + \eta_2 u_2$. However, for $V > V_3$ the amplitude for u_1 component abruptly increases and for $V \ll V_3$ only the u_1 component

survives, leading to the gapless superconducting phase, originally proposed in Ref. [67].

Note that all the transitions are taking place at much larger interactions in comparison to that for the Kekule state ($V_c/t \approx 2.063$). Therefore upon increasing the the strength of the attractive interactions among the fermions on the nearest-neighbour sites of the honeycomb lattice first the system suffers a transition towards the Kekule state. Once the Dirac points are gapped, it preempts appearance of any further transitions. Moreover, these transitions are first order and the size of the order parameter at criticality is $\sim t/2$. Superconducting phases are therefore formed by pairing the states far from the Fermi energy. Away from the Fermi energy the quasi particle states are broad and hence cannot be treated as ordinary single-particle fermions. Therefore, the BSC-mean-field type of instability performed here, suffers from the lack of self-consistency.

3.6 p-Kekule state

We turn to a general Kekule state with the parameter $\alpha \neq 0$ next. Select the spin axis so that $\Delta_\uparrow = \Delta_\downarrow = 0$ by setting the angle $\theta = 0$ in Eq. [3.26]. Without a loss in generality one may choose then the order parameter to be real, and write the BdG Hamiltonian *in real space* as

$$H_{BdG} = \sum_{\vec{x}_1,\vec{x}_2} \Phi(\vec{x}_1)[(\tau_0 \otimes T) + \Delta(\tau_1 \otimes K)]\Phi(\vec{x}_2), \tag{3.31}$$

where $\vec{x}_1$ and $\vec{x}_2$ belong to the same sublattice, and

$$\Phi^\top(\vec{x}) = (u_\uparrow(\vec{x}), v_\uparrow(\vec{x}+\vec{b}), u_\downarrow^\dagger(\vec{x}), -v_\downarrow^\dagger(\vec{x}+\vec{b})). \tag{3.32}$$

$\vec{b}$ is one of the three vectors that connect the nearest neighbours of the honeycomb lattice. The elements of the connectivity matrices T and K represent the uniform and Kekule hopping integrals between the nearest-neighbours, respectively. By rotating τ_1 in the second term into τ_3 then, we find that the energy of the Dirac-Fermi sea in presence of a superconducting Kekule order parameter K is given by the sum of the energies of the *two* copies of the Dirac-Fermi seas for the spinless fermions: one in presence of the Kekule hopping pattern $+K$, and the other in the pattern $-K$. We have therefore computed the energy $f(\alpha)$ for the single copy as a function of the parameter α at various values of the amplitude

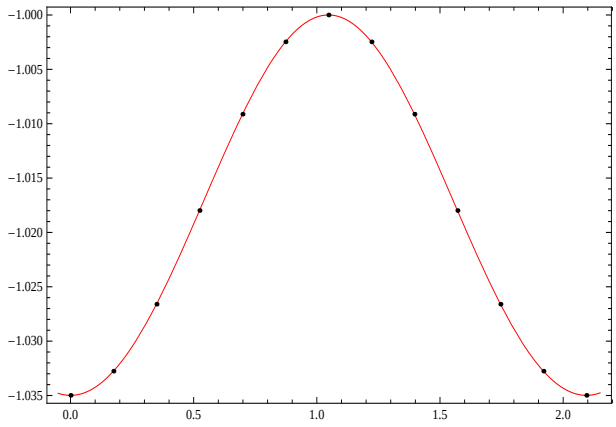

Figure 3.2: The energy per site $f(\alpha)$ of the Dirac-Fermi sea of spinless fermions, hopping between nearest neighbors of the honeycomb lattice with the Kekule hopping amplitude $1 + |\Delta| \cos(\vec{Q} \cdot (\vec{x} + \vec{y}) + \alpha)$ for $|\Delta| = 1$, as a function of the parameter α. The precise type of the Kekule superconducting order depends on the sign of the combination $f(0) + f(\pi/3) - 2f(\pi/6)$. The points are the computed values, and the red line is our best fit $-1.018 - 0.0175 \cos(3\alpha) + 0.000248 \cos(6\alpha) + O(10^{-5} \cos(9\alpha))$. This implies the p-Kekule order (see the text). The transition into the s-Kekule state at $|\Delta| = 2.725$ essentially corresponds to the change in sign of the second harmonic of this function. The blue dots correspond to the local strength of the inhomogeneous magnetic field. Figure reprinted with permission from B. Roy et. al., [64]. Copyright 2010 by the American Physical Society.

$|\Delta|$. The typical result is depicted in Fig. 3.2. The function $f(\alpha)$ may be shown in general to be even, and periodic with the period $2\pi/3$, which reflects the rotational symmetry of the honeycomb lattice. The computation shows that its absolute minimum is always at $\alpha = 0$, in agreement with the recent work [83], and the maximum at $f(\pi/3) = f(\pi)$. We then find that $2f(\pi/2) < f(0) + f(\pi)$, as long as $|\Delta| < 2.725$. The transition from the semimetallic phase is therefore into the superconducting Kekule phase with $\alpha = \pi/2$, which we therefore name *p-Kekule*. For $|\Delta| > 2.725$, deep within the superconducting phase, we find $\alpha = 0$ solution to eventually become energetically favorable, with a discontinuous transition between the s-Kekule and p-Kekule superconductors.

3.7 Other superconducting states in graphene

Let us also recognize the other gapped superconducting states, as the possible mass-terms that anticommute *both* with the Dirac Hamiltonian H_D and with the number operator N:

1. the standard s-wave superconductor with on-site pairing,

$$\langle \Psi^\dagger [(\tau_1 \cos\phi + \tau_2 \sin\phi) \otimes \sigma_0 \otimes i\gamma_0\gamma_3]\Psi\rangle, \tag{3.33}$$

   which is translationally invariant, even under the valley and/or sublattice exchange, but odd under the exchange of spin labels (spin singlet).

2. the f-wave [66]

$$\langle \Psi^\dagger [(\tau_1 \cos\phi + \tau_2 \sin\phi) \otimes \vec{\sigma} \otimes i\gamma_0\gamma_5]\Psi\rangle, \tag{3.34}$$

   which is translationally invariant, even under the sublattice and spin exchanges (spin triplet), but odd under valley exchange.

3. the p-Kekule state discussed above written explicitly is

$$\langle \Psi^\dagger [(\tau_1 \cos\phi + \tau_2 \sin\phi) \otimes \vec{\sigma} \otimes i\gamma_1\gamma_2]\Psi\rangle. \tag{3.35}$$

One can further construct all the gapless (hidden) condensates, as $i\langle \Psi^\dagger M H_D \Psi\rangle$ where M is a mass-matrix for *any* of the above gapped superconducting states. Choosing the matrix M to correspond to the s-wave order as in the above yields the original hidden order of Ref. [67]. Since the Hermitian matrix iMH_D by construction then anticommutes with the Dirac Hamiltonian H_D while at the same time being proportional to it, its addition to H_D will effectively only renormalize the velocity of the Bogoliubov excitations, as manifest in Eq. [3.27] [1].

Of course, one can imagine many other matrices that do not commute with the number operator, and will therefore represent some superconducting order, which nevertheless do

[1] For mass gaps in Dirac spectrum see Appendix D

not fall into any of the categories listed above. These fail to anticommute with the Dirac Hamiltonian, and as such neither gap out, nor increase the velocity of the Dirac fermions. Development of these order parameters would not therefore be particularly energetically advantageous, which is the reason behind their omission here.

One can expect the gapped superconducting states to compete in the phase diagram for attractive interactions in a close parallel with the competition between insulators when the interactions are repulsive [80]. As an illustration, in Fig. 3.3 we present the mean-field phase diagram in the presence of both the on-site and the nearest-neighbour attractions at half filling. In analogy with the insulating case, there is a discontinuous transition between the ordered phases, whereas the transitions out of the semimetallic phase may be expected to be continuous [75, 56]. One novel feature is that because of the $U(1)$ symmetry in the superconducting phase the matrices representing different superconducting states can be chosen so as to *anticommute*. Consider the above p-Kekule state with the phase $\phi = 0$ and the spin axis along z-direction, for example. Choosing the uniform s-wave state with $\phi = \pi/2$ makes the two representative mass-matrices anticommuting, so that right at the boundary between the two phases the system acquires a larger symmetry $O(5)$. Adding the third axis for the second-nearest neighbour interaction introduces then a region of the f-wave order, with the discontinuous transitions between any two of the three phases. Interestingly, there is a unique anticommuting f-wave state, with $\phi = \pi/2$ and with the spin axis along z-direction, that may be added to the above combination of the already anticommuting Kekule and s-wave order parameters. At the point in the phase diagram where the three phases would meet, an even larger, $O(6)$, symmetry emerges.

If the preferred non-uniform superconducting state is the s-Kekule, on the other hand, the possible anticommuting states are again the uniform s-wave and f-wave condensates, but this time both with the same phase as the one of the s-Kekule state.

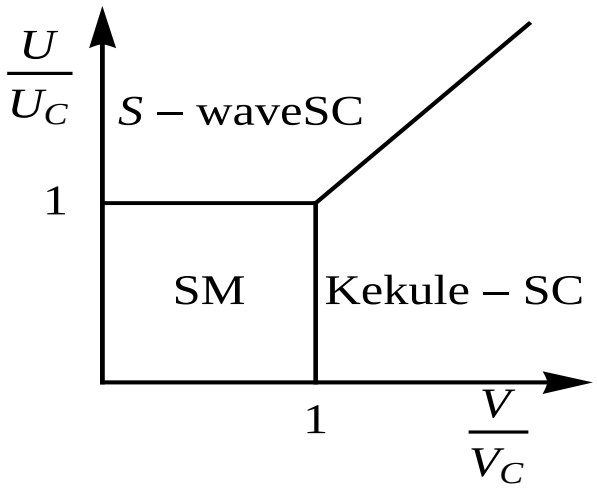

Figure 3.3: The schematic $T = 0$ phase diagram in the model with the on-site (U) and the nearest-neighbour (V) attractions. At the boundary between the two superconducting states the order parameter acquires the larger $O(5)$ symmetry, as the energy becomes invariant under the rotations of the Kekule into the s-wave order with the relative phase of $\pi/2$. Figure reprinted with permission from B. Roy et. al., [64]. Copyright 2010 by the American Physical Society.

3.8 Insulating orders

In the previous section we listed all possible superconducting masses available for Dirac fermions in honeycomb lattice to condense into. Here we would like to take the opportunity to tabulate all possible insulating masses that can develop a gap in the quasi-particle excitation if the interactions are purely repulsive.

1. Charge density wave

$$\langle \Psi^\dagger [\tau_0 \otimes \sigma_0 \otimes \gamma_0] \Psi \rangle, \tag{3.36}$$

which is translationally invariant and breaks the chiral symmetry, odd (even) under sub-lattice (valley) exchange. Yet another chiral symmetry breaking mass is

2. anti-ferromagnetic order

$$\langle \Psi^\dagger [\tau_3 \otimes \vec{\sigma} \otimes \gamma_0] \Psi \rangle, \tag{3.37}$$

which additionally breaks the spin rotational symmetry (triplet).

3. Quantum anomalous Hall (QAH) state

$$\langle \Psi^\dagger [\tau_0 \otimes \sigma_0 \otimes i\gamma_1\gamma_2]\Psi \rangle, \tag{3.38}$$

which corresponds the circulating current among the sites on same sub-lattice, hence breaks the time reversal symmetry.

4. Quantum spin Hall (QSH) state

$$\langle \Psi^\dagger [\tau_3 \otimes \vec{\sigma} \otimes i\gamma_1\gamma_2]\Psi \rangle, \tag{3.39}$$

which on the other hand breaks the time reversal symmetry for each spin species only. Both the QAH and QSH state are odd under sub-lattice and Dirac point exchange.

All these insulating orders break certain class of either discreet or continuous symmetry of the free Dirac quasi particle, however uniform in space. The existence of two nonequivalent Dirac points provides an opportunity for the Dirac fermions with momentum $\vec{Q}+\vec{q}$ and $-\vec{Q}-\vec{q}$ to pair up and that way to develop a gap in the spectrum. Such orders are :

5. spin singlet Kekule bond density waves:

   (a)

$$\langle \Psi^\dagger [\tau_3 \otimes \sigma_0 \otimes i\gamma_0\gamma_3]\Psi \rangle, \tag{3.40}$$

   is even, while

   (b)

$$\langle \Psi^\dagger [\tau_0 \otimes \sigma_0 \otimes i\gamma_0\gamma_5]\Psi \rangle, \tag{3.41}$$

   is odd under Dirac point exchange

6. and spin triplet Kekule bond density waves :

(a)

$$\langle \Psi^\dagger [\tau_0 \otimes \vec{\sigma} \otimes i\gamma_0\gamma_3]\Psi \rangle, \tag{3.42}$$

and

(b)

$$\langle \Psi^\dagger [\tau_3 \otimes \vec{\sigma} \otimes i\gamma_0\gamma_5]\Psi \rangle \tag{3.43}$$

are however, inhomogeneous in space with periodicity $2\vec{Q}$ and correspond to a periodic modulation of the nearest-neighbour hopping.

Therefore, altogether there are 4 superconducting and 8 insulating orders available for the Dirac fermions in graphene, which leads to 36 linearly independent mass matrices, in accordance with a previous study [84]. [2]

3.9 Topology and defects

Let us now get back to the Kekule superconductor and study the topological aspects of the ordered phase. In the ordered phase, the mass-matrix for the Kekule order parameter in Eq. [3.26] lives on the $S_2 \times S_1$ target space, but with opposite points identified. In other words, the order parameter space is the product of S_2 for the spin direction and half of S_1 for the superconducting phase, which is equivalent to S_3, the sphere in four dimensions. That this is indeed the target space becomes clear upon recalling that the minimum with $\vec{n} = 0$, the mean-field free energy in Eq. [3.21] depends only on the mass $m^2 = |\Delta|^2 + |\Delta_\uparrow|^2$, where the two complex order parameters Δ and $\Delta_\uparrow$ are constrained only by the condition that m is the solution of the gap equation.

Since the first and the second homotopy groups of S_3 are trivial, $\pi_1(S_3) = \pi_2(S_3) = 1$, there are no stable topological defects, and the massless fluctuations in the ordered phase should be correctly described by the $O(4)$ non-linear sigma model [40]. We therefore do not expect a true finite temperature phase transition from a semimetal into the Kekule superconductor, but only a crossover when the superconducting correlation length $\xi \propto \exp(cm_0/T)$,

[2] See Appendix E for detail computation of the order parameters.

with c as a (non-universal) numerical constant, reaches the size of the sample. [3]

A reduction of the rotational symmetry would change the target space and allow stable vortex excitations. Let us consider the case of a possible easy plane first. Such an anisotropy may be introduced most simply by placing the Kekule superconductor into a magnetic field. The Zeeman term representing the coupling of the magnetic field to the electron spin will be proportional to the generator of rotations along the direction of the magnetic field, $\tau_0 \otimes \sigma_3 \otimes I$, for example. Since this matrix commutes with the Dirac Hamiltonian and with the third term in the Kekule mass-matrix M in Eq. [3.14] that is proportional to Δ, while it anticommutes with the two other terms in M that are proportional to Δ_σ, the minimization of the energy in the presence of Zeeman coupling is formally equivalent to the problem of Néel ordering in graphene catalyzed by the magnetic field [81, 20]. The result is that $\Delta = 0$, since that way the Kekule mass matrix anticommutes with the Zeeman term. The way to understand this physically is to realize that in such a state the spins of paired electrons are all orthogonal to the magnetic field, so it becomes easier for them to tilt and provide a finite magnetization in the field direction. The minimum condition $\vec{n} = 0$ then translates into $|\Delta_\uparrow| = |\Delta_\downarrow|$, the same as without the magnetic field, but without a further constraint on the phases of the two complex order parameters. The s-Kekule mass-matrix in Eq. [3.14] for such an easy plane may be then rewritten differently as

$$M = m_0 \left(\tau_2 \cos \frac{\phi_\uparrow + \phi_\downarrow}{2} + \tau_1 \sin \frac{\phi_\uparrow + \phi_\downarrow}{2} \right) \otimes \left(\sigma_2 \cos \frac{\phi_\uparrow - \phi_\downarrow}{2} + \sigma_1 \sin \frac{\phi_\uparrow - \phi_\downarrow}{2} \right) \otimes \gamma_0. \tag{3.44}$$

The target space with the easy plane anisotropy is thus $S_1 \times S_1$, with the factors corresponding to the two phases $\phi_\uparrow$ and $\phi_\downarrow$. Since the first homotopy group of S_1 is non-trivial, $\pi_1(S_1) = Z$, there are different types of topologically distinct vortex excitations. For example, winding just one of the phases by 2π causes both $(\phi_\uparrow + \phi_\downarrow)/2$ and $(\phi_\uparrow - \phi_\downarrow)/2$ to change from zero to π, i.e. both the first, phase term, and the second, spin-axis term in the above matrix make half a circle. This is sometimes referred to as "half-vortex" [86]. On the other hand, winding both the phases $\phi_\uparrow$ and $\phi_\downarrow$ in the same sense by 2π leaves the angle of

[3] The third homotopy group of S_3 is non-trivial, however, $(\pi_3(S_3) = Z)$ and the topologically non-trivial skyrmion textures at $T = 0$, which would depend both on space and imaginary time, are possible to construct. They are nevertheless, in general unstable excitations [85]

the spin-axis intact, and produces the standard full vortex in the superconducting phase. Finally, winding the two phases $\phi_\uparrow$ and $\phi_\downarrow$ in the opposite sense by 2π produces a third type of vortex, this time in the direction of the spin-axis only.

An easy axis, on the other hand, is introduced by spin-orbit coupling, for example. Consider adding a weak perturbation to the Dirac Hamiltonian proportional to $\tau_3 \otimes \sigma_3 \otimes i\gamma_1\gamma_2$, which in our representation corresponds to the third component of the spin-triplet version of the time-reversal symmetry breaking mass, introduced by Haldane [38] and discussed in the context of spin-orbit interaction in graphene by Kane and Mele [87]. The presence of such a term would again select the piece of the Kekule mass matrix that anticommutes with it, but due to the τ_3 matrix in the first, Nambu's factor, this now implies that $\Delta_\uparrow = \Delta_\downarrow = 0$. The s-Kekule matrix assumes the form as in Eq. [3.26], with $\theta = 0$. The target space therefore in this case reduces to the usual S_1, with only the standard vortices as the topological excitations. The internal structure of such a vortex has already been studied in Ref. [70].

Finally, it should be understood that we discussed the breaking of the rotational symmetry in the s-Kekule state for simplicity only, and that everything said applies equally to the p-Kekule state as well.

3.10 Summary and discussion

To summarize, we introduced the non-uniform superconducting state on graphene's honeycomb lattice, and argued that it is the mean-field solution of the simple model with nearest-neighbour attraction. The order parameter for this state lives on the bonds of the lattice, and forms a Kekule lattice with the period three. Competition between different Kekule superconducting states, as well as between the Kekule and the other possible gapped and gapless superconducting states was discussed. The Kekule superconductor has a spin-triplet order parameter, which lives on the surface of the S_3 sphere. Target spaces for the order parameter and the topological defects in presence of some simple symmetry breaking terms were determined.

A Kekule insulator which breaks the translational invariance of the honeycomb lattice

has been previously proposed and discussed in literature [39, 77]. However, it appears that this state is not the ground state of the simplest model with only the nearest-neighbour repulsion, since there is an energetically superior charge-density-wave that breaks the sublattice exchange symmetry available. This should be contrasted with the situation for the attractive interactions considered here, where the competing superconducting state is the gapless superconductor, which we argued should have a higher energy. It was argued recently, however, that the Kekule insulator does become the mean-field ground state when there is a balance between the nearest-neighbour and the second-nearest-neighbour components of the repulsive interactions [83].

We described here only the problem at half-filling in detail, where a finite interaction is needed to cause the superconducting transition. At a finite filling the density of states at the Fermi level also becomes finite, and there is the usual BCS instability at an infinitesimal attraction. For small deviations from half-filling, however, the symmetry of the superconducting state is essentially determined by the solution at the Dirac point. For the nearest-neighbour attraction as the dominant component of the interaction one should therefore expect the non-uniform Kekule state we discussed to persist at a finite doping as well. As long as the Fermi surface around the Dirac points stays circular [88] the states with momenta $\vec{Q} + \vec{q}$ and $\vec{Q} - \vec{q}$ may both be near the Fermi surface and be paired up by the Kekule order parameter with momentum $2\vec{Q}$, essentially the same way as at half-filling.

Chapter 4

Integer quantum Hall effect in graphene

When placed in a magnetic field graphene exhibits plateaus in Hall conductivity at integer filling $\nu = \pm(4n + 2)$, with $n = 0, 1, 2, \cdots$. Such anomalous quantization of the Hall conductivity can be understood from a simple picture of non-interacting fermions living on the honeycomb lattice of carbon atoms. With increasing magnetic field additional Hall states at fillings $\nu = 0, \pm 1, \pm 4$ become discernible. Scaling of the activation gap at $\nu = 4$ points its origin toward the Zeeman coupling of electron's spin with the magnetic field. However, vanishing longitudinal resistivity at other odd integer fillings, e.g., $\nu = \pm 3, \pm 5, \cdots$, has not been seen yet[1]. These observations imply that the four-fold degeneracy of the zeroth Landau level is completely lifted, which calls for the inclusion of the Coulomb interaction among the electrons into consideration. On the other hand, the remaining Landau levels lose only the spin degeneracy. Together with these observations, a Kosterlitz-Thouless scaling of the resistivity at neutral filling, sub-linear scaling of the activation gap at $\nu = 1$ with the field's perpendicular component only, make the problem of interacting fermions on graphene's honeycomb lattice in the presence of a magnetic field theoretically as well as experimentally appealing. Here we attempt to shed some light on these issues.

[1] See text for recent experimental results

4.1 Current perspectives

The nature of the electronic ground state in graphene in the presence of a uniform magnetic field attracted lots of attention in the recent past. The formation of additional plateaus in the Hall conductivity at filling $\nu = 0, \pm 1$, besides those at $\nu = \pm\ (4\ n + 2)$ with $n = 0, 1, \cdots$ [10, 11] which can be understood solely from the picture of noninteracting fermions [89, 90, 91], raised considerable interest about the underlying mechanism giving birth to the new Hall states. The formation of the plateaus in the off diagonal elements of the conductivity matrix at *neutral* as well as *unit* filling implies that the zeroth Landau level no longer enjoys the four fold degeneracy arising from the valley and spin degrees of freedom. Such degeneracy lifting can not be explained within the framework of free fermion model, and thus calls for the electron-electron interaction to be taken into account. The Coulomb repulsion may break either the 'sublattice' [28] or 'valley' [92, 93, 94] degeneracy, which happens to be equivalent only in the zeroth Landau level. Neglecting the Zeeman coupling of electron's spin with the magnetic field, such a symmetry breaking mechanism would lead to a staggered pattern, either in charge or in average magnetization, if the symmetry breaking is of equal or opposite sense for two projections of spin respectively. The exact nature of the electronic ground state, however, depends on the details of various components of the Coulomb interaction at the lattice scale. Concomitantly the broken symmetric phases also lead to a gap in the quasi particle excitations [95]. On the other hand, coupling of electron spin with the magnetic field (Zeeman coupling) always tends to place the system in an ordered phase, with finite magnetization, pointing in the direction of the field, due to the familiar physics of Hund's rule [30]. Interplay among various possible ordered phases in the zeroth Landau level is currently an unresolved issue [96, 97] and here we take the opportunity to explore some of its aspects.

Plateaus in Hall conductivity at non zero, even integer fillings have been observed in experiment at relatively low magnetic fields ($\sim$ 10 T). At stronger magnetic fields ($> 15-20$ T) however, additional Hall plateaus appears at fillings $\nu = 0, \pm 1, \pm 4$. Nevertheless, plateaus at the remaining of the integer fillings, e.g., $\nu = \pm 3, \pm 5, \cdots$ are yet to be observed, even at the highest laboratory magnetic field (~ 45 T) [98].[2] The activation gap in the longitudinal

[2]However, Hall state at $\nu = 3$ has been observed in graphene deposited on boron-nitride substrate. See text for further details.

resistivity for $\nu = 1$ state appears to be independent of the field's component parallel to the graphene plane and varies sub-linearly with its perpendicular component. In stark contrast, the activation gap for $\nu = \pm 4$ scales linearly with the *total* magnetic field, which implies that only the spin degeneracy from the higher Landau levels are lifted by finite Zeeman coupling. The size of such a gap ($\sim$ 10 K) provides a rough estimate of the g-factor (≈ 2) for electrons in graphene. The estimated strength of the g-factor is in very good agreement with the past studies [99]. These observations conform to the following fact that Hall state at *unit* filling is likely to be originating from electron-electron interaction, whereas those at $\nu = \pm 4$ develop by liberating the higher Landau levels from the spin degeneracy. However, we are still left to answer the most crucial and debated issue: what mechanism is responsible behind the formation of the Hall state at $\nu = \pm 1$.

A natural estimation may be the following. Being unscreened in neutral graphene, the long ranged tail of the Coulomb interaction may remove the 'valley degeneracy' from the zeroth Landau level. However, the long range Coulomb interaction lifts the valley degeneracy not only from the zeroth Landau level, but at the same time from the other ones as well. This mechanism is named '*Quantum Hall ferromagnetism*' [92]. Taking into account Zeeman splitting of all the Landau levels including the zeroth one, one expects to observe Hall states at $\nu = \pm 3, \pm 5$ etc. as well. So far these Hall states have not been observed when the sample is deposited on a SiO_2 substrates. Absence of Hall states at higher odd integer fillings has recently been attributed to their lack of robustness against disorder [100], which in graphene is always present in form of *ripples*. In a normal graphene flake, ripples are unavoidably present and can be induced by strains produced by the substrate. Nonetheless, a Hall state at $\nu = 3$ has been discerned in a recent experiment by depositing graphene on boron nitride. However, the activation gap is $\sim$ 10 K *only* [101]. In the presence of a magnetic field the Coulomb interaction scales as $e^2/\epsilon l_B$, where l_B is the magnetic length. Therefore, the size of the activation gap at odd integer fillings should be of the order of Landau level spacing $\sim$ 1000 K, much larger than the experimentally observed one.

Here we would to like to bring another mechanism to attention, which appears to explain a majority of the experimental observations, and may therefore replace the previous one. This mechanism, however takes only the short ranged components of the Coulomb interaction into account. In the absence of a magnetic field, a sufficiently strong interaction may

place the system in an ordered phase by breaking the chiral symmetry of the symmetric semimetallic ground state. For example, an imbalance of the electron density lowers the energy of the filled Dirac-Fermi sea if the fermions on nearest-neighbour sites of the honeycomb lattice experience a large repulsion. The magnetization at each site prefers to alter its sign from its neighbour if onsite repulsion among the fermions is large. Such quantum metal-insulator transitions out of the symmetric phase are believed to be continuous and belong to the Gross-Neveu universality class [9, 80]. Nonetheless, such order-disorder transitions in neutral graphene can only take place at finite interaction, which is solely due to the vanishing density of states at the Fermi energy. However, in the presence of a magnetic field, the kinetic energy is completely quenched and the energy spectrum is comprised of a set of Landau levels at well separated energies. When the system is at the charge neutral point, Landau levels at positive energy are empty, whereas those at negative energies are completely filled, leaving only half of the zeroth Landau level occupied. Hence, pushing half of the states below the chemical potential, while keeping the remaining ones empty, the quasiparticle spectrum becomes gapped. This mechanism is named '*magnetic catalysis*'[102, 28]. Within the framework of this mechanism, the 'sublattice' degeneracy from the zeroth Landau level is lifted and the symmetry breaking can be equal or opposite for the two projections of spin, depending on the details of the interaction strength on the lattice scale. Such symmetry breaking order can be identified as charge density wave or antiferromagnet. Within the zeroth Landau level the two proposed mechanisms are identical, though they yield a completely different spectrum in the rest of the band. Instead of splitting the other Landau levels, a finite chiral symmetry breaking order only shifts them in energy. Consequently, Hall states are found to reside at fillings $\nu = 0, \pm 1, \pm 2, \pm 4, \pm 6, \cdots$, after incorporating a finite Zeeman coupling. Furthermore, we will show later in the chapter that a reasonably strong short ranged interaction can explain the sublinear scaling of the activation gap at $\nu = 1$ with the field's perpendicular component [103].

Our discussion starts with a simple model of free fermions hopping only among the nearest-neighbour sites of the honeycomb lattice. The orbital effect of the magnetic field then leads to the observed anomalous quantization of the Hall conductivity. Following that we will present some aspects of electronic ground state at $\nu = 0$. We show that irrespective of the exact nature of the correlated ground state at neutral filling, a chiral symmetry breaking order exists at filling $\nu = \pm 1$. Under the assumption that the Hall state at unit

filling lacks chiral symmetry, we present a detailed analysis of the scaling of the activation gap at $\nu = 1$ with field strength and interaction.

4.2 Free electron spectrum and Landau levels

Let us start our discussion by considering a collection of non-interacting electrons, living on the honeycomb lattice, subject to a magnetic field. Keeping the Fourier modes in the vicinity of two non-equivalent Dirac points, one can write down the effective Hamiltonian, corresponding to the tight binding model in the low energy limit as,

$$H_0 = \int d\vec{x} \sum_{\sigma=\pm} \Psi^\dagger_\sigma(\vec{x}) i\gamma_0\gamma_i D_i \Psi_\sigma(\vec{x}), \tag{4.1}$$

with

$$\Psi^\dagger_\sigma(\vec{x}) = \int^\Lambda \frac{d\vec{q}}{(2\pi a)^2} e^{-i\vec{q}\cdot\vec{x}} (u^\dagger_\sigma(\vec{K}+\vec{q}), v^\dagger_\sigma(\vec{K}+\vec{q}), u^\dagger_\sigma(-\vec{K}+\vec{q}), v^\dagger_\sigma(-\vec{K}+\vec{q})). \tag{4.2}$$

Here, we conveniently rotate the frame of reference to $q_x = \vec{q}\cdot\vec{K}/K$ and $q_y = (\vec{K}\times\vec{q})\times\vec{K}/K^2$. We adopt natural units, $\hbar = e = v_F = 1$, where $v_F = ta\sqrt{3}/2$ is the Fermi velocity and a is the lattice spacing. $\Lambda \approx 1/a$ is the ultraviolet cut-off over which the linear approximation of the tight binding density of states holds. Over repeated space-time indices, the summation convention is assumed. The mutually anti-commuting four component Hermitian gamma matrices belong to the 'graphene' representation, namely, $\gamma_0 = I_2 \otimes \sigma_3, \gamma_1 = \sigma_3 \otimes \sigma_2$ and $\gamma_2 = -I_2 \otimes \sigma_1$. We define the two remaining gamma matrices as $\gamma_3 = \sigma_1 \otimes \sigma_2$ and $\gamma_5 = \sigma_2 \otimes \sigma_2$ [9, 80]. One can include the orbital effect of the magnetic field by defining $D_i = -i\partial_i - A_i$, with magnetic field $B = -\epsilon_{3ij}\partial_i A_j$ set to be perpendicular to the graphene plane.

To compute the energy spectrum of H_0, consider an auxiliary Hamiltonian [95]

$$\tilde{H_0} = i\gamma_0\gamma_i D_i. \tag{4.3}$$

The existence of M, such that $\{\tilde{H_0}, M\} = 0$ guarantees spectral symmetry about zero energy. Here $M \in \{\gamma_0, i\gamma_0\gamma_3, i\gamma_0\gamma_5, i\gamma_1\gamma_2\}$. Squaring the Hamiltonian one gets

$$\tilde{H_0}^2 = D_i^2 - B\,(\sigma_3 \otimes \sigma_3)\,. \tag{4.4}$$

Thus $\tilde{H}_0$ is in close resemblance to the Schrödinger equation in magnetic field and its eigenvalues are at $2nB$, with $n = 0, 1, 2, \cdots$. Therefore, the spectrum of $\tilde{H}_0$ is as follows. For $n \neq 0$ eigenvalues of $\tilde{H}_0$ are at $\pm\sqrt{2nB}$ with degeneracies B/π per unit area and the eigenvectors read as

$$\Psi^K_{n,+} = \begin{pmatrix} \phi_n \\ -\phi_{n-1} \\ 0 \\ 0 \end{pmatrix} \quad \text{and} \quad \Psi^{-K}_{n,+} = \begin{pmatrix} 0 \\ 0 \\ \phi_{n-1} \\ -\phi_n \end{pmatrix}, \tag{4.5}$$

for $E_n = \sqrt{2nB}$ and

$$\Psi^K_{n,-} = \begin{pmatrix} \phi_n \\ \phi_{n-1} \\ 0 \\ 0 \end{pmatrix} \quad \text{and} \quad \Psi^{-K}_{n,-} = \begin{pmatrix} 0 \\ 0 \\ \phi_{n-1} \\ \phi_n \end{pmatrix}, \tag{4.6}$$

for $E_n = -\sqrt{2nB}$. However, for $n = 0$ the eigenstates associated with the different 'valley's read as

$$\Psi^K_0 = \begin{pmatrix} \phi_0 \\ 0 \\ 0 \\ 0 \end{pmatrix} \quad \text{and} \quad \Psi^{-K}_0 = \begin{pmatrix} 0 \\ 0 \\ 0 \\ \phi_0 \end{pmatrix}. \tag{4.7}$$

Hence, in the zeroth Landau level, states near the Dirac points live on complementary sublattices, namely, states near $+K$ reside on the A-sublattice, whereas those near the other Dirac point (at $-K$) on the B-sublattice. Here ϕ_n corresponds to the Schödinger wave function in presence of the magnetic field, i.e.,

$$\phi_n(y) \propto H_n\left(\frac{y}{l} - lk\right)\, e^{-\left(y - l^2k\right)^2 / \, 2l^2}, \tag{4.8}$$

in the Landau gauge $\vec{A} = (-y\ B, 0)$. $H_n(x)$ is the Hermite polynomial of order n and

$$l \equiv \left(\frac{\hbar\, c}{e\ B}\right)^{1/2}, \tag{4.9}$$

is the magnetic length [104].

Restoring the spin degrees of freedom one finds that each of the Landau levels including the one at zero energy, has an additional *four fold degeneracy*, arising from the 'valley' and the spin degrees of freedom. In neutral graphene, all the states at positive energy are empty, with those at negative energy completely filled. However, only half of the states in the zeroth Landau level are filled. Therefore, plateaus in the Hall conductivity (σ_{xy}) are expected to reside at integer fillings $\nu = (4n + 2)$, with $n = 0, 1, 2, \cdots$ [90]. Measurement of the Hall conductivity at relatively low magnetic fields (~ 10 T) confirmed such quantization [10, 11].

4.3 Magnetic catalysis and order parameters

Next we consider the effect of electron-electron interactions, when the system is at filling one-half. In the zeroth Landau level, states in the vicinity of different Dirac points live on complementary sub-lattices. Hence, half of these states are associated with $+1$ eigenvalue of γ_0, whereas the remaining ones are anchored to -1. In the two dimensional sub-space $\mathcal{H}_0$ of $\tilde{H}_0$, γ_0 is proportional to the *diagonal* Pauli matrix. Therefore, addition of a term $m\gamma_0$ to the auxiliary Hamiltonian $\tilde{H}_0$, leads to the following eigenvalue spectrum. For $n \neq 0$, a macroscopic number of states are located at $\pm\sqrt{2\ n\ B\ +\ m^2}$ with degeneracy B/π. Besides these, for n=0, states are at $\pm|m|$, however with degeneracy being halved ($B/2\pi$). Therefore, the Landau levels at finite energies are only shifted in energy, whereas those at zero energy get split. Hence the quasi-particle excitations are spontaneously gapped by breaking the chiral symmetry of the free Dirac Hamiltonian H_0 [95]. Chiral symmetry for spinless fermions in $2+1$ dimension corresponds to a $SU_c(2)$ symmetry generated by $\{\gamma_3, \gamma_5, i\gamma_3\gamma_5\}$. As one restores the spin degrees of freedom, the chiral symmetry is enlarged to a $U_c(4)$ symmetry, accomplished by $\{\tau_0, \vec{\tau}\} \otimes \{I_4, \gamma_3, \gamma_5, i\gamma_3\gamma_5\}$, where the two dimensional Pauli matrices $\{\tau_0, \vec{\tau}\}$ act on the spin indices [9]. If the fermions are assumed to be spinless a chiral symmetry breaking gap may develop by inducing a density imbalance among the two sub-lattices. In standard nomenclature, such order is known as *charge density wave*. Even though the critical interaction strength for insulation in graphene is finite, a macroscopic density of states in the presence of magnetic field may place the system in an ordered phase, even at an *infinitesimal* interaction. The mechanism of driving the system towards an insulating phase at sufficiently weak interactions is named 'magnetic catalysis'. Two other

matrices that anti-commute with $\tilde{H}_0$, $i\gamma_0\gamma_3$ and $i\gamma_0\gamma_5$ are proportional to the two off diagonal Pauli matrices within the zero energy manifold $\mathcal{H}_0$. They correspond to the Kekule realization of the hopping. These states, on the other hand break the translation symmetry of the lattice into the Keukule pattern [39]. The remaining anti-commuting matrix $i\gamma_1\gamma_2$ is proportional to the *identity* matrix in the zeroth Landau level. Therefore at charge neutrality, this order cannot develop any finite expectation value. However, changing the chemical potential of the system one may induce such a phase. Therefore, it corresponds to *quantum anomalous Hall* state. In graphene, such order relates to a finite current circulating among the sites on the same sub-lattice [38]. The reader can find a detailed discussion of the energy spectrum in Appendix G.

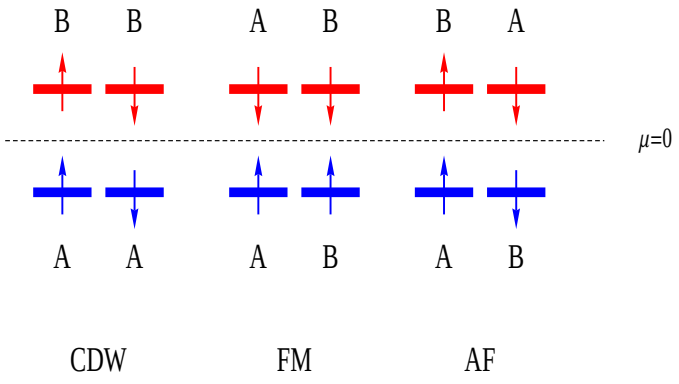

Figure 4.1: Various order parameters in graphene in presence of magnetic field

Restoration of the spin degrees of freedom opens up possibilities for various other order parameters which may develop finite expectation value within the zeroth Landau level. For instance, if the onsite Hubbard interaction (U) is bigger than the nearest neighbour (V) repulsion the system lowers its energy by pushing states on two sub-lattices, however, with opposite spin projections below the chemical potential (μ), as in the absence of a magnetic field. The antiferromagnet order parameter reads as $\langle\Psi(\vec{x})[\vec{\tau}\otimes\gamma_0]\Psi(\vec{x})\rangle \neq 0$. Conversely, if $V \gg U$, the system develops a charge density wave order by pushing all the states on one sub-lattice below the chemical potential, with $\langle\Psi(\vec{x})[\tau_0\otimes\gamma_0]\Psi(\vec{x})\rangle \neq 0$ [9, 80]. In the presence of a magnetic field, the electron's spin is also coupled to the field via Zeeman

coupling. The Zeeman term reads as

$$H_z = g\, B(\vec{x})\ (\tau_3 \otimes I_4)\,, \tag{4.10}$$

assuming the field is perpendicular to the plane and $g \approx 2$ for electrons in graphene. For sufficiently strong Zeeman coupling, the ground state acquires a finite magnetization in the direction of the magnetic field. Such a ground state can also be stabilized by increasing the component of the magnetic field parallel to the graphene plane. If the ground state achieves a finite magnetization, the system simultaneously develops a finite expectation value of $\sigma_3 \otimes i\gamma_1\gamma_2$. Such an order parameter corresponds to the third component of the time reversal symmetry breaking mass, originally introduced by Haldane [38] and later discussed in the context of spin-orbit coupling in graphene [87]. The reader may consult Table 4.1, which shows that both the matrices $(\tau_3 \otimes I_4, \tau_3 \otimes i\gamma_1\gamma_2)$ have identical sets of eigenvalues within the zeroth Landau level and therefore may coexist. We may also resolve this issue by establishing an important general property of the zero energy states.

Consider the following sum

$$q(\vec{x}) = \sum_{E\in R} \Psi_E^\dagger(\vec{x}) Q \Psi_E(\vec{x}), \tag{4.11}$$

where Q is a traceless Hermitian matrix and $\{\Psi_E(\vec{x})\}$ is the set of eigenstates for any Hamiltonian H. Therefore if one performs the sum over the entire spectrum then $q(\vec{x}) = 0$. Whereas if R includes only the occupied state then $q(\vec{x})$ stands for the expectation value of physical observable associated with the operator Q. By subtracting a half of the vanishing sum one can rewrite the same average as

$$\langle q(\vec{x})\rangle = \frac{1}{2}\left(\sum_{occup} - \sum_{empty}\right) \Psi_E^\dagger(\vec{x}) Q \Psi_E(\vec{x}). \tag{4.12}$$

If there exists a unitary matrix, say T, that anti-commutes with H and at the same time commutes with Q, then only the zero energy states contribute to the sum [20, 105]. For the Hamiltonian $\tilde{H}_0$, one can choose T to be $\tau_0 \otimes \gamma_0$. If one chooses $Q = \tau_3 \otimes i\gamma_1\gamma_2$, then $[T, Q] = 0$. Notice that half of the states in the zeroth Landau level are associated with $+1$, whereas remaining ones with -1, eigenvalues of the matrix Q. Hence pushing all the states with, say -1 eigenvalue of Q, below the chemical potential, the system acquires a finite expectation value for Q. From table 4.1, one can convince oneself that such ordering

wave function	$\tau_0 \otimes \gamma_0$	$\tau_3 \otimes \gamma_0$	$\tau_3 \otimes i\gamma_1\gamma_2$	$\tau_3 \otimes I_4$
$\Psi^{K}_{\uparrow}$	+1	+1	+1	+1
$\Psi^{-K}_{\uparrow}$	-1	-1	+1	+1
$\Psi^{K}_{\downarrow}$	+1	-1	-1	-1
$\Psi^{-K}_{\downarrow}$	-1	+1	-1	-1

Table 4.1: Order parameters in zeroth Landau levels in the presence of real magnetic field

leads to finite magnetization of the ground state.

The nature of the electronic ground state at $\nu = 0$ is still an issue of debate. Taking into account a finite Zeeman coupling of electrons spin with the magnetic field, it can be shown that the Neél order parameter is restricted to the easy plane ($\vec{N}_\perp$), while the ground state achieves a finite magnetization in the direction of the field. If the Zeeman coupling ($\lambda < \lambda_c = 2(g_a - g_f)/\pi l^2$) is small, the ground state is in a mixed phase with finite Neél order $\vec{N}_\perp = [g_a/(g_a - g_f)]\,\sqrt{\lambda_c^2 - \lambda^2}$ and magnetization $m_3 = [g_f/(g_a - g_f)]\,\lambda$. Beyond the critical Zeeman coupling (λ_c), the magnetization saturates at $m_3 = [g_f/(g_a - g_f)]\,\lambda_c$, while $\vec{N}_\perp = 0$. Within the framework of the Hubbard model with only onsite repulsion (U), $g_a = g_f = U/16$ at the lattice scale. However, as one integrates out the fast Fourier modes within the momentum shell $(1/a, 1/l)$ and enters into the low energy regime $g_a \gg g_f$, and hence $\lambda_c > 0$, where a and l are the lattice spacing and magnetic length. A schematic phase diagram is shown in Fig. 4.2. In an real experimental environment which side of the transition graphene lies, is hard to answar at this moment. Nevertheless, the activation gap at $\nu = 1$ scales with the perpendicular component of the magnetic field only. This observation suggests that in a real graphene system the strength of the Zeeman coupling is probably above the critical one (λ_c) [81]. A recent experiment observed a Kosterlitz-Thouless scaling of the resistivity in the presence of magnetic field at neutral filling [106]. This observation indicates a underlying vortex structure with requisite $U(1)$ symmetry. The possible candidates are: Kekule vortex which is favored by electron-phonon interaction [107], Neél order parameter with an easy axis for the spin degrees of freedom [81]. A controlled $\epsilon-$expansion near $d = 3$ showed that such projection of the Neél order is unlikely to arise from an anisotropic Hubbard interaction [108]. Spin splitting has also been proposed as a possible origin of such divergent resistivity at filling $\nu = 0$ [109]. However, we leave the issue of electronic ground state at neutral filling for future investigation. Next we focus on

the scaling behavior of the interaction induced gap at $\nu = 1$ with the magnetic field.

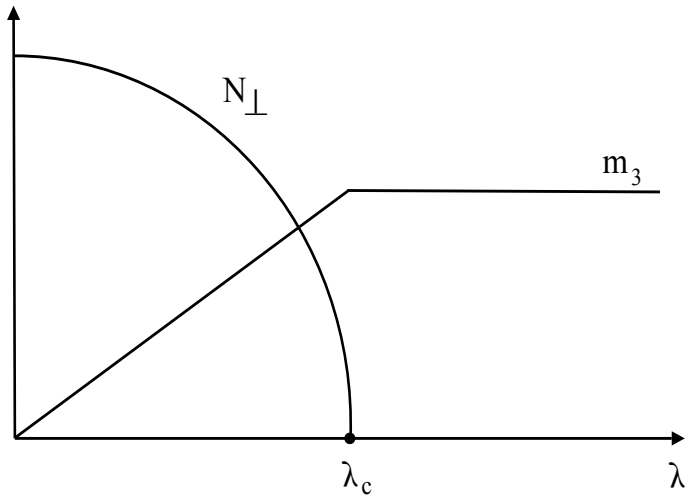

Figure 4.2: Schematic variation of the Neél order ($\vec{N}_\perp$) perpendicular to and magnetization m_3, parallel to the external magnetic field. The field is set to be perpendicular to the graphene plane. Here $\lambda_c = 2(g_a - g_f)/\pi l^2$ [81]. Figure reprinted with permission from I. F. Herbut, [81]. Copyright 2007 by the American Physical Society.

The sublinear field dependence of the gap at $\nu = 1$ in particular conforms to the expectation that the interaction-induced gap should scale with the Coulomb energy scale, $e^2/\epsilon l$, where $l = 1/\sqrt{B}$ is the magnetic length. This natural interpretation, however, runs into the following difficulty: with the commonly assumed dielectric constant $\epsilon \approx 5$ the measured gap at $\nu = 1$ (of $\sim 100K$) is more than an order of magnitude smaller than the theoretical prediction, which would require it to be of a similar size as the energy of the first Landau level. The observed energy gap at $\nu = 1$ therefore provides an unanticipated intermediate energy scale, in between the Landau level separation ($\sim 1000K$) and the much lower Zeeman energy ($\sim 10K$). The origin of such an energy scale in graphene in a magnetic field is presently unknown. In the next section we will try to shed some light on this issue.

4.4 Quantum critical scaling at $\nu = 1$ in a magnetic field

A possible reason for the smallness of the energy gap at $\nu = 1$ may be almost trivial: assuming an order of magnitude larger dielectric constant, which may be due to an accumulated layer of water for example, would obviously bring the theory and the observation closer together [110]. Here we wish to put forward an alternative and more general explanation which relies only on the short-range effects of the electron-electron repulsion, and as such completely avoids the ambiguities in the size of graphene's effective dielectric constant. The summary of our theory is the follow. As argued in the previous chapters that a purely short-range repulsion, if above a critical value, would open a gap in graphene even at zero magnetic field. Such a metal-insulator transition is found to be continuous one. In the following we will show that right at the critical point the system becomes scale invariant. This implies that upon the introduction of the magnetic field the gap at $\nu = 1$ behaves as

$$m = \frac{v_F\sqrt{2B}}{C}. \tag{4.13}$$

v_F is the Fermi velocity at the Dirac point, $\sqrt{2B}$ the energy of the first Landau level in units $\hbar = e/c = 1$, and C is a universal number. We determine the universal number in Eq. [4.13] to be

$$C = 5.985 + O(1/N), \tag{4.14}$$

with N as the number of Dirac fermions. Since $1/N$ corrections to simpler universal quantities in the problem, such as the critical exponents at zero magnetic field, are known to be only a few percent even for N as low as 2 [9, 50], we expect the above number to be quite indicative of the real value of C. At a subcritical value of the short-range interactions, likely to be realized in real graphene, the sublinear dependence $m \sim \sqrt{B}$ crosses over to the linear dependence $m \sim B$ at lower fields, with the values of the gap at all magnetic fields bounded from above by the critical curve in Eq. [4.13]. We compute the universal scaling function for the gap dependence on the magnetic field and the deviation from the criticality in the large-N limit. The family of resulting curves is depicted in Fig. 4.3. The question posed by the experiment is then whether there exists a line with enough curvature within the range of the laboratory fields which also agrees with the observed magnitude of the gaps. In Fig. 4.3 we argue that the answer is yes. Our conclusion is strengthened further by the inclusion of the long-range part of the Coulomb interaction, which provides the leading (logarithmic) corrections to scaling at the large-N critical point. We find its effect to be an additional

curvature to the universal function, and its inclusion thus always improves the comparison with the available experimental data (see Fig. 4.6).

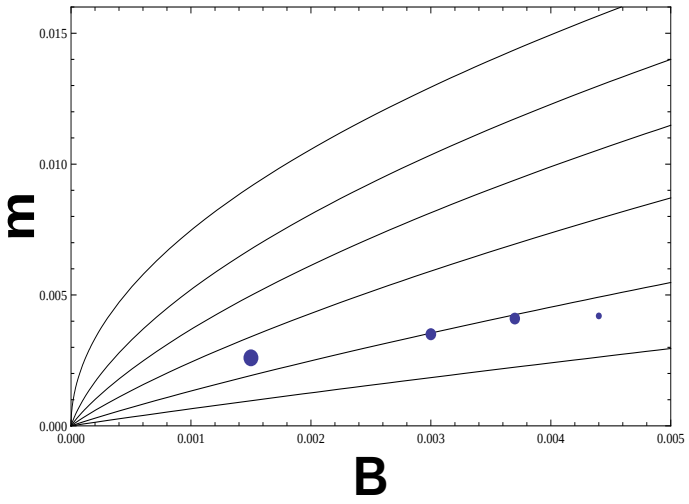

Figure 4.3: The gap m (in units of $v_F\Lambda$) at filling factor $\nu = 1$ as a function of the magnetic field B (in units of $B_0 = \Lambda^2$) below the zero-field critical value of the short-range coupling g, for $N = \infty$. The top curve corresponds to the critical point $\delta = 0$ (Eq. (1)), and the remaining ones to $\delta = 0.03, 0.07, 0.14, 0.31, 0.7$ (top to bottom), with $\delta = (g_c - g)/gg_c\Lambda$. The best fit to the experimental data (dots) assuming $1/\Lambda = 2.5\mathring{A}$ (i. e. $B_0 = 10^4 T$) is for $\delta = 0.31$. Figure reprinted with permission from I. F. Herbut et. al., [103]. Copyright 2008 by the American Physical Society.

A necessary condition for the applicability of our theory is that the external magnetic field is low compared to the characteristic lattice magnetic field scale, or equivalently, that the magnetic length is much longer than the lattice constant. Even at the highest fields of ~ 45 T this condition is comfortably satisfied. Provided that the system is not too far in the coupling space from its quantum critical point, in the next section we show that in general under this condition a single relevant coupling constant needs to be included, and a simple scaling law in the magnetic field emerges.

4.5 Scaling

Let us now establish the scaling behaviour of the interaction induced gap. To be specific, we assume the spin degeneracy to be removed by the Zeeman splitting, and that the chemical potential is close enough to the Zeeman-shifted Dirac point so that $\nu = 1$. Assuming further a simple quantum critical point at $B = 0$ we retain a single relevant short-range coupling constant g. We will also include the coupling representing the $\sim 1/r$ tail of the Coulomb interaction, which remains unscreened in graphene: $\lambda = 2\pi e^2/\epsilon v_F$ [3]. At "weak" magnetic fields, at which $l/a \gg 1$, one is at liberty to use the continuum field-theoretic description, with the underlying lattice entering only at energies above the ultraviolet cutoff $\Lambda = 1/a$. The internal consistency of such a description requires that if another value of the cutoff, say Λ/b, is chosen, the gap in the spectrum m satisfies

$$m/\Lambda = b^{-1} v_F(b) F_{\pm}(|\delta(b)|, \lambda(b), b^2 B), \tag{4.15}$$

where the functions $v_F(b)$, $\delta(b)$ and $\lambda(b)$ are such that the measurable value of m is independent of the arbitrary factor b. Here we defined a dimensionless parameter $\delta = (g\Lambda)^{-1} - (g_c\Lambda)^{-1}$ for later convenience, with g_c as the critical value of the short-range coupling. The (engineering) scaling of the magnetic field in the last equation follows from gauge-invariance. The two functions F_+ and F_- refer to $\delta > 0$ ($g < g_c$) and $\delta < 0$ ($g > g_c$), respectively.

We may then choose $b = (B_0/B)^{1/2} = l/a$, with $B_0 = 1/a^2$, and write

$$m = l^{-1} v_F(l/a) F_{\pm}[\delta(l/a), \lambda(l/a), B_0]. \tag{4.16}$$

If $l/a \gg 1$ the flow of the couplings is essentially determined as at zero magnetic field. Omitting all but the single relevant parameter δ from the outset becomes justified, as all the other couplings are much smaller at a large (magnetic) length scale, provided that in the coupling space the system was not too far from the critical point. Assuming a simple critical point at $B = 0$ near which $|\delta(b)| = |\delta| b^{1/\nu}$, $\lambda(b) = \lambda^*$, and $v_F(b) = v_F b^{1-z}$, where ν and z are the usual correlation length and dynamical critical exponents, we may finally write

$$m/(v_F\Lambda) = (a/l)^z G_{\pm}[l/\xi, \lambda^*], \tag{4.17}$$

[3] Such a long-range coupling is also irrelevant at the metal-insulator quantum critical point to the leading order in $1/N$, but only marginally so.

with $\xi = a|\delta|^{-\nu}$, as the correlation length. This is the universal scaling form of the gap at low magnetic fields, dictated by the critical point at $\delta = 0$, $\lambda = \lambda^*$, and $B = 0$ [37, 111]. The last expression is analogous to the finite-size scaling, with the magnetic length playing the role of the system's size [4].

Before proceeding with the computation of the universal scaling function, let us consider its limits first. At the critical point,

$$G_-[0, \lambda^*] = G_+[0, \lambda^*]. \tag{4.18}$$

In particular, for $z = 1$ this yields the announced Eq. [4.13]. At $x \gg 1$, we must have

$$G_+[x, \lambda^*] \sim x^{z-2}, \tag{4.19}$$

so that for $g < g_c$ one finds $m \sim B$, as appropriate to "magnetic catalysis" [102]. For $g > g_c$, on the other hand, at $x \gg 1$,

$$G_-[x, \lambda^*] \sim x^z, \tag{4.20}$$

which yields $m \sim |\delta|^{z\nu}$ above the critical coupling and at $B = 0$. This is the familiar scaling of the gap near a quantum critical point [40].

4.6 Large-N calculation

Let us now take $\lambda = 0$, and compute the scaling function $G_+(x, 0)$ in the limit of large number of Dirac fermions. The discussion of the effects of long-range interaction will be presented in the next section. The ground state energy for N species of four-component Dirac fermions in magnetic field and when $N \to \infty$ reads as [5]:

$$\frac{E(m) - E(0)}{N} = \frac{m^2}{4g} + \frac{B}{4\pi^{3/2}} \int_0^\infty \frac{ds}{s^{3/2}} (e^{-sm^2} - 1)[p + 2K(s\Lambda^2)(\coth(sB) - 1)]. \tag{4.21}$$

m is the gap to be determined by the minimization of $E(m)$, and g is the dominant among the quartic couplings that represent the short-range part of Coulomb repulsion [9]. $K(x)$ is the cutoff function introduced to sum over $n \neq 0$ Landau levels, which satisfies $K(x \to \infty) = 1$ and $K(x \to 0) = 0$, but is otherwise arbitrary. The parameter $p = 2$ for $\nu = 0$, when the zeroth Landau level of each Dirac fermion contributes to the energy difference $E(m) - E(0)$,

[4] For other scaling laws in graphene reader may consult [31, 112]

[5] See Appendix G and Ref. [81, 95]

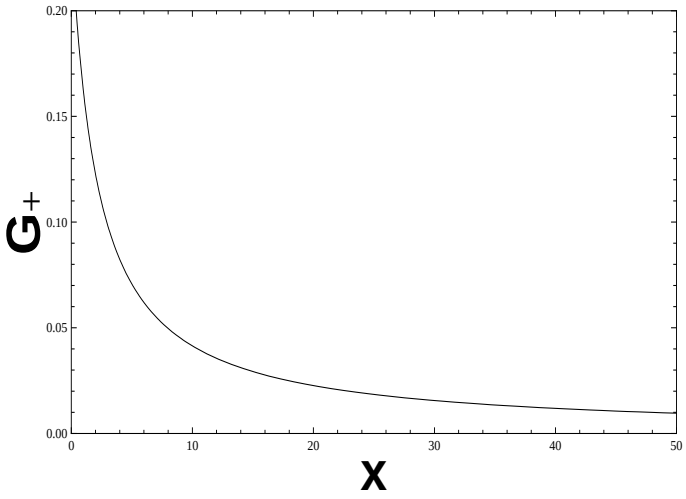

Figure 4.4: The universal scaling function $G_+(x,0)$ at $N=\infty$. Figure reprinted with permission from I. F. Herbut et. al., [103]. Copyright 2008 by the American Physical Society.

and $p=1$ for $\nu=N/2$, when half of the zeroth Landau levels do not [81, 95]. $E(m)$ may also be understood as the variational ground state energy of electrons with an on-site, or nearest-neighbour, repulsion on a honeycomb lattice and in low magnetic field, in the Hartree approximation.

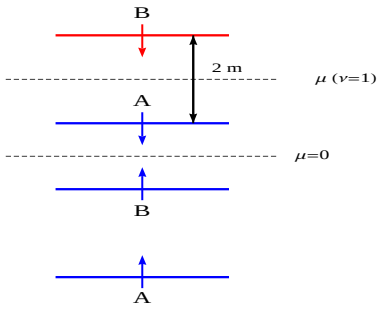

Figure 4.5: Chiral symmetry breaking gap at $\nu=1$

Hereafter we set $p=1$, which would correspond to the filling factor $\nu=1$ for the

physical case of $N = 2$. Minimizing $E(m)$, after some transformations the gap equation can be written in a compact form as

$$y = f(y) + 2\delta(yB_0/B)^{1/2}, \tag{4.22}$$

where the variable $y = B/m^2$, and δ is as defined below Eq. [4.15], with

$$\frac{1}{g_c} = \frac{\Lambda}{\sqrt{\pi}} \int_0^\infty dt \frac{K(t)}{t^{3/2}}. \tag{4.23}$$

The function $f(y)$ is defined as

$$f(y) = \frac{2}{\sqrt{\pi}} \int_0^\infty \frac{dt}{t^{3/2}} K\left(\frac{tyB_0}{B}\right) \left[1 - \frac{2yte^{-t}}{e^{2yt} - 1}\right]. \tag{4.24}$$

The ultraviolet cutoff enters the gap equation by providing the scale for the magnetic field (B_0). In the limit of weak magnetic field, $B/B_0 \ll 1$, we may replace the cutoff function $K(x)$ in the last equation with unity. In this (continuum) limit the dimensionless variable y becomes a *universal* function of the ratio $\delta(B_0/B)^{1/2}$. The only remaining dependence on the cutoff then is in the value of the critical point g_c which is therefore, as usual, non-universal.

The gap equation may be solved essentially analytically for $\delta > 0$ by noticing first that at $\delta = 0$ the (numerical) solution is at $y_0 = 17.913$. This immediately yields the result in Eqs. [4.13] and [4.14], with $C = \sqrt{2y_0}$. Since at $\delta > 0$ the solution will be at $y > y_0$, one in fact needs the function $f(y)$ only for large arguments, where it can be expanded as

$$f(y) = uy^{1/2} + vy^{-1/2} + O(y^{-3/2}), \tag{4.25}$$

with $u = 4.13031$ and $v = 1.84723$. The difference between $f(y)$ and the first two terms in the expansion on the right-hand side is less than a percent already for $y > 3$, and decreases further with y. Comparing with the general form in Eq. [4.17] we may then write the Eq. [4.22] in terms of the universal function $G_+(x, y)$ as

$$-1 + (u + 2x)\, G_+(x, 0) + v\, G_+^3(x, 0) = 0, \tag{4.26}$$

with the higher order terms in G_+ entirely negligible. This way we find $G_+(0, 0) = 0.236$, and $G_+(x, 0) = 1/2x$ for $x \gg 1$, and uniformly decreasing in between. In sum, at $N = \infty$ and $\lambda = 0$ the Eq. [4.17] becomes

$$m = \frac{v_F}{l^z} G_+\left(\frac{l\delta^\nu}{a}, 0\right) \tag{4.27}$$

with $z = 1$ and $\nu = 1 + O(1/N)$, and the function $G_+(x, 0)$ depicted in Fig. 4.4.

Although it may not be directly relevant to graphene, for completeness we also briefly describe some of the results when $\delta < 0$. Since the gap is finite even at zero field above the critical coupling, the solution of Eq. [4.22] now lies at $y < y_0$. For weak fields, the relevant regime is $y \ll 1$, where $f(y) = 4 + 2y + O(y^2)$. This implies, for example, $G_-(x, 0) \to x/2$ when $x \gg 1$, in agreement with the Eq. [4.20]. We thus find $m = |\delta|/2 + O(\delta^2)$ in the zero-field limit, and at $N = \infty$.

4.7 Leading correction to scaling

Let us now turn on a weak long-range interaction $\lambda \ll 1$. It represents a marginally irrelevant perturbation at the large-N critical point $\delta = 0$, $\lambda^* = 0$ [9], and thus provides logarithmic corrections to the scaling law in Eq. [4.17]. At $b \gg 1$, the Coulomb interaction scales as

$$\lambda(b) = \frac{8\pi}{\ln b} + O\left(\left(\frac{1}{\ln b}\right)^2\right). \tag{4.28}$$

The effect of the long-range Coulomb interaction is to break the pseudo-relativistic invariance of the problem and renormalize the velocity as [18, 19]

$$v_F(b) = v_F\left(1 + \left(\frac{\lambda}{8\pi} + O(\lambda^2)\right)\ln b\right). \tag{4.29}$$

The Eq. [4.16] then yields, for $l/a \gg 1$

$$m = \left(\frac{\lambda}{8\pi} + O(\lambda^2)\right) v_F \frac{\ln(l/a)}{l} G_+\left(\frac{l\delta^\nu}{a}, 0\right). \tag{4.30}$$

Interestingly, the inclusion of such corrections improves the agreement with experiment. As an illustration, in Fig. 4.6 we display the fit to

$$m = v_F\sqrt{B}\left(1 + \frac{\lambda}{16\pi}\ln\frac{B^*}{B}\right) G_+\left(\frac{l\delta^\nu}{a}, 0\right). \tag{4.31}$$

$1/\sqrt{B^*}$ defines the length scale appropriate to the measured value of $v_F = 10^6$ m/s, which we will treat as a fitting parameter. The best fit for $\epsilon = 1$, for example, is obtained for $B^* = 29$ T. More data seems needed, however, to distinguish between this and the alternative forms such as a simple $m \sim \sqrt{B}$ considered in Ref. [99].

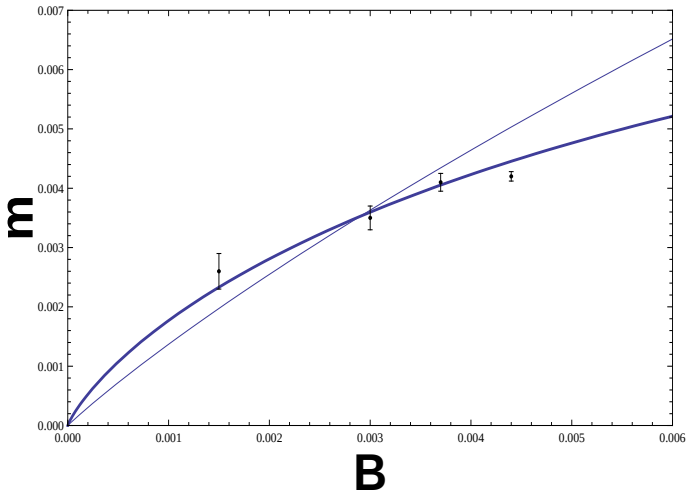

Figure 4.6: The same as in Fig. 4.3 at $\delta = 0.3$, without (dashed line) and with ($\lambda/16\pi = 0.27$, ($\epsilon = 1$), thick line) the logarithmic corrections to scaling in Eq. [4.31]. Figure reprinted with permission from I. F. Herbut et. al., [103]. Copyright 2008 by the American Physical Society.

4.8 Discussion and summary

We have argued that taking into account only the short-range parts of the repulsive electron-electron interaction in graphene suffices to provide a qualitative, and even semi-quantitative understanding of the observed magnetic field dependence of the gap at $\nu = 1$. Our main assumption is that the value of the dominant short-range coupling is below but not too far from its critical value, so that the aforementioned magnetic field dependence resembles itself as right at the criticality at the laboratory fields.

Note that the precise nature of the short-range coupling, i.e. whether it is on-site or nearest-neighbour interaction, for example, does not matter for the form of the scaling function in the large-N limit we considered. It is only the resulting order parameter that will depend on this [81, 95]. Any order parameter which breaks the chiral symmetry of the Dirac Hamiltonian and lifts the valley degeneracy in the magnetic field will lead to the same large-N scaling function as obtained here. $1/N$-corrections may depend on the type of the order parameter, however.

The best fit to the experimental data is provided by $\delta = 0.31$ (Fig. 4.3), which places the system relatively far from the critical point. On the other hand, assuming the simplest Hubbard model for short-range interactions, for example, would place the critical point at $U_c/t = 4 - 5$. With $t = 2.5eV$, the usual estimate $U \approx 10eV$ [24] is then in a reasonable agreement with the value of δ obtained from the fit. It is in fact not uncommon that a simple single-parameter scaling works well even reasonably far from the critical point. A celebrated example is provided by the scaling plot for classical liquids, where very good scaling of the data is found even at $T/T_c \approx 0.5$ [40].

For weak Zeeman splitting the gap at $f = 0$ will also obey the critical scaling in magnetic field, and the critical function can be found in the large-N limit by choosing $p = 2$ in the Eq. [4.21]. At $\nu = 0$, however, the Zeeman gap is in competition with the "mass"-gap studied here, and there are reasons to believe that the gap at $\nu = 0$ in reality may be a pure (albeit interaction enhanced) Zeeman gap.

A test of relevancy of the presented theory would be a measurement of the field-dependent gap at the filling factor $\nu = 1$ on a suspended graphene, for example, where the dielectric constant $\epsilon \approx 1$. If the gaps are still of the same size as in Ref. [99] this would eliminate the alternative explanation we mentioned in the introduction, that the smallness of the gap is caused by the extra screening by the surrounding medium. Alternatively, one may want to enhance screening by bringing a metallic plate to the graphene layer. If the gap is indeed caused primarily by the short-range electron-electron interaction as discussed here, this should not alter its size much either.

In the next chapter, we will confirm the 'magnetic catalysis' mechanism on a finite size honeycomb lattice. By numerically diagonalizing the interacting Hamiltonian at Hartree level, scaling of the interaction induced gap is found to be to be in good accordance with the analytical one, computed here in the large-N limit. However, the main purpose will be to establish the robustness of catalysis mechanism under the relaxation of the condition of uniformity of the magnetic field. We will show that a finite density of states at zero energy can take the system to an ordered phase even at an infinitesimal interaction when the system is at filling one-half.

Chapter 5

Inhomogeneous magnetic catalysis

We investigate the ordering instability of interacting (and for simplicity, spinless) fermions on graphene's honeycomb lattice by numerically computing the Hartree self-consistent solution for the charge-density-wave order parameter in presence of both uniform and non-uniform magnetic fields. For a uniform field the overall behaviour of the order parameter is found to be in accord with the continuum theory, discussed in the previous chapter. In the inhomogeneous case, the spatial profile of the order parameter resembles qualitatively the form of the magnetic field itself, at least when the interaction is not overly strong. We find that right at the zero-field critical point of the infinite system the local order parameter scales as the square-root of the local strength of the magnetic field, apparently independently of the assumed field's profile. The finite size effects on various parameters of interest, such as the critical interaction and the universal amplitude ratio of the interaction-induced gap to the Landau level energy at criticality are also addressed. The main motivation of the following discussion is to study the behaviour of the interacting fermions in presence of inhomogeneous magnetic field, with special emphasis given to the spatial variation of the order parameter.

5.1 Introduction

Even though successful fabrication of graphene opened a new frontier in condensed matter physics, the reason it has not been used in electronics successfully is mainly a large overlap of the electronic wave functions of the neighboring carbon atoms ($t \sim 2.5$ eV), which

protects the semimetal phase against weak electron-electron interactions [113]. In the language of renormalization group, such a stability corresponds to a large domain of attraction of the non-interacting Gaussian fixed point [114]. Nevertheless, fermions in graphene may condense into various insulating orders, however the critical strength for insulation is fairly large, due to the vanishing density of states at charge neutral point. As we have seen in the previous chapter, a metal-insulator transition can take place at sufficiently weak interactions in the the presence of magnetic field [115, 116, 95, 81]. Yet another qualitatively different gauge field, which may arise from specific deformation of the graphene flake [117, 118], can also drive metal-insulator transitions at weak interactions. However, we resume this issue until the next chapter.

Magnetic catalysis in the presence of uniform magnetic field is by now well understood and was the subject of our previous discussion. It has been proposed as a mechanism behind the formation of the Hall states in graphene at filling factors $\nu = 0$ and $\nu = 1$ [95, 81, 28], which become discernible at higher magnetic fields. [98] Sublinear scaling of the gap with the magnetic field, for example, strongly suggests that electron-electron interactions are the cause of the gap at $\nu = 1$ [99, 103]. In contrast, the behaviour of interacting electrons in presence of an *inhomogeneous* magnetic field has not been studied much, although the issue of order parameter's dependence on the local value of the magnetic field has been addressed analytically, for specific spatial profiles of the field [119, 120]. In this work we attempt to develop a more detailed understanding of the spatial variation and the field dependence of the order parameter when an inhomogeneous magnetic field penetrates through the system. The motivation for such a study comes in part from a closely related problem of interacting electrons in a pseudomagnetic field [43, 117], where the field's profile is typically non-uniform in space. On a methodological level, it seems also interesting to inquire how much of the catalysis mechanism remains in effect when the condition of uniformity of the magnetic field is relaxed.

A self-consistent profile of the local gap in the insulating phase is computed therefore numerically on a discrete lattice and at the level of Hartree approximation, with special attention given to its spatial variation. We find that the system stills suffers a metal-insulator transition at weak nearest-neighbour interactions even in the presence of a inhomogeneous magnetic field. In the continuum, this phenomenon would be attributed to the delta-function

density of states when the Fermi energy is at the Dirac point [121]. Interestingly, we find that the spatial profile of the interaction-induced gap (order parameter) in presence of a localized magnetic flux, although not matching exactly, still mimics closely the profile of the local strength of the magnetic field. Moreover, right at the zero-field metal-insulator quantum criticality, the *local* order parameter seems to vary very much like the square-root of the *local* magnetic field. This behaviour is analogous to what we previously found analytically in a uniform magnetic field [103]. Away from the critical point, at weak interactions the expectation value of the local order parameter reverts to a linear dependence of the local magnetic field, as one might expect.

For a uniform magnetic field, we in general find a very good agreement between the previous field theoretic results and our numerical calculations. We focus on the finite-ranged components of the Coulomb repulsion, and choose to keep only the simplest one, which acts between the nearest neighbours. The system at filling one-half and in a magnetic field then develops a gap in the spectrum, even when the interaction is weak. Right at the metal-insulator quantum critical point the gap behaves as

$$m = \frac{E(1)}{C}, \tag{5.1}$$

where $E(n)$ is the n^{th} LL energy. Here C is a universal number, found to be 6.1 in the largest system considered here, within the the Hartree approximation. This is in satisfactory agreement with the same quantity computed previously in the field-theoretic description [103], where we found it to be 5.985, in the limit of infinite number of fermion components. These two procedures being equivalent, we indeed find that upon increasing system's size the constant C slowly approaches its value in the continuum.

5.2 Free fermions

Let us define the system of non-interacting electrons on honeycomb lattice in the presence of a uniform magnetic field. The tight-binding model with nearest-neighbour hopping is defined as

$$H_t = -t \sum_{a,i} c_a^\dagger c_{a+b_i} + H.c., \tag{5.2}$$

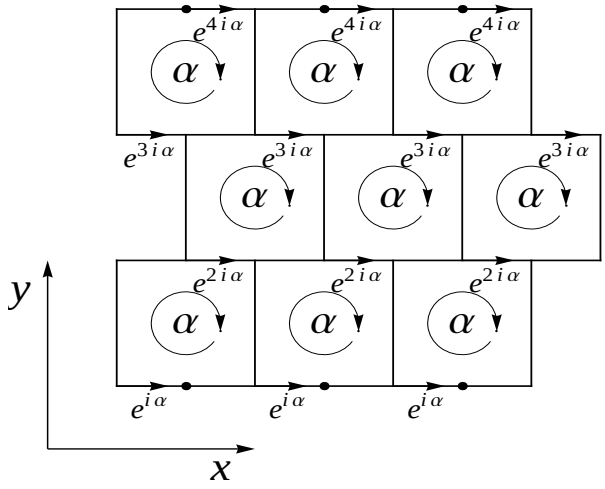

Figure 5.1: Brickwall realization of honeycomb lattice. Here the magnetic flux of $\alpha\Phi_0$ pierces through each hexagon, corresponding to a uniform magnetic field through the system. This particular choice of gauge is equivalent to the Landau gauge $A = (-By, 0)$ in the continuum description. This construction is straightforward to generalize to an inhomogeneous magnetic field. Figure reprinted with permission from B. Roy et. al., [135]. Copyright 2011 by the American Physical Society.

where c and $c^\dagger$ are the usual fermionic annihilation and creation operators, respectively. Here we omitted the spin degrees of freedom, for simplicity. $\vec{a}$ denotes the sublattice generated by the linear combination of basis vectors $\vec{a}_1 = (\sqrt{3}, -1)a$ and $\vec{a}_2 = (0, 1)a$, for example. The second sublattice is then at $\vec{b} = \vec{a} + \vec{b}$, with $\vec{b}$ being either $\vec{b}_1 = (1/\sqrt{3}, 1)a/2, \vec{b}_2 = (1/\sqrt{3}, -1)a/2$ or $\vec{b}_3 = (-1/\sqrt{3}, 0)a$, where a is the lattice spacing. The magnetic field may be introduced through the Peierls substitution $t \to te^{(i2\pi e/h)\int \vec{A}\cdot d\vec{l}}$, where $h/e = \Phi_0$ is the usual flux-quantum, and $(1/\Phi_0)\int \vec{A} \cdot d\vec{l} = \Phi/\Phi_0$ counts the magnetic flux through each plaquette of the honeycomb lattice. In case of graphene, Φ_0 corresponds to a magnetic field $\sim 10^4$ T, with commonly assumed lattice constant, $a \approx 3$ $\mathring{A}$. Such a high magnetic field corresponds to a magnetic length close to the lattice scale, $B_0 \sim 1/a^2$. Therefore Φ/Φ_0 is equivalent to B/B_0, where $B/B_0 = 0.05$ corresponds to $B = 500$ T. In Fig. [5.1] we have shown one way to introduce a uniform magnetic field on honeycomb lattice. By solving numerically the tight-binding model on a 80×65 lattice with periodic boundary in x-direction and the field $B = 160$ T, we clearly see the first few (5) LLs as the well-separated energies where the DOS is sharply peaked (black curve Fig. [5.2]). The energy spectrum is

symmetric about zero and the spacing among the LLs decreases with the LL index. The energy of the LLs varies as the square root of the magnetic field, due to the relativistic nature of the quasi-particles (top curve Fig. [5.3]). We also found that the maximum energy of the free electron system is $2.97t(< 3t)$, in agreement with the previous results [122]. It may be worth mentioning that in presence of the periodic boundary conditions the choice of gauge requires some care, and $A(\vec{r})$ is chosen here so that only one out of the three bonds emanating from a site contributes to it. Such a choice is then equivalent to the Landau gauge in the continuum description.

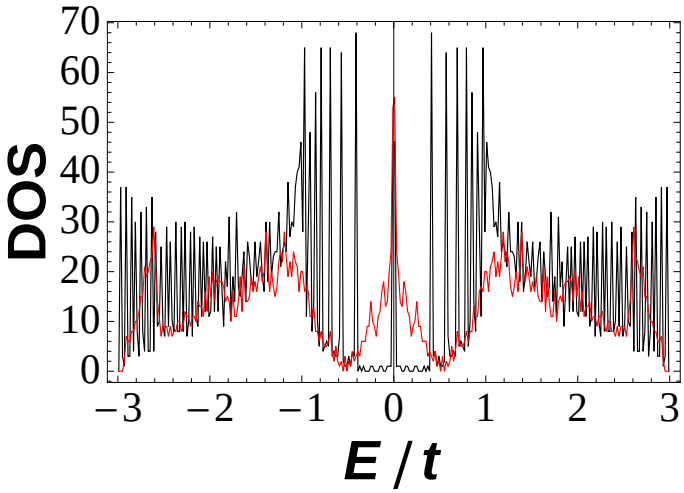

Figure 5.2: DOS as a function of energy in presence of uniform (black) and non-uniform (red) magnetic field. The first five LLs are well formed in the case of a uniform magnetic field, on a lattice of size 80×65, with periodic boundary in x-direction. In contrast, the DOS is sharply peaked only at zero energy in presence of an inhomogeneous magnetic field, computed on a 70×55 lattice with open boundary. Figure reprinted with permission from B. Roy et. al., [135]. Copyright 2011 by the American Physical Society.

Next, we consider still non-interacting electrons on the honeycomb lattice, but now subject to an inhomogeneous magnetic field. Numerically diagonalizing the free electron Hamiltonian, the DOS is found to be a smooth function of energy, and peaked only at the zero energy (red curve in Fig. [5.2]). There we considered a 70×55 lattice, with a open

boundary and total flux $\Phi_{total} = 4.59\Phi_0$. We assumed the field to be uniform in the x-direction, and bell-shaped in y-direction, with the maximum at the center. The number of near zero energy states is proportional to the total flux of the magnetic field enclosed by the system.[121] The maximum energy in the free electron spectrum is found to be $2.93t(< 3t)$.

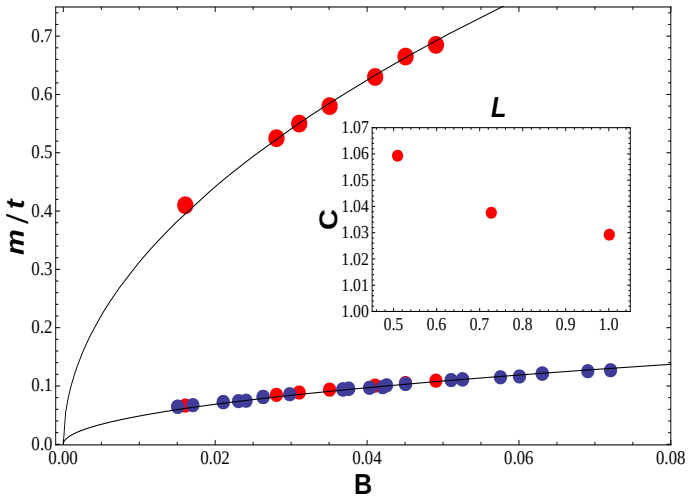

Figure 5.3: The top curve corresponds to the first LL energies at various magnetic fields B (measured in the unit of B_0) in a finite lattice. The energy spectrum is computed in a system of 40×31 points with a periodic boundary in x-direction. The bottom one shows the interaction induced gap, as a function of magnetic field at the zero-field metal-insulator critical point $V/t = 0.75$, in the same system. The red dots correspond to the OPs for the uniform field, whereas the blue ones correspond to that in an inhomogeneous field, at different regions in the bulk of the system. The inset shows the variation of the universal ratio (C) relative to its field-theoretic value (5.985) with the system size. Here L corresponds to the ratio of system size to the maximum one. The largest lattice considered here has 40×31 lattice points. Figure reprinted with permission from B. Roy et. al., [135]. Copyright 2011 by the American Physical Society.

5.3 Interactions and magnetic catalysis

Next, we turn on the short-range electron-electron interaction. The Hamiltonian in the presence of only the nearest-neighbor Coulomb repulsion (V) is given by

$$H = H_t + \frac{V}{2}\sum_{\langle i,j\rangle} n_i n_j - \mu N, \tag{5.3}$$

where $\langle i,j\rangle$ stands for the summation over the nearest-neighbor sites, N is the total number of electrons and μ is the chemical potential. After the usual Hartree decomposition the effective single-particle Hamiltonian for interacting electrons becomes

$$H_{HF} = H_t + V\sum_{<i,j>}(< n_{B,j} > n_{A,i} + < n_{A,j} > n_{B,i}) - \mu N, \tag{5.4}$$

where $\langle n_{B(A)}\rangle$ counts the self-consistent site-dependent average electron density on sublattice B(A). Let us measure these relative to the uniform density at half-filling by defining

$$< n_{A,i} >= \frac{1}{2} + \delta_{A,i}, \quad < n_{B,i} >= \frac{1}{2} - \delta_{B,i}. \tag{5.5}$$

The positive quantities δ_A, δ_B determine the local charge-density-wave order parameter (OP). Both δ_A and δ_B will be functions of position with the constraint that the system is precisely at half filling,

$$\sum_i \delta_{A,i} - \sum_i \delta_{B,i} = 0. \tag{5.6}$$

We also choose the value of $\mu = V/2$.

We have computed the (Hartree) self-consistent solutions for the OPs, for different values of the flux and for a variety of interaction strengths (V/t), at $T = 0$. Consider a lattice with a periodic boundary in the x direction and let us conveniently define the local OP as,

$$\delta_R = \frac{1}{2}(\delta_A + \delta_B), \tag{5.7}$$

where B is either one of the two nearest-neighbors to the site A, on the same row in x-direction. δ_R this way measures the order parameter in a unit cell. On the other hand, the OP will be averaged over the points connected by the C_6 symmetry, when we considered a quasi-circular system with an open boundary. In the presence of a uniform magnetic field,

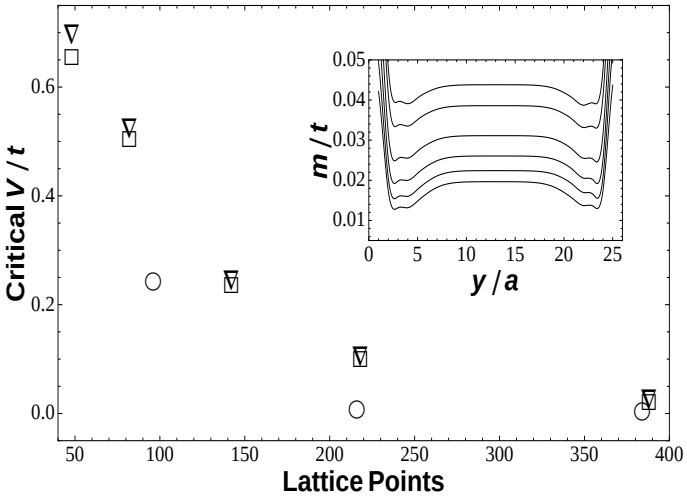

Figure 5.4: The variation of finite-size "critical interaction" $(V/t)_C$ (see the text) as a function of the lattice size. $\bigtriangledown$ and $\square$ stand for $(V/t)_C$ in a cylindrical lattice with open boundary in different gauges $A = (0, Bx)$ and $A = (-By, 0)$, respectively. $\bigcirc$ stands for $(V/t)_C$ in a lattice with open boundary, preserving the C_6 symmetry of the honeycomb lattice, with $A = (0, Bx)$. Here the critical interactions are computed for $\Phi/\Phi_0 = 0.05$. The inset shows the variation of the size of the order parameter (δ_R) as a function of V/t, in the entire system, computed on a 36×25 lattice. V/t reads as $0.5, 0.4, 0.3, 0.2, 0.1, 0.05$ from top to bottom. Figure reprinted with permission from B. Roy et. al., [135]. Copyright 2011 by the American Physical Society.

δ_R is found to be uniform in the bulk of the system. However, δ_R becomes position dependent and proportional to the local field when the system is subject to a inhomogeneous field.

Before we proceed, it is worth pausing to establish a practical definition of the "critical interaction" associated with the metal-insulator transition in the finite size system like ours. For a sufficiently strong nearest-neighbour interaction, fermions reside only on one sublattice, with the other one completely empty. The system is then deep in the insulating phase. As the interaction is weakened, the size of the order parameter decreases and we numerically find the system to go through a well-defined transition into the semi-metallic phase, where the order parameters δ_A, δ_B are zero in the entire system. Right above that particular interaction (V/t) which we call critical, there is a finite, but slightly inhomogeneous staggered density *everywhere* in the system. We will designate that value as the

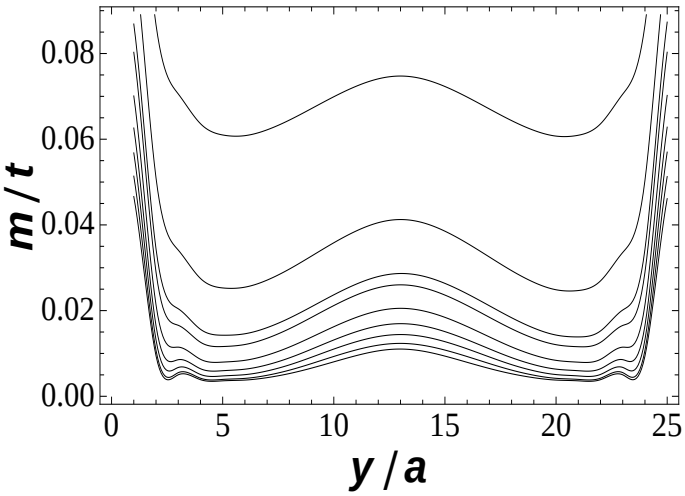

Figure 5.5: Spatial distribution of the order parameter in the presence of a localized flux of magnetic field, with total flux $\Phi_{total} = 5.6\Phi_0$. The top curve corresponds to $V/t = 0.76$ and the rest read as $V/t = 0.65, 0.55, 0.5, 0.4, 0.3, 0.2, 0.1, 0.05, 0.01$ from top to bottom. Figure reprinted with permission from B. Roy et. al., [135]. Copyright 2011 by the American Physical Society.

critical interaction $(V/t)_C$ corresponding to the metal-insulator transition. The described scenario is quite generic and occurs both in the absence and presence of magnetic fields, which also may be either uniform or nonuniform. The observed non-analytic behaviour in a finite system, however, is clearly an artifact of the Hartree approximation, i. e. of the requirement of the self-consistency of the solution.

We computed the variation of the critical interaction defined this way with the lattice size and the geometry, for a particular magnetic flux $\Phi/\Phi_0 = 0.05$ ($B = 500T$) through each plaquette of the lattice. As may be seen from the Fig. [5.4], for a small system size the critical interaction is large even in the presence of a magnetic field, and also depends on the geometry of the lattice, as well as on the choice of the gauge. Upon increasing the size of the system, the value of the critical interaction decreases and appears to approach *zero* in the thermodynamic limit, in agreement with the results obtained in the continuum theory. A typical distribution of the OP in a lattice with periodic boundary is shown in inset of Fig. [5.4]. From that one can conclude that upon decreasing (V/t), the size of the

order parameter decreases in the entire system, both in the bulk and at the edge. However a finite gap in the spectrum exists even at a rather weak interaction, $V/t = 0.05$ (bottom curve). Hence, in the presence of a uniform magnetic field, we expect that a large system would find itself in a gapped insulating phase even at an infinitesimal interaction, as found in the continuum theory.

On the other hand, when the system is exposed to a localized flux of magnetic field OP develops a local expectation value (see Fig. [5.5]). The local OP is found to be proportional to the local magnetic field. As one enters the regime of weaker interaction the OP decreases both in the bulk and the edge of the system. Yet we managed to observe finite expectation value of the OP in the entire system even at the smallest interaction considered here, $V/t = 0.01$. Therefore, the system can also find itself in an ordered phase at weak interaction when an *inhomogeneous* flux of the magnetic field pierces through it. This phenomenon can be attributed to the finite density of states at zero energy, where the chemical potential lies at filling one-half.

Besides the condensation in the bulk of the system, the OP acquires spikes near the edges of the system, in presence of both uniform (Inset of Fig. [5.4]) and non-uniform (Fig. [5.5]) field. The spikes in the OP near the edge of the system arise as a finite size effect. Such edge effects die out as one increases the system size. Moreover, with the increasing magnetic field, those spikes also dissolve and give rise to a uniform condensation throughout the system, at sufficiently large magnetic field. These effects on the OP are demonstrated in Fig. [5.6]. We exhibit the finite-size effects in presence of a uniform flux only, but the result is qualitatively the same in the presence of a localized flux as well.

5.4 Scaling in uniform magnetic field

We now investigate the dependence of the gap on the magnetic field (B) and the interaction (V/t). First we take the field to be uniform, and still consider the lattice with the periodic boundary in the x direction. The functional dependence of δ_R, defined in Eq. 5.7, on the magnetic fields and interactions is shown in Fig. [5.7]. Here, δ_R is computed on a 36×25 lattice and we considered OP only in the bulk of the system. With the parametrization as

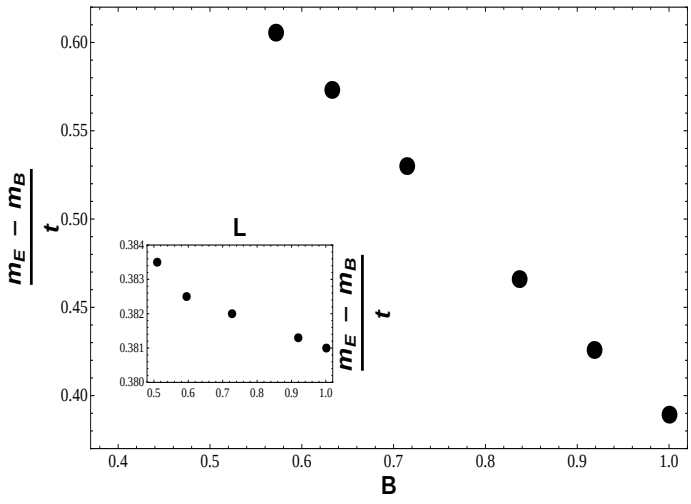

Figure 5.6: Difference of the masses at the edge (m_E) and in the bulk (m_B) as a function of the magnetic field (B/B_{max}) in a 36×25 lattice, at $V/t = 0.5$. Inset: same quantity as a function of system size (L), at fixed magnetic field $B/B_0 = 0.028$, at $V/t = 0.76$. Here $B_{max} = 490T$ and $L_{max} = 40 \times 31$. Figure reprinted with permission from B. Roy et. al., [135]. Copyright 2011 by the American Physical Society.

in Sec. 5.2, the lowest value of the magnetic field (160 T), considered here, is about four times larger than the current highest constant laboratory magnetic field. However, upon using a larger system one can get down to a more realistic strength of the field.

For sufficiently small interactions, the order parameter (δ_R or m) varies almost linearly with B/B_0 (bottom curve in Fig. [5.7]). As one increases the strength of interaction, there is a crossover to a sub-linear dependence of the mass (m) on B [103]. In particular, right at $V/t = 0.75$, we find the best overall $\sqrt{B}$ fit of the mass to the magnetic field. We therefore designate that interaction to be the critical interaction $(V/t)_C$ at $B = 0$. When we computed the ratio of the first LL energy to the interaction induced gap (m) at $V/t = 0.75$, it came out to be a universal number (C) ≈ 6.21, independent of the magnetic field B (inset Fig. [5.3]). The value of the number is in satisfactory agreement with the same quantity previously calculated in the continuum description and in the large-N limit [103]. There we obtained $C = 5.985$, with the difference between the two values that can be attributed to the finite size (Inset Fig. [5.3]).

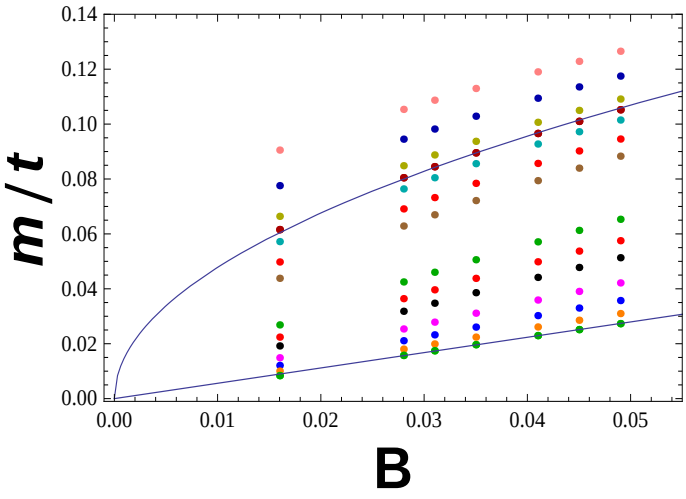

Figure 5.7: OP (δ_R or m) as a function of Φ/Φ_0 or B/B_0 at different V/t. The top points corresponds to $V/t = 0.8$ and the remaining ones to $V/t = 0.78, 0.76, 0.75, 0.74, 0.72, 0.7, 0.6, 0.55, 0.5, 0.4, 0.3, 0.2, 0.1$ from top to bottom. For $V/t = 0.75$ we found the best $\sqrt{B}$ fit of the mass with magnetic field. Figure reprinted with permission from B. Roy et. al., [135]. Copyright 2011 by the American Physical Society.

We also found a similar dependence of the mass on interactions and magnetic fields, computed on a quasi-circular lattice with open boundary, preserving the C_6 symmetry of a hexagon. A spatial variation of the interaction induced gap in the presence of a uniform magnetic field is shown in Fig. [5.8] (black curves). In that case, we found the ratio of the first LL energy to the interaction induced gap (C) to be 6.29, in a system of 384 lattice points. Such a particular choice of lattice turns out to be useful when one imposes rotationally symmetric inhomogeneous magnetic field. By considering a graphene sheet with open boundary, we computed the OP in two different gauges, equivalent to $A = (0, Bx)$ and $A = (-By, 0)$ and it turned out to be gauge independent, as expected.

5.5 Interacting fermions in inhomogeneous field

Next, we consider spinless interacting fermions on a honeycomb lattice subject to a inhomogeneous magnetic field in more detail. It was previously shown that, for a specific realization of the inhomogeneous magnetic field and in the limit of a large magnetic flux, the order parameter in the insulating phase computed within the zero-energy manifold matches exactly the local profile of the magnetic field [119]. Here we determine the order parameter self-consistently (at $T = 0$) and on the honeycomb lattice, and include the contributions from all the states into account. We will consider two specific configurations of spatially modulated magnetic field. (a) Localized field in one direction, y in our case, but extended in the orthogonal direction, and (b) rotationally symmetric localized field with the maximum strength at the center. We imposed the field of type (a) on a lattice with a periodic boundary in x direction. On the other hand, a quasi-circular lattice with open boundary, preserving the C_6 symmetry of a hexagon, is exposed to a localized field of type (b). As mentioned previously, even in presence of a non-uniform field, there is a large (and in the continuum limit, infinite) DOS at zero energy. Therefore, right at the filling one half, one expects that even a weak interaction can place the system into a insulating phase.

In the presence of a non-uniform field, but with a finite total magnetic flux, the system develops a gap in the spectrum even at sub-critical interactions ($V/t \ll (V/t)_c$) (Fig. [5.5]). The spatially variation of the order parameter (δ_R) in the presence of a inhomogeneous magnetic field of type (a) is depicted in Fig. [5.9]. We considered the OP only far from the edges of the system, and normalized the OP as well the magnetic fields with respect to their maximum values at the center of the system. The order parameter appears to follow the spatial profile of the magnetic field, and to depend on its local strength for $V/t < (V/t)_c$. Near the zero-field criticality the profile of the OP follows the magnetic field's more closely, whereas at large interactions the effect of inhomogeneous magnetic field becomes irrelevant, leading to uniform condensation. In Fig. [5.8] (red curves), we exhibit the spatial distribution of the OP in presence of a non-uniform magnetic field, applied on a lattice that preserves the C_6 symmetry of a hexagon. Our computation yields an interaction induced OP as a function of space qualitatively similar to the assumed profile of the magnetic field itself.

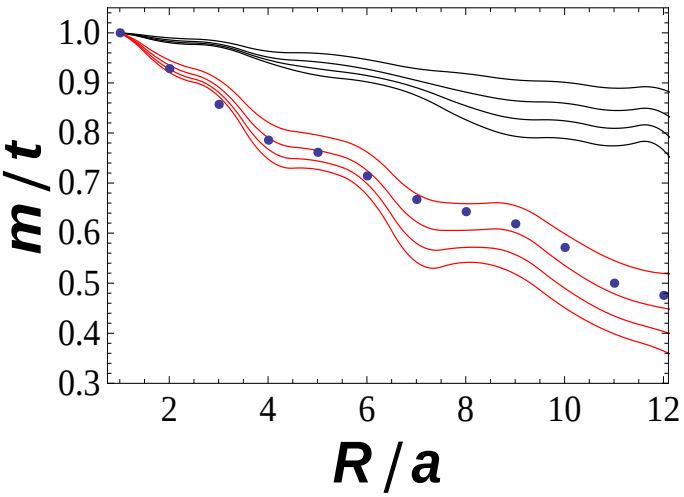

Figure 5.8: Normalized OP in presence of a uniform (black) and a non-uniform (red) magnetic field for different values of V/t. From top to bottom V/t reads $0.6, 0.5, 0.4, 0.3$. For the inhomogeneous field the total flux through the system is $\Phi_{total} = 7.1\Phi_0$. The blue dots correspond to the local strength of the inhomogeneous magnetic field. Figure reprinted with permission from B. Roy et. al., [135]. Copyright 2011 by the American Physical Society.

Let us now turn to functional dependence of the OP on the magnetic field and interaction, when the former is space dependent. At sufficiently weak interactions, the size of the gap at different region of the bulk of the system varies almost precisely linearly with the *local* strength of magnetic field. The linear dependence of the local OP at $V/t = 0.05(\ll (V/t)_c)$ with the local magnetic field is shown in Fig. [5.10]. As the interaction is increased there is a crossover to a sub-linear dependence of the mass on the local magnetic field. This situation is quite similar to the one in presence of a uniform field. Right at the zero-field criticality ($V/t = 0.75$), the local OPs in the entire bulk of the system varies as $\sqrt{B}$, independent of the position (blue dots in Fig. [5.3]). This suggests that the OP in the insulating phase may be a universal function of the *local* magnetic field, independent of its spatial distribution.

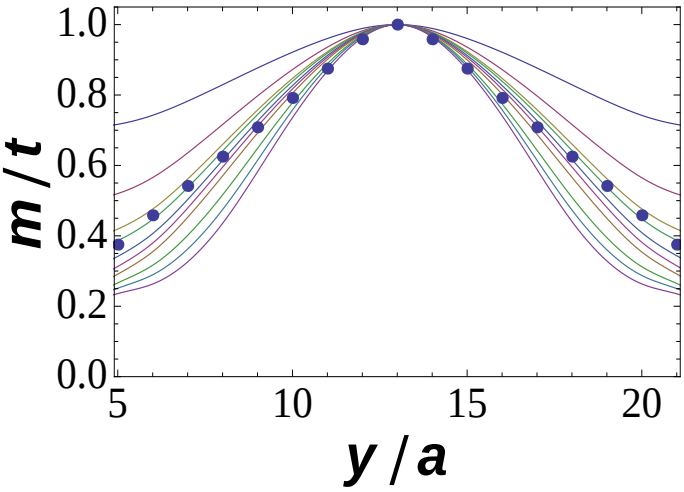

Figure 5.9: Normalized OP in presence of inhomogeneous magnetic field at $\Phi_{total} = 9.86\Phi_0$. Average magnetic field at different rows is denoted by the dots. V/t reads $0.75, 0.65, 0.55, 0.5, 0.4, 0.3, 0.2, 0.1, 0.05, 0.01$ from top to bottom. The blue dots corresponds to the local strength of the inhomogeneous magnetic field. Figure reprinted with permission from B. Roy et. al., [135]. Copyright 2011 by the American Physical Society.

5.6 Summary and Discussion

In the present work we systematically studied magnetic catalysis for spinless interacting electrons on a honeycomb lattice of finite extension, both for uniform and spatially modulated magnetic fields. In presence of the magnetic field, either uniform or non-uniform, the semimetal-insulator transition takes place at weak interaction in a large system. We here considered only the nearest-neighbor component (V) of the Coulomb interaction, and omitted its long-ranged ($\sim 1/r$) tail [18, **?**] for simplicity. We computed the self-consistent Hartree solution of the interaction-induced gap while keeping the system at filling one half and presented the scaling behavior of the interaction-induced order parameter (or a gap (m)) with the magnetic field and interaction, at $T = 0$. At weak interaction we observed a linear variation of the interaction induced local OP with the local magnetic field. With increase in the strength of the interaction we find a crossover from linear to a sub-linear dependence of the mass on the local magnetic field. A perfect $\sqrt{B}$ dependence of the OP emerges when the system is tuned to be precisely at the zero-field criticality, which we identified to be at $V/t = 0.75$. This is close to the value found analytically [83].

In our analysis we have considered only the nearest-neighbour hopping amplitude t, while neglecting the next-nearest-neighbour hopping t', which in graphene, for example, is finite but rather small. The main effect of a finite t' is the violation of the perfect particle-hole symmetry of the free electron spectrum. On the basis of continuum theory we expect, however, that the inclusion of t' would not change our results in a significant way, once the chemical potential is adjusted so that the central (formerly zero-energy) LL is half filled. A more detailed analysis is left for future study.

If we were to restore the spin of electrons, we would need to include a finite on-site Hubbard interaction as well. In absence of a magnetic field, an anti-ferromagnetic (AF) ground state is energetically favored for a large on-site Hubbard interaction when the chemical potential is at the Dirac point [9, 80]. The presence of magnetic field stabilizes such a ground state even at an infinitesimal on-site interaction (U) [95, 81, 123]. [1] We therefore expect that the system would develop a local expectation value of the N*é*el order parameter when in a inhomogeneous magnetic field, if $U \gg V$. If $V \gg U$, on the other hand, the system would decrease the energy more by forming a charge density wave (CDW) order of the type we considered here. At zero magnetic field the two quantum phase transitions belong to distinct Gross-Neveu universality classes [56, 124]. AF order, in contrast to the CDW breaks the spin rotational symmetry. In the ordered phase there will be two soft modes and one massive mode. Therefore, at finite temperature there will be no long ranged order in the AF phase, but only a crossover from semimetal to AF phase when the correlation length reaches the sample extension. A scaling behavior in a similar model has also been studied recently in presence of both real and pseudo magnetic fields [125]. We will discuss this issue in Chapter in detail.

5.7 Supplementary information

During the discussion of inhomogeneous magnetic catalysis on the honeycomb lattice we presented the spatial variation of the order parameter for only one particular flux enclosed

[1] About the possible appearance of a spin-liquid phase at an intermediate strength of Hubbard U see Ref. [123].

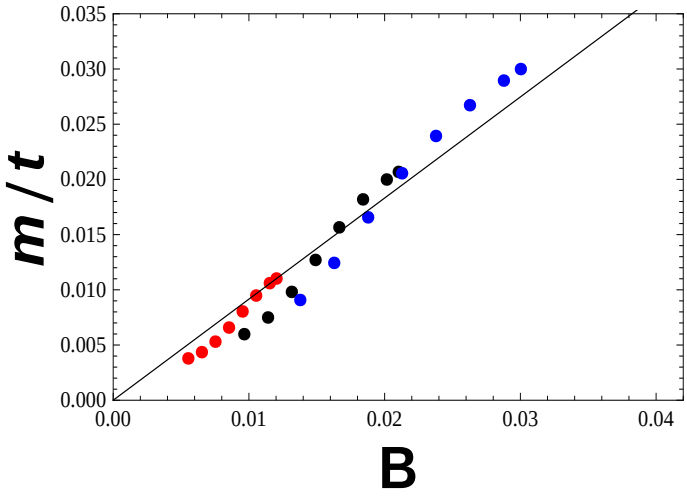

Figure 5.10: The scaling of the local OP with local magnetic field (measured in units of B_0) at $V/t = 0.05$ at various values of the total flux. Red, black and blue dots correspond to $\Phi_{total} = 5.86\Phi_0, 10.14\Phi_0$ and $14.6\Phi_0$, respectively. Different dots of the same color signify local OP at various positions in the bulk. Figure reprinted with permission from B. Roy et. al., [135]. Copyright 2011 by the American Physical Society.

by the system. However, we analyzed the distribution of the order parameter in presence of a inhomogeneous field, with different total flux enclosed by the system. Here we take the opportunity to present the same family of curves at various bell shaped localized fluxes on the honeycomb lattice with cylindrical boundary, with the maximum magnetic field strength at the center in Fig. 5.11 to Fig. 5.13. Similar quantities computed on a quasi circular lattice, in the presence of a rotationally symmetric inhomogeneous flux with a maximum strength at the center of the system is shown in Fig. 5.14.

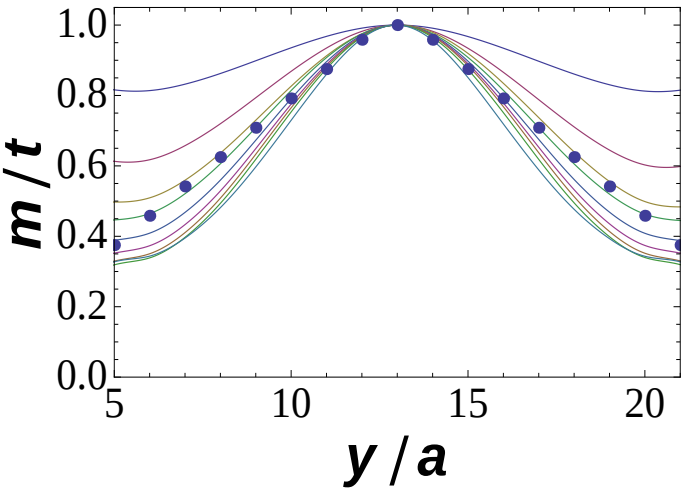

Figure 5.11: Normalized OP in the presence of an inhomogeneous magnetic field at $\Phi_{total} = 5.6\Phi_0$. The average magnetic field at different rows is denoted by the dots. V/t reads $0.75, 0.65, 0.55, 0.5, 0.4, 0.3, 0.2, 0.1, 0.05$ from top to bottom. The blue dots correspond to the local strength of the inhomogeneous magnetic field.

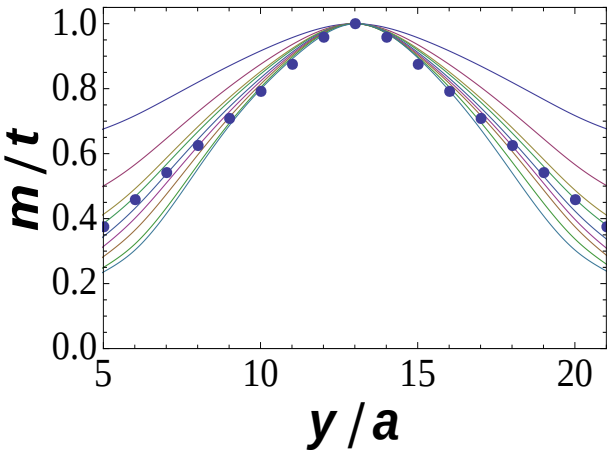

Figure 5.12: Normalized OP in the presence of an inhomogeneous magnetic field at $\Phi_{total} = 14.04\Phi_0$. The average magnetic field at different rows is denoted by the dots. V/t reads $0.75, 0.65, 0.55, 0.5, 0.4, 0.3, 0.2, 0.1, 0.05$ from top to bottom. The blue dots correspond to the local strength of the inhomogeneous magnetic field.

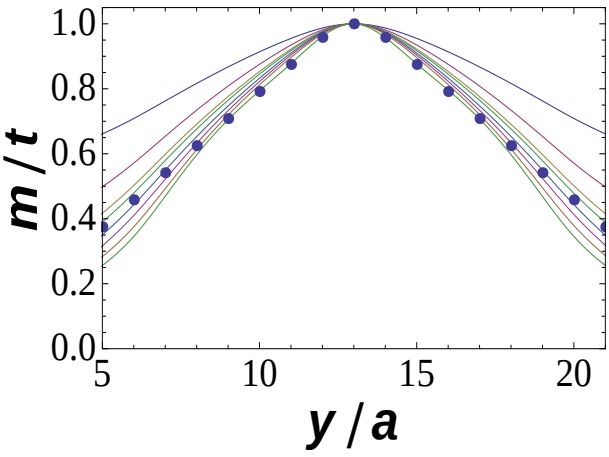

Figure 5.13: Normalized OP in the presence of an inhomogeneous magnetic field at $\Phi_{total} = 16.484\Phi_0$. The average magnetic field at different rows is denoted by the dots. V/t reads $0.75, 0.65, 0.55, 0.5, 0.4, 0.3, 0.2, 0.1$ from top to bottom. The blue dots correspond to the local strength of the inhomogeneous magnetic field.

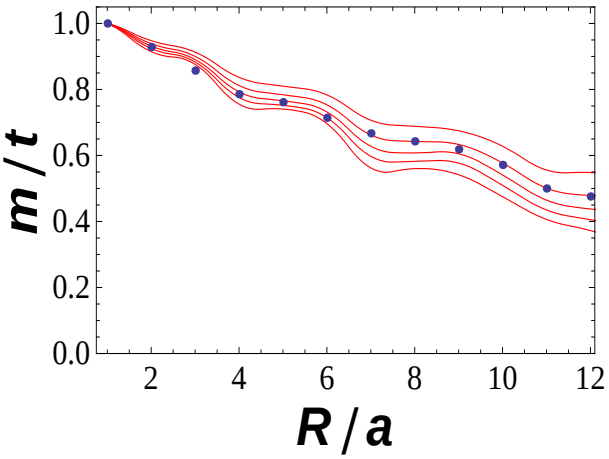

Figure 5.14: Normalized OP in the presence of a uniform (black) and a non-uniform (red) magnetic field for different values of V/t. From top to bottom V/t reads $0.6, 0.5, 0.4, 0.3, 0.2$. For the inhomogeneous field the total flux through the system is $\Phi_{total} = 10.0\Phi_0$. The blue dots correspond to the local strength of the inhomogeneous magnetic field.

Chapter 6

Pseudo Magnetic catalysis

Previous chapters were concerned with the behaviour of interacting electrons on the honeycomb lattice at and near filling one half, in the absence and presence of a magnetic field, which can be either uniform or nonuniform. Our study showed that fermions in graphene can find themselves in variety of insulating or superconducting ground states, depending on the relative strength of finite ranged repulsive or attractive Coulomb interactions. When the chemical potential coincides with the charge-neutral point, a finite strength of the interactions is necessary to drive the system out of the semi-metal ground state into an ordered phase, due to the vanishing density of states at the Fermi energy. The ordered phases lack some particular discrete or continuous symmetry of the free electron system. In the presence of a real magnetic field, the kinetic energy is completely quenched by developing a set of Landau levels with macroscopic density of states at well separated energies. The spectrum, however, still retains the particle-hole symmetry with a Landau level forming at vanishing energy. Therefore, in the presence of a magnetic field, the system can develop a chiral symmetry breaking gap, even at an infinitesimal onsite or nearest neighbour interaction, when only half of the band is filled. Yet another class of gauge potential may arise in graphene from specific deformations of the flake, which preserves the time reversal symmetry but breaks the chiral symmetry, in contrary to the real gauge field. A random distribution of such gauge fields have been realized in graphene due to ripples existing on the graphene flake, arising partially due to the strain induced by the SiO_2 substrate. Nevertheless, a finite flux of such fictitious gauge fields may bring a macroscopic number of states at zero energy, and may catalyze the formation of a time reversal symmetry breaking

order. In this chapter, we will show using analytical and numerical methods that the insulating phase lacking in time reversal symmetry can be realized even at a sufficiently weak second nearest-neighbour repulsion, upon introducing a specific strain on the graphene flake.

6.1 Introduction

Even though graphene is an arrangement of carbon atoms in a two dimensional honeycomb lattice, ripples are unavoidably present. In a long wavelength limit, one can capture its effect in terms of fictitious gauge potentials. A crude estimation yields the strength of fictitious gauge field ~ 1 T, produced by a single wrinkle in graphene sheet [126]. In a normal graphene flake, such ripples are randomly distributed giving zero net flux of the pseudo magnetic field. However the ripples play a crucial role in the low energy conductivity of graphene [31]. On the other hand, specific corrugation can give rise to a finite pseudo magnetic field [117]. In a recent experiment, such a deformation was produced by depositing graphene on a metallic substrate, e.g. platinum, at relatively high temperature (~ 800 K) and followed by cooling the system. Due to a mismatch in compressibility between the substrate and graphene, the latter experiences a strain. Such strain leads to bulging of the flake, giving rise to a finite *uniform* pseudo magnetic field of strength ~ 350 T [118]. The Landau level quantization of the energy spectrum (particularly the one at zero energy) has been confirmed in the presence of the fictitious gauge field. The existence of the zeroth Landau level may take the half filled system into an ordered phase, which lacks time reversal symmetry at weak interactions among the fermions residing at the next nearest-neighbour sites of the honeycomb lattice. During the rest of the chapter we will present some aspects of the interacting fermions, when a finite fictitious field penetrates the system. In particular we will focus on the nature of the ordered phase and the scaling of the interaction induced gap.

The underlying catalysis mechanism in the presence of either real or pseudo magnetic field is the same. Only half of the zeroth Landau level being filled and associated with distinct eigenvalues of some particular mass matrix may place the system in an ordered phase at weak interactions. The character of the electronic ground state, however, differs depending on the gauge fields. The nature of the catalyzed order parameter is dictated by

the zeroth Landau level only, as shown in Chapter 4. We will try to make an educated guess about the order parameter first formulating the problem in the continuum limit. During our study, we establish an excellent agreement among the observable quantities such as the gap sizes and its scaling with the field strengths computed in the field theoretic description and on a finite size honeycomb lattice. The order parameter giving rise to a gap in the quasi-particle spectrum however breaks the time reversal symmetry. On graphene, such a phase is associated with a current connecting the sites on same sublattice. The circulating Haldane current is therefore computed self consistently at Hartree level, at weak interactions. A finite order parameter exists even at sufficiently weak interaction, while varying linearly with the field. As the interaction acquires strength, the gap scales sublinearly with field, followed by a perfect square root dependence at zero field semimetal-insulator quantum criticality. In the presence of finite, but inhomogeneous pseudo flux, the order parameter is found to develop only in the vicinity of the regime where the field is localized. Taking into account finite size effects, the results are found to be in good accordance with ones computed in the continuum limit.

6.2 Landau levels in pseudo magnetic field

Let us start with a collection of free fermions (and for simplicity spinless) and try to gain some insight about the behaviour of interacting fermions in the presence of a fictitious gauge potential. Restricting ourselves only to nearest-neighbour hopping, the tight binding Hamiltonian takes the usual form

$$H_t = t \sum_{\langle \vec{x}, \vec{y} \rangle} u^\dagger(\vec{x}) v(\vec{y}) + H.c. \tag{6.1}$$

$u(\vec{x})$ and $v(\vec{y})$ are the fermionic operators on the two triangular sub-lattices A and B of the honeycomb lattice respectively. In the low energy limit, only the Fourier modes in the vicinity of the two inequivalent Dirac points at the corners of the first Brillouin Zone are of dynamical importance. In the continuum approximation, such excitations can be described in terms of massless chiral Dirac fermions when the chemical potential coincides with the apex of the doubly degenerate conical bands. Let us construct a $4-$ component Dirac fermion as

$$\Psi^\top(\vec{q}) = (u(\vec{K}+\vec{q}), v(\vec{K}+\vec{q}), u(-\vec{K}+\vec{q}), v(-\vec{K}+\vec{q})), \tag{6.2}$$

where $\pm\vec{K} = \pm(1, 1/\sqrt{3})(2\pi/a\sqrt{3})$ are the Dirac points. In this representation, the tight binding Hamiltonian takes the following form

$$H_t = \sum_q \Psi^\dagger(\vec{q}) H_D \Psi(\vec{q}) \; + \; \sum_q \Psi^\dagger(\vec{q}) \left(O(q^2)\right) \Psi(\vec{q}), \tag{6.3}$$

in first quantization, with H_D the Dirac Hamiltonian in two spatial dimensions

$$H_D = v_F i\gamma_0\gamma_i q_i. \tag{6.4}$$

Here the four-component anticommuting Hermitian gamma matrices belong to the 'graphene' representation, $\gamma_0 = \sigma_0 \otimes \sigma_3, \gamma_1 = \sigma_3 \otimes \sigma_2, \gamma_2 = \sigma_0 \otimes \sigma_1$. The remaining two gamma matrices can be defined as $\gamma_3 = \sigma_1 \otimes \sigma_2$, and $\gamma_5 = \sigma_2 \otimes \sigma_2$. Summation over the repeated space indices is assumed. Hereafter we set the Fermi velocity $v_F = \sqrt{3}ta/2$, as well as $\hbar$ and the electronic charge (e) to unity [9, 80].

One can study the orbital effect of the pseudo magnetic field by writing the Dirac Hamiltonian in the presence of a general pseudo vector potential as

$$H[a] = i\gamma_0\gamma_i(q_i - a_i). \tag{6.5}$$

Here, a_i is a member of the general $SU(2)$ gauge field

$$a_i = a_i^3\gamma_3 + a_i^5\gamma_5 + a_i^{35}\gamma_{35}, \tag{6.6}$$

where $\gamma_{35} = -i\gamma_3\gamma_5 = -\sigma_3 \otimes I_2$. It is worth noticing that the Hamiltonian $H[a]$ respects time reversal symmetry (TRS). The time reversal symmetry is represented by an anti-unitary operator $I_t = U_t K$, where U_t is unitary and K is complex conjugation. In the graphene representation, $U_k = i\gamma_1\gamma_5 = \sigma_1 \otimes I_2$. Assuming that the corrugation of the graphene flake is smooth, one is at the liberty to omit any valley mixing, which leaves us with only one of the components (namely a^{35}) of a general gauge field. Note that the gauge potential proportional to γ_{35} couples with opposite signs at the two Dirac points and hence respects time reversal symmetry. In contrary to a real gauge potential, which violates the time reversal symmetry, the pseudo vector potential breaks the low energy emergent chiral $SU_c(2)$ symmetry (CS) of the free Dirac Hamiltonian H_D. In $2-$ dimensions the chiral symmetry for spinless fermions is generated by $\{\gamma_3, \gamma_5, \gamma_{35}\}$ and a finite a_i^{35} leaves the Hamiltonian with only a $U_c(1)$ invariance generated by γ_{35}. These two symmetries will play a crucial

role when we discuss the electron-electron interaction and spontaneous generation of mass.

Next we study the free electron spectrum when a finite flux of pseudo field penetrates the honeycomb lattice. In light of previous studies, it is easy to appreciate that the energy spectrum is comprised of a set of Landau levels, living at well-separated energies $\sqrt{2nb}$, for $n = 0, 1, 2, \cdots$, where $\vec{b} = \vec{\bigtriangledown} \times \vec{a}^{35}$ is the pseudo magnetic field, which is uniform. Landau levels at finite energy are still enriched by valley degeneracy, and quite similar to those in the presence of a real magnetic field. To obtain the spectrum, let us define an auxiliary Hamiltonian similar to the one defined in Chapter 3,

$$\tilde{H}_0 = i\gamma_0\gamma_i D_i, \tag{6.7}$$

but with a slightly different definition of the covariant derivative, $D_i = q_i - \gamma_{35} a_i^{35}$. Squaring the Hamiltonian one finds

$$\tilde{H_0}^2 = D_i^2 - (I_2 \otimes \sigma_3)\, b. \tag{6.8}$$

Eigenstates at $E_n = \sqrt{2nb}$ read as

$$\Psi^K_{n,+} = \begin{pmatrix} \phi_n \\ -\phi_{n-1} \\ 0 \\ 0 \end{pmatrix} \quad \text{and} \quad \Psi^{-K}_{n,+} = \begin{pmatrix} 0 \\ 0 \\ \phi_{n-1} \\ -\phi_n \end{pmatrix}, \tag{6.9}$$

and for $E_n = -\sqrt{2nb}$

$$\Psi^K_{n,-} = \begin{pmatrix} \phi_n \\ \phi_{n-1} \\ 0 \\ 0 \end{pmatrix} \quad \text{and} \quad \Psi^{-K}_{n,-} = \begin{pmatrix} 0 \\ 0 \\ \phi_n \\ \phi_{n-1} \end{pmatrix}. \tag{6.10}$$

Each of these Landau levels has $\Omega b/\pi$ state, Ω being the area of the sample. However, the zeroth Landau levels are different from those in presence of ordinary magnetic field and they read as

$$\Psi^K_0 = \begin{pmatrix} \phi_0 \\ 0 \\ 0 \\ 0 \end{pmatrix} \quad \text{and} \quad \Psi^{-K}_0 = \begin{pmatrix} 0 \\ 0 \\ \phi_0 \\ 0 \end{pmatrix}, \tag{6.11}$$

with degeneracy $b/2\pi$ per unit area for each set of the zero energy states. Hence, both sets of zeroth Landau level live on the same sub-lattice, A, whereas those living on the other sub-lattice (B) are not normalizable. Therefore, they appear on the boundary of a finite size system. We will confirm this shortly, when we discuss the zeroth Landau level on a finite size honeycomb lattice.

Let us now add $i\gamma_1\gamma_2 m$ to the auxiliary Hamiltonian. This term violates TRS and corresponds to circulating current among the sites on the same sublattice. The energy spectrum of the new auxiliary Hamiltonian

$$\tilde{H_0} = i\gamma_1\gamma_2 D_i + mi\gamma_1\gamma_2 \tag{6.12}$$

is as follows. For $n \neq 0$, particle and hole Landau levels are mixed and eigenstates are placed at $\pm\sqrt{2nb + m^2}$, with degeneracy b/π per unit area. The energy spectrum for $n \neq 0$ is similar to that in a real magnetic field. However, the states in zeroth Landau level, Ψ_0^K and Ψ_0^{-K} are eigenstates of $i\gamma_1\gamma_2$, with eigenvalues $+1$ and -1 respectively. If such a time reversal symmetry breaking mass term arises from interactions, the zeroth Landau level splits, leading the system to an ordered phase even at sufficiently weak interactions. From our previous studies, the reader may convince themselves that such a mass term can be generated from next nearest-neighbour interactions, upon decomposing it in the particle-hole channel via a Hubbard-Stratonovich transformation. Unlike the catalysis scenario in the presence of a real magnetic field, the Hermitian γ_0 matrix acts like an *identity* matrix, thus cannot be catalyzed while keeping the system at charge neutrality. The effect of such mass term will be discussed in detail later. The underlying mechanism being the same, it is interesting but may be not entirely unexpected that the scaling behavior of such TRS breaking order with the strength of second neighbour interactions and magnetic field is identical to that for a CS breaking mass with nearest-neighbour interactions, and real magnetic field [43].

6.3 Pseudo magnetic field on a lattice

We first develop a formalism to impose a finite pseudo magnetic flux through the system. Notice that $H[a]$ in Eq. 6.5, with only non-vanishing a_i^{35} component, can be also written as

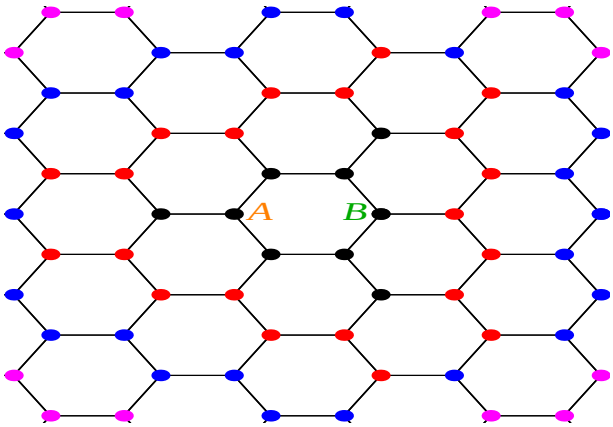

Figure 6.1: Phase configuration attached to each site of the honeycomb lattice. The phase increases its value towards the edge. Therefore the black dots corresponds to the minimum of the phase. Then it reads as red, blue, magenta in increasing order. When we modulate the hopping integrals according to $t_{\alpha\beta} = e^{\chi(\alpha)} t^{(0)}_{\alpha\beta} e^{-\chi(\beta)}$, a finite flux of pseudo magnetic field is introduced. It is evident that such a deformed lattice is only invariant under a C_3 symmetry.

[127]

$$H[a] = i\gamma_0\gamma_i(q_i - \gamma_{35}a_i) = e^{\chi(\vec{x})\gamma_0} H[0] e^{\chi(\vec{x})\gamma_0}, \tag{6.13}$$

where $H[0] \equiv H_D$. Note that γ_0 assigns a $+1$ eigenvalue on the A sub-lattice and -1 on the B sub-lattice. Therefore a finite pseudo flux can be incorporated by making the following substitution in the nearest-neighbour hopping amplitude [128]

$$t_{\alpha\beta} = e^{\chi(\alpha)} t^{(0)}_{\alpha\beta} e^{-\chi(\beta)}, \tag{6.14}$$

where $\alpha \in A$ and $\beta \in B$ and $t^{(0)}_{\alpha\beta}$ is the underlying uniform hopping. We assume $\chi(\vec{x})$ to be a function of radial co-ordinate only, thus $\chi(\vec{x}) = \chi(r)$. Consequently, the hopping amplitudes will be modulated only along the bonds that are oriented radially outward from the center of the system. Next we assign a phase to each of the lattice points, with a restriction that at any particular distance from the center $\chi(A) > \chi(B)$. One particular way to assign the phases is shown in Fig. 6.1. Once the phases are assigned according to the prescribed scheme, the system no longer has the C_6 symmetry of a honeycomb plaquette. It rather enjoys a reduced C_3 symmetry. Upon deforming the nearest-neighbour hopping amplitude in this scheme, the system experiences a vector potential, $\vec{A} = (A_r, A_\phi) = \left(0, \frac{\partial\chi(r)}{\partial r}\right)$ and

the concomitant flux enclosed by the system is

$$\Phi_{encl} = \oint \vec{A} \cdot \vec{dl} = \frac{\partial \chi(\vec{r})}{\partial r}|_{r=R} R\ \Phi_0, \tag{6.15}$$

where $\Phi_0 = h/e$ is the flux quanta. Unlike the real magnetic field, which can be implemented on a lattice via Peierls substitution (Chapter 4), a finite flux of the pseudo magnetic field is introduced to the system through a modulation of the hopping amplitudes, while they remain real. Therefore, the time reversal symmetry is preserved, when $\Phi_{encl} \neq 0$. Depending on the variation of $\chi(r)$ with radial distance (r), one can implement various profiles of the pseudo flux. For example, choosing $\chi(r) \propto r^2$ yields a flux enclosed by the system being proportional to its area, yielding a uniform magnetic field. A localized pseudo flux, on the other other hand, can be realized by taking $\chi(r) \propto \ln(r)$.

6.4 Zero energy states

In the continuum description, the normalizable states in the zeroth Landau level are localized on one sublattice in the presence of a fictitious magnetic field. Here we numerically diagonalize the free Hamiltonian with finite pseudo magnetic fields and show that near zero energy modes on A-sublattice reside in the bulk, whereas those on the B-sublattice can only be found near the boundary of finite systems. States in the zeroth Landau level can be represented as

$$\Psi_{0,n}\left[a\right](\vec{x}) \propto e^{-\Phi(\vec{x})\gamma_0} \Psi_{0,n}\left[0\right](\vec{x}). \tag{6.16}$$

This correspondence implies that the normalizable zero energy states, are associated with $+1$ eigenvalue of γ_0. In the 'graphene' representation $\gamma_0 = I_2 \otimes \sigma_3$. Hence, the normalizable zero energy modes live on the A sub-lattice. The other set of zero energy modes accompanied by a -1 eigenvalue of γ_0 are not normalizable in the thermodynamic limit since their normalization constant grows with the size of the system. Therefore in a finite size system, under consideration here, these states reside near the edge of the system. In stark contrast to this situation, the normalizable zero energy states in a real field are equally populated among both the sub-lattices. Numerically diagonalizing the free Hamiltonian on a 2400 site lattice, with hoppings modified according to Eq. [6.14] we registered the following features:

1. Even when a uniform pseudo magnetic field is implemented by setting $\chi(r) \propto r^2$, we could not see any Landau level quantization. However, there exists a spike in the density of states near zero energy.

2. Relaxing the condition of uniformity of the field, we found a discontinuity in the density of states near zero energy.

3. The number of zero energy states in both cases is found to be proportional to the total flux enclosed by the system.

4. The probability amplitude of the zero energy states on A sub-lattice found to be localized in the bulk, whereas that on the B sub-lattice exists near the edge of the system.

These observations confirm that the specific deformation of the lattice, implemented here, indeed imposed a finite pseudo flux in the system. Characteristics of the zero energy states are also in accord with the continuum calculation [129].

6.5 Electron-Electron interaction

So far we focused on the behaviour of non-interacting fermions on the honeycomb lattice in the presence of a background pseudo magnetic flux. Besides their free motion, fermions in the quasi two dimensional system built of carbon atoms interact via Coulomb interactions. Fermions in graphene may find themselves in a plethora of insulating phases. However, the exact nature of the ordered phase depends on the detail of the interactions at lattice scale. For example, a density wave of average charge may develop if the first neighbour interaction becomes sufficiently large ($V_{1c}/t \approx 1$) [9, 80]. The insulating phase develops a mass for the quasi-particle excitations by spontaneously breaking the CS. Yet another insulating phase may develop if the second neighbour component of the Coulomb repulsion (V_2) is strong enough [55]. A mean field calculation showed that for $V_2/t > 1.3$ [83], the ground state supports a finite current, circulating among the sites on same sub-lattice, thus breaks

the TRS. However, it propagates in opposite directions in two sub-lattices. This state is named as *quantum anomalous Hall insulator*. Beyond the mean field approximation, it is found that fluctuating massless Goldstone modes ultimately stabilize the *spin Hall insulator* (QSH) ground state, which however breaks the TRS for each spin component [38, 87]. The *two* soft modes arise from the spontaneous selection of the orientation of the spin axis of the QSH order parameter. As a consequence of the vanishing density of states at the Fermi level, the critical strength for insulation is *finite*. Due to the reduced dimensionality of the lattice, presence of finite magnetic field (either real or pseudo) brings a macroscopic number of states near zero energy and may also reduce the critical interaction down to zero. This mechanism of developing a mass is referred as *magnetic catalysis*.

First we will try to answer the following question: what is the nature of the interacting ground state when a pseudo field pierces through the system. This can be answered by studying the zero energy states, as shown previously. Here we would like to answer this question from slightly different perspective. The expectation value of of a traceless operator Q can be written as [1]

$$\langle q(\vec{x})\rangle = \frac{1}{2}\left(\sum_{occup} - \sum_{empty}\right)\Psi_E^\dagger(\vec{x})Q\Psi_E(\vec{x}), \tag{6.17}$$

where $\{\Psi_E(\vec{x})\}$ is the set of eigenstates for any Hamiltonian H. If there exists a unitary matrix T, that anti-commutes with H and commutes with Q, then, only the zero energy states contribute to the sum [20, 105]. For the Hamiltonian $H[a]$ in Eq. [6.5] , T can be chosen to be γ_0. Choosing $Q = \gamma_0$, one gets charge density wave (CDW) order. Within the zero energy sub-space of $H[a]$, γ_0 has only the eigenvalue $+1$. Thus the above sum vanishes. Hence CDW order cannot be catalyzed in presence of a pseudo flux. Formation of a CDW is associated with changing the chemical potential, as it acts like the *identity* matrix within the zero energy space and therefore may exist for $\nu = \pm 1$. In contrast, half of the zero energy states has $+1$ eigenvalue and the rest -1 for $i\gamma_1\gamma_2$. On the honeycomb lattice $i\gamma_1\gamma_2$ represents the Haldanes circulating current. Therefore, upon choosing $Q = i\gamma_1\gamma_2$, the above sum provides a non-zero expectation value of the Haldane order, which implies that a TRS breaking mass can be catalyzed in the presence of a finite pseudo flux. In Chapter 4, we found that in the presence of a real magnetic field CS breaking CDW ordering can

[1] See section 4.3 for the derivation

acquire a finite expectation value even at infinitesimal nearest-neighbour repulsion. Upon incorporating the spin degrees of freedom, an anti-ferromagnetic order can also develop if $U \gg V_1$ [9].

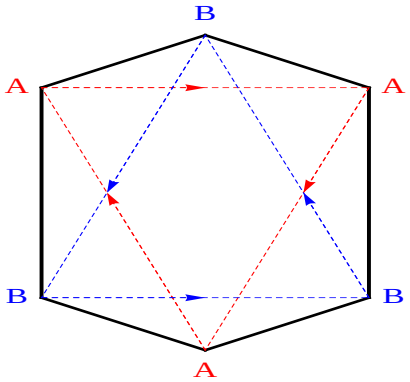

Figure 6.2: Time reversal symmetry breaking order in honeycomb the lattice.

Hereafter, we consider only the repulsive interaction among the fermions residing on the second neighbours of the honeycomb lattice. The interacting Hamiltonian for spinless fermions on the honeycomb lattice is

$$H_I[a] = H_t + V \sum_{\langle\langle \vec{x},\vec{y} \rangle\rangle} n(\vec{x})n(\vec{y}), \tag{6.18}$$

where $V > 0$, and $\langle\langle \dots \rangle\rangle$ stands for the sum over next nearest-neighbour sites. H_t stands for the free Hamiltonian with pseudo flux. After the usual Hartree decomposition one can write down the effective single particle Hamiltonian as

$$H_{HF} = H_t + \left(\sum_{\langle\langle i,j \rangle\rangle} \eta_{ij} c_j^\dagger c_i + H.c. \right), \tag{6.19}$$

where $\eta_{ij} = V\langle c_i^\dagger c_j \rangle$, corresponds to the Haldane circulating current, to be determined self consistently on a finite lattice.

First we set $\Phi_{encl} = 0$. Removing the pseudo flux from the system we thereafter searched for the self consistent solution of the Haldane current in a finite system of 600 lattice points

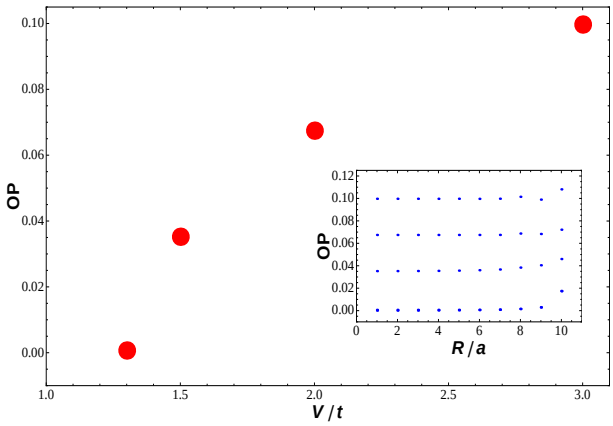

Figure 6.3: Variation of the Haldane current with interaction at zero field predicts that the critical interaction $V_c/t \approx 1.27$. Inset: Shows the variation of Haldane current in the entire system on both A or B sub-lattices at various interaction strength. V reads as $2.5, 2, 1.5, 1.3$ from top t bottom. The small spikes near the edge are solely due to finite size effects.

at various strengths of next nearest-neighbour repulsion. The self consistency is checked up to the 7th decimal place. A family of such curves is shown in the inset of Fig. 6.3. At very large interaction, the order parameter acquires a finite value both in the bulk and and at the edge of the system. As one enters the regime of weaker interactions, the size of the gap reduces both in the bulk and in the vicinity of the edge of the system. Below certain interaction strength, the gap vanishes everywhere. Just above that particular interaction, the order parameter achieves a slightly inhomogeneous expectation value everywhere in the system. We designate that interaction to be the critical interaction for insulation. This definition of the critical interaction will be used for remainder of the discussion. Such non analytic behaviour in a finite size system is an artifact of self-consistency of the solution. A similar behavior is also been reported in the presence of real magnetic field. It is evident from Fig. 6.3, second nearest-neighbour repulsion needs to be strong enough to open up a gap in the system and the critical interaction for insulation is found to be $V_c/t \approx 1.27$. This value is in very good agreement with the critical interaction found analytically [83].

The amplitudes of the Haldane current in this situation are equal on both the sub-lattices, but circulating in opposite directions. Apart from the uniform condensation in the bulk of the system, there are small spikes in the order parameter in the vicinity of the edge

of the system. Those spikes can be attributed to finite size effects, and upon analyzing the self consistent profile of the gap in a larger system, spikes are found to be localized only far from the bulk. Estimating the critical value of the interaction for the insulation, we now search for the insulating ground state when $V/t \ll V_c/t$, once pseudo flux penetrates the system.

6.6 Uniform pseudo magnetic field

Next, we study the role of the electron-electron interaction, living on next nearest-neighbour sites, in the presence of a uniform pseudo magnetic field, particularly when it is sub-critical, i.e., $V < V_c \approx 1.27\, t$. A spatially homogeneous field can be achieved by choosing $\chi(r) \propto r^2$. Upon exposing the system to a uniform field we numerically computed the self consistent solution of the Haldane current in the honeycomb lattice. A family of curves showing the typical spatial variation of the gap is presented in Fig. 6.4. The OP is computed on a quasi circular lattice of 600 points. The self consistent OP found to have only imaginary component even when the interaction strength is sufficiently small, hence breaks TRS. This result is in agreement with previous studies in the absence of a gauge field. A finite real component of the η_{ij}s would correspond to a shift of the Dirac points in energy.

Let us now discuss some features of the self consistent solutions of the OP. First of all, one can immediately notice from Fig. 6.4 that there exists a non-zero expectation value of the Haldane circulating current even when $V \ll V_c$. For small values of the interaction ($V/t \approx 0.5$) the OP on the 'A' sub-lattice develops in the bulk of the system whereas it is localized at the boundary of the system on the other sub-lattice (B). This behaviour can be explained from the fact that the zero energy states on the A sub-lattice are localized near the center of the system, whereas those on the other sub-lattice live near the boundary. For weak interactions, the size of the gap on the A sub-lattice is much bigger than that on the B sub-lattice. These observations are in clear accordance with the continuum calculation. In the bulk of the system ($R/a < 6$ in Fig. 6.4) the OP on the A sub-lattice is approximately uniform. However, the OP in the bulk on the B sub-lattice is negligibly small far from the edge, at weak interactions. As the interaction is strengthened, OP in the bulk on two sub-lattices starts to become comparable. At sufficiently large interactions the effect of the

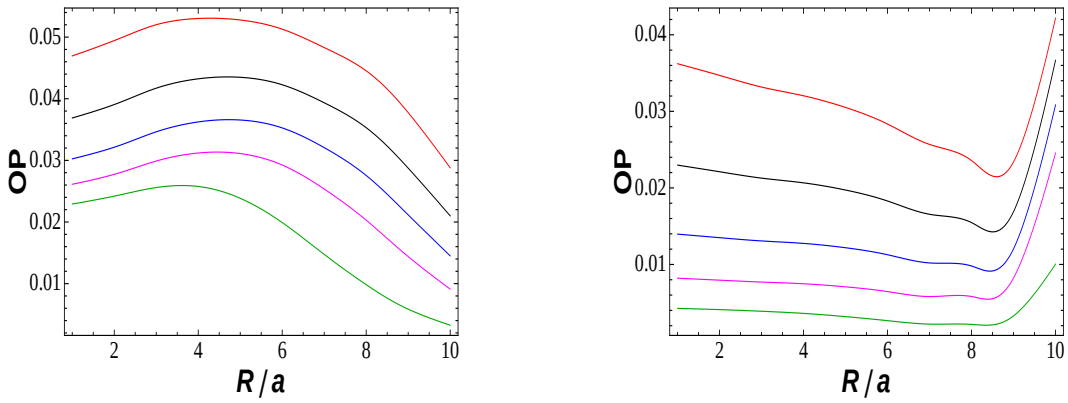

Figure 6.4: Self consistent solution of the Haldane current on a honeycomb lattice in the presence of a uniform magnetic field with $\Phi/\Phi_0 = 0.025$. Here $\Phi_0 = h/e$ is the flux quantum. The left figure shows the OP on the A sub-lattice, whereas the right one represents that on the B sub-lattice. The top curves correspond to the interaction $V = 1.5$ and the remaining ones to $V = 1.27(V_c), 1.0, 0.75, 0.5$ from top to bottom.

gauge potential becomes irrelevant and the amplitude of the Haldane currents are found to be equal on both sub-lattices, in the entire system.

Besides these features, the OP also preserves an additional symmetry, not discernible in Fig. 6.4. Upon exposing the system to a finite pseudo magnetic field, the lattice no longer respects the C_6 symmetry of a hexagon. It is evident from Fig. 6.1, the system then is only invariant under a C_3 symmetry. Being invariant under this symmetry, the next nearest neighbour electron-electron interaction is expected to give rise to a finite Haldane current with the requisite C_3 symmetry. The self consistent solution of the Haldane's current is indeed found to respect the C_3 symmetry.

Let us now turn to the scaling behaviour of the gap with interactions and the pseudo magnetic fields. Here we consider the OP on the A sub-lattice only. A set of OPs at various interaction and field strengths is shown in Fig. 6.5. The OP is conveniently averaged over the bulk ($R/a < 6$) of the system. At weak interactions the OP varies almost linear with the pseudo magnetic field (bottom curve in Fig. 6.5). As one enters the domain of stronger interaction, there is a cross over to a sub-linear dependence of the gap with the magnetic

field. Particularly at zero field criticality $V = V_c \approx 1.27$, it reverts to a perfect square root dependence on the magnetic field ($m \sim \sqrt{b}$). One might wish to spot the zero field quantum critical point from such square root scaling of the gap. Such scaling can also be confirmed from the linear variation of the square of the gap size with pseudo magnetic fields (Inset of Fig. 6.5). The scaling behaviour of the TRS breaking mass is exactly similar to the one for the CS breaking mass in the presence of a real magnetic field. The perfect $\sqrt{b}$ scaling of the gap happens to appear at zero field semimetal-insulator quantum criticality. For $V = 1.5 > V_c$ there is a non-vanishing gap even when there is no pseudo flux, as expected [103].

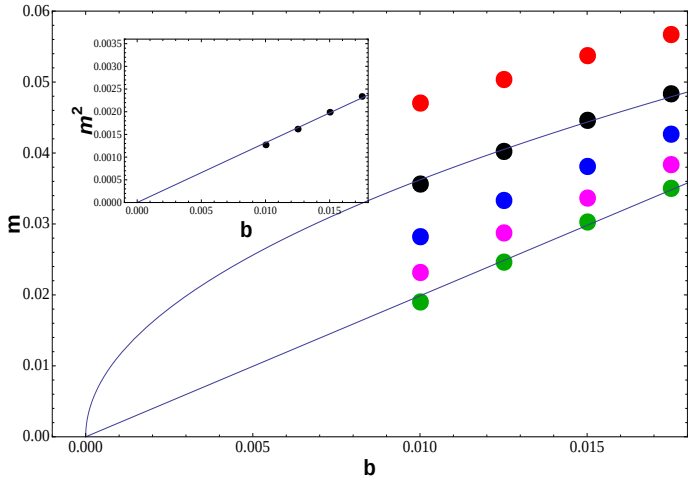

Figure 6.5: Mass is presented for various strength of interaction and pseudo magnetic field. The red dots correspond to $V = 1.5$. The black, blue, magenta,and the green dots stand for $V = 1.27, 1, 0.75, 0.5$ respectively. Inset: shows the variation of m^2 with b, revealing a excellent linear dependence among these two quantities at zero field criticality, $V/t \approx 1.27$.

6.7 Finite size effects in uniform condensation

In this section, we attempt to gain some insight about the finite size effects on the OP. It can been be seen in Fig. 6.4 that the OP on the A-sublattice is quite uniform in the bulk of the system ($R/a < 6$), but it decays as one proceeds towards the boundary. We found that such spatial modulation of the OP arises as a finite size effect and in the limit of large

system size the OP is expected to be uniformly distributed in the entire system. These finite size effects are shown in Fig. 6.6. Moreover, we found that the bulk OP on the B- sublattice achieves reduced expectation value upon increasing the system size and OP is localized in the edge of the system.

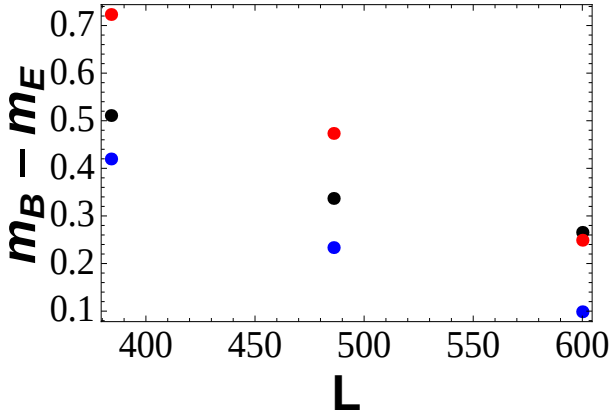

Figure 6.6: Difference in the OP in bulk (m_B) and edge (m_E) as function of system size. The red dots corresponds to $V = 1.27 \approx V_c$, whereas the black and the blue dots to $V = 1.0, 0.75$, respectively.

6.8 Inhomogeneous pseudo magnetic catalysis

Previously, we were concerned with the behaviour of interacting electrons in the presence of a *uniform* pseudo field. Let us now take the field to be *non-uniform* and bell-shaped, with its maximum strength near the center of the system. The motivation for studying such a configuration comes from the fact that a finite pseudo field can be produced by some specific deformation of the lattice, hence it is typically *inhomogeneous*. In the presence of finite non-uniform flux, there is a sharp peak in the density of states near zero energy, with the number of near zero energy states being proportional to the flux enclosed by the system. Due to the finite density of states near zero energy, the system is expected to develop a gap in the spectrum, even at sub-critical interactions, at filling one-half. Next we consider the effect of interactions among the fermions (spinless) living at the next nearest neighbour sites of the honeycomb lattice. To minimize finite size effects, we numerically compute the self consistent Hartree solution of the OP in a larger system, comprised of 726 lattice points.

The typical result is depicted in Fig. 6.7, with total pseudo flux $3\Phi_0$.

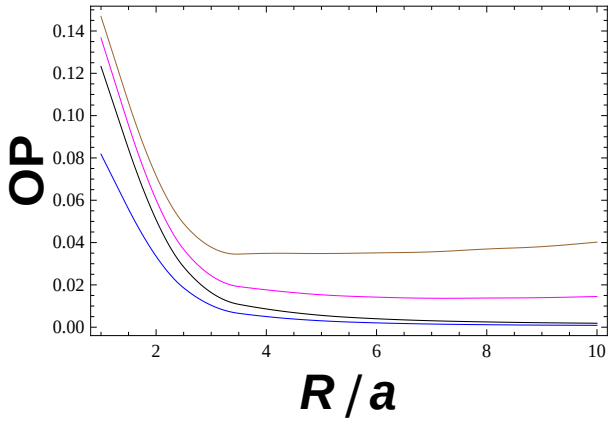

Figure 6.7: Mass is presented at various strength of interaction with $\Phi_{encl} = 7.85\Phi_0$. The red curve corresponds to $V = 1.5$. The magenta,black and the blue curve stand for $V = 1.27, 1, 0.75$ respectively.

As shown in Fig. 6.7, the gap develops mainly in the bulk of the system, at sub-critical interactions when an inhomogeneous magnetic field penetrates the system, accompanied by a rapidly decaying tail towards the edge. In the figure, we focused on the OP on the A-sublattice only. The behaviour of the OP on the other sublattice is found to be identical to that in the presence of homogeneous flux. The gap in the system mimics the profile of the pseudo magnetic field which in this case is localized near the center. The situation is quite similar to the one in the presence of localized real magnetic field, where the chiral symmetry breaking order is found to be proportional to the local strength of the magnetic field. At sufficiently weak interaction we found that the gap scales linearly with the flux enclosed by the system. Within the sub-critical range of interaction the size of the gap increases upon increasing the interaction, but mainly in the bulk. Whereas once the interaction is stronger than the zero field semimetal-insulator critical interaction, the OP starts to become comparable in the entire system (top curve in Fig. 6.7). Unless the interaction is overly strong, the OP in the bulk remains larger than that in the vicinity of edge. At sufficiently strong interaction, the signature of localized flux washes out, leading to a uniform condensation in the entire system. The Haldane current is found to be invariant under rotation by $2\pi/3$, as

in the presence of uniform flux.

It is worth mentioning that the self consistent solution of the OP at weak interactions is not purely imaginary, in contrast to the scenario in presence of uniform field. A finite real amplitude of the OP is found to persist up to the zero field critical point. However, it is always at least two orders of magnitude smaller than its imaginary component. Such real amplitudes count the shift of the Dirac points in energy. Shortly we will argue this behaviour can be attributed to a finite size effect. As one approaches zero field criticality, the real component of the OP gets smaller and is found to have only a trivial value beyond the criticality. The effect of finite extension of the system will be the subject of discussion in the next section.

6.9 Finite size effects in nonuniform condensation

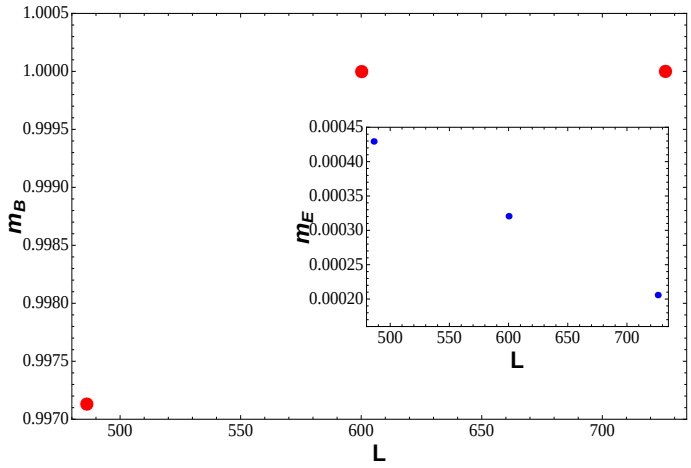

Figure 6.8: OP at the center of the system as a function of the system size, in the presence of localized flux. Here we normalized the OP with respect to the maximum one. The OP achieves the maximum value in a system of 726 lattice points. Inset: variation of the OP at the boundary with system size, in the presence of identical flux. It shows that as one approaches the thermodynamic limit the OP near the edge disappears, and hence the gap develops only in the bulk of the system.

As mentioned in the previous section, below the critical interaction at zero field the OP develops only on the A sub-lattice at the bulk of the system. Such spatial variation of the gap mimics the profile of the inhomogeneous field penetrating the system. This behaviour happens to be quite similar to that for CS breaking order in presence of localized flux of real magnetic field and is independent of the size of the system. First we would like to confirm that the OP saturates with respect to the size of the system. With the increasing size of the lattice, the gap in the spectrum increases and finally saturates in a large lattice, as shown in Fig. 6.8. From that figure, we can also confirm that in the system under consideration (726 lattice points), the OP saturates quite well to its thermodynamic limit. However, the same quantity, near the edge of the system, gradually disappears in a larger system. Hence in the thermodynamic limit a finite gap appears to exist only in the bulk of the system, following the profile of the flux.

Let us now focus on the variation of the real part of the self-consistent solution on the extension of system. Fig. 6.9 discerns that upon increasing the size of the system the real amplitude of the OP decreases in the bulk and near the edge of system as well. Hence it is expected that in the thermodynamic limit, the self consistent solution would be purely imaginary and hence break TRS.

6.10 Discussion and summary

To summarize we studied the behaviour of interacting fermions on the honeycomb lattice in presence of a pseudo magnetic field, which may arise from specific deformation of the graphene sheet. We pursued both analytical as well as numerical approaches to show that system finds itself in a ordered phase even at an infinitesimal next nearest neighbour interaction, upon exposing it to a finite pseudo flux. The ordered phase breaks the time reversal symmetry, at least when the fermions are spinless. Here we also present a scheme to introduce a finite flux of fictitious gauge field in a honeycomb lattice of finite extent. There we showed how one can implement the gauge field by some specific modulation of the nearest neighbour hopping amplitudes. Diagonalizing the free Hamiltonian with periodically modulated hoppings, on a sufficiently large lattice, we established a good agreement with the analytical predictions. The lattice, however loses the luxury of the C_6 symmetry of the

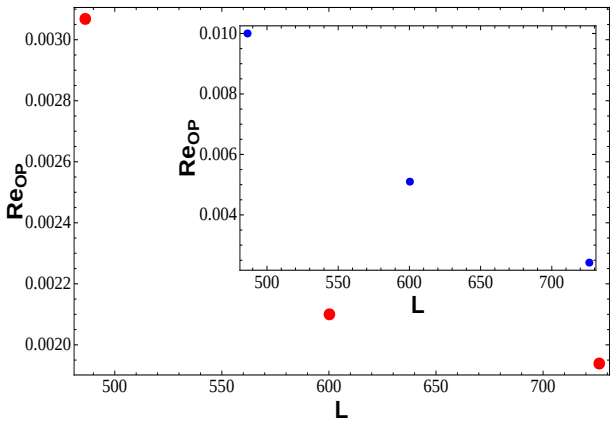

Figure 6.9: Modulation of the the real amplitude of the OP in the bulk with system size. Figure shows that upon increasing the system size it vanishes smoothly. Inset: shows the same functional plot but the parameter is measured far from the bulk. Its variation qualitatively agrees with the one in the bulk.

hexagon when a finite field penetrates the system. The energy spectrum then hosts a finite number of near zero energy modes out of which only half are filled.

Our main concern was to study the nature of the insulating gap, which develops in the spectrum when electron-electron interactions are taken into account. Keeping only the second neighbour component of the finite ranged Coulomb interaction, we numerically found the self consistent Hartree solution of the order parameter. The order parameter in this situation corresponds to a current circulating among the sites on same sublattice. The existence of such time reversal symmetry breaking order was originally proposed by Haldane. In the presence of finite field, being either uniform or inhomogeneous, we found a non zero expectation value of such an order parameter at sufficiently weak interaction (well below the zero field metal-insulator critical interaction) when the system is at filling one half.

At zero field criticality, the gap scales as the square root of the uniform magnetic field. At sufficiently weak interaction it reverts to a linear dependence with the magnetic field. These observations are in accordance with the analytical predictions. Even though the order parameter in the system is not entirely uniform, upon ramping up the system size it appears to achieve a uniform condensation in the entire system. However, a finite current

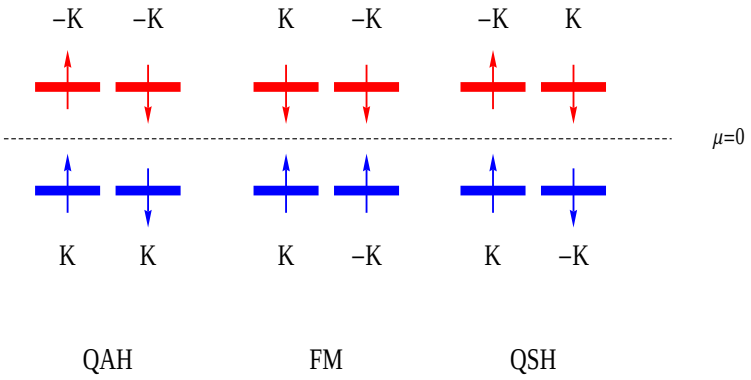

Figure 6.10: Different ordered phases which can be catalyzed in presence of finite pseudo field.

circulates among the sites of only one sublattice in the bulk and of the other one near the perimeter of the system. This can be explained from the nature of the near zero energy modes, catalyzing the formation of the ordered phase. This scenario is quite generic and happens in the presence of finite pseudo flux, being either uniform or nonuniform. On the other hand, when a localized flux pierces through the system, the order parameter develops in that particular regime of the system where the flux is localized. The order parameter appears to have only the time reversal symmetry breaking component with increasing size of the system.

Restoration of the real spin degrees of freedom offers the possibility of two other ordered phases, which might develop within the zero energy manifold, a quantum spin Hall (QSH) insulator and ferromagnetic order. The possible scenarios of the ordered phase are shown in Fig. 6.10. It may also be confirmed by noting the eigenvalues of different order parameters in the zero energy subspace (See Table 1). To develop a phase with finite magnetization one requires Zeeman coupling between the electrons' spin and a magnetic field. However, the pseudo magnetic field does not couple with the electrons' spin. Therefore, one can discard the possibility of a ground state with all the spins aligned. The competition among the QAH and QSH phase is more subtle. These two phases are degenerate in the Hartree limit. However, the QSH phase additionally breaks the spin rotational symmetry. In the absence of a gauge field, the spin fluctuations make the QSH phase energetically superior to the

wave function	$\tau_0 \otimes i\gamma_1\gamma_2$	$\tau_3 \otimes I_4$	$\tau_3 \otimes i\gamma_1\gamma_2$
$\Psi^{K}_{\uparrow}$	+1	+1	+1
$\Psi^{-K}_{\uparrow}$	- 1	+1	- 1
$\Psi^{K}_{\downarrow}$	+1	- 1	- 1
$\Psi^{-K}_{\downarrow}$	- 1	- 1	+1

Table 6.1: Order parameter within zeroth Landau level in the presence of pseudo magnetic field

QAH phase. Unlike the situation in the presence of a real magnetic field which couples with the spin degrees of freedom via Zeeman coupling, thereby projecting the N*é*el order onto an easy plane, the QSH order parameter breaks the $SO(3)$ spin rotational symmetry by spontaneously selecting its orientation. Hence the ordered phase is accompanied by one massive and two massless modes. Therefore, it is likely that even in presence of fictitious flux the QSH phase remains a variational ground state for Dirac fermions to condense into. However, at this moment it impossible to say anything quantitative about this competition. A detailed analysis of this issue is left for future investigation.

6.11 Supplementary information

During the discussion of pseudo magnetic catalysis we presented a family of order parameters for one particular strength of uniform and inhomogeneous pseudo magnetic field. However, our conclusion is supported by similar computation at various other pseudo magnetic fields. Here we would like to exploit the opportunity to present the results from similar numerical computations, carried at different pseudo magnetic fields. In Fig. 6.11 we present the various of the order parameter in the entire system at various strength of the uniform pseudo magnetic field. A similar set of plots for the order parameter is shown in Fig. 6.12, however when a inhomogeneous field penetrates the honeycomb lattice.

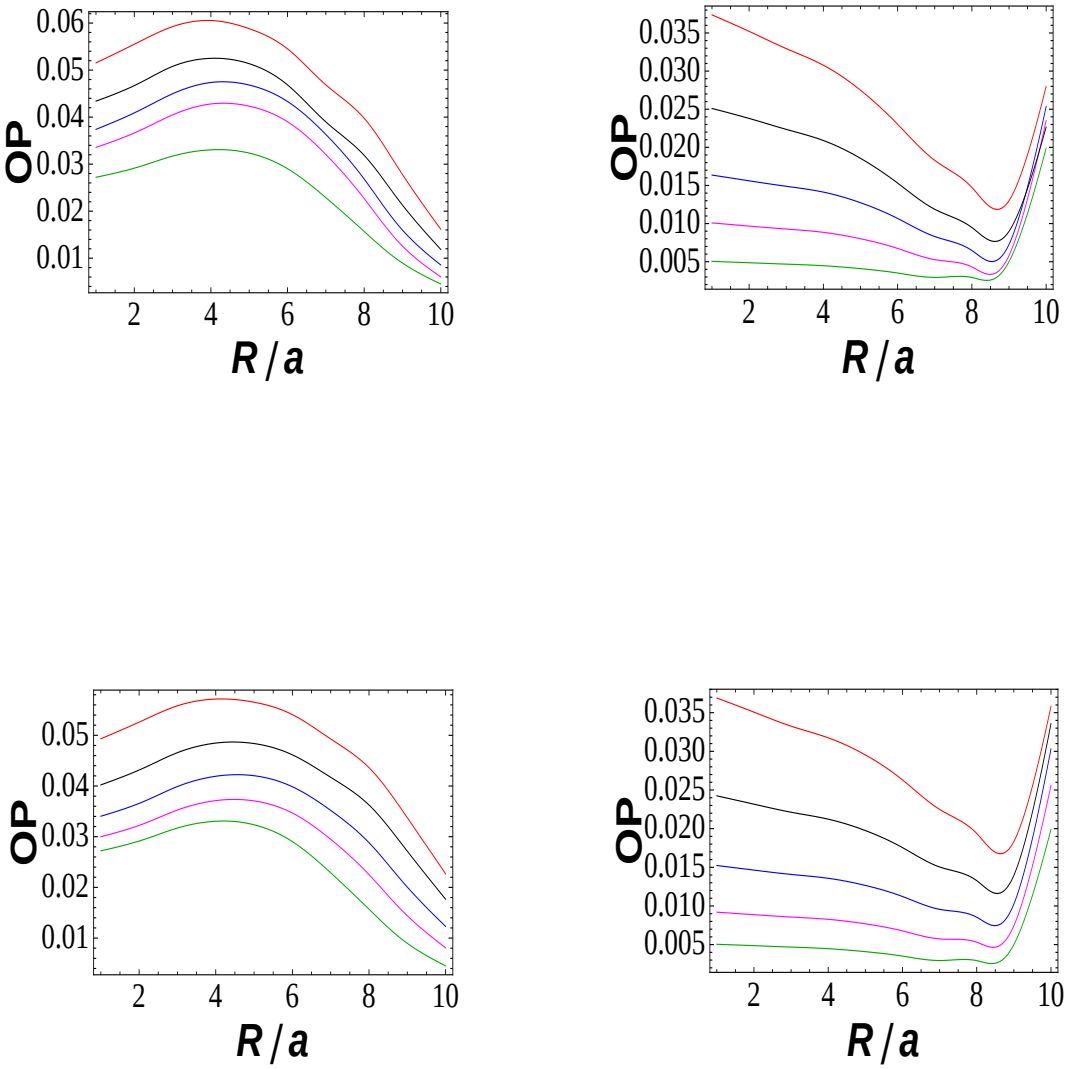

Figure 6.11: The top two figures show the self consistent solution of the Haldane current on a honeycomb lattice in the presence of uniform pseudo magnetic field with $\Phi/\Phi_0 = 0.035$. The left figure shows the OP on the A sub-lattice, whereas the right one represents that on the B sub-lattice. The top curves correspond to $V = 1.5$ and the remaining ones to $V = 1.27(V_c), 1.0, 0.75, 0.5$ from top to bottom. The bottom ones show the same family of curves, however for $\Phi/\Phi_0 = 0.03$.

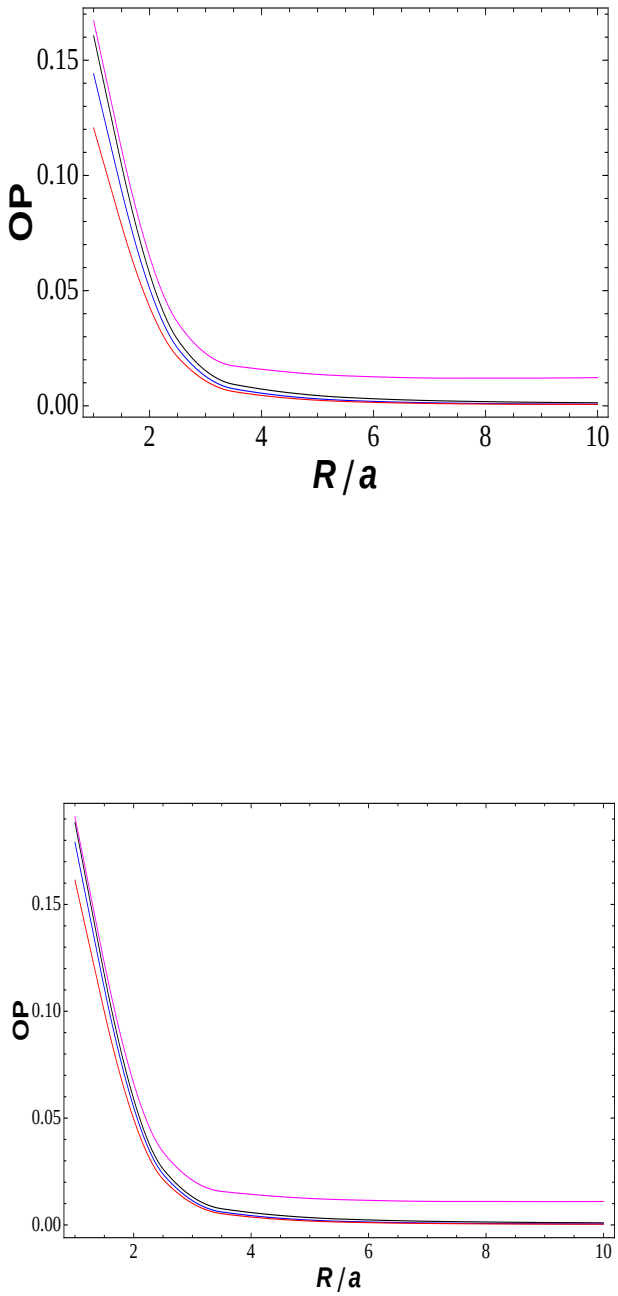

Figure 6.12: Self consistent solution of the Haldane current on the honeycomb lattice in the presence of nonuniform magnetic field with $\Phi_{total} = 9.42\Phi_0$ (top curves). The bottom ones are computed for $\Phi_{total} = 10.99\Phi_0$. The strength of the interaction reads as $V/t = 1.27, 1, 0.75, 0.5$ from top to bottom.

Chapter 7

Odd integer quantum Hall effect in graphene

A possible realization of Hall conductivity, quantized at odd integer factors of e^2/h for graphene's honeycomb lattice is proposed. We argue that, in the presence of *uniform* real and pseudo-magnetic fields, the valley degeneracy from the higher Landau levels can be removed. A pseudo magnetic field may arise from bulging or stretching of the graphene flake. This may lead to the observation of plateaus in the Hall conductivity at quantized values fe^2/h, with $f = \pm 3, \pm 5$ etc, which have not been observed in measurements of Hall conductivity. However, in a collection of noninteracting Dirac fermions living on the honeycomb lattice subject to real and pseudo magnetic fields, the zeroth Landau level enjoys valley and spin degeneracy. Upon including the Zeeman coupling, the spin degeneracy is removed from all the Landau levels. The effects of short ranged electron-electron interactions are also considered, particularly, the onsite Hubbard repulsion (U) and the nearest-neighbour Coulomb repulsion (V). Within the framework of the extended Hubbard model with only those two components of finite ranged Coulomb repulsion, it is shown that infinitesimally weak interactions can place the system in a gapped insulating phase by developing a *ferrimegnatic* order, if $U \gg V$. Therefore, one may expect to see plateaus in the Hall conductivity at all the integer values, $f = 0, \pm 1, \pm 2, \pm 3, \cdots$. The scaling behaviour of the interaction induced gap at $f = 1$ in the presence of finite pseudo flux is also addressed. A qualitative discussion of finite size effects and behaviour of the interaction induced gap when the restriction on uniformity of the fields is relaxed, is presented as well. A possible experimental set up that

can test the relevance of our theory is proposed.

7.1 Motivation and introduction

Before we get to the details of the announced problem, it is worth pausing to realize the physical motivation behind this work. Placed in a magnetic field, graphene exhibits the integer quantum Hall effect, where the Hall states reside at filling factors $\nu = \pm(4n+2)$ with $n = 0, 1, 2, \cdots$ at low magnetic fields ($\sim$ 10 T) [10]. Upon exposing the system to stronger magnetic fields ($>$ 20 T), additional Hall states appear at filling factors $\nu = 0, \pm 1, \pm 4$ [11]. However, the plateaus in the Hall conductivity at other odd integer fillings (for example $\nu = \pm 3$ or ± 5 etc.) are absent even at the highest laboratory magnetic field ($\sim$ 45 T) [101]. These observations confirm that the four fold degeneracy of the zeroth Landau level (LL) is completely lifted, whereas the remaining LLs lose only the spin degeneracy. Within the framework of the extended Hubbard model with onsite and nearest-neighbour repulsion, one can show that the valley degeneracy only from the zeroth LL can be lifted, due to a spontaneous breaking of the chiral symmetry. However, the higher LLs gain a finite shift in energy only. Therefore, one can explain the absence of Hall states at odd integer fillings (e.g., $\nu = \pm 3, \pm 5$) from the protected valley degeneracy of the higher LLs [28, 95]. Here we propose one particular way to observe plateaus in the Hall conductivity at odd integer values of e^2/h, as follows.

As we discussed previously, ripples are randomly distributed on the graphene sheet arising from the strain induced by the SiO_2 substrate [130] and introduce a fictitious gauge potential in the long wavelength limit. Perhaps, bulging or stretching of the graphene sheet can give rise to a finite pseudo flux [117]. One such specific modulation is shown in the previous chapter. Recently, it has been argued that specific distortions of a flake can give rise to a uniform pseudo magnetic field up to 10 T [131]. However a pseudo magnetic field of strength $\sim$ 350 T, is produced by depositing a graphene layer on a platinum substrate, followed by cooling of the system [118]. In the presence of both real and pseudo magnetic fields, valleys are exposed to distinct effective magnetic fields, and may also allow the formation of plateaus in Hall conductivity at odd integer values of e^2/h which were previously absent.

7.2 Free electron spectrum

The tight binding Hamiltonian for spin-1/2 electrons on the honeycomb lattice in the presence of only nearest-neighbour hopping is defined as

$$H_t = -t \sum_{\vec{A},i,\sigma=\pm} u^\dagger_\sigma(\vec{A}) v_\sigma(\vec{A}+\vec{b_i}) + H.c.. \tag{7.1}$$

Here $u^\dagger(\vec{A})$ denotes the fermionic creation operator on the sites of one of the triangular sublattices (A). As argued previously, retaining the Fourier modes only near these two points, one can write down the effective Hamiltonian corresponding to the tight binding model in the low energy limit as

$$H_0 = \int d\vec{x} \sum_{\sigma=\pm} \Psi^\dagger_\sigma(\vec{x}) i\gamma_0\gamma_i D_i \Psi_\sigma(\vec{x}), \tag{7.2}$$

with

$$\Psi^\dagger_\sigma(\vec{x},\tau) = \int^\Lambda \frac{d\vec{q}}{(2\pi a)^2} e^{-i\vec{q}\cdot\vec{x}} (u^\dagger_\sigma(\vec{K}+\vec{q}), v^\dagger_\sigma(\vec{K}+\vec{q}), u^\dagger_\sigma(-\vec{K}+\vec{q}), v^\dagger_\sigma(-\vec{K}+\vec{q})), \tag{7.3}$$

with the convenient frame of reference $q_x = \vec{q}\cdot\vec{K}/K$ and $q_y = (\vec{K}\times\vec{q})\times\vec{K}/K^2$. Here mutually anti commuting gamma matrices belong to the 'graphene representation'. The low energy Hamiltonian H_0 preserves the emergent "chiral" $U(4)$ symmetry generated by $\{\tau_0,\vec{\tau}\}\otimes\{I_4,\gamma_3,\gamma_5\,\gamma_{35}\}$ where, $\gamma_{35} = i\gamma_3\gamma_5 = \sigma_3\otimes I_2$ [9, 80]. The two component Pauli matrices $\{\tau_0,\vec{\tau}\}$, operate on spin indices. One can study the response to a magnetic field by defining $D_i = -i\partial_i - A_i$, with magnetic field $B = \epsilon_{3ij}\partial_i A_j$ set to be perpendicular to the graphene plane.

The Dirac Hamiltonian in the presence of both the real and pseudo magnetic fields reads as

$$H_0[A,a] = \tau_0 \otimes i\gamma_0\gamma_i(p_i - A_i - a^{35}_i\gamma_{35}), \tag{7.4}$$

where, a^{35}_i is the member of a general non-Abelian $SU(2)$ gauge field,

$$a_i = a^3_i\gamma_3 + a^5_i\gamma_5 + a^{35}_i\gamma_{35}. \tag{7.5}$$

A smooth enough deformation in the graphene sheet, does not mix two inequivalent valleys at $\vec{K}$ and $-\vec{K}$. Assuming that the bump in the graphene flake varies slowly on the

lattice scale we kept only one component of a general $SU(2)$ gauge potential [1]. One way to introduce both gauge potentials in experiment is the following. First deposit graphene over a metallic substrate, e.g. platinum [118], at a relatively high temperature and then cool the system. Due to a mismatch in compressibility of the substrate and graphene, one produces a strain on the graphene sheet. This way one might expose the system first to a finite pseudo magnetic field. Once the fictitious field is introduced, the system can then be placed in a real magnetic field.

It is informative to cast the Hamiltonian $H_0[A,a]$ in the following block-diagonal form, $H_0[A,a] = H_+[A,a] \oplus H_-[A,a]$, where

$$H_\pm = \pm I_2 \otimes \sigma_1(-i\partial_1 - A_1 \mp a_1^{35}) - I_2 \otimes \sigma_2(-i\partial_2 - A_2 \mp a_2^{35}). \tag{7.6}$$

H_+ and H_- represent the Hamiltonian near the $\vec{K}$ and $-\vec{K}$ points, respectively. From the Eq. [7.6] one can register that the net magnetic field near one Dirac point ($\vec{K}$) is enhanced to the value $B^+_{total} = B + b$, with $b = \epsilon_{3ij}\partial_i a_j^{35}$. Near the other Dirac point at $-\vec{K}$ the net magnetic field is attenuated to $B^-_{total} = B - b$. Unless mentioned otherwise we assume $B > b$ for the rest of our discussion. Both the fields are assumed to be uniform as well. One can see that both $H_\pm$ are unitarily equivalent to a generic Dirac Hamiltonian $H_D[A,a]$ in two dimensions in the presence of gauge fields, where

$$H_D[A,a] = i\gamma_0\gamma_i(p_i - A_i - a_i^{35}). \tag{7.7}$$

Specifically, $H_+ = U_1^\dagger H_D[A,a]U_1$, with $U_1 = I_2 \oplus i\sigma_2$ and $H_- = U_2^\dagger H_D[A,-a]U_2$, with $U_2 = i\sigma_2 \oplus I_2$ [20].

In the absence of the pseudo magnetic field ($b = 0$) the Hamiltonian $H_0[A,0]$, exhibits a series of LLs at well separated energies $\pm\sqrt{2nB}$, $n = 0, 1, 2, \cdots$, with degeneracies of B/π per unit area. At half filling, all the negative energy LLs are completely filled, whereas the LLs at positive energies are totally empty, with only half of the zero energy states occupied. As a consequence, the Hall conductivity shows plateaus at integer fillings $\nu = \pm(4n+2)$, $n = 0, 1, 2, \cdots$ [90]. Measurement of the Hall conductance at relatively low magnetic fields ($B \sim 10$ T) confirmed such quantization [10, 98]. The additional four-fold degeneracy of the

[1] Two other components of the fictitious gauge potential, proportional to γ_3 and γ_5 are off diagonal in valley index, hence mixe two inequivalent valleys.

LLs arises from the spin and the valley degrees of freedom. The same story follows when one switches off the real magnetic field, and only a pseudo magnetic field penetrates the system, with the difference that now the LLs appear at energies $\pm\sqrt{2nb}$. A recent experiment confirmed such quantization in the presence of a pseudo magnetic field of strength ~ 350 T [118]. On the other hand, the presence of finite real and pseudo magnetic field removes the valley degeneracy from each LL. Consequently, each of the LLs at energy $\sqrt{2nB}$, upon imposing a finite pseudo magnetic field, gives rise to two new LLs at energies $\sqrt{2n(B \pm b)}$, with degeneracies $D_\pm = (B \pm b)/2\pi$ per unit area, respectively, but only for $n \neq 0$. It is worth noticing that the Dirac points are decoupled from each other even in the presence of a finite pseudo field. Hence, there are two sets of zero energy states, one is localized near the $\vec{K}$ point, and the other one near $-\vec{K}$ (or $\vec{K}'$) with degeneracies $\Omega(B \pm b)/2\pi$, respectively. Here Ω is the area of the sample. Thus, the zeroth LL does not split even when the system experiences finite real and pseudo fields [2] [132]. However, in presence of uniform real and pseudo magnetic field the higher LLs split, thereby pushing the states near the K point up in energy, and those in the vicinity of the K' point down in energy. Hence, with some particular strength of B and b, states from two successive LLs, localized near different Dirac points can be degenerate. This situation can easily be bypassed by tuning the ratio B/b close to an *even integer*.

Upon including a finite Zeeman coupling, the spin degeneracy can be lifted from all the LLs including the zeroth one. The Zeeman splitting scales as Δ_Z (in Kelvin) $\sim B$, where B is measured in Tesla, thus much smaller than the LL energies. For our purposes we tune the magnetic fields so that, $5 < B/b < 10$. Within this range of parameters, the energy difference between the Hall states with same LL index (n) but localized near two different valleys is $\sim 200 - 400$ K. Energies corresponding to different LLs for one particular set of realistic values of the magnetic fields are shown in Table 7.1. Without considering the many body effects arising from the electron-electron interactions, one can expect the Hall conductivity to exhibit plateaus at integer values $f = 0, \pm 2, \pm 3, \pm 4, \pm 5, \cdots$ of e^2/h. It is worth noticing that the LLs associated with different Dirac points do not enjoy the luxury of equal degeneracy. Therefore, plateaus of Hall conductivity at integer values of e^2/h, are not associated with the integer fillings. For further illustration of the computation of the

[2] There is one copy of 4-component Dirac fermions near each of the Dirac points. Hence each of them host zero energy modes.

Hall conductivity the reader may refer to the Appendix H.

Table 7.1: Energies of LLs with real field $B = 32$ T and pseudo field $b = 4$ T

n	1	2	3
E_0	2.4×10^3 K	3.4×10^3 K	4.1×10^3 K
E_+	2.5×10^3 K	3.5×10^3 K	4.4×10^3 K
E_-	2.2×10^3 K	3.2×10^3 K	3.8×10^3 K

Energies of the LLs (measured from the charge neutral point) for a particular choice of the magnetic fields. Here n stands for the LL index in absence of pseudo field. E_0 stands for the energy of the LL without any pseudo field. $E_{+(-)}$ denotes the energy of the LL lives in the vicinity of the $+\vec{K}(-\vec{K})$ Dirac point.

7.3 Electron-electron interactions

Diagonalizing the Dirac Hamiltonian in the presence of uniform real and pseudo magnetic fields we found that the valley degeneracy is lifted only from higher LLs. In the absence of interactions the zeroth LL still enjoys the valley degeneracy. In this section we will consider the effect of the short ranged electron-electron interactions in the spectrum. The interacting Hamiltonian in presence of only on-site (U) and nearest-neighbour (V) repulsion is defined as

$$H_U = \frac{U}{2} \sum_{\vec{X},\sigma} n_\sigma(\vec{X}) n_{-\sigma}(\vec{X}) + \frac{V}{2} \sum_{\vec{A},i,\sigma,\sigma'} n_\sigma(\vec{A}) n_{\sigma'}(\vec{A} + \vec{b_i}). \tag{7.8}$$

For graphene, $U \approx 5 - 12$ eV and $U/V \approx 2 - 3$ [133]. After the usual Hartree-Fock decomposition, one can write down an effective single-particle Hamiltonian in that background as

$$H_{HF} = \tau_0 \otimes H_0[A, a] + ma \otimes \gamma_0, \tag{7.9}$$

where $a = \tau_0$ corresponds to $m = C = \langle n(\vec{A}) - n(\vec{A} + \vec{b}) \rangle$ (charge density wave (CDW)) and $a = \tau_3$ to $m = N = \langle m(\vec{A}) - m(\vec{A} + \vec{b}) \rangle$ (anti-ferromagnet (AF)). Here $n(\vec{A}) = u^\dagger_\sigma(\vec{A}) u_\sigma(\vec{A})$ is the average electron density and $m(\vec{A}) = u^\dagger_\sigma(\vec{A}) \sigma_3 u_\sigma(\vec{A})$ corresponds to the average magnetization on sub-lattice A. Similar quantities are analogously defined on the B sub-lattice in terms of fermionic operators $v_\sigma(\vec{B})$ and $v^\dagger_\sigma(\vec{B})$. Here we omitted the Zeeman term for

convenience. The effect of Zeeman splitting will be discussed later.

The spectrum of the Hamiltonian H_{HF} is as follows. For $n \neq 0$ the eigenvalues are at $\pm\sqrt{2n(B \pm b) + m^2}$, for each spin projection, with degeneracies per unit area $D_\pm = (B \pm b)/2\pi$, respectively. Besides these, for $n = 0$, the eigenvalues of H_{HF} for each spin components are $\pm|m|$ with degeneracies $D^0_\pm = (B \pm b)/2\pi$ per unit area, respectively. Therefore filling up only the states at negative energy while leaving those at positive energy empty one immediately develops a gap even at small enough interaction. Generating a gap at infinitesimal interactions in the presence of a magnetic field is termed as 'magnetic catalysis' [102]. This has been proposed as a mechanism behind the formation of the Hall states in graphene at filling factor $\nu = 0$ and 1 in presence of an ordinary magnetic field [90, 95]. In the zeroth LL, states associated with $\vec{K}$ and $-\vec{K}$ are localized on complimentary sub-lattices A and B respectively. Hence, for each spin projection, there are $(B + b)/2\pi$ states per unit area on the A sub-lattice, whereas the other sub-lattice hosts only $(B - b)/2\pi$ states. In the absence of pseudo field, states on each of the sub-lattices enjoy equal degeneracy. Therefore, even infinitesimally strong interactions can develop a gap at filling one-half by spontaneously breaking the chiral symmetry of the Dirac quasi-particles. However, the nature of the insulating ground state depends on the strength of the interactions at the lattice scale. For example, if $U > V$, AF ordering lowers the the energy of the ground state. A CDW order can develop within the zeroth LL if on the other hand, the nearest-neighbour component of the finite range Coulomb repulsion is the dominant one. However, due to imbalance in the number of states living on two sub-lattices in the zeroth LL, only *ferrimagnetic* order can be developed while keeping the system at charge neutrality. The electron-electron interactions remove either the valley degeneracy or the sub-lattice degeneracy from the zeroth LL. These two are equivalent however only within the zeroth LL. Alternatively, a large enough Zeeman coupling will orient the magnetization at all the sites in the direction of the magnetic field and hence lower the energy of the filled Dirac-Fermi sea. Such a ground state with finite magnetization can also be stabilized by increasing the component of the magnetic field parallel to the graphene plane. The exact nature of the ground state at $\nu = 0$ in graphene in the presence of only a real field is still a subject of debate [96, 81, 30, 134]. The activation gap of longitudinal resistivity for $\nu = 1$ was found to be independent of the component of the magnetic field parallel to the graphene plane, and varies sublinearly with its perpendicular component. This observation strongly suggests that it originates from electron-electron

interactions [99].

Therefore upon including the Zeeman splitting and finite ranged interactions the four fold degeneracy from all the LLs is completely removed. Within the zeroth LL, a gap develops by lifting the valley or sub-lattice degeneracy. Under this circumstance, one can expect the Hall conductivity to exhibit quantized plateaus at $\sigma_{xy} = fe^2/h$, with $f = 0, \pm 1, \pm 2, \pm 3, \cdots$. [3]

7.4 Scaling of interaction induced gap

Let us now focus on the scaling behaviour of the interaction induced gap. The validity of our theory relies on the assumption that the magnetic fields are low in comparison to the characteristic lattice magnetic field, or equivalently the magnetic length is much larger than the lattice spacing. This condition is easily satisfied even at the highest laboratory magnetic field $B \sim 45$T and $0 < b/B < 0.2$. In a current experimental situation with $b \sim 350$ T [118], the magnetic length ($\approx 35\mathring{A}$) is more than an order magnitude larger than the lattice spacing ($a \sim 2.5\mathring{A}$). Hereafter we assume that the spin degeneracy is completely lifted by the Zeeman splitting and the chemical potential lies close to the Zeeman shifted 'Dirac' point, thus $f = 1$. After integrating out the fast Fourier modes within the momentum shell $1/a < k < 1/l_B$, one can write down the effective low energy Lagrangian corresponding to H_U in Eq. [7.8] as

$$L = i \sum_{\sigma} \overline{\Psi}_{\sigma} \gamma_{\mu} D_{\mu} \Psi_{\sigma} - g_1 \left(\sum_{\sigma} \overline{\Psi}_{\sigma} \Psi_{\sigma} \right)^2 - g_2 \left(\sum_{\sigma} \sigma \overline{\Psi}_{\sigma} \Psi_{\sigma} \right)^2, \tag{7.10}$$

where $\overline{\Psi}_{\sigma} = \Psi_{\sigma}^{\dagger} \gamma_0$, $D_0 = -i\partial_{\tau}$, and τ is the imaginary time. $\mu = 0, 1, 2$ runs over the space-time indices and summation over repeated indices is assumed. Here, $l_B \sim B^{-1}$ is the magnetic length and we kept only the least irrelevant couplings $g_1 = (3V - U)a^2/8$ and $g_2 = Ua^2/8$. Assuming a uniform background of either staggered electron density or *ferrimagnetic* order, the ground state energy for N four component fermions in the magnetic

[3] Consult Appendix H

fields is given by

$$\frac{E(m)-E(0)}{N} = \frac{m^2}{4g_2}+\sum_{\sigma=\pm}\frac{B+\sigma b}{4\pi^{3/2}}\int_0^\infty \frac{ds}{s^{3/2}}(e^{-sm^2}-1) \left[\frac{1+\sigma}{2}+K(s\Lambda^2)\left(\coth(s(B+\sigma b))-1\right)\right], \tag{7.11}$$

as $N\to\infty$. Setting $b=0$, one recovers the ground state energy in the presence of only real magnetic field [95]. Here $K(x)$ is the cut-off function introduced to sum over the $n\neq 0$ LLs. This function satisfies $K(x\to\infty)=1$ and $K(x\to 0)=0$, but is otherwise arbitrary. $E(m)$ can be understood as the Hartree-Fock variational ground state energy of the electrons either in a CDW or ferrimagnetic background. Due to the different degeneracies of the states localized near $\vec{K}$ and $\vec{K}'$, the energy of the ground state is maximally lowered by pushing down all the states on the A sub-lattice below the chemical potential while leaving those on the B sub-lattice empty. In the absence of pseudo flux, the A and B sub-lattice host equal numbers of states. The system then spontaneously chooses the ground state by breaking the Ising like symmetry of either sub-lattice or the valley degrees of freedom. The first term in the parentheses in Eq. [7.11] counts the contribution from the zeroth LL whereas the second one includes the contributions from higher LLs. Minimizing $E(m)$, one can cast the gap equation in the following form

$$\frac{X}{2}=f(X,q)+\frac{\delta}{m}, \tag{7.12}$$

where $X=(B+b)/m^2$, $\delta=(g\Lambda)^{-1}-(g_c\Lambda)^{-1}$ measures the deviation from the critical interaction (g_c) and $q=(B+b)/(B-b)$, yielding $B/b=(q+1)/(q-1)$. The non-universal value of the critical interaction is determined by

$$\frac{1}{g_c}=\frac{\Lambda}{\sqrt{\pi}}\int_0^\infty ds\frac{K(t)}{s^{3/2}}, \tag{7.13}$$

and the function $f(X,q)$ is defined as

$$f(X,q)=\frac{1}{\sqrt{\pi}}\int_0^\infty \frac{ds}{s^{3/2}}K\left(\frac{sXB_0}{B+b}\right)\left(1-\frac{Xse^{-s}}{e^{2Xs}-1}-\frac{1}{q}\cdot\frac{Xse^{-s}}{e^{2Xs/q}-1}\right). \tag{7.14}$$

In the limit of low magnetic fields $B,b\ll B_0$, where $B_0\sim a^{-2}$ is the magnetic field corresponding to the lattice scale, one can substitute $K(x)$ by *unity*. Upon setting $q=1$, one gets the gap equation in presence of the ordinary magnetic field, obtained previously [103].

However, for $1 \leq q \leq 1.5$, or equivalently $0 \geq b/B \geq 0.2$, the solution of the gap equation lies in the range $17.913 \geq X = X_0 \geq 14.0$, when $\delta = 0$. Realizing that the solution of the gap equation for $\delta > 0$ or $g < g_c$ will exist at $X > X_0$, one can expand $f(X, q)$ for large X, at least when q is not far from *unity*. Keeping the terms up to second order one can write

$$f(X,q) = u\left(1 + \frac{1}{\sqrt{q}}\right)\sqrt{X} + \frac{v}{\sqrt{X}}\left(1 + \sqrt{q}\right) + O(X^{-3/2}), \tag{7.15}$$

with $u = 1.03258$ and $v = 0.461808$. Hence one can cast the self consistent equation of the gap in terms of an algebraic equation

$$u\sqrt{\frac{2q}{q+1}}\left(1 + \frac{1}{\sqrt{q}}\right)m + v\frac{\sqrt{1+q}}{\sqrt{2q}}(1+\sqrt{q})\frac{m^3}{B} + \frac{\delta}{\sqrt{B}}m - \frac{q}{1+q}\sqrt{B} = 0. \tag{7.16}$$

At criticality, i.e. $\delta = 0$, the interaction induced mass varies as $m = \sqrt{2B}/C$, where C now depends on q, otherwise it is a universal number. Particularly for $q = 1$, i.e., $b = 0$, this ratio was found to be $C = 5.985 + O(1/N)$ [103]. Recently the same universal number is been computed numerically on a finite honeycomb lattice, where we found this number to be extremely close to the one computed in continuum limit [135]. From the solution of the gap equation at $\delta = 0$, one finds that the size of the gap at $f = 1$ increases upon introducing a finite pseudo flux. This issue can be resolved by considering the zeroth LL only. In the presence of real and pseudo fields, the Hall conductivity develops a plateau at $f = 1$ by filling $\Omega(B + b)/2\pi$ states from the charge neutrality, where Ω is the area of the sample. Hence the zeroth LL contribution to the ground state energy is proportional to $\Omega m(B + b)/2\pi$, where m is the activation gap for $f = 1$. Therefore, one finds that the zeroth LL contribution is enhanced in the presence of pseudo flux. In the gap equation this contribution is dominant whereas, the higher LL contributions are $O(m^2/B_{\pm})$ and hence sub dominant. After some tedious, otherwise straight-forward calculations it can be shown that the higher LL contribution also increases the size of the gap at $f = 1$. We computed the gap as a function of B for $q = 1$ and 1.285 for various δ and a family of such curves is shown in Fig. 1. The first case, $q = 1$ corresponds to $b = 0$ and $q = 1.285$ implies $B/b \approx 8$.

The gap at $f = 1$ is generated by breaking either the sub-lattice or the valley degeneracy within the zeroth LL. The semimetal-insulator transition belongs to the Gross-Neveu universality class. Therefore, near transition the dynamical critical exponent z is equal to *unity* and the correlation length exponent $\nu = 1 + O(1/N)$ [80]. The $1/N$ corrections are found

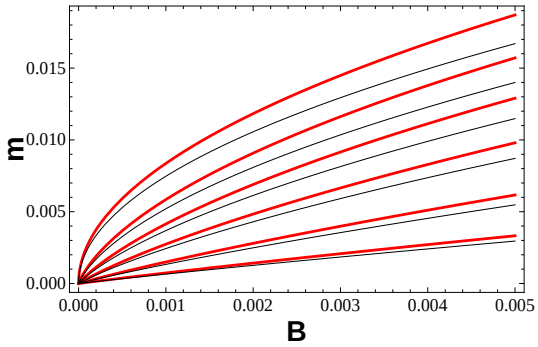

Figure 7.1: Gap (m) at $f = 1$ as function of B, with $q = 1.285$ (red), i.e. $B/b = 8$ and $q = 1$ (black), i.e. $b = 0$. Here m and B are measured in units of $v_F\Lambda$ and $B_0 = \Lambda^2$, respectively. The top curves correspond to the critical point $\delta = 0$ and the remaining ones to $\delta = 0.03, 0.07, 0.14, 0.31, 0.7$ (top to bottom), where $\delta = (g_c - g)/g_c g\Lambda$. Figure reprinted with permission from B. Roy, [125]. Copyright 2011 by the American Physical Society.

to be small in comparison to the leading order contribution. This is the reason behind their omission here [50]. One can also confirm the critical exponents from the linear variation of the gap with magnetic field B, for small interaction ($\delta \ll 0$) [4]. As one enters the regime of stronger interaction, a sub-linear dependence of the gap on magnetic field emerges. At criticality $\delta = 0$, the gap shows a perfect square-root dependence on magnetic field [103]. For $q = 1.285$, one finds the universal ratio C to be $5.55878 + O(1/N)$. To the leading order, the scaling function does not depend on the exact nature of the short-ranged interactions. Any order parameter that lifts the valley degeneracy from the zeroth LL will lead to identical scaling behavior. However, $1/N$ corrections may depend on the exact nature of the order parameters [9, 56].

A pseudo magnetic field may arise from a specific deformation of the graphene sheet, thus the field profile is typically *inhomogeneous*. Hence it natural to study the behaviour of a collection of interacting fermions on the honeycomb lattice when the fields are inhomogeneous. A recent numerical study [135] in the presence of a nonuniform, but real magnetic field, established that the catalysis mechanism survives even when the condition of uniformity of the field is relaxed. The system finds itself in an ordered phase at sufficiently weak

[4] See Ref. [103]

interaction by developing a local expectation value of the order parameter, which more or less is found to follow the profile of the magnetic field. The system finds itself in an ordered phase by lifting the chiral symmetry. A similar behaviour of the *local* order parameter on the *local* strength of the field is been observed, when only an inhomogeneous pseudo magnetic field penetrates through the system [5]. The order parameter in presence of fictitious field breaks TRS [43]. Hence, in presence of inhomogeneous fields, we expect the order parameter to develop a space modulated expectation value. However, we leave this issue for further investigation.

7.5 Discussion and Summary

To summarize, we consider Dirac fermions in two spatial dimensions in the presence of real and pseudo magnetic fields. For simplicity, we assumed both of them to be uniform and the real one directed perpendicular to the graphene plane. Diagonalizing the free Hamiltonian under that circumstance we found that all the LLs at finite energy lack valley degeneracy, whereas the one at zero energy enjoys it. Taking into account the onsite and nearest neighbour interaction we have shown that the zero energy level splits by developing either a CDW or ferrimagnetic order when the real magnetic field is stronger than the fictitious one. Upon including the Zeeman splitting, the spin degeneracy of all the LLs is lifted and one expects to see plateaus in the Hall conductivity at all the integer factors of e^2/h. Previously the plateaus at odd integer fillings $f = \pm 3, \pm 5, \cdots$ could not be observed due to the valley degeneracy of the higher LLs. Here we proposed that a finite pseudo flux can, in principle, release the LLs from the valley degeneracy. However, due to distinct degeneracies of the LLs localized in the vicinity of two Dirac points, the plateaus in Hall conductivity at integer values of e^2/h, would be observed at non integer fillings. A scaling behavior of the interaction induced gap at $f = 1$ is presented, assuming either onsite Hubbard or nearest-neighbour repulsion is the dominant finite range interaction. Within the mean field approximation, the size of the gap is found to be enhanced in the presence of a finite pseudo flux. One way to test the enhancement of the gap is as follows. As mentioned in Ref. [118], the bulging of the graphene sheet does not take place everywhere on the sample. Only

[5] See Chapter 6 for some detailed discussion.

some portion of the flake develops a bump and experiences a finite pseudo field. Therefore placing the system in a magnetic field one can measure the order parameter in two different domains of the flake, where the flake is bulged and the other where it is reasonably flat. This way one can determine the effect of the finite pseudo flux on the interaction driven gap.

In a finite system, pseudo field can be achieved by means of an inhomogeneous strain. Particular deformations that might give rise to a such field were proposed in Ref. [117] and in Ref. [131] as well. One feature of such a deformation is that it leaves the lattice with only a C_3 symmetry, which has also been confirmed experimentally [118]. As long as the extension of the bump in the graphene flake and the magnetic length are larger than the lattice spacing, the continuum description is valid. In recent experiment [118], $l_b \approx 35\mathring{A}$ at $b = 350$ T and the extension of the bump is $\sim 40 - 100\mathring{A}$. Hence, both the length scales are much larger than the lattice spacing in graphene ($a \approx 2.5\mathring{A}$). However, for the true thermodynamic limit, one requires the extension of the bump to be much larger than the magnetic length.In the present experimental situation these two length scales are comparable. However, with a smoother bump with broader extension, one can get to the regime where the constraint is easily satisfied.

Finally let us turn to the situation when $b > B$. Recently a *uniform* pseudo field of strength 350 T was produced by bulges in the graphene layer deposited on Platinum substrate [118]. Hence this limit seems quite achievable. Particularly for $B = 0$ the zero energy states near two Dirac points live on the same sub-lattice. Hence, an infinitesimal next-nearest-neighbour Coulomb repulsion may open up a gap by spontaneously breaking time reversal symmetry (TRS) [43]. The order parameter in the insulating phase is given by $\langle \Psi_\sigma^\dagger (I_2 \otimes i\gamma_1\gamma_2)\Psi_\sigma \rangle$. The TRS is represented by an anti-unitary operator $I_t = U_t K$, where U_t is unitary and K is the complex conjugation operator. In the graphene representation U_t is given by $i\gamma_1\gamma_5 = \sigma_1 \otimes I_2$ [80]. The correlated ground state this circumstance corresponds to an intra sub-lattice Haldane circulating current, propagating in opposite direction on the two sub-lattices [38]. This state is named the *quantum anomalous Hall insulator* (QAH). The exact nature of the correlated ground state in the presence of a pseudo magnetic field is yet to be determined and we leave this issue for future investigation. However, in the absence of any gauge potentials ($B = 0, b = 0$) fluctuations preempt the appearance of the QAH and stabilize the *spin Hall insulator* (QSH) ground state. The correlated ground state

in the QSH phase breaks the TRS for each spin component and the order parameter reads as $\langle \Psi_\sigma^\dagger (\vec{\sigma} \otimes i\gamma_1\gamma_2)\Psi_\sigma \rangle$ [55].

Here we focused only on the finite-ranged components of the Coulomb interaction. On the other hand, its long range $1/r$ tail is unscreened due to the vanishing density of states at the charge neutral point. If one turns off the pseudo magnetic field the long range Coulomb interaction will lead to a similar splitting of the LLs. However, it introduces an energy scale $e^2/\epsilon l_B$, which is on the same order of the LL energy with commonly assumed dielectric constant $\epsilon \approx 5$ for SiO_2 substrate. This immediately contradicts the experimentally observed gap of ~ 100 K at $f = 1$, an order of magnitude smaller than the LL energy [99]. This issue can be resolved by assuming an order of magnitude larger value of the dielectric constant, which attributes the accumulation of water layer between the graphene flake and SiO_2 substrate [110]. In recent work [100], it was shown that even though the long range Coulomb interaction liberates all the LLs from the valley degeneracy, the critical strength of the disorder above which the $f = 3$ plateau is destroyed is much smaller than that for $f = 1$. This scenario, may explain the absence of odd integer Hall plateaus in graphene [98, 99]. In contrast, the presence of a finite flux of pseudo field leads to an activation gap $\sim 200 - 400$ K for $f = \pm 3, \pm 5$ Hall states (Table 7.1). Consequently, the Hall states at those fillings should be much more robust against disorder. Thus, one may expect to see the quantization of Hall conductivity at odd integer factors of e^2/h in a cleaner system. Assuming a sufficiently large dielectric constant, one can restrict oneself to the short-ranged components of the Coulomb interaction. The effect of weak long-ranged Coulomb interaction on the interaction mediated gap is discussed in Ref. [103].

Chapter 8

Summary and concluding remarks

In the final chapter we present an overview of our work and present some possible extensions. Our voyage started with the collection of noninteracting fermions on graphene's honeycomb lattice. Some elementary computation led us to the Dirac nature of the quasiparticles in the vicinity of the edges of the Brillouin zone. In the low energy limit those quasiparticles determine the electronic behavior of graphene.

8.1 Interactions and insulation

In this work we attempt to gain some insights of the interacting fermions on honeycomb lattice. In neutral graphene, a vanishing density of states leaves the long range Coulomb interaction unscreened. Nevertheless, the finite ranged components of the Coulomb interaction are strong as well. For example, the onsite Hubbard interaction $U \sim 10$ eV, the nearest-neighbour repulsion $V_1 \sim 5$ eV, whereas the nearest-neighbour hopping amplitude $t \sim 2.5$ eV, leading to the Fermi velocity $v_F = 10^6$ m/s. Recent measurement of the Fermi velocity found a logarithmic variation as one approaches the charge neutral point. This observation confirms the imprint of long ranged Coulomb interactions in the system. Depending on the relative strength of different finite ranged repulsive interactions fermions in graphene may condense into plethora of insulating ground states. The strength of interactions seems to be below the critical strength for insulation, however not too far from the criticality. Instead of starting from a particular lattice model of interaction, we wrote down the most general form of the interacting Lagrangian on the honeycomb lattice of carbon atoms. For simplicity we considered the fermions to be spinless. However, our study can

easily be generalized once the spin degrees of freedom are restored. Even though, at the beginning the number of coupling constants appears to be too many, symmetries present in the lattice considerably reduce that number. Implementation of the low energy emergent symmetries restricts the allowed quartic interactions even further. The maximally symmetric theory preserving additional Lorentz and chiral symmetry, can be described in terms of four terms. The existence of an algebraic identity, known as the Fierz identity, which allows one to write down any bilinear as a linear combination of the others, reduced that number to two. Removal of the chiral symmetry increases that number to three, while the interacting theory consistent with the symmetries offered by the lattice can be described in terms of only four independent quartic interaction.

A renormalization group study of the interacting theory allowed us to capture its low energy behaviour and simultaneously provided insights about the possible phase transitions in graphene. We found that all the critical points through which system takes itself out of the semimetallic ground state to an ordered phase belong to the Lorentz symmetric hyperplane. Weak violation of the Lorentz symmetry turned out to be irrelevant near the meta-insulator quantum critical point. As a consequence the Fermi velocity remains non-critical near the criticality. Our conclusion is necessarily based on an uncontrolled one loop renormalization group study. However, such scale invariant behaviour has been confirmed by performing a controlled $\epsilon-$expansion near four dimensions.

In three dimensions, the cutoff ($\Lambda \sim 1/a$) in the momentum integral, representing the range of energy over which the linear approximation of the density of states hold, explicitly appears in the definition of renormalized coupling constants. It makes the outcome of the low energy theory dependent on the procedure to eliminate the high energy Fourier modes. Such a problem can be eliminated by defining the theory near two dimensions, at which all the quartic interactions are dimensionless and hence one can performed a controlled $\epsilon-$expansion near the lower critical dimension.

8.2 Superconductivity

If on the other hand, the net interaction has an attractive component, numerous superconducting states become available to fermions to pair into, and that way to lower the energy of the filled Dirac Fermi sea. For example, a strong on-site attraction favors a spin singlet s-wave superconductor. Other superconducting orders are not so conventional. A strong second nearest-neighbour attraction leads to a f-wave superconducting ground state and the order parameter changes its sign six times around the Brillouin zone. Yet another non trivial order appears when the fermions living on the nearest-neighbour sites of the honeycomb lattice attract each other strongly. We found a spatially inhomogeneous, spin triplet superconducting state as a variational ground state. It is however, odd under sublattice exchange and breaks the translational symmetry of the lattice into a Kekule pattern.

Upon increasing the nearest-neighbour interaction first there is a transition from the semimetallic phase to a p-Kekule state, odd under the Dirac point exchange. Deep inside the superconducting phase, there is an additional discontinuous transition from p-Kekule to s-Kekule state. The s-Kekule state is however, even under the Dirac point exchange. The Kekule order is inhomogeneous in space with periodicity $2\vec{Q}$, where $\vec{Q}$ is the momentum of the Dirac point, and opens up a gap near the Dirac point. The critical interaction of such an instability is almost half that for the 'hidden' order, which on the other hand lowers the energy of Dirac quasiparticles by increasing the Fermi velocity, hence it is not a gapped superconductor at filling one-half. As one increases the interaction strength first there is a transition to Kekule order and it also preempts any appearance of 'hidden' order. However, our study mainly focused on the neutral graphene system. Upon chemically doping the system existence of a pure 'hidden' order or coexistence of these two phases seems conceivable. We leave this issue for future investigation.

The target space of the Kekule order parameter lives on the surface of S_3, the sphere in four dimensions. As the first and the second homotopy group of S_3 are trivial, there are no stable topological defects in the ordered phase. The massless fluctuations are therefore described by an $O(4)$ nonlinear sigma model. Nevertheless, the target space can be reduced by external perturbations, e.g. Zeeman coupling, spin-orbit splitting. A finite Zeeman coupling selects an easy plane for the spin axis and the target space becomes $S_1 \times S_1$. Apart

from the standard superconducting or easy spin plane vortex, another non-trivial topological excitation becomes stable, known as 'half-vortex'.

8.3 Catalysis

A large overlap of the electronic wave function among the nearest neighbour sites of the honeycomb lattice protects its semimetallic ground state against any weak electron-electron interaction. Moreover interactions need to be sufficiently strong in order to place the system in a ordered phase, because of the vanishing density of states at the Fermi energy in neutral graphene. However, due to the reduced dimensionality of the system, in the presence of a magnetic field, the kinetic energy is completely quenched and the energy spectrum is comprised of a series of Landau levels. The existence of the Landau level at zero energy, therefore brings the critical interaction for insulation down to zero. Consequently, the system suffers a metal-insulator transition even at an infinitesimal strength of the interactions. We confirmed this phenomenon by pursuing both analytical and numerical approaches. In the presence of a real magnetic field, a chiral symmetry breaking order can be catalyzed, where a time reversal symmetry breaking order can only be catalyzed when a finite pseudo magnetic flux penetrates the system. Even though, a pseudo magnetic flux may arise from the ripples existing in the graphene flake, a random distribution of such defects provides only a net zero flux of the pseudo field. However, a specific modulation of the nearest neighbour hopping can give rise to a finite flux of pseudo field. One specific way to incorporate a finite pseudo flux has been shown in Chapter 6.

Qualitatively, the scaling behaviour of the chiral and time reversal symmetry breaking orders with interaction and magnetic field are the same. At weak interactions, they scale linearly with the magnetic field, whereas sublinear variation of the gap with the magnetic field emerges at intermediate strength of interaction. At zero field criticality, the gap scales as the square root of the field. Even though, in the presence of inhomogeneous fields the gap becomes nonuniform and follows the profile of the field, the scaling features of the local order parameter with the local magnetic field retain the behaviour of the uniform gap with uniform field. Our numerical and analytical results are in very good agreement with each other when finite size effects are taken into account for various quantities, e.g. Landau level

energy to interaction induced gap ratio at zero field criticality.

In the presence of a uniform real magnetic field we investigate the nature of the electronic ground state at neutral filling. Performing a self consistent Hartree-Fock calculation we showed the possible existence of a topological order, which also happens to be proportional to the magnetization in the zeroth Landau level. Our study revealed that the Néel order is always projected to the easy plane of the spin axis, whereas the topological order (Quantum spin Hall insulator (QSH)) acquires an easy axis.

One possible issue that need to be answered is the nature of the electronic ground state in the presence of pseudo magnetic field, once the spin degrees of freedom are incorporated. Towards the end of the Chapter 6, we shed some light on that issue and claimed that possibly the quantum spin Hall insulator becomes energetically the best solution. Nevertheless, a more quantitative argument is needed.

8.4 Two magnetic fields

In the presence of either real or pseudo magnetic field, Landau levels other than the zeroth Landau level retain the valley degeneracy. Therefore, Hall states do not exist at odd integer fillings except *unity*. In the previous Chapter we showed that when both real and pseudo magnetic field penetrates the system uniformly, all the Landau levels, except the zeroth one are liberated from the valley degeneracy, because the valleys are then exposed to distinct effective magnetic fields. Taking into account the effect of short ranged electron-electron interactions as well as the Zeeman coupling of electrons spin with the real magnetic field, we showed that the Hall conductivity is quantized at all the integer multiples of e^2/h. However, the quantization of the Hall conductivity is no longer associated with integer filling, due to the different degeneracies of the Landau levels.

We also considered the scaling of the interaction induced gap for a fixed ratio of the strength of the fields, when the real one is stronger than the pseudo magnetic field. We found a formation of *ferrimagnet* order when the Hall conductivity is quantized at e^2/h. The size of the gap is also found to be enhanced by the existence of a finite flux of pseudo

magnetic field.

An interesting issue, left for future investigation, is the electronic ground state in neutral graphene when these two types of magnetic fields pierce the system.

Appendix A

Symmetries and free Hamiltonian

Here we will show how one can derive the free Hamiltonian from the symmetries discussed in Chapter 2. We will restrict ourselves to the hopping of fermions among nearest neighbour sites of the honeycomb lattice. Therefore, particle-hole symmetry is always respected. Let us first consider the free Hamiltonian, linear in momentum. In general, the non-interacting Hamiltonian to linear order in momentum can be written as

$$H_{linear} = \alpha\ A\ p_x + \beta\ B\ p_y, \tag{A.1}$$

where A and B are 4-component Hermitian matrices and α , β are associated with the strength of the nearest neighbor hopping. The Hamiltonian in Eq. [A.1] is written in a four component basis $\Psi\ (\vec{q})$, where

$$\Psi^{\top}(\vec{q}) \ = \ (u(\vec{Q}+\vec{q}), v(\vec{Q}+\vec{q}), u(-\vec{Q}+\vec{q}), v(-\vec{Q}+\vec{q})). \tag{A.2}$$

$\vec{Q}$ here, corresponds to the momentum associated with the Dirac point, i.e. $\vec{Q} = \pm\left(1, 1/\sqrt{3}\right) 2\pi/a\sqrt{3}$, a being the lattice constant. The Free Hamiltonian must be invariant under the exchange of two sub-lattices as well as two inequivalent Dirac points. These two reflections can be achieved via rotations by γ_2 and $i\gamma_1\gamma_5$, respectively. Note that these two operations are accompanied by inversions of particular momentum axes, namely $p_y \rightarrow -p_y$ and $p_x \rightarrow -p_x$, respectively. Therefore, the two matrices A and B must satisfy the following algebra

$$[A, \gamma_2] = \{A, i\gamma_1\gamma_5\} = 0, \tag{A.3}$$

$$\{B, \gamma_2\} = [B, i\gamma_1\gamma_5] = 0. \tag{A.4}$$

These constrains leave two possibilities for each of the matrices, $A \in \{i\gamma_3\gamma_5, i\gamma_0\gamma_1\}$ and $B \in \{\gamma_0, i\gamma_0\gamma_2\}$. As H_{linear} reflects the low energy behaviour of *real* hopping of the fermions on lattice, it must be even under the time reversal symmetric. Time reversal symmetry in 'graphene representation' reads as $I_t = i\gamma_1\gamma_5 K$, where K is complex conjugation. Recall that momentum operator is odd under time reversal symmetry, i.e., $I_t p_a I_t^{-1} = -p_a$, with $a = x, y$. Hence the free Hamiltonian (linear in momentum) reads as

$$H_{linear} = \alpha\, i\gamma_0\gamma_1\, p_x + \beta\, i\gamma_0\gamma_2\, p_y. \tag{A.5}$$

H_{linear} commutes with the generator of translation $i\gamma_3\gamma_5$, while anticommutes with γ_0. The matrix γ_0 in the 'graphene representation' is the generator of particle-hole symmetry. Hence the spectrum of H_{linear} is symmetric about zero energy.

Next we find a connection between the two arbitrary parameters α and β. Let us define two quantities

$$p = p_x + i\, p_y \quad \text{and} \quad \gamma = \gamma_1 + i\, \gamma_2 \tag{A.6}$$

which transform as vectors under the rotation around the Dirac points. Rewriting H_{linear} in terms of these two quantities, one gets

$$H_{linear} = \frac{i\,\gamma_0}{4}\,(\,\alpha + \beta\,)\,(\,\gamma^*\, p + \gamma\, p^*\,) + \frac{i\,\gamma_0}{4}\,(\,\alpha - \beta\,)\,(\,\gamma^*\, p^* + \gamma\, p\,) \tag{A.7}$$

Setting $\alpha = \beta$, which offers H_{linear} the requisite invariance under a rotation by an angle $2\pi/3$, one finds the celebrated free Dirac Hamiltonian, linear in the momentum operator

$$H_{linear} = \alpha\,(\, i\gamma_0\gamma_1\, p_x + i\gamma_0\gamma_2\, p_y\,), \tag{A.8}$$

where α is proportional to the Fermi velocity. To linear order the free Hamiltonian enjoys a larger $U(1)$ symmetry. However, this is an artifact of the lowest order expansion of the free Hamiltonian in momentum. Since, both $\vec{p} = (p_x, p_y)$ and $\vec{\gamma} = (i\gamma_0\gamma_1, i\gamma_0\gamma_1)$ are vectors under rotation, the only quantity invariant under this operation is their scalar product, which leads to the announced form of the Hamiltonian. Soon we will see that such an extra degree of symmetry is immediately violated by the next to leading order term.

The most general Hamiltonian quadratic in momentum can be written as

$$H_{quadratic} = M_1\, p_x^2 + X\, M_2\, p_y^2 + Y\, M_3\, p_x p_y, \tag{A.9}$$

where M_i, with $i = 1, 2, 3$ are 4-component Hermitian matrices and X and Y are arbitrary parameters. Invariance of $H_{quadratic}$ under the two reflection symmetries, time reversal symmetry, particle-hole symmetry, as well as translation, determines the matrices M_i uniquely

$$M_1 \;=\; M_2 \;=\; \gamma_2 \quad \text{and} \quad M_3 = \gamma_1. \tag{A.10}$$

Hence in terms of p and γ, $H_{quadratic}$ can be written as

$$\begin{aligned} H_{quadratic} \;\; = \;\; & \frac{1}{8\,i}[\,\gamma\, p^2\;(\,1 - X + Y\,)\;+\;\gamma\, p^{*^2}\;(\,1 - X - Y\,)\;+\;2\gamma\, p\, p^*\,(1 + X) \\ & -\,2\gamma^*\, p\, p\,(1 + x)\;+\;\gamma^* p^2\;(-1 + X + Y)\;+\gamma^*\, p^{*^2}\,(-1 + X - Y)\,]. \end{aligned} \tag{A.11}$$

The C_3 invariance of the Hamiltonian imposes a constraint among the two arbitrary parameters

$$X = -1 \quad \text{and} \quad Y = 2. \tag{A.12}$$

Therefore, one can write down the free Hamiltonian (quadratic in momentum) as

$$H_{quadratic} = \alpha\,\left(\,\gamma_2\,\left(p_x^2 - p_y^2\right)\;+\;\gamma_1\,(-2p_x\,p_y)\,\right). \tag{A.13}$$

This also happens to be the low energy dispersion in bilayer graphene, with $\alpha = 1/2m$, where m is the mass of the quasiparticle excitation spectrum.

One can use this prescription to determine the free Hamiltonian up to any order in momentum. We also proceeded to to third order in momentum, which yields

$$H_{cubic} \;=\; i\gamma_0\gamma_1\;\left(p_x^3 \;+\; p_x p_y^2\right)\;+\;i\gamma_0\gamma_2\;\left(p_y^3 \;+\; p_y p_x^2\right). \tag{A.14}$$

Appendix B

Lorentz symmetry breaking momentum shell integration

In Chapter 2, we considered the quartic interaction among the spinless fermions living on the honeycomb lattice. Integrating out the fast Fourier modes in a momentum shell $\Lambda < \left(\omega^2 + k^2\right)^{1/2} < \Lambda/b$, with $b > 1$, we found the low energy behaviour of the interacting fermions. Performing a calculation of the stability of the renormalization group flow equations of the coupling constants, we found that all the critical points leading to the semimetal-insulator instabilities belong to the Lorentz symmetric hyperplane. As a consequence, one finds the *dynamical critical exponent* (z) to be exactly equal to *unity*, and concomitant scale invariant behaviour of the Fermi velocity. However, one might wonder about the robustness of such behaviour against the procedure to eliminate the high energy modes. In Chapter 2, we arrived at the effective low energy theory by performing a momentum shell integration, which preserves the Lorentz invariance. Nevertheless, such procedure might be the legitimate prescription when both the free and the interacting Lagrangians are pseudo-relativistic invariant. However, one is under no obligation to follow that particular methodology once the interacting theory is no longer Lorentz invariant. Here, we will show the nature of the interacting theory at the infrared regime by performing the momentum shell integration in a different, albeit; non-Lorentz symmetric fashion; namely we integrate out the fast Fourier modes within the momentum shell $-\infty < \omega < \infty$ and $\Lambda/b < |\vec{k}| < \Lambda$. Let us write down the interacting theory in terms of the linearly independent coupling

constants, when it loses both the chiral and the Lorentz symmetry

$$L_{int,rot} = g_{C1}\ (\bar{\Psi}\Psi)^2 + g_{D2}(\bar{\Psi}\gamma_{35}\Psi)^2 + g_\alpha\ \left[(\bar{\Psi}i\ \gamma_3\Psi)^2 + (\bar{\Psi}i\ \gamma_5\Psi)^2\right] + g_{A1}(\bar{\Psi}\gamma_0\Psi)^2. \quad \text{(B.1)}$$

The remaining *five* coupling constants can be written as a linear combination of these four couplings, as mentioned in Chapter 2. Performing the momentum shell integration in the announced method one gets the following flow equations

$$\begin{aligned}
\frac{dg_{C1}}{d\ln b} &= -g_{C1} - 2g_{C1}^2 + 2g_{C1}g_{D2} - 2g_{C1}g_\alpha + g_{C1}g_{A1} - g_{D2}g_{A1} \\
&\quad +2g_\alpha g_{A1} - 3g_\alpha^2, && \text{(B.2)}\\
\frac{dg_{D2}}{d\ln b} &= -g_{D2} - 2g_{D2}^2 + 2g_{C1}g_{D2} + 4g_{D2}g_\alpha - 4g_{C1}g_\alpha - 2g_\alpha^2, && \text{(B.3)}\\
\frac{dg_\alpha}{d\ln b} &= -g_\alpha - 3g_\alpha^2 - 4g_\alpha g_{C1} + 2g_\alpha g_{D2} + 2g_\alpha g_{A1} + g_{C1}g_{A1} - g_{D2}g_{A1}, && \text{(B.4)}\\
\frac{dg_{A1}}{d\ln b} &= -g_{A1} - 2g_{C1}g_\alpha + g_{C1}g_{A1} - g_{D2}g_{A1} + 2g_\alpha g_{A1} - g_\alpha^2, && \text{(B.5)}
\end{aligned}$$

after conveniently redefining the coupling constants as $g_i\Lambda/2\pi \to g_i$, with $i = C1, D2, \alpha$ and $A1$. Two chirally symmetric critical points are now located at $g_{C1} = g_\alpha = g_{A1} = 0, g_{D2} = -0.5$ and $g_{C1} = g_\alpha = -0.21325, g_{D2} = -0.134, g_{A1} = -0.089$. The first one corresponds an instability of the semimetallic ground state towards an insulating phase, which lacks time reversal symmetry. On the other hand, the second drives the system to a phase with a non zero expectation value of a triplet order parameter

$$\langle \vec{n} \cdot \vec{V} \rangle \neq 0, \quad \text{(B.6)}$$

with

$$\vec{V} = \left(\ \bar{\Psi}\Psi\ ,\ \bar{\Psi}i\ \gamma_3\Psi\ ,\ \bar{\Psi}i\ \gamma_5\Psi\ \right). \quad \text{(B.7)}$$

The third and the remaining critical point resides at $g_{C1} = -0.33, g_{D2} = 0.167, g_\alpha = 0.211$ and $g_{A1} = 0.089$, and corresponds to transition toward a broken chiral symmetric phase, namely a charge density wave in graphene.

The central message of this exercise is that the restoration of the pseudo Lorentz symmetry near the metal-insulator quantum critical point is no longer valid near all the critical points. However, all the insulating phases as well as the semimetallic phase are Lorentz symmetric. This behaviour is an artifact of a continuum description near three-dimension ($d = 2 + 1$). While performing the momentum shell integration, the cut-off explicitly shows

up in the redefinition of the coupling constants. Therefore, the low energy behaviour of the interacting theory explicitly depends on how one eliminates the fast Fourier modes. To avoid this catastrophe we are after an $\epsilon-$ expansion near two-dimensions ($d = 1 + 1$). At $d = 1 + 1$ all the coupling constants are dimensionless. Therefore, one may expand the theory in a small parameter $\epsilon = D - 2$. This is an ongoing work and lives outside the main theme of this thesis.

Appendix C

Energy spectrum in Kekule lattice

In this appendix we provide some details of the computation of the function $f(\alpha)$, the energy in presence of Kekule distorsion, where α corresponds to various realizations of the Kekule pattern. In the presence of the Kekule modulation the unit cell consists of *six* points and *nine* bonds (Fig. 3.1), hence thrice that in the presence of uniform hopping. The Hamiltonian in k-space then reads as

$$H_k = \sum_k \Psi_k^\dagger H_k \Psi_k, \tag{C.1}$$

with Ψ_k a six component spinor. H_k reads as

$$H_k = \begin{pmatrix} 0 & 0 & 0 & t_3 & t_2 & t_1 \\ 0 & 0 & 0 & t_2 & t_1 & t_3 \\ 0 & 0 & 0 & t_1 & t_3 & t_2 \\ t_3^* & t_2^* & t_1^* & 0 & 0 & 0 \\ t_2^* & t_1^* & t_3^* & 0 & 0 & 0 \\ t_1^* & t_3^* & t_2^* & 0 & 0 & 0 \end{pmatrix}. \tag{C.2}$$

Here $t_a = (t + \eta_a)\, e^{ik_a}$, where t is the uniform hopping and $\eta_a = \eta \cos\left(\alpha + a\,\frac{2\pi}{3}\right)$ yields Kekule hopping. The reduced Brilluoin zone is comprised of the following points

$$(k_1, k_2, K_3) = \frac{2\pi}{3}\frac{1}{L}(n - m, m, -n), \tag{C.3}$$

with $m, n = 1, 2, \cdots, L$, and $6L^2 = N$ is the total number of sites. Before we proceed to compute the energy spectrum $f(\alpha)$, it is worth pausing to register some characteristics of

this function:

1. $f(\alpha)$ is an even function of α, i.e., $f(\alpha) = f(-\alpha)$.

2. $f(\alpha)$ has a global maximum at $\alpha = \pi/3$ and minimum at $\alpha = 0$.

3. $f(\alpha)$ is a periodic function of α with periodicity $2\pi/3$. The periodicity arises from C_3 symmetry around a site of the honeycomb lattice. Hence one can write

$$f(\alpha) = \sum_n a_n \cos(\, 3\, n\, \alpha\,) \tag{C.4}$$

The energy of the p-Kekule superconductor is given by

$$E_{\text{p-Kekule}} = 2f\left(\alpha = \frac{\pi}{2}\right) = \sum_{n \in even} (-1)^{\frac{n}{2}} a_n, \tag{C.5}$$

whereas that for s-Kekule reads as

$$E_{\text{s-Kekule}} = \left[f\,(\alpha = 0) + f\left(\alpha = \frac{\pi}{3}\right)\right] = \sum_{n \in even} a_n. \tag{C.6}$$

Therefore, the difference in the energy for s- and p- Kekule superconducting ground states is

$$E_{\text{p-Kekule}} - E_{\text{s-Kekule}} = -\,2 \sum_n a_{2\,+\,4\,n} \tag{C.7}$$

Hence, for $a_2 > (<)\ 0$ s-(p-) Kekule state is the energetically superior, assuming that $a_6, a_{10} \ll a_2$. Numerically diagonalizing H_k we presented the typical curve for $\eta = 1$ in Chapter 3, after setting $t = 1$. As mentioned previously, upon increasing the strength of nearest-neighbour attraction, first there is a continuous transition from semimetal to p-kekule (odd under Dirac point exchange), followed by an additional discontinuous transition from p- to s-Kekule phase deep inside the superconducting phase, associated with the change of sign of the parameter a_2.

Next, we determine the the susceptibilities for the hidden and Kekule order used in Chapter 3, evaluated over the whole Brillouin zone. For the hidden order, the energy per

site may be written as

$$\frac{E(\Delta')}{2N} = \left(\frac{3}{V} - \frac{1}{2N} \sum_{\vec{k}} |f(\vec{k})| \right) |\Delta'|^2 + O(|\Delta'|^4) \tag{C.8}$$

where

$$f(\vec{k}) = \sum_{i=1,2,3} e^{i\vec{k}\cdot\vec{b}_i} \tag{C.9}$$

and $\vec{b}_i$ are the three vectors connecting the nearest neighbours on the honeycomb lattice. The sum over the wavevectors is performed over the entire Brillouin zone with N points. We find

$$\frac{1}{2N} \sum_{\vec{k}} |f(\vec{k})| = 0.786 \tag{C.10}$$

in agreement with [83]. This yields the value of V_c' cited in the Chapter 3.

For the critical interaction for Kekule order we need the energy as a function of the Kekule mass m to the leading order. Diagonalizing the six-dimensional matrix given in Eq. [C.2] [83] and summing over the reduced first Brillouin zone for the Kekule lattice we find

$$\frac{E(m)}{2N} = \left(\frac{3}{2V} - 0.727 \right) m^2 + O(|m|^3). \tag{C.11}$$

Note that the the electronic susceptibilities for the hidden and Kekule orders are rather close numerically, and the Kekule state wins mainly due to the geometrical factor of two in the first term.

Appendix D

Susceptibilities of Dirac fermions in (2+1)-dimensions

In this appendix we answer the question as to which bilinear has the largest susceptibility in $(2+1)$- dimensions. For simplicity we consider a collection of spinless Dirac fermions, for which the free Lagrangian reads as

$$L_{free} = \overline{\psi}\gamma_\mu \partial_\mu \psi \tag{D.1}$$

One can then add bilinears $\overline{\psi}M\psi$ coupled with the source fields, so that the total Lagrangian becomes

$$L = \overline{\psi}\gamma_\mu \partial_\mu \psi + ij\overline{\psi}M\psi, \tag{D.2}$$

where i, j are source fields. Here M is a four component matrix. The bilinear $\overline{\psi}M\psi$ serves as an 'order parameter'. The source fields are composite fermions, hence can also serve the purpose of the 'order parameter'. Next integrating out the fermions yields

$$L = \frac{1}{2} j\chi j, \tag{D.3}$$

where χ is the susceptibility associated with the order parameter $\overline{\psi}M\psi$ and given by

$$\chi(q) = -Tr\int d^D\vec{k} \quad \frac{ik_\mu\gamma_\mu}{k^2} \quad M \quad \frac{i(k_\nu+q_\nu)\gamma_\nu}{(k+q)^2} \quad M. \tag{D.4}$$

Here our main concern is to find the static susceptibility $\chi_0 = \chi(q=0)$, given by

$$\chi_0 = \int \frac{d^d\vec{k}}{k^4} \quad k_\mu k_\nu \quad \{Tr(\gamma_\mu M\gamma_\nu M)\}. \tag{D.5}$$

For $d = 3$ one finds

$$\chi_0 = \int \frac{d^3k}{3k^2} \quad Tr(\gamma_\mu M \gamma_\mu M). \tag{D.6}$$

Hence our task is to find the M which gives the largest trace.

Let us now introduce a basis $\Gamma_\alpha \in$

$$\{I \quad \gamma_0 \quad \gamma_1 \quad \gamma_2 \quad \gamma_3$$

$$i\gamma_0\gamma_1 \quad i\gamma_0\gamma_2 \quad i\gamma_0\gamma_3 \quad i\gamma_1\gamma_2 \quad i\gamma_1\gamma_3 \quad i\gamma_2\gamma_3$$

$$i\gamma_0\gamma_1\gamma_2 \quad i\gamma_0\gamma_1\gamma_3 \quad i\gamma_0\gamma_2\gamma_3 \quad i\gamma_1\gamma_2\gamma_3$$

$$\gamma_0\gamma_1\gamma_2\gamma_3 = \gamma_5\}.$$

All the elements in this basis satisfy the following properties

$$\Gamma_\alpha{}^\dagger = \Gamma_\alpha, \quad \Gamma_\alpha{}^2 = I. \tag{D.7}$$

These 16 Γ matrices spans the basis for any 4 dimensional Hermitian matrix. Expanding M in this basis one gets

$$T = \sum_{\mu,a,b} C_a C_b \quad Tr(\gamma_\mu \Gamma_a \gamma_\mu \Gamma_b), \tag{D.8}$$

where, $T = Tr(\gamma_\mu M \gamma_\mu M)$ and $M = \sum_a C_a \Gamma_a$. Using the fact that the elements in Γ_α either commute or anti-commute with γ_μ one can decompose T as follows

$$T = \sum_\mu \sum_b C_b \left\{ \sum_a{}' C_a Tr(\Gamma_a \Gamma_b) - \sum_a{}'' C_a Tr(\Gamma_a \Gamma_b) \right\}, \tag{D.9}$$

since $\gamma_\mu{}^2 = I$ for all μ. In the above expression $\sum_a{}'$ runs over Γ_a which commutes with γ_μ and $\sum_a{}''$ runs over Γ_a which anti-commute with γ_μ. Since

$$Tr\{\Gamma_a \Gamma_b\} = 4\delta_{a,b}, \tag{D.10}$$

one gets

$$T = 4 \sum_\mu \left(\sum_a{}' C_a{}^2 - \sum_a{}'' C_a{}^2 \right). \tag{D.11}$$

Therefore we get the bounds on T as

$$-4 \times 3 \quad \leq \quad T \quad \leq 4 \times 3, \tag{D.12}$$

assuming $\sum_a {C_a}^2 = 1$. Thus the trace is optimized in two cases, either

$$\{M, \gamma_\mu\} = 0, \tag{D.13}$$

$\forall\ \mu$, implying $M = \gamma_3, \gamma_5$; or

$$[M, \gamma_\mu] = 0, \tag{D.14}$$

$\forall\ \mu$, implying $M = I, i\gamma_3\gamma_5$. Hence from these solutions one immediately finds that the susceptibility of Dirac fermions in $(2+1)$-dimensions is maximized for $M = I, i\gamma_3, i\gamma_5$, and $i\gamma_3\gamma_5$, whereas it is minimum for $M = \gamma_3, \gamma_5$, and $\gamma_3\gamma_5$. Therefore the maximal susceptibility corresponds to the opening of the relativistic mass gap that either breaks the chiral symmetry $(\gamma_0, i\gamma_0\gamma_3, i\gamma_0\gamma_5)$ or respects the chiral symmetry $(i\gamma_0\gamma_3\gamma_5)$. This conclusion is independent of the representation of the gamma matrices. However, the physical interpretation of the mass gaps explicitly depends on the representation. For example, if we go back to the 'graphene representation', γ_0 relates to the charge density wave order, while the remaining two chiral symmetry breaking orders $(i\gamma_0\gamma_3, i\gamma_0\gamma_5)$ correspond to the Kekule pattern of the nearest-neighbour hopping amplitudes. On the other hand, a finite current circulating among the sites of the same sublattice leads to $M = i\gamma_3\gamma_5$. Dirac fermions maximally lower the energy of the filled Fermi sea by developing a finite expectation value of these order parameters, as we have seen in Chapter 2.

For $d = 4$, the susceptibility of the Dirac fermions is largest only for $M = \gamma_0, i\gamma_0\gamma_5$ for $d = 3 + 1$ [137].

Appendix E

Masses in graphene

Here we will present a detailed computation of various insulating and superconducting order parameters, which can develop finite expectation values if the interactions are sufficiently strong. For the purpose let us consider the 16-compoent Nambu-Dirac fermion, defined in Chapter 3. Namely, $\Psi = (\Psi_p, \Psi_h)^\top$, with $\Psi_p = (\Psi_{p\uparrow}, \Psi_{p\downarrow})^\top$ and $\Psi_h = (\Psi_{h\downarrow}, -\Psi_{h\uparrow})^\top$, and

$$\Psi^\top_{p\sigma}(\vec{q}) = (u_\sigma(\vec{Q}+\vec{q}), v_\sigma(\vec{Q}+\vec{q}), u_\sigma(-\vec{Q}+\vec{q}), v_\sigma(-\vec{Q}+\vec{q})), \tag{E.1}$$

$$\Psi^\top_{h\sigma}(\vec{q}) = (v^\dagger_\sigma(\vec{Q}-\vec{q}), u^\dagger_\sigma(\vec{Q}-\vec{q}), v^\dagger_\sigma(-\vec{Q}-\vec{q}), v^\dagger_\sigma(-\vec{Q}-\vec{q})). \tag{E.2}$$

In this representation the tight binding Hamiltonian with only nearest-neighbour hopping reads as

$$H_D = \sum_{\vec{q}} \Psi^\dagger(\vec{q}) \left[\tau_0 \otimes \sigma_0 \otimes i\gamma_0\gamma_i \; q_i\right] \Psi(\vec{q}). \tag{E.3}$$

Here we omitted the terms higher order in momentum. The two component Pauli matrices $(\tau_0, \vec{\tau})$ and $(\sigma_0, \vec{\sigma})$ act on Nambu's and spin indices. In this representation the three generators of rotations of electron spin are $\vec{S} = \tau_0 \otimes \vec{\sigma} \otimes I_4$, hence they commute with H_D. H_D also commutes with the number operator $N = \tau_3 \otimes \sigma_0 \otimes I_4$. Here the four component, mutually anti commuting, Hermitian gamma matrices belong to the 'graphene representation' [1]. Therefore all the matrices or their products are either purely real or purely imaginary. Next we will list all the insulating orders in graphene.

[1] See for example Chapter 2

Note that insulating orders must commute with the number operator N. Therefore, one can have either τ_0 or τ_3 in the Nambu's index. Before we proceed, it is useful to define a different representation of 16 component Nambu-Dirac fermions as $\tilde{\Psi} = [I_8 \oplus (-i\sigma_2 \otimes \gamma_2)]\,\Psi$. The advantage of using the $\tilde{\Psi}$ representation can be understood from the following relation

$$\psi_h^\dagger\, A\, \psi_h \;=\; -\psi_p^\dagger\, A^\top\, \psi_p. \tag{E.4}$$

The general form of an insulating order is

$$\Psi^\dagger\,[M_1 \oplus M_2]\,\Psi, \tag{E.5}$$

where M_1 and M_2 are 8-dimensional matrices. With τ_0 in the Nambu space, $M_1 = M_2$, leads to the constraint

$$M_1 \;=\; -\,(\sigma_2 \otimes \gamma_2)\,M_1^\top\,(\sigma_2 \otimes \gamma_2)\,, \tag{E.6}$$

for an order parameter with finite expectation value. This constraint yields the following insulating orders

1. $\tau_0 \otimes \sigma_0 \otimes \gamma_0$: charge density wave
2. $\tau_0 \otimes \sigma_0 \otimes i\gamma_1\gamma_2$: quantum anomalous Hall insulator
3. $\tau_0 \otimes \sigma_0 \otimes i\gamma_0\gamma_5$: singlet bond-density wave (odd under Dirac point exchange)
4. $\tau_0 \otimes \vec{\sigma} \otimes i\gamma_0\gamma_5$: triplet bond-density wave (even under Dirac point exchange).

With τ_3 ($M_1 = -M_2$) in the Nambu space on the other hand yields

$$M_1 \;=\; (\sigma_2 \otimes \gamma_2)\,M_1^\top\,(\sigma_2 \otimes \gamma_2)\,, \tag{E.7}$$

which leads to the other set of insulating orders

5. $\tau_3 \otimes \vec{\sigma} \otimes \gamma_0$: antiferromagnet
6. $\tau_3 \otimes \vec{\sigma} \otimes i\gamma_1\gamma_2$: quantum spin Hall insulator
7. $\tau_3 \otimes \vec{\sigma} \otimes i\gamma_0\gamma_5$: triplet bond-density wave (odd under Dirac point exchange)
8. $\tau_3 \otimes \sigma_0 \otimes i\gamma_0\gamma_5$: singlet bond-density wave (even under Dirac point exchange).

Therefore we recover all the 8 insulating order parameters listed in Chapter 3. However, these insulating orders are comprised of 16 linearly independent matrices.

Finally we focus on the superconducting orders into which fermions in honeycomb lattice can condense into. A general superconducting order parameter can be written as

$$\Psi^\dagger \left[\begin{array}{c|c} 0 & M \\ \hline M^\dagger & 0 \end{array}\right] \Psi, \tag{E.8}$$

where M is a 8-dimensional matrix. The superconducting order parameter needs to satisfy the requisite constraint

$$(M\ \sigma_2 \otimes \gamma_2\ )^\top\ =\ -M\ \sigma_2 \otimes \gamma_2. \tag{E.9}$$

In graphene, there are following 4 superconducting states available for the fermions to pair into

1. $(\tau_1, \tau_2) \otimes \sigma_0 \otimes i\gamma_0\gamma_3$: s-wave,
2. $(\tau_1, \tau_2) \otimes \vec{\sigma} \otimes i\gamma_0\gamma_5$: f-wave,
3. $(\tau_1, \tau_2) \otimes \vec{\sigma} \otimes \gamma_0$: s-Kekule,
4. $(\tau_1, \tau_2) \otimes \vec{\sigma} \otimes i\gamma_1\gamma_2$: p-Kekule,

as mentioned in Chapter 3. However, one needs twenty linearly independent matrices to describe all the possible superconducting orders.

All together, hence we have

$$16 \text{ (insulators)} + 20 \text{ (superconductors)} = 36 \text{ mass matrices}$$

in graphene which may open up gaps in the quasi-particle spectrum. From these orders one can also get all the 'hidden orders' by multiplying any of the orders with the Dirac Hamiltonian. However, the hidden orders lower the energy of the filled Dirac-Fermi sea by effectively increasing the Fermi velocity of the excitations.

Appendix F

Topological defects of a Kekule superconductor

In Chapter 3, we introduced the concept of the Kekule superconductor which was found to be the variational ground state within the framework of simple attractive interactions among the fermions living on the nearest neighbour sites of graphene's honeycomb lattice. The s-Kekule order parameter reads as

$$M = m_0(\tau_1 \cos\phi - \tau_2 \sin\phi) \otimes [\sin\theta(\sigma_1 \cos(\phi_\downarrow - \phi) + \sigma_2 \sin(\phi_\downarrow - \phi)) + \sigma_3 \cos\theta] \otimes \gamma_0, \quad \text{(F.1)}$$

where

$$\Delta \;=\; m\;\cos\theta\, e^{i\phi} \quad \text{and} \quad \Delta_\downarrow \;=\; m\;\sin\theta\, e^{i\phi_\downarrow} \qquad \text{(F.2)}$$

The topology of the order parameter is $S_2 \times S_1$, but with opposite sides identified. In other words, the mass matrix lives on the surface of S_3, the sphere in four dimensions. Hence there is no stable topological defect in the ordered phase, since both the first and second homotopy group of S_3 are trivial, i.e. $\pi_1(S_3) = \pi_2(S_3) = 1$. Here will convey this observation by constructing a few vortex like excitations and then show that they are equivalent to the vacuum:

a) $\theta = 0$ and $\phi \;\in\; (\,0, 2\pi\,)$ and the order parameter reads as

$$M(\theta = 0) = \Delta\,(\tau_1 \cos\phi - \tau_2 \sin\phi) \otimes \sigma_3 \otimes \gamma_0. \qquad \text{(F.3)}$$

Even though $M(\theta = 0)$ can support a vortex in Δ, it can be continuously deformed into $\Delta = 0$ and $\Delta_\downarrow = m$ by taking the angle θ from 0 to $\pi/2$.

b) One can construct a vortex by twisting the angle $\phi_\downarrow \in (0, 2\pi)$, after setting $\theta = \pi/2$ or $\Delta = 0$ and $\phi = 0$. The order parameter then becomes

$$M = \tau_1 \otimes (\cos\phi_\downarrow \sigma_1 + \sin\phi_\downarrow \sigma_2) \otimes \gamma_0. \tag{F.4}$$

This order parameter can be shrunk into a point by taking θ from $\pi/2$ to 0.

c) Half-vortex: setting $\phi_\downarrow = \phi \in (0, \pi)$ and $\theta \in (0, \pi)$, yielding

$$M = m_0 \, (\tau_1 \cos\phi - \tau_2 \sin\phi) \otimes (\sin\theta\sigma_1 + \cos\theta\sigma_3) \otimes \gamma_0. \tag{F.5}$$

Let us construct a three component vector

$$\Psi = \begin{pmatrix} \sin\phi \\ \cos\phi\cos\theta \\ \cos\phi\sin\theta \end{pmatrix}, \tag{F.6}$$

which goes from $(0, 1, 0)$ back to $(0, 1, 0)$ at the end of the rotation. Define the three component vector Ψ slightly differently as

$$\Psi = \begin{pmatrix} \cos(\frac{\pi}{2} - \phi) \\ \sin(\frac{\pi}{2} - \phi)\cos\theta \\ \sin(\frac{\pi}{2} - \phi)\sin\theta \end{pmatrix}, \tag{F.7}$$

so that the angles $(\frac{\pi}{2} - \phi)$ and θ corresponds to the polar and azimuthal angles respectively, we can identify Ψ as a vector living on the surface of S_2, the sphere in three dimensions. Hence the order parameter can be continuously shrunk into a point.

Finally let us consider a different type of half-vortex, by setting $\theta = \pi/2$ and the $\phi \in (0, \pi)$ and $\Delta\phi = \phi_\downarrow - \phi \in (0, \pi)$. The order parameter then assumes the following form

$$M = m_0 \, (\tau_1 \cos\phi - \tau_2 \sin\phi) \otimes (\sigma_1 \cos\Delta\phi + \sigma_2 \sin\Delta\phi) \otimes \gamma_0. \tag{F.8}$$

Let us define a four component vector Ψ as

$$\Psi = \begin{pmatrix} \cos\phi \, \cos\Delta\phi \\ \cos\phi \, \sin\Delta\phi \\ \sin\phi \, \cos\Delta\phi \\ \sin\phi \, \sin\Delta\phi \end{pmatrix}, \tag{F.9}$$

with $|\Psi|^2 = 1$. Under a particular parameterization $\phi = \Delta\phi = t \cdot \pi$ with $t \in (0, 1)$, Ψ takes the form

$$\Psi = \begin{pmatrix} \psi_1 \\ \psi_2 \\ \psi_3 \\ \psi_4 \end{pmatrix} = \begin{pmatrix} \cos^2 t\pi \\ \cos t\pi \ \sin t\pi \\ \sin t\pi \ \cos t\pi \\ \sin^2 t\pi \end{pmatrix}. \tag{F.10}$$

Under this parameterization $\psi_2 \equiv \psi_3 \, \forall \, t$. Hence it is useful to define a 3-component vector Ψ' as

$$\Psi' = \begin{pmatrix} \psi_1 \\ \sqrt{\psi_2^2 + \psi_3^2} \\ \psi_4 \end{pmatrix}, \tag{F.11}$$

which resides on the surface of a three sphere S_2 and $\Psi'(t = 0) \equiv \Psi'(t = 1) = (1, 0, 0)$. Therefore, the half-vortex excitations are loops on the surface of the sphere, which are smoothly connected to the vacuum.

In the previous examples, we constructed various topological defects and showed that they can be continuously deformed into a point in the target space. However, in the presence of external perturbations such as spin-orbit coupling or Zeeman splitting the target space of the order parameter is reduced to $S_1 \times S_1$, which restores the possibility of various stable topological excitations. These are discussed in detail in Chapter 3.

Appendix G

Gap equation in a magnetic field

Here we compute the energy spectrum of interacting electrons in the presence of a magnetic field. For simplicity we assume a collection of spinless fermions. Consider the following auxiliary Hamiltonian

$$\tilde{H} = i\gamma_0\gamma_i p_i + m\gamma_0. \tag{G.1}$$

Since $\gamma_0 = I_2 \otimes \sigma_3$ is block diagonal in the valley index, one can focus on the spectrum near each Dirac point. Consider a two dimensional basis

$$|a(+\vec{K})\rangle = \begin{pmatrix} \phi_{n-1} \\ -\phi_n \end{pmatrix} \quad \text{and} \quad |b(+\vec{K})\rangle = \begin{pmatrix} \phi_{n-1} \\ \phi_n \end{pmatrix}, \tag{G.2}$$

with energies $\pm\sqrt{2nB}$, respectively, when $m = 0$. In this two dimensional basis the auxiliary Hamiltonian takes the following form

$$H_+ = \left(\begin{array}{c|c} \sqrt{2nB} & m \\ \hline m & -\sqrt{2nB} \end{array}\right). \tag{G.3}$$

The eigenvalues of H_+ are at $E = \pm\sqrt{2nB + m^2}$, with eigenvectors

$$|+\sqrt{2nB+m^2}\rangle = \frac{1}{N_1}\left(\frac{m}{\sqrt{2nB+m^2}-\sqrt{2nB}}|a(+\vec{K})\rangle, +|b(+\vec{K})\rangle\right) \tag{G.4}$$

and

$$|-\sqrt{2nB+m^2}\rangle = \frac{1}{N_2}\left(\frac{-m}{\sqrt{2nB+m^2}+\sqrt{2nB}}|a(+\vec{K})\rangle, +|b(+\vec{K})\rangle\right) \tag{G.5}$$

respectively. The N_i, with $i = 1, 2$ are the normalization constants. One gets an identical energy spectrum for the lower component. Assuming such a chiral symmetry breaking term

arises from electron-electron interactions, one finds that Landau levels at finite energy are shifted in energy, but the particle and hole Landau levels are now mixed. However, their valley degeneracy is still protected for $n \neq 0$. For $n = 0$ the Hamiltonian becomes

$$H_+\Psi_0^+ = \left(\begin{array}{c|c} m & D^* \\ \hline D & -m \end{array}\right)\left(\begin{array}{c} \phi_0 \\ 0 \end{array}\right) = +m\left(\begin{array}{c} \phi_0 \\ 0 \end{array}\right), \tag{G.6}$$

near the Dirac point at $+\vec{K}$. Near the other Dirac point it takes the following form

$$H_-\Psi_0^- = \left(\begin{array}{c|c} m & -D \\ \hline D^* & -m \end{array}\right)\left(\begin{array}{c} 0 \\ \phi_0 \end{array}\right) = -m\left(\begin{array}{c} 0 \\ \phi_0 \end{array}\right). \tag{G.7}$$

Therefore the zeroth Landau levels are eigenstates of γ_0. For $m \neq 0$, half of the states in the zeroth Landau level have eigenvalue $+m$, and the remaining ones have eigenvalue $-m$. Hence even an infinitesimal amount of interaction splits the zeroth Landau level and develops a gap in the spectrum. This mechanism is named 'magnetic catalysis'. A pictorial demonstration of magnetic catalysis is given in Fig. G.1.

Next, we derive the gap equation of the interaction induced gap in the magnetic field. We define the Lagrangian

$$L_{int} = \overline{\Psi}_i \not{D} \Psi_i - g\left(\overline{\Psi}_i \Psi_i\right)^2. \tag{G.8}$$

After a Hubbard-Stratonovich transformation one can write down the action associated with L_{int} as

$$S = \frac{\Omega}{T}\frac{m^2}{4g} - 2\frac{N}{2}\sum_{\omega_n} Tr \ln\left(i\omega_n + \tilde{H}\right), \tag{G.9}$$

where $\tilde{H}$ is the auxiliary Hamiltonian defined in Eq. G.1, T is the temperature, Ω is the area of the sample, $\omega_n = (2n+1)/T$ is the fermionic Matsubara frequency and m is the interaction induced gap. The spectrum of $\tilde{H}$ is as following

$$\begin{aligned} E_n &= \pm\sqrt{2nB + m^2} \quad \text{with degeneracy } D_\pm = 2D, \\ E_0^+ &= +m \quad \text{with degeneracy } D_0^+ = D, \\ E_0^- &= -m \quad \text{with degeneracy } D_0^- = D, \end{aligned} \tag{G.10}$$

where $D = \Omega/2\pi l_B^2$ is the degeneracy of Landau level for non-relativistic particles, with $l_B^2 = \hbar/eB$ being the magnetic length. As $T \to 0$, the Mastubara frequencies form a

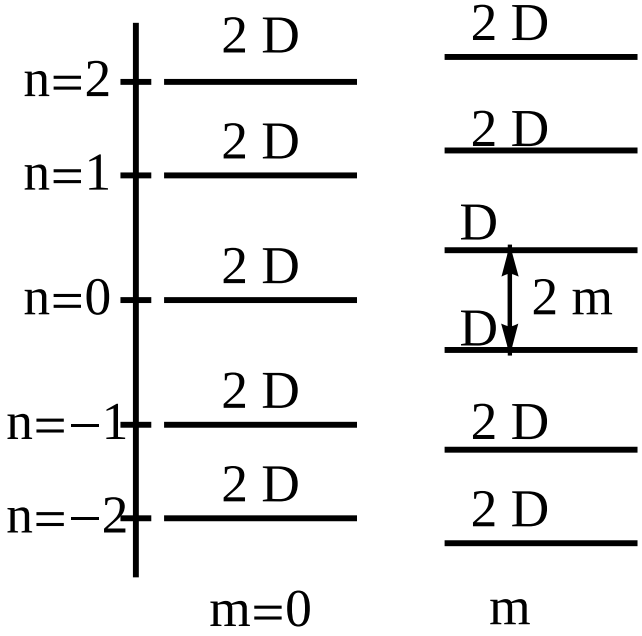

Figure G.1: 'Magnetic catalysis': developing a chiral symmetry breaking gap (2 m) close to the charge neutral point in graphene.

continuum. Minimizing the action one can write down the self-consistent gap equation as

$$\frac{1}{4g} = \frac{N}{\Omega}\int_{-\infty}^{\infty}\frac{d\omega}{2\pi}\left(\sum_{n=1}^{\infty} 2\cdot\frac{1}{2\sqrt{2nB+m^2}} + \frac{1}{2}\cdot\frac{1}{m}\right). \tag{G.11}$$

Implementing the trick

$$\frac{1}{m} \equiv \frac{1}{\sqrt{m^2}} = \frac{1}{\sqrt{\pi}}\int_0^{\infty}\frac{ds}{\sqrt{s}}e^{-sm^2}, \tag{G.12}$$

one can rewrite down the previous equation as

$$\frac{1}{4g} = \frac{N}{2\pi^{3/2}l_B^2}\int_0^{\infty}\frac{ds}{\sqrt{s}}e^{-sm^2}\left(\sum_{n=0}^{\infty}e^{-2snB} - \frac{1}{2}\right). \tag{G.13}$$

Realizing the identity

$$\sum_{n=0}^{\infty}e^{-2snB} - \frac{1}{2} = \frac{1}{2}\coth(sB), \tag{G.14}$$

the gap equation can be expressed compactly as

$$\frac{1}{g} = \frac{NB}{\pi^{3/2}}\int_{\Lambda^{-2}}^{\infty}\frac{ds}{\sqrt{s}}e^{-sm^2}\coth(sB). \tag{G.15}$$

Upon including the spin degrees of freedom one needs to multiply the contribution on the right hand side by a factor of 2 for $\nu = 0$, since both the Landau levels contribute and the gap equation then becomes

$$\frac{1}{g} = 2 \cdot \frac{NB}{\pi^{3/2}} \int_{\Lambda^{-2}}^{\infty} \frac{ds}{\sqrt{s}} e^{-sm^2} \cdot \coth(sB). \tag{G.16}$$

However, for $\nu = 1$, only half of the the Landau levels contribute and the free energy reads as

$$\frac{E(m) - E(0)}{N} = \frac{m^2}{4g} + \frac{B}{4\pi^{3/2}} \int_0^{\infty} \frac{ds}{s^{3/2}} (e^{-sm^2} - 1) \cdot [1 + 2(\coth(sB) - 1)]. \tag{G.17}$$

Here for simplicity we omitted the function $K(x)$, introduced to sum over the higher Landau levels. The reader can consult Fig. G.2 for further clarification. Here it is assumed that the spin degeneracy is completely lifted by Zeeman splitting and the chemical potential lies close to the Zeeman shifted Dirac point.

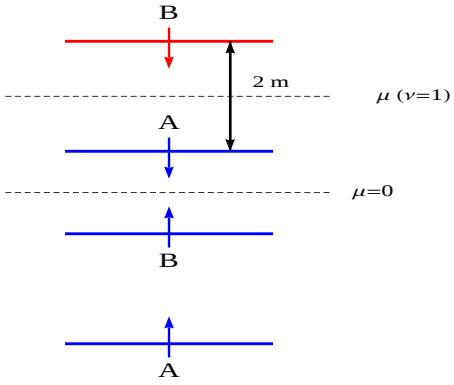

Figure G.2: $\nu = 1$ gap generation by 'magnetic catalysis' after the spin degeneracy is completely lifted by Zeeman splitting.

Next we derive the form of the gap equation, mentioned in Chapter 4. After introducing the function $K(x)$ and minimizing the free energy, we arrive at

$$\frac{1}{\sqrt{yB}} \left(\frac{1}{g} - \frac{K}{\sqrt{\pi}} \right) = 1 + \frac{1}{y\sqrt{\pi}} \int_0^{\infty} K\left(\frac{sy}{B}\right) \left[\frac{2yse^{-s}}{e^{2ys} - 1} - 1 \right], \tag{G.18}$$

where $y = B/m^2$ and

$$\frac{K}{m} = \frac{1}{m} \int_0^{\infty} dt \frac{K(t)}{t^{3/2}} = \int_0^{\infty} \frac{ds}{s^{3/2}} \cdot K\left(\frac{s}{m^2}\right). \tag{G.19}$$

The previous equation can also be put in the following compact form

$$y = \frac{1}{\sqrt{\pi}} \int_0^\infty \frac{ds}{s^{3/2}} \cdot \left[1 - \frac{2yse^{-s}}{e^{2ys} - 1} \right] + \sqrt{\frac{y}{B}} \delta, \tag{G.20}$$

after conveniently defining

$$\delta = \frac{1}{g} - \frac{1}{g_c}, \tag{G.21}$$

where the non-universal value of the critical interaction at $B = 0$ for the metal-insulator transition reads as

$$\frac{1}{g_c} = \frac{K}{\sqrt{\pi}}. \tag{G.22}$$

To arrive at the algebraic form of the gap equation announced in Chapter 3, first we compactly write the gap equation as

$$y = f(y) + 2\delta \sqrt{\frac{y}{B}}, \tag{G.23}$$

where

$$\begin{aligned} f(y) &= \frac{2}{\sqrt{\pi}} \int_0^\infty \frac{dt/2y}{(t/2y)^{3/2}} \left[1 - \frac{te^{-t/2y}}{e^t - 1} \right] \\ &= \frac{2^{3/2}\sqrt{y}}{\sqrt{\pi}} \int_0^\infty \left[\left(1 - \frac{t}{e^t - 1} \right) + \frac{t^2}{e^t - 1} \cdot \frac{1}{2y} + \cdots \right] \\ &= \frac{2^{3/2}\sqrt{y}}{\sqrt{\pi}} \left[2.58829 + \frac{2.31516}{2y} + \cdots \right] \\ &= (4.1303)\sqrt{y} + \frac{1.8472}{\sqrt{y}} + O\left(\frac{1}{y^{3/2}} \right) \\ &\equiv u\sqrt{y} + vy^{-1/2} + O\left(\frac{1}{y^{3/2}} \right), \end{aligned} \tag{G.24}$$

as mentioned in Chapter 3.

Appendix H

Středa formula and Hall conductivity

In this appendix, we determine the quantization of the Hall conductivity that we mentioned in Chapter 7, when the real and pseudo magnetic fields penetrating the graphene system are both finite. One notices that upon introducing a finite pseudo magnetic flux, all the LLs do not enjoy equal degeneracies. LLs localized in the neighborhood of the Dirac point at $\vec{K}$ have a degeneracy $(B+b)/2\pi$ per unit area, whereas those living in the vicinity of the other Dirac point, at $-\vec{K}$, carry $(B-b)/2\pi$ states per unit area. Using the Středa formula, one can write the expession for the Hall conductivity as

$$\sigma_{xy} = \left(\frac{\partial N}{\partial B}\right)_{\mu}, \tag{H.1}$$

after setting $e = c = 1$ [136]. Here N is the electronic density in the bulk and the derivative with respect to B is taken at fixed chemical potential (μ). The chemical potential is measured from the charge neutral point. Moreover, all the LLs have an additional two fold spin degeneracy. Upon changing the magnetic field B, the number of states below the chemical potential is changed to

$$\delta N = \Omega f_{+} \delta B + \Omega f_{-} \delta B. \tag{H.2}$$

f_{+} and f_{-} counts the number of LLs below the chemical potential (μ), but above the charge neutral point, with degeneracies $(B \pm b)/2\pi$ per unit area for each spin species, respectively. Therefore the Hall conductivity is

$$\sigma_{xy} = f_{+} + f_{-} = f. \tag{H.3}$$

Hence, quantization of the Hall conductivity only takes the number of filled LLs below the chemical potential into account. That leads to the the announced result of the Hall conductivity in the presence of real and pseudo magnetic fields. However, one should notice that due to the different degeneracies of the LLs, quantization of the Hall conductivity at integer values of e^2/h is not associated with integer fillings. The filling factor explicitly depends on the ratio b/B.

Bibliography

[1] V.P. Gusynin, S.G. Sharapov, J.P. Carbotte, Int. J. of Mod. Phys. B, **21**, 4611 (2007); A. H. Castro Neto, F. Guinea, N. M. R. Peres, K. S. Novoselov, and A. K. Geim, Rev. Mod. Phys. **81**, 109 (2009).

[2] I. Affleck and J. B. Marston, Phys. Rev. B **37**, 3774 (1988).

[3] P. Hosur, S. Ryu and A. Vishwanath, Phys. Rev. B **81**, 045120 (2010).

[4] I. F. Herbut, Phys. Rev. B **83**, 245445 (2011).

[5] P. R. Wallace, Phys. Rev. **71**, 622 (1947).

[6] G. W. Semenoff, Phys. Rev. Lett. **53**, 2449 (1984).

[7] T. A. Gloor and F. Milla, Eur. Phys. J. B **38**, 9 (2004).

[8] F. Bassani and G. Pastori Parravicini, Electronic States and Optical Transitions in Solid (Pergamon, New York, 1975).

[9] I. F. Herbut, Phys. Rev. Lett. **97**, 146401 (2006).

[10] K. S. Novoselov, A. K. Geim, S. V. Morozov, D. Jiang, M. I. Katsnelson, I. V. Grigorieva, S. V. Dubonos, and A. A. Firsov, Nature (London) **438**, 197 (2005).

[11] Y. Zhang, Y.-W. Tan, H. L. Stormer, and P. Kim, Nature (London) **438**, 201 (2005).

[12] T. Taychatanapat, K. Watanabe, T. Taniguchi, and P. Jarillo-Herrero, arxiv:1104.0438 (2011).

[13] J. W. Negele and H. Orland, Quantum many-particle systems (Addison-Wesley Pub. Co., the Advanced Book Program, 1988).

[14] M. J. Luttinger, Phys. Rev. **118**, 1417 (1960).

[15] R. Shankar, Rev. Mod. Phys. **66**, 129 (1994).

[16] J. E. Drut and T. A. Lahde, Phys. Rev. Lett, **102**, 026802 (2009); Phys. Rev. B **79**, 165425 (2009); Phys. Rev. B **79**, 241405(R) (2009).

[17] V.Juričić, I. F. Herbut, and G. W. Semenoff, Phys. Rev. B, **80**, 081405 (R) (2009).

[18] J. Gonzalez, F. Guinea, and M. A. H. Vozmediano, Nucl. Phys. **B424**, 595 (1994); Phys. Rev. B **59**, 2474 (1999).

[19] O. Vafek, Phys. Rev. Lett. **98**, 216401 (2007); O. Vafek and M. J. Case, Phys. Rev. B **77**, 033410 (2008).

[20] I. F. Herbut, Phys. Rev. Lett. **99** 206404, (2007).

[21] S. Sorella and E. Tosatti, Europhys. Lett. **19**, 699 (1992).

[22] L. M. Martelo, M. Dzierzawa, L. Siffert, and D. Baeriswyl, Z. Phys. B **103**, 335 (1997).

[23] T. Paiva, R. T. Scalettar, W. Zheng, R. R. Singh, and J. Oitmaa, Phys. Rev. B **72**, 085123 (2005).

[24] T. O. Wehling, E. Sasioglu, C. Friedrich, A. I. Lichtenstein, M. I. Katsnelson, and S. Blügel, Phys. Rev. Lett. **106**, 236805 (2011)

[25] Y. Zhang, Z. Jiang, J. P. Small, M. S. Purewal, Y.-W. Tan, M. Fazlollahi, J. D. Chudow, J. A. Jaszczak, H. L. Stormer, and P. Kim, Phys. Rev. Lett. **96**, 136806 (2006); Z. Jiang, Y. Zhang, H. L. Stormer, and P. Kim, Phys. Rev. Lett. **99**, 106802 (2007).

[26] Joseph G. Checkelsky, Lu Li, and N. P. Ong, Phys. Rev. Lett. **100**, 206801 (2008); preprint arXiv:0808.0906.

[27] D. V. Khveshchenko, Phys. Rev. Lett. **87**, 206401 (2001); *ibid.* **87**, 246802 (2001).

[28] V. P. Gusynin, V. A. Miransky, S. G. Sharapov, and I. A. Shovkovy, Phys. Rev. B **74**, 195429 (2006); E. V. Gorbar, V. P. Gusynin, V. A. Miransky, I. A. Shovkovy, Phys. Rev. B **78** 085437 (2008); E. V. Gorbar, V. P. Gusynin, V. A. Miransky, Low Temp. Phys. **34**, 790 (2008).

[29] I. F. Herbut, Phys. Rev. B **75**, 165411 (2007).

[30] J. Alicea and M. P. A. Fisher, Phys. Rev. B **74**, 075422 (2006); R. L. Doretto and C. Morais-Smith, Phys. Rev. B **76**, 195431 (2007).

[31] I. F. Herbut, V. Juričić, and O. Vafek, Phys. Rev. Lett. **100** 046403 (2008); I. F. Herbut, V. Juričić, O. Vafek, and M. J. Case, preprint, arxive:0809.0725 (2008); V. Juričić, O. Vafek, and I. F. Herbut, Phys. Rev. B **82**, 235402 (2010).

[32] L. Fritz, J. Schmalian, M. Mueller, and S. Sachdev, Phys. Rev. B **78**, 085416 (2008).

[33] D. C. Elias, R. V. Gorbachev, A. S. Mayorov, S. V. Morozov, A. A. Zhukov, P. Blake, K. S. Novoselov, A. K. Geim, and F. Guinea, arxiv:1104.1396 (2011).

[34] See for example, Y. Takahashi, in *Progress in Quantum Field Theory*, ed. by H. Ezawa and S. Kamefuchi (North Holland, 1986).

[35] O. Vafek, Phys. Rev. B **82**, 205106 (2010).

[36] I. F. Herbut, Phys. Rev. B **66**, 094504 (2002); Phys. Rev. Lett. **88**, 047006 (2002); Phys. Rev. Lett. **94**, 237001 (2005); D. J. Lee and I. F. Herbut, Phys. Rev. B **66**, 094512 (2002); B. Seradjeh and I. F. Herbut, Phys. Rev. B **66**, 184507 (2002); Z. Tešanović, O. Vafek, and M. Franz, Phys. Rev. B **65**, 180511 (2002); M. Franz, T. Pereg-Barnea, D.E. Sheehy, and Z. Tešanović, Phys. Rev. B **68**, 024508 (2003); I. O. Thomas and S. Hands, Phys. Rev. B **75**, 134516 (2007).

[37] I. F. Herbut, Phys. Rev. Lett. **87**, 137004 (2001).

[38] F. D. M. Haldane, Phys. Rev. Lett. **61**, 2015 (1988).

[39] C-Y. Hou, C. Chamon, and C. Mudry, Phys. Rev. Lett. **98**, 186809 (2007).

[40] I. Herbut, *A Modern Approach to Critical Phenomena*, (Cambridge University Press, Cambridge, 2007).

[41] W. F. Brinkman and T. M. Rice, Phys. Rev. B **2**, 4302 (1970).

[42] Y. Hasegawa, R. Konno, H. Nakano, and M. Kohmoto, Phys. Rev. B **74**, 033413 (2006).

[43] I. F. Herbut, Phys. Rev. B. **78**, 205433 (2008).

[44] Dj. Mušicki and B. Milić, *Matematicke osnove teorijske fizike*, (Univerzitet u Beogradu, Beograd, 1984), sec. 5.3 (in Serbian).

[45] Here we treat the frequency integrals in the loops analogously to momentum integrals. For an alternative, see ref. 2, for example.

[46] K. Kaveh and I. F. Herbut, Phys. Rev. B **71**, 184519 (2005).

[47] A. M. Vasil'ev, S. E. Derkachov, N. A. Kilev, and A. S. Stepanenko, Teor. Mat. Fiz. **92**, 486 (1992); *ibid.* **97**, 364 (1993);

[48] J. A. Gracey, Int. J. Mod. Phys. A **9**, 727 (1994).

[49] L. Kärkkäinen, L. Lacaze, P. Lacock, and B. Petersson, Nucl. Phys. B **415**, 781 (1994); **438** 650(E) (1995).

[50] L. Rosa, P. Vitale, and C. Wetterich, Phys. Rev. Lett. **86**, 958 (2001); F. Höfling, C. Novak, and C. Wetterich, Phys. Rev. B **66**, 205111 (2002).

[51] S. Christofi, S. Hands, and C. Strouthos, Phys. Rev. D **75**, 101701 (2007), and references therein.

[52] Y. Nambu and G. Jona-Lasinio, Phys. Rev. **122**, 345 (1961).

[53] H. Gies and L. Janssen, Phys. Rev. D **82**, 085018 (2010).

[54] P. Calabrese, A. Pelissetto, and E. Vicari, Phys. Rev. B **67**, 054505 (2003).

[55] S. Raghu, Xiao-Liang Qi, C. Honerkamp, and S.-C. Zhang, Phys. Rev. Lett. **100**, 156401 (2008).

[56] I. F. Herbut, V. Juričić, and O. Vafek, Phys. Rev. B **80**, 075432 (2009).

[57] I. L. Aleiner, D. E. Kharzaev, and A. M. Tsvelik, Phys. Rev. B **76**, 195415 (2007)

[58] D. T. Son, Phys. Rev. B **75**, 235423 (2007); J. E. Drut and D. T. Son, Phys. Rev. B **77**, 075115 (2008).

[59] E. V. Gorbar, V. P. Gusynin, V. A. Miransky, and I. A. Shovkovy , Phys. Rev. B **66**, 045108 (2002).

[60] D. V. Khveshchenko and H. Leal, Nucl. Phys. B **687**, 323 (2004).

[61] S. Hands and C. Strouthos, Phys. Rev. B **78** 165423, (2008).

[62] See the ref. 21, and the problem 8.10 in ref. 25.

[63] I. F. Herbut and Z. Tešanović, Phys. Rev. Lett. **76**, 4588 (1996); *ibid.* **78**, 980 (1997); I. F. Herbut, J. Phys. A: Math. Gen. **30**, 423 (1997).

[64] B. Roy and I. F. Herbut, Phys. Rev. B **82**, 035429 (2010).

[65] E. Zhao and A. Paramekanti, Phys. Rev. Lett. **97**, 230404 (2006).

[66] C. Honerkamp, Phys. Rev. Lett. **100**, 146404 (2008).

[67] B. Uchoa and A. H. Castro Neto, Phys. Rev. Lett. **98**, 146801 (2007).

[68] A. M. Black-Schaffer and S. Doniach, Phys. Rev. B **75**, 134512 (2007); J. Linder, A. M. Black-Schaffer, T. Yokoyama, S. Doniach, and A. Sudbo, Phys. Rev. B **80**, 094522 (2009).

[69] D. V. Khveshchenko, J. Phys. Cond. Matt. **21**, 075303 (2009).

[70] I. F. Herbut, Phys. Rev. Lett. **104**, 066404 (2010).

[71] Y. Kopelevich, P. Esquinazi, J. H. S. Torres, and S. Moehlecke, J. Low Temp. Phys. **119**, 691 (2000).

[72] P. Ghaemi and F. Wilczek, arXiv:0709.2626 (2007).

[73] P. Ghaemi, S. Ryu, and D.-H. Lee, Phys. Rev. B **81**, 081403(R) (2010).

[74] C. W. J. Beenakker, Phys. Rev. Lett. **97**, 067007 (2006); Rev. Mod. Phys. **80**, 1337 (2008).

[75] P. Strack, S. Takei, and W. Metzner, Phys. Rev. B **81**, 125103 (2010).

[76] L.-K. Lim, A. Lazarides, A. Hemmerich, and C. Morais Smith, Europhys. Lett. **88**, 36001 (2009).

[77] C. Chamon, Phys. Rev. B **62**, 2806 (2000).

[78] A. I. Larkin and Y. N. Ovchinnikov, Zh. Eksp. Teor. Fiz. **47**, 1136 (1964), [Sov. Phys. JETP **20**, 762 (1965)].

[79] P. Fulde and R. A. Ferrell, Phys. Rev. **135**, A550 (1964).

[80] I. F. Herbut, V. Juričić, and B. Roy, Phys. Rev. B **79**, 085116 (2009).

[81] I. F. Herbut, Phys. Rev. B **76**, 085432 (2007).

[82] D. Poletti, C. Miniatura, and B. Gremaud, Eur. Phys. Lett. **93**, 37008 (2011).

[83] C. Weeks and M. Franz, Phys. Rev. B **81**, 085105 (2010).

[84] S. Ryu, C. Mudry, C.-Y. Hou, and C. Chamon, Phys. Rev. B **80**, 205319 (2009).

[85] I. F. Herbut and M. Oshikawa, Phys. Rev. Lett. **97**, 080403 (2006), A. Tokuno, Y. Mitamura, M. Oshikawa, and I. F. Herbut, Phys. Rev. A **79**, 053626 (2009), for a detailed discussion.

[86] D. Vollhardt and P. Woelfle, *The Superfluid Phases of Hellium 3*, (Taylor & Francis, 1990).

[87] C. L. Kane and E. J. Mele, Phys. Rev. lett. **95**, 226801 (2005).

[88] I. F. Herbut, Phys. Rev. B **79**, 193405 (2010).

[89] Y. Zheng and T. Ando, Phys. Rev. B **65**, 245420 (2002).

[90] V. P. Gusynin and S. G. Sharapov, Phys. Rev. Lett. **95**, 146801 (2005); N. M. R. Peres, F. Guinea, and A. H. Castro Neto, Phys. Rev. B **72**, 174406 (2005).

[91] N. M. R. Peres, F. Guinea, and A. H. Castro Neto, Phys. Rev. B **72**, 174406 (2005).

[92] K. Nomura and A. H. MacDonald, Phys. Rev. Lett. **96**, 256602 (2006).

[93] M. O. Goerbig, R. Moessner, and B. Doucot, Phys. Rev. B **74**, 161407(R) (2006).

[94] V. M. Apalkov and T. Chakraborty, Phys. Rev. Lett. **97**, 126801 (2006).

[95] I. F. Herbut, Phys. Rev. B **75**, 165411 (2007).

[96] J.-N. Fuchs and P. Lederer, Phys. Rev. Lett. **98**, 016803 (2007).

[97] K. Yang, Solid State Commun. **23**, 147 (2007).

[98] Y. Zhang, Z. Jiang, J. P. Small, M. S. Purewal, Y. -W. Tan, M. Fazlollahi, J. D. Chudow, J. A. Jaszczak, H. L. Stormer, and P. Kim, Phys. Rev. Lett. **96**, 136806 (2006).

[99] Z. Jiang, Y. Zhang, H. L. Stromer,and P. Kim, Phys. Rev. Lett. **99**, 106802 (2007).

[100] L. Sheng, D. N. Sheng, F. D. M. Haldane, L. Balents, Phys. Rev. Lett. **99**, 196802 (2007).

[101] C. R. Dean, A. F. Young, I. Meric, C. Lee, L. Wang, S. Sorgenfrei, K. Watanabe, T. Taniguchi, P. Kim, K. L. Shepard and J. Hone, Nat. Nanotech., **5**, 722 (2010).

[102] V. P. Gusynin, V. A. Miransky, and I. A. Shovkovy, Phys. Rev. Lett. **73**, 3499 (1994); Phys. Rev. D **52**, 4718 (1995).

[103] I. F. Herbut, and Bitan Roy, Phys. Rev. B **77**, 245438 (2008).

[104] *The Quantum Hall effect* Edited by R. E. Prange and S. M. Girvin, (Springer-Verlag, 1987).

[105] G. W. Semenoff, I. A. Shovkovy, and L. C. R. Wijewardhana, Phys. Rev. D **60**, 105024 (1999).

[106] J. G. Checkelsky, L. Li, and N. P. Ong, Phys. Rev. B **79**, 115434 (2009).

[107] C.-Y. Hou, C. Chamon, and C. Mudry, Phys. Rev. B **81**, 075427 (2010).

[108] B. Roy, arxiv:1106.1419 (2011).

[109] D. A. Abanin, K. S. Novoselov, U. Zeitler, P. A. Lee, A. K. Geim, and L. S. Levitov, Phys. Rev. Lett. **98**, 196806 (2007).

[110] F. Schedin, A. K. Geim, S. V. Morozov, D. Jiang, E. H. Hill, P. Blake, K. S. Novoselov, Nat. Mater. **6**, 652 (2007).

[111] D.T. Son, Phys. Rev. B **75**, 235423 (2007).

[112] D. Sheehy and J. Schmalian, Phys. Rev. Lett. **99**, 226803 (2007).

[113] K. S. Novoselov, A. K. Geim, S. V. Morozov, D. Jiang, Y. Zhang, S. V. Dubonos, I. V. Grigorieva, and A. A. Firsov, Science **306**, 666 (2004).

[114] I. F. Herbut, Physics **2**, 57 (2009).

[115] V. P. Gusynin, V. A. Miransky, and I. A. Shovkovy, Phys. Rev. Lett. **73**, 3499 (1994); Phys. Rev. D **52**, 4718 (1995).

[116] D. V. Khveshchenko, Phys. Rev. Lett. **87**, 246802 (2001); H. Leal and D. V. Khveshchenko, Nucl. Phys. B **B687**, 323 (2004).

[117] F. Guinea, M. I. Katsnelson, and A.K. Geim, Nat. Phys. **6**, 30 (2010).

[118] N. Levy, S. A. Burke, K. L. Meaker, M. Panlasigui, A. Zettl, F. Geimkatguinea, and A. H. Castro Neto, M. F. Crommie, Science **329**, 544 (2010).

[119] G. Dunne and T. Hall, Phys. Rev. D **53**, 2220 (1996).

[120] A. Raya and E. Reyes, Phys. Rev. D **82**, 016004 (2010).

[121] Y. Aharonov and A. Casher, Phys. Rev. A **19**, 2461 (1979).

[122] Y. Hasegawa, M. Kohmoto, Phys. Rev. B **74**, 155415 (2006); D. R. Hofstadter, Phys. Rev. B. **14**, 2239 (1976).

[123] Z. Y. Meng, T. C. Lang, S. Wessel, F. F. Assaad, and A. Muramatsu, Nature **464**, 847 (2010).

[124] S. Sachdev, arXiv:1012.0299 (2010).

[125] B. Roy, Phys. Rev. B **84**, 035458 (2011).

[126] S. V. Morozov, K. S. Novoselov, M. I. Katsnelson, F. Schedin, L. A. Ponomarenko, D. Jiang, and A. K. Geim, Phys. Rev. Lett. **97**, 016801 (2006).

[127] R. Jackiw, and S.-Y. Pi, Phys. Rev. Lett. **98**, 266402 (2007).

[128] O. Motrunich, K. Damle, and D. Huse, Phys. Rev. B **65**, 064206 (2002).

[129] F. Guinea, M. I. Katsnelson, and M. A. H. Vozmediano, Phys. Rev. B **77**, 075422 (2008).

[130] M. Ishigami, J. H. Chen, W. G. Cullen, M. S. Fuhrer, and E. D. Williams, Nano Lett. **7**, 1643 (2007).

[131] F. Guinea, A. K. Geim, M. I. Katnelson, and K. S. Novoselov, Phys. Rev. B **81**, 035408 (2010).

[132] R. Jackiw, Phys. Rev. D **29**, 2375 (1984).

[133] A. L. Tchougreeff and R. Hoffmann, J. Phys. Chem. **96** 8993 (1992).

[134] J. Jung, and A. H. MacDonald, Phys. Rev. B **80**, 235417 (2009).

[135] B. Roy and I. Herbut, Phys. Rev. B **83**, 195422 (2011).

[136] P. Středa, J. Phys. C: Solid State Phys. **15**, L717 (1982).

[137] C. Itzykson and J. B. Zuber, *Quantum Field Theory*, (Dover Publication, 2005)